Methods in Molecular Biology 1583

Springer Protocols

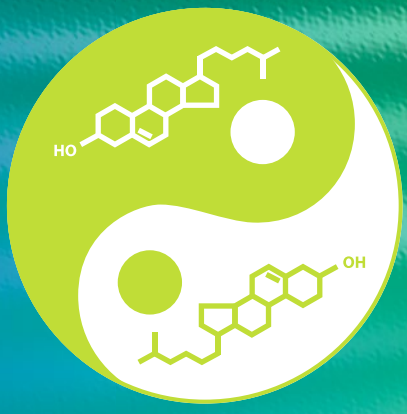

Ingrid C. Gelissen
Andrew J. Brown *Editors*

Cholesterol Homeostasis

Methods and Protocols

EXTRAS ONLINE

Humana Press

METHODS IN MOLECULAR BIOLOGY

Series Editor
John M. Walker
School of Life and Medical Sciences
University of Hertfordshire
Hatfield, Hertfordshire, AL10 9AB, UK

For further volumes:
http://www.springer.com/series/7651

Cholesterol Homeostasis

Methods and Protocols

Edited by

Ingrid C. Gelissen

Faculty of Pharmacy, The University of Sydney, Sydney, NSW, Australia

Andrew J. Brown

School of Biotechnology and Biomolecular Sciences,
The University of New South Wales, Sydney, NSW, Australia

Humana Press

Editors
Ingrid C. Gelissen
Faculty of Pharmacy
The University of Sydney
Sydney, NSW, Australia

Andrew J. Brown
School of Biotechnology
and Biomolecular Sciences
The University of New South Wales
Sydney, NSW, Australia

ISSN 1064-3745 ISSN 1940-6029 (electronic)
Methods in Molecular Biology
ISBN 978-1-4939-6873-2 ISBN 978-1-4939-6875-6 (eBook)
DOI 10.1007/978-1-4939-6875-6

Library of Congress Control Number: 2016963794

Printed on acid-free paper

This Humana Press imprint is published by Springer Nature
The registered company is Springer Science+Business Media LLC
The registered company address is: 233 Spring Street, New York, NY 10013, U.S.A.

Preface

> *Cholesterol is a Janus-faced molecule. The very property that makes it useful in cell membranes, namely its absolute insolubility in water, also makes it lethal.*

This quote from the 1985 Nobel Laureates Michael Brown and Joseph Goldstein (Brown and Goldstein, 1985 *Nobel Lecture*: 284–324) aptly introduces the concept of cholesterol homeostasis. We need cholesterol, but too much cholesterol can be detrimental, even lethal. And so biology's elegant solution to this conundrum is the intricate, multilayered homeostatic mechanisms that mammals have evolved. Furthermore, the absolute insolubility of cholesterol in water presents special technical challenges to the study of cholesterol homeostasis. This volume of Methods in Molecular Biology brings together a compendium of "How-to" guides for many key techniques in tackling the investigation of cholesterol homeostasis.

Sydney, NSW, Australia

Ingrid C. Gelissen
Andrew J. Brown

Contents

Contributors

Andrew J. Brown • *School of Biotechnology and Biomolecular Sciences, The University of New South Wales, Sydney, NSW, Australia*

Simon H.J. Brown • *School of Biology and Illawarra Health and Medical Research Institute, University of Wollongong, Wollongong, NSW, Australia*

Anna C. Calkin • *Lipid Metabolism and Cardiometabolic Disease Laboratory, Baker IDI Heart and Diabetes Institute, Melbourne, VIC, Australia; Central Clinical School, Monash University, Clayton, VIC, Australia*

Ta-Yuan Chang • *Department of Biochemistry, Geisel School of Medicine at Dartmouth, Hanover, NH, USA*

Mark Charman • *Department of Biochemistry and Molecular Biology, Dalhousie University, Halifax, NS, Canada*

Amitabha Chattopadhyay • *CSIR-Centre for Cellular and Molecular Biology, Hyderabad, India*

Jen-Chieh Chuang • *Division of Digestive and Liver Diseases, Department of Internal Medicine, University of Texas Southwestern Medical Center, Dallas, TX, USA*

Russell A. DeBose-Boyd • *Department of Molecular Genetics, University of Texas Southwestern Medical Center, Dallas, TX, USA*

Ximing Du • *School of Biotechnology and Biomolecular Sciences, The University of New South Wales, Sydney, NSW, Australia*

Jacques Fantini • *EA-4674, Interactions Moléculaires et Systèmes Membranaires, Aix-Marseille Université, Marseille, France*

Ingrid C. Gelissen • *Faculty of Pharmacy, The University of Sydney, Sydney, NSW, Australia*

Vicky Howe • *BABS, School of Biotechnology and Biomolecular Sciences, The University of New South Wales, Sydney, NSW, Australia*

Md. Jafurulla • *CSIR-Centre for Cellular and Molecular Biology, Hyderabad, India*

Andrew M. Jenner • *Bioanalytical Mass Spectrometry Facility, Mark Wainwright Analytical Centre, University of New South Wales, Sydney, NSW, Australia; School of Biology and Illawarra Health and Medical Research Institute, University of Wollongong, Wollongong, NSW, Australia*

Wendy Jessup • *ANZAC Research Institute, Concord Repatriation General Hospital, Concord, NSW, Australia*

Barbara Karten • *Department of Biochemistry and Molecular Biology, Dalhousie University, Halifax, NS, Canada*

Barry E. Kennedy • *Department of Biochemistry and Molecular Biology, Dalhousie University, Halifax, NS, Canada*

Maaike Kockx • *ANZAC Research Institute, Concord Repatriation General Hospital, Concord, NSW, Australia*

Leonard Kritharides • *ANZAC Research Institute, Concord Repatriation General Hospital, Concord, NSW, Australia*
Peter L. Lee • *Department of Biochemistry, Stanford University School of Medicine, Stanford, CA, USA*
Jian Li • *Department of Biochemistry, Stanford University School of Medicine, Stanford, CA, USA*
Ya-Cheng Liao • *State Key Laboratory of Molecular Biology, Institute of Biochemistry and Cell Biology, Shanghai Institutes for Biological Sciences, Chinese Academy of Sciences, Shanghai, China*
Adam M. Lopez • *Division of Digestive and Liver Diseases, Department of Internal Medicine, University of Texas Southwestern Medical Center, Dallas, TX, USA*
Anke Loregger • *Department of Medical Biochemistry, Academic Medical Center, University of Amsterdam, Amsterdam, The Netherlands*
Ivan Lukmantara • *School of Biotechnology and Biomolecular Sciences, The University of New South Wales, Sydney, NSW, Australia*
Frederik W. Lund • *Department of Biochemistry and Molecular Biology, University of Southern Denmark, Odense, Denmark; Department of Biochemistry, Weill Medical College of Cornell University, New York, NY, USA*
Jie Luo • *Hubei Key Laboratory of Cell Homeostasis, College of Life Sciences, Wuhan University, Wuhan, China*
Winnie Luu • *School of Biotechnology and Biomolecular Sciences, The University of New South Wales, Sydney, NSW, Australia*
Leslie A. McCauliff • *Department of Nutritional Sciences and Rutgers Center for Lipid Research, Rutgers University New Brunswick, New Brunswick, NJ, USA*
Maciej Modzel • *Department of Biochemistry and Molecular Biology, University of Southern Denmark, Odense, Denmark*
Lindsey L. Morris • *Department of Molecular Genetics, University of Texas Southwestern Medical Center, Dallas, TX, USA*
Jessica K. Nelson • *Department of Medical Biochemistry, Academic Medical Center, University of Amsterdam, Amsterdam, The Netherlands*
Suzanne R. Pfeffer • *Department of Biochemistry, Stanford University School of Medicine, Stanford, CA, USA*
Anika V. Prabhu • *School of Biotechnology and Biomolecular Sciences, The University of New South Wales, Sydney, NSW, Australia*
Coralie Di Scala • *EA-4674, Interactions Moléculaires et Systèmes Membranaires, Aix-Marseille Université, Marseille, France*
Laura J. Sharpe • *School of Biotechnology and Biomolecular Sciences, The University of New South Wales, Sydney, NSW, Australia*
Bao-Liang Song • *Hubei Key Laboratory of Cell Homeostasis, College of Life Sciences, Wuhan University, Wuhan, China*
Judith Storch • *Department of Nutritional Sciences and Rutgers Center for Lipid Research, Rutgers University New Brunswick, New Brunswick, NJ, USA*
Stephen D. Turley • *Division of Digestive and Liver Diseases, Department of Internal Medicine, University of Texas Southwestern Medical Center, Dallas, TX, USA*
Daniel Wüstner • *Department of Biochemistry and Molecular Biology, University of Southern Denmark, Odense, Denmark*

Jian Xiao • *Hubei Key Laboratory of Cell Homeostasis, College of Life Sciences, Wuhan University, Wuhan, China*
Yoshio Yamauchi • *Department of Biochemistry II, Nagoya University Graduate School of Medicine, Nagoya, Japan; ; Department of Applied Biological Chemistry, Graduate School of Agricultural and Life Sciences, The University of Tokyo, Tokyo, Japan*
Alryel Yang • *Faculty of Pharmacy, The University of Sydney, Sydney, NSW, Australia*
Hongyuan Yang • *School of Biotechnology and Biomolecular Sciences, The University of New South Wales, Sydney, NSW, Australia*
Shinji Yokoyama • *Nutritional Health Science Research Center, and Department of Food and Nutritional Sciences, Chubu University, Kasugai, Japan*
Noam Zelcer • *Department of Medical Biochemistry, Academic Medical Center, University of Amsterdam, Amsterdam, The Netherlands*
Eser J. Zerenturk • *Lipid Metabolism and Cardiometabolic Disease Laboratory, Baker IDI Heart and Diabetes Institute, Melbourne, VIC, Australia*

Chapter 1

An Overview of Cholesterol Homeostasis

Ingrid C. Gelissen and Andrew J. Brown

Abstract

Cholesterol has long been implicated in diverse aspects of human health and disease. As this lipid is both vital and lethal, ensuring that its levels are kept in check is important for maintaining health. However, studying cholesterol homeostasis can be challenging due to the extreme hydrophobic nature of cholesterol and the membranous world it inhabits. This volume of Methods in Molecular Biology brings together 21 techniques covering the gamut of cholesterol homeostasis.

Key words Cholesterol sensing, Cholesterol uptake, Cholesterol transport, Cholesterol synthesis, Cholesterol efflux

1 Introduction

At its simplest, cholesterol homeostasis in the cell involves sensing sterol levels and appropriately responding by altering the balance between cholesterol uptake and synthesis on the one hand, with cholesterol export or efflux on the other. Regulated transport of cholesterol is also needed; from where it enters the cell (plasma membrane) or is made (endoplasmic reticulum) to other organelles and extracellular locations. Here, we briefly review each of these major aspects of cholesterol homeostasis (*see* Fig. 1), introducing the chapters that relate to each.

2 Cholesterol Sensing

Michael Brown and Joseph Goldstein labeled cholesterol "a Janus-faced molecule" during their Nobel Prize acceptance speech in 1985 [1]. Figuratively, cholesterol may be Janus-faced, but physically this planar molecule does in fact have two faces, one rough and one smooth. These features help cholesterol interact with specific lipids and proteins in the membrane, underpinning its functions as well as its homeostasis.

Ingrid C. Gelissen and Andrew J. Brown (eds.), *Cholesterol Homeostasis: Methods and Protocols*, Methods in Molecular Biology, vol. 1583, DOI 10.1007/978-1-4939-6875-6_1,

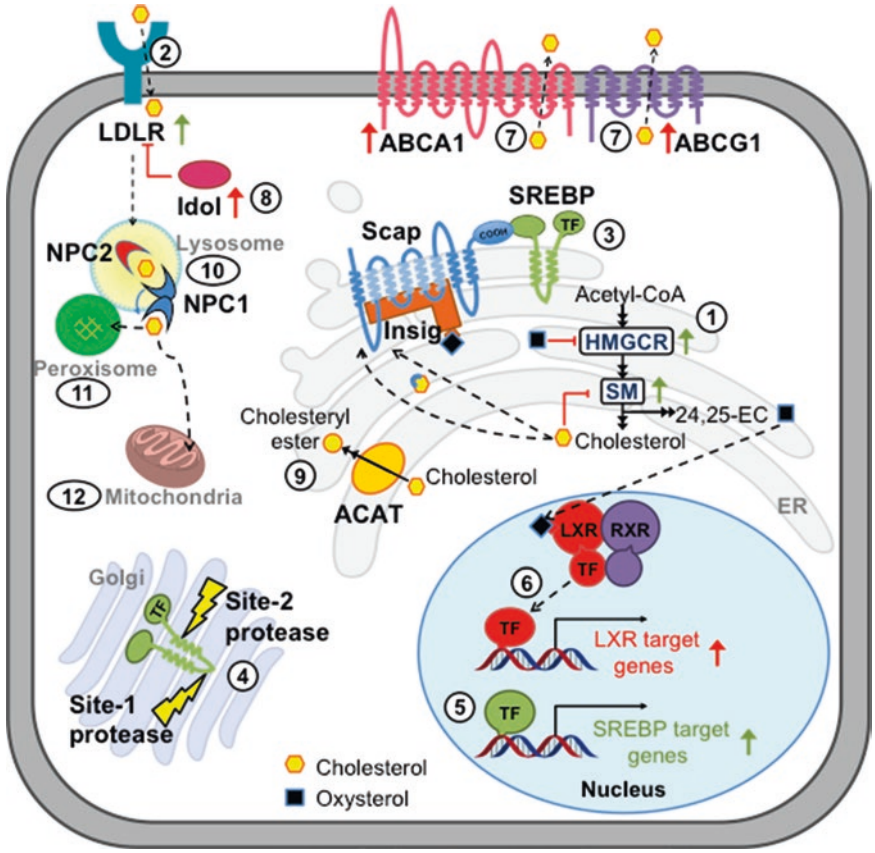

Fig. 1 Overview of the cholesterol homeostatic machinery. Cholesterol (*yellow* hexagon) is synthesized from acetyl-CoA in the endoplasmic reticulum (ER) (1) or taken up through the LDLR (2). When sterol levels are low, Insig (*orange*) dissociates from Scap (*blue*), enabling Scap to escort SREBP (*green*) (3) to the Golgi for processing by Site-1 and Site-2 proteases (4). This releases an SREBP TF that translocates to the nucleus and upregulates SREBP target genes (5). These include HMGCR, SM, and LDLR (indicated by *green arrows*). When sterol levels are high, cholesterol negatively regulates SM and oxysterols (*black squares*) negatively regulate HMGCR (indicated by the *red barred lines*), causing their degradation. Cholesterol binds to Scap, and oxysterols bind to Insig, causing the retention of Scap/SREBP in the ER. Oxysterols, such as 24(*S*), 25-epoxycholesterol (denoted 24,25-EC), also act as ligands for the LXR (*bright red*)-retinoid X receptor (RXR, *purple*) heterodimer, releasing the LXR TF and upregulating transcription of LXR target genes (indicated by *red arrows*) (6). These include ABCA1 and ABCG1, which synergize to export cholesterol from the cell (7), and Idol (*pink*), which mediates degradation of LDLR (indicated by the *red barred line*) (8). Excess cholesterol can also be esterified by ACAT (*light orange*) for storage in an inactive form (9). LDL-derived cholesterol entering the cell via the LDLR is transported via the endosomes to fuse with lysosomes where cholesteryl esters are hydrolyzed. Free cholesterol is released from lysosomes in a process involving handoff between soluble NPC2 and membrane-bound NPC1 (10). Cholesterol can be transported to other organelles including peroxisomes (11) and mitochondria (12). Adapted from [2]

Cholesterol homeostasis begins with sterol sensing in the membranes of the cell, which then governs homeostasis at the level of the whole organism. Cholesterol sensing occurs either directly by binding to specific proteins, and/or by altering the properties

of the membrane in which the cholesterol and sensing proteins reside (reviewed in ref. [2]).

In Chapter 2, Di Scala and Fantini provide a computational approach to model cholesterol–protein interactions, before presenting an in vitro experimental approach for their validation. In Chapter 3, Jafurulla and Chattopadhyay review the many approaches to manipulating cell cholesterol levels in culture, including cyclodextrins to deliver or deplete cholesterol, agents to complex cholesterol in the plasma membrane, and inhibitors that block cholesterol synthesis at different points in the pathway. Moreover, they focus on stereoisomers of cholesterol, which have particular utility in interrogating the structural stringency of cholesterol-membrane protein interactions. We then follow with step-by-step guides for some of the key approaches to manipulating cell cholesterol levels in Chapter 4.

3 Cholesterol Uptake

The discovery of the low-density lipoprotein (LDL) receptor was central to the work Michael Brown and Joseph Goldstein won their Nobel prize for in 1985. Typically, cholesterol packaged in lipoproteins like LDL enters the cell via receptor-mediated endocytosis. Levels of the LDL receptor are thus a key determinant of LDL levels, which as the major cholesterol-carrying lipoprotein in the circulation contributes to the cholesterol deposits seen in atherosclerosis. In Chapter 5, Loregger, Nelson, and Zelcer describe a fluorescent assay for measuring LDL uptake in cells. Zerenturk and Calkin follow (Chapter 6) with a new model of atherosclerosis which overexpresses Idol. This inducible E3 ubiquitin ligase targets LDL receptors for proteasomal degradation. The resulting reduced levels of LDL receptors in the livers of the mice give rise to a more human-like lipoprotein profile and increased atherosclerosis, especially on a Western diet.

4 Intracellular Cholesterol Transport

After receptor-mediated endocytosis of LDL, the endosomes fuse with lysosomes that hydrolyze the cholesteryl esters in the core of the lipoprotein particles to free cholesterol. From there, the itinerary of cholesterol remains rather sketchy. But recent insights have been gleaned from the study of a rare lysosomal storage disease, Niemann-Pick Type C (NPC), sometimes called Childhood Alzheimer's Disease. The molecular defects are in either of two proteins, NPC1 or NPC2, and at the cellular level this disease is characterized by striking cholesterol accumulation. In Chapter 7, Du, Lukmantara, and Yang generate a cell model for this disease by

deleting NPC1 using CRISPR/Cas9 technology. The ability to detect cholesterol accumulation is not only important for the diagnosis of cholesterol defects like NPC, but also in depth characterization of transport pathways. In Chapter 8, Li, Lee, and Pfeffer utilize a bacterial toxin that binds to cholesterol, Perfringolysin O (engineered so that it is nontoxic), as a tool to measure intracellular cholesterol accumulation using flow cytometry. McCauliff and Storch (Chapter 9) describe assays of cholesterol transfer between model membranes and purified NPC2. Modzel, Lund, and Wustner (Chapter 10) use sophisticated imaging and computational approaches to track fluorescent analogs of cholesterol.

Membrane contacts exist between many organelles, including between peroxisomes and lysosomes [3]. These contacts are enhanced by LDL, and indeed cholesterol is transported from lysosomes to peroxisomes [4]. In Chapter 11, Luo, Liao, Xiao, and Song present a biochemical method for monitoring cholesterol transfer from lysosomes to peroxisomes.

Membrane cholesterol content increases dramatically from the endoplasmic reticulum to the plasma membrane. The mitochondrion, echoing its prokaryotic origin, is a particularly cholesterol-poor organelle, but still needs cholesterol for membrane maintenance and for the synthesis of steroids, oxysterols, and bile acids. Kennedy, Charman, and Karten (Chapter 12) trace cholesterol trafficking to mitochondria by taking advantage of a mitochondrial-specific enzyme approach.

5 Cholesterol Synthesis

Cholesterol is not a simple molecule. At 27-carbons, it comprises four fused rings, an aliphatic side-chain, and a hydroxyl group. Constructing this complicated molecule from the two-carbon building blocks of acetyl-CoA clearly requires a lengthy biosynthetic pathway that comprises more than 20 steps [5]. Like other processes in cholesterol homeostasis, there are multiple levels of regulation, including transcriptionally and posttranslationally. Nearly all of the cholesterol synthetic enzymes are under the control of the chief transcriptional conductor of lipid metabolism, sterol-regulatory element binding protein (SREBP), which as the name suggests binds to sterol responsive elements (SREs) in the promoters for many of the genes involved in cholesterol homeostasis. In Chapter 13, we describe in silico and luciferase-based experimental approaches for mapping SREs in gene promoters that we have used successfully to pinpoint dual SREs in the promoters of two cholesterol synthesis genes, DHCR7 and DHCR24.

The best known example of posttranslational regulation in cholesterol synthesis is the proteasomal degradation of the key

rate-limiting step, 3-hydroxy-3-methylglutaryl-coenzyme A reductase (HMGCR). In response to increased sterol status, HMGCR becomes ubiquitinated and then extracted from the membranes of the endoplasmic reticulum into the cytosol for degradation by 26S proteasomes. In Chapter 14, Morris and Debose-Boyd detail an assay to monitor this extraction using an in vitro protease digestion method of an epitope engineered into a luminal loop of HMGCR.

A key rate-limiting step beyond HMGCR is squalene monooxygenase (SM). We provide an approach to probe the membrane topology of cholesterol-related proteins, using SM as an example (Chapter 15).

The activity of individual enzymes in cholesterol synthesis can be assayed by determining the conversion of a stably labeled sterol substrate into a deuterated product by gas chromatography linked to mass spectrometry (GC-MS), as we describe in Chapter 16. Jenner and Brown (Chapter 17) present a GC-MS method for an array of sterols, including cholesterol synthetic precursors, phytosterols, and oxysterols. They also utilize direct infusion of tissue extracts onto tandem MS for analyzing cholesteryl esters.

Rates of cholesterol synthesis can be measured in tissue slices or whole animal models using tritiated water, as detailed by Lopez, Chuang, and Turley in Chapter 18. This landmark method has been applied over many decades and been instrumental in developing our current understanding of cholesterol synthesis in the whole animal as well as contributions from individual organs.

6 Cholesterol Efflux

Apart from SREBP, cholesterol excess is sensed by another transcription factor, the nuclear Liver X Receptor (LXR), which is activated by sterol ligands (oxysterols and certain intermediates in cholesterol synthesis). LXR upregulates a suite of genes, including those encoding two proteins that export cholesterol from the cell. The ATP-binding cassette proteins, ABCA1 and ABCG1, facilitate cell cholesterol export to nascent and mature high-density lipoproteins (HDL), respectively. Yamauchi, Yokoyama, and Chang (Chapter 19) describe methods for monitoring ABCA1-dependent sterol efflux. Importantly, they note that newly synthesized cholesterol is preferentially effluxed over premade cholesterol, say from LDL. Yang and Gelissen (Chapter 20) focus on a tritiated cholesterol assay in cultured cells for assessing ABC-transporter mediated cholesterol export, using various cell systems. And finally turning to another in vivo model, Kockx, Jessup, and Kritharides (Chapter 21) present a macrophage-specific reverse cholesterol transport assay in mice.

7 Beginnings and Endings

And thus ends the first chapter of this book. It is appropriate that we began the chapter with Janus, the Roman god of beginnings and endings. With his two faces, he looks to the past and to the future. The past of cholesterol research is long and distinguished, and considering the wealth of talented researchers active in this field (just some of whom have contributed to this volume), the future looks very bright indeed.

References

1. Brown MS, Goldstein JL (1985) A receptor-mediated pathway for cholesterol homeostasis. Nobel Lectures:284–324
2. Howe V, Sharpe LJ, Alexopoulos SJ, Kunze SV, Chua NK, Li D, Brown AJ (2016) Cholesterol homeostasis: how do cells sense sterol excess? Chem Phys Lipids 199:170–178
3. Du X, Brown AJ, Yang H (2015) Novel mechanisms of intracellular cholesterol transport: oxysterol-binding proteins and membrane contact sites. Curr Opin Lipidol 35:37–42
4. Chu BB, Liao YC, Qi W, Xie C, Du X, Wang J, Yang H, Miao HH, Li BL, Song BL (2015) Cholesterol transport through lysosome-peroxisome membrane contacts. Cell 161(2): 291–306
5. Brown AJ, Sharpe LJ (2015) Cholesterol synthesis. In: Biochemistry of lipids, lipoproteins, and membranes, 6th edn. Elsevier, The Netherlands.

Chapter 2

Hybrid In Silico/In Vitro Approaches for the Identification of Functional Cholesterol-Binding Domains in Membrane Proteins

Coralie Di Scala and Jacques Fantini

Abstract

In eukaryotic cells, cholesterol is an important regulator of a broad range of membrane proteins, including receptors, transporters, and ion channels. Understanding how cholesterol interacts with membrane proteins is a difficult task because structural data of these proteins complexed with cholesterol are scarce. Here, we describe a dual approach based on in silico studies of protein–cholesterol interactions, combined with physico-chemical measurements of protein insertion into cholesterol-containing monolayers. Our algorithm is validated through careful analysis of the effect of key mutations within and outside the predicted cholesterol-binding site. Our method is illustrated by a complete analysis of cholesterol-binding to Alzheimer's β-amyloid peptide, a protein that penetrates the plasma membrane of brain cells through a cholesterol-dependent process.

Key words Alzheimer's β-amyloid peptide, Cholesterol-binding motif, Langmuir monolayer, Molecular docking, Molecular dynamics simulations, Transmembrane domain

1 Introduction

Among eukaryotic membrane lipids, cholesterol (Fig. 1) is unique for several reasons. In contrast with other membrane lipids, which contain one (sphingolipids) or two (glycerophospholipids) acyl chains, whose variability may generate a high degree of biochemical diversity, cholesterol has only one molecular structure [1]. It contains two structural elements that are not found in other membrane lipids, i.e., carbon rings (the sterane backbone) and branched aliphatic groups (methyl and iso-octyl). The asymmetric distribution of these chemical groups defines two topologically distinct surfaces of the cholesterol molecule: one with reliefs, referred to as the "rough" face, and the other one devoid of this roughness, referred to as the "smooth" face (Fig. 1). According to the nomenclature of cyclic compounds proposed by Rose et al. [2], the smooth and rough faces are respectively identified as the α and β faces [1, 3].

Ingrid C. Gelissen and Andrew J. Brown (eds.), *Cholesterol Homeostasis: Methods and Protocols*, Methods in Molecular Biology, vol. 1583, DOI 10.1007/978-1-4939-6875-6_2,

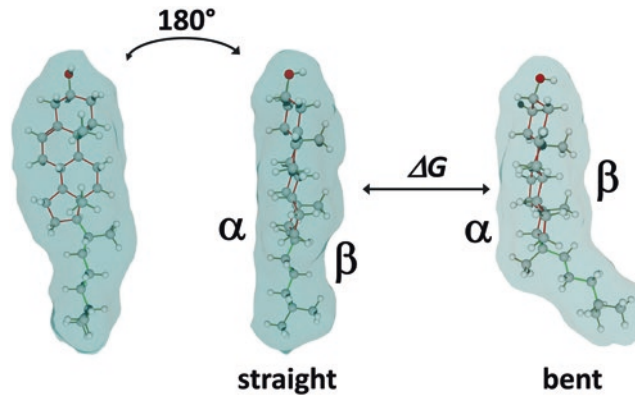

Fig. 1 Structure and conformational flexibility of cholesterol. In textbooks, cholesterol is often represented in such a way that the four rings of the sterane backbone are clearly visible (left panel). In this case, it is not possible to assess the distinct topologies of the α (smooth) and β (rough) faces. A 180 ° rotation of the molecule (middle panel) unmasks the two faces of cholesterol. Note that the iso-octyl chain of this particular conformer is not tilted with respect to the main axis of cholesterol, giving the molecule a "straight" structure that is compatible with an interaction with membrane lipids. Upon protein binding (a process that can be quantified by a variation in free energy, ΔG), cholesterol may adopt a "bent" shape due to the rotational flexibility of the iso-octyl chain (right panel)

Apart from its bifacial geometry, cholesterol has unexpected conformational flexibility properties that are conferred by the rotational movements of the carbon–carbon bonds at the level of the iso-octyl chain. Schematically, two types of cholesterol conformers have to be considered for studying protein–cholesterol interactions at the molecular level [4]. As shown in Fig. 1, these conformers differ by the angle between the sterane unit and the iso-octyl chain, which defines either "straight" or "bent" structures. Straight conformers are particularly adapted for interacting with the apolar part of sphingolipids, whereas bent conformers are generally bound to a membrane-spanning protein [5].

Finally, the amphipathic nature of cholesterol, with its polar OH group at one end and the iso-octyl group at the opposite, suggests a preferential orientation of the cholesterol molecule within a lipid bilayer, i.e., parallel to bulk membrane lipids with the OH group facing the polar-apolar interface. This thermodynamic constraint facilitates the search for a fit between cholesterol and a membrane-embedded domain of the studied protein because it significantly restricts the possibilities of forming a biologically relevant complex.

In this chapter, we describe a procedure for the prediction of a cholesterol-binding site on Alzheimer's β-amyloid peptide (Aβ). The choice of this particular protein is motivated by the fact that it lacks any predictable cholesterol-binding motif based on amino

acid sequences such as CARC or CRAC motifs [3]. Therefore, the molecular modeling study in this case has to start from zero ("ab initio" modeling). Nevertheless, we will also give some clues for generating a cholesterol-protein complex based on the detection of a consensus cholesterol-binding motif. Finally, we will describe the experimental procedure used in our laboratory for checking the validity of the models obtained in silico.

2 Materials

2.1 Computers, Websites, and Softwares

For modeling studies, we suggest using a high performance gaming computer (either Mac or PC) with a large HD monitor, a good video card, and at least 8 GB RAM. The websites that we regularly use are UniProt (http://www.uniprot.org) for protein sequence data and the Protein Databank (http://www.rcsb.org) for 3D structures. The software packages used for molecular modeling, structure analysis, and visualization are Hyperchem Professional (Hypercube, Inc., Gainesville, FL), DeepView - Swiss-PdbViewer (http://spdbv.vital-it.ch), and Molegro Molecular Viewer (CLC bio, Waltham, MA, http://www.clcbio.com). The surface pressure data were analyzed with the FilmWare X program (Kibron Inc., Helsinki, Finland). We developed our own software (NTB extractor) for transferring the FilmWare data (.ntb) to Microsoft Exel (.xls). The graphs are generated using Origin (OriginLab Corp., Northampton, MA).

2.2 Langmuir Trough

Surface pressure measurements are performed with a microtensiometer specifically designed for small working volumes (800 μL of the aqueous phase in which the protein or peptide is diluted), the MicroTroughX (Kibron Inc., Helsinki, Finland). A simple but reliable homemade setup for measuring surface tension has also been described by Fantini and coworkers [6].

3 Methods

3.1 Cholesterol Modeling

1. The first step is to obtain a workable file for the cholesterol molecule. Whatever the modeling program used, it should accept **.pdb** files, so that you can download the cholesterol molecule from the Protein Data Bank (cholesterol as ligand of cholesterol-binding protein) or by searching "cholesterol molecule pdb" in Google. The other solution is to generate cholesterol ab initio with your modeling software, but this may be painful because there are several asymmetric carbons that require special attention. As an example we have used the Swiss-PDB viewer program to extract a cholesterol molecule

from the PDB file 3D4S (cholesterol bound to the human β2-adrenergic receptor) [7].

2. Go to the 3D4S entry of the ProteinDatabank. Download the file in pdb format and save it on your computer desktop.
3. Open Swiss-PDB viewer, then open the 3D4S file. In the control panel window, you have the list of all amino acid residues and ligands. At the end of the list, there are two cholesterol molecules noted CLR402 and CLR403. You can create a .pdb file with one of these cholesterol molecules, e.g., CLR403. To do so, you can select all listed items other than CLR403 and delete these items with the "Remove selected residue" command of the "Build" menu. Then you just have to save the file now containing only CLR403 ("File" menu, "Save," "Current layer"). At this point, you have a cholesterol.pdb file.
4. Open this file with Hyperchem. Check the cholesterol molecule for atom valence, double bond (ring B of sterane), and hydrogen atoms (Fig. 2). Correct the structure if necessary.
5. Start an energy minimization process. In the Hyperchem program, geometry optimization is achieved using the unconstrained optimization rendered by the Polak–Ribière conjugate gradient algorithm. A typical process is shown in Fig. 2. In starting conditions, the value of the gradient is 2.3 kcal/(Å mol). At the end of the process (termination condition), the gradient is <0.01. These conditions can be changed

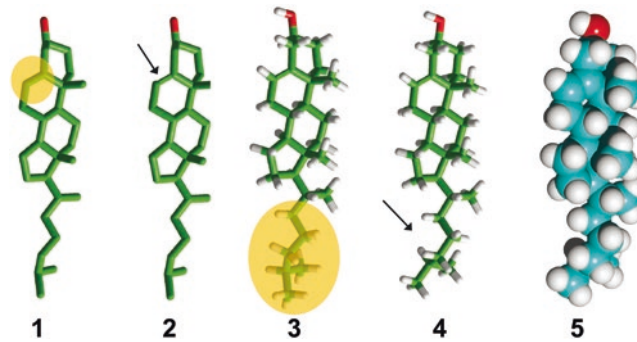

Fig. 2 Generating a workable cholesterol file. (1) Cholesterol downloaded from a PDB file (e.g., 3D4S). Note that it lacks the double bond (*orange disk*). (2) Cholesterol with the double bond (*arrow*). (3) Cholesterol with hydrogen, yet displaying a specific orientation of the iso-octyl chain (*orange disk*). (4) Cholesterol after geometry optimization with the Polak–Ribière algorithm (the change in the orientation of the iso-octyl chain is indicated by an *arrow*). (5) A sphere model of the cholesterol molecule shown in panel 4 (carbon in *blue*, oxygen in *red*, hydrogen in *white*). The molecule is viewed from the β face, in a typical "textbook" representation

in the software but are usually fine for small biomolecules such as cholesterol and peptides.

6. Save the file as a new file, e.g., "chol PR" (for cholesterol Polak–Ribière), not to be confused with the initial file you have downloaded from PDB or generated ab initio with Hyperchem. You can save this file with various extensions, but here we will use the pdb compatible **.ent** format. In this case, your file is named "**chol PR.ent.**"

3.2 Docking a Phenylalanine Tetrapeptide (Phe_4) onto Cholesterol: Looking for CH-π Stacking

1. As a first example of protein docking onto a simple protein motif, we will study the interaction of cholesterol with a minimal cholesterol-binding motif, e.g., a phenylalanine tetrapeptide (Phe_4). This modeling exercise will illustrate the process of formation of coordinated CH-π stacking interaction, a hallmark of protein–cholesterol interaction [8]. A workable structure of the Phe_4 tetrapeptide can be generated ab initio with Hyperchem by using the "Databases menu" and select four times the amino acid Phe. Apply the Polak–Ribière algorithm and save the file in the **.pdb** format.
2. Keep the Phe_4 file open and use the "Merge" function of the "File" menu of Hyperchem to insert cholesterol (**chol PR.ent**) in the same window. Now you can select cholesterol and Phe_4 independently.
3. Select the rendering method. For modeling purposes, "sticks" or "tubes" are suitable, but you may use the "sphere" rendition as well if you prefer. At this stage, you may also adjust the background (black or white) and the atom colors (carbon in green, oxygen in red, hydrogen in white).
4. Search for a potential geometric fit between Phe_4 and cholesterol. There are many possibilities for starting conditions, including totally random orientations. For instance, you can put two phenyl rings (Phe-2 and Phe-3) of the Phe_4 tetrapeptide onto the α face of cholesterol (Fig. 3a).
5. Apply the Polak–Ribière algorithm. The result is shown in Fig. 3b. Note that Phe-1 and Phe-4 are still in the same conformation, whereas the orientations of the phenyl rings of Phe-2 and Phe-3 have changed. In fact, both rings now form a flat structure that lies on the α face of cholesterol (Fig. 3c). The driving force of this process is the formation of CH-π stacking interaction between the first ring of sterane and the phenyl ring of Phe-3 (Fig. 3d). From this point, you can proceed for several rounds of molecular dynamics simulations to evaluate the robustness of this docking exercise. A typical example of molecular dynamics (MD) simulations of a protein–cholesterol complex with iterative snapshot and energy measurements has been published by Fantini et al. [9]. MD simulations

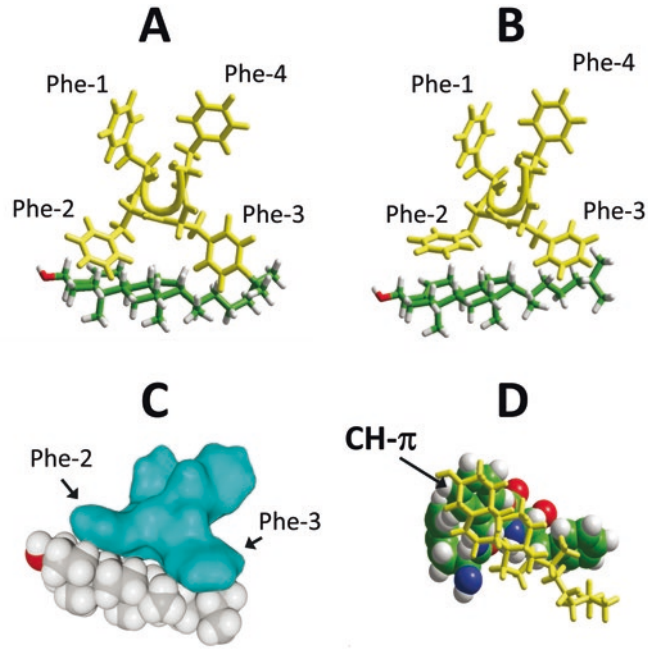

Fig. 3 Docking a phenylalanine tetrapeptide (Phe_4) onto cholesterol. (**a**) Starting conditions: the Phe_4 tetrapeptide is in *yellow* and cholesterol in atoms colors (carbon *green*, oxygen *red*, hydrogen *white*). (**b**) Obtaining a complex after applying the Polak–Ribière algorithm. (**c**) Evaluation of the surface of interaction between the Phe_4 tetrapeptide (in *blue*) and cholesterol. (**d**) Visualization of the CH-π interaction between the first ring of sterane (cholesterol in *yellow*) and the phenyl ring of Phe-2

are mandatory to check the robustness of the docking process before any experimental validation. Indeed, there are many examples of protein-ligand complexes obtained with docking programs that reached a high dock score but failed in MD simulations [10]. Such cases are particularly frustrating since the ligand literally "flies away" from its initial binding site as MD simulations are running. As emphasized by Chen in a recent review on potential docking caveats [10], the key "*difference between docking and MD is the variable, time.*" In essence, docking considers chiefly the binding affinity. In contrast, MD simulations calculate the movement of the complex and predict its evolution over the time. Unfortunately, due to hardware limitations, the simulation time of MD is usually less than 1 ms (and most often in the sub-ms range). Under these circumstances, further validation of docking results with appropriate bioassays is strongly recommended [10]. In the last part of this chapter, we will discuss how to assess the validity of in silico predicted protein–cholesterol interactions by experimental approaches.

3.3 Protein Modeling: Generating a α-Helix Structure from an Amino Acid Sequence

1. Open a window on your computer screen with the amino acid sequence. As an example we will study the 21–38 fragment of Aβ (21-AEDVGSNKGAIIGLMVGG-38).
2. Run Hyperchem. Use the "Databases" menu and the "amino acid" command to build the peptide fragment. Since you plan to generate an α-helix structure, check that "α-helix" is selected in the "Databases" window.
3. Once the peptide is built, apply the Polak–Ribière algorithm. Save the file.

3.4 Docking of Cholesterol onto a α-Helix (Aβ21–38)

1. Open the Aβ21–38 file with Hyperchem.
2. Merge with the cholesterol file (**chol PR.ent**).
3. Bring Aβ21–38 and cholesterol together in random or user-defined orientations and run the Polak–Ribière algorithm. You may try several possible starting conditions before you reach a good geometric fit. An example of a possible fit is illustrated in Fig. 4. In this case, the β face of cholesterol interacts tightly with the Aβ peptide. The binding process has significantly tilted the iso-octyl chain in a perfect example of a protein-bound cholesterol conformer. The amino acid residues that interact with cholesterol are chiefly Gly-25, Lys-28, and Ile-32 (Fig. 4). The identification of these residues is important for validating the model by physico-chemical approaches (i.e., test of mutant vs. wild-type peptides).

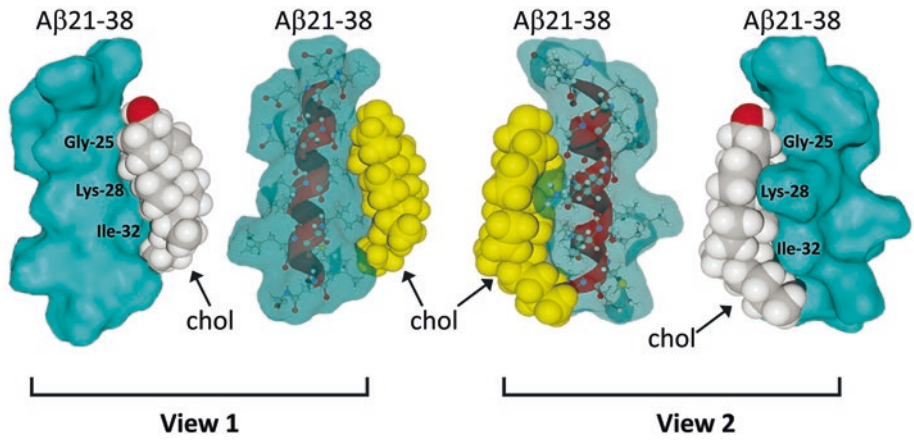

Fig. 4 Interaction of cholesterol with Aβ21–38. This model illustrates two major concepts of molecular interactions: geometry complementarity and chemical compatibility. Note that the β face of cholesterol interacts with the α-helical peptide. The complex is reinforced by the bending of the iso-octyl chain of the sterol which optimally spouses the peptide shape. Two distinct views of the complex are shown. In each case, a surface view is accompanied by a transparent rendition, allowing location of the α-helix (*red*) and the atoms of amino acid residues

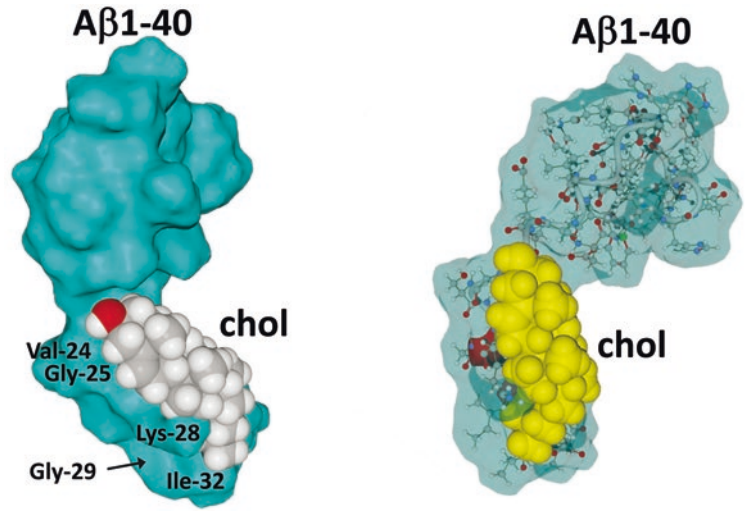

Fig. 5 Interaction of cholesterol with Aβ1–40. This model has been previously described by Di Scala et al. [4, 11, 14]. The location of Val-24, Gly-25, Lys-28, Gly-29, and Ile-32 is indicated on the model on the left. The model on the right is shown in a membrane compatible orientation with respect to cholesterol

3.5 Comparison of Data with a Published Model of the Aβ-Cholesterol Complex

The model of the Aβ21–38/cholesterol complex can be compared with published in silico studies of the Aβ/cholesterol interaction. As an example, we will analyze the data obtained with Aβ1–40 (Fig. 5). When merged with this longer peptide (compared with Aβ21–38), cholesterol spreads on a large region comprised between Phe-20 and Met-35 [11]. MD simulations of this complex allowed characterization of a very good fit, which involves a series of van der Waals interactions. Interestingly, the three amino acid residues of Aβ21–38 that were predicted to be in physical contact with cholesterol, i.e., Gly-25, Lys-28, and Ile-32, were also found to be important for cholesterol/Aβ1–40 complex [11]. In particular, in both cases the closest contact was with the methylene groups of Lys-28. Therefore, a first approach to validate both models is to assess the importance of this amino acid residue for the cholesterol/Aβ-binding reaction. For the sake of comparison, a residue that is not involved in the process (e.g., Gly-29) should be evaluated in parallel. We will now describe the way to measure the binding of cholesterol to wild-type and mutant Aβ peptides.

3.6 Langmuir Monolayer Technique

This technique is based on surface tension measurements of a simple system consisting of a lipid monolayer spread on the surface of a water phase [4, 6]. The surface tension of pure water is **72.8 mN/m**. When a surfactant (e.g., a lipid) is present at the water surface, it decreases the value of the surface tension proportionally to its amount. The surface pressure π is defined as the difference between γ_0, the surface tension of pure water, and γ, the surface tension measured in the presence of the surfactant:

$\pi = \gamma 0 - \gamma$. For instance, if a lipid monolayer decreases the initial surface tension to **56.3 mN/m**, the surface pressure for this monolayer is $\pi = 72.8 - 56.3 = 16.5$ **mN/m**. Increasing the amount of lipid molecules in the monolayer will further decrease surface tension, resulting in an increased surface pressure [12]. This rule applies as long as the monolayer is intact. If the area is maintained constant, the monolayer eventually collapses when the number of lipid molecules exceeds the available surface on water, resulting in a precipitous drop of surface pressure. For this reason, protein-lipid interactions measured this way are usually performed within the range of 10–30 mN/m. The injection of a protein (or a peptide) underneath a lipid monolayer induces an increase of the surface pressure when the protein (or the peptide) penetrates the monolayer. This process can be followed in real-time (kinetics studies) by dipping a platinum probe in the water bathing the monolayer [4].

1. Clean the platinum probe in the flame of a Bunsen burner (1 s) and hang it on its support.
2. Add 800 μL of ultrapure water into the tank, dip the microtensiometer probe at the air-water interface (about 1–2 mm is enough), and calibrate the apparatus to adjust the surface tension to 72.8 mN/m. Accordingly, the surface pressure π is 0 mN/m.
3. The purity of the aqueous subphase (pure water or buffer) can be assessed by following the surface pressure value over the time which should remain perfectly stable at the basal value of $\pi = 0$ mN/m.
4. Start again steps 1 and 2 and then inject 8 μL of peptide in the subphase to check its surfactancy. This control ensures that you are working with the appropriate concentration of peptide, and confirms that under these conditions, the molecule of interest does not modify the surface pressure by itself.
5. Start again steps 1 and 2 and spread a few drops (ideally less than 1 μL with a 10 μL Hamilton microsyringe) of lipid solution at the air-water interface. Wait 5 min for evaporation of the solvent. Check that the monolayer remains stable and note the initial surface pressure value (π_0).
6. Inject the protein or peptide (8 μL) in the subphase at the appropriate concentration. Do not worry that the needle of the microsyringe goes through the monolayer: once the needle is removed, the monolayer reseals instantaneously. Record surface pressure variations and note the final surface pressure value (π_{max}). The difference between the final and the initial surface pressure ($\Delta\pi_{max} = \pi_{max} - \pi_0$) is characteristic of the type of interaction. The kinetics of interaction of wild-type and mutant Aβ22–35 peptides with cholesterol monolayers are shown in Fig. 6.

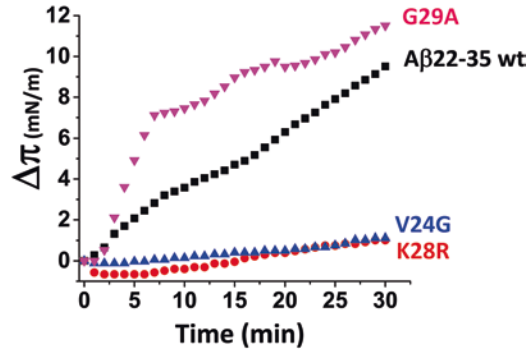

Fig. 6 Kinetics of interaction of Aβ22–35 wild-type (wt) and mutant peptides with cholesterol monolayers. Cholesterol monolayers were prepared at an initial surface pressure of 20 mN/m. After equilibration (5 min to allow solvent evaporation), the indicated peptide was injected underneath the monolayer at a concentration of 10 μM. The data show the evolution of the surface pressure as a function of time

In agreement with in silico studies, the K28R mutant did not interact with cholesterol. In contrast, a mutation at position 29 (G29A), which is not involved in cholesterol binding, had no inhibitory effect on Aβ–cholesterol interactions.

7. It is important to perform the experiments at various values of the initial surface pressure. In fact, the insertion of the protein into the lipid monolayer is expected to become more and more difficult as the initial pressure surface increases, i.e., with condensed monolayers containing a high number of lipid molecules. Indeed, the strength of lipid–lipid interactions is higher in a densely packed monolayer than in a loose monolayer. Thus, when the lipid-protein interaction is specific, the value of $\Delta\pi_{max}$ gradually decreases as π_0 increases. The extrapolated value of π_0 at $\Delta\pi_{max} = 0$ is referred to as the critical pressure of insertion π_c (Fig. 7). When the value of critical pressure of insertion is ≥30 mN/m (i.e., the mean surface pressure of the plasma membrane) the interaction is considered biologically relevant [12].

4 Notes

4.1 Docking Algorithms

Docking is becoming more and more popular, especially for drug screening and design. In a recent overview, Chen listed no less than 50 docking programs [10]. The strategy described in the present article does not use any of these programs. Instead, we propose an alternative process that combines both the search for an optimal protein-cholesterol fit and the possibility to run MD simulations with the same software. Our method takes into account the

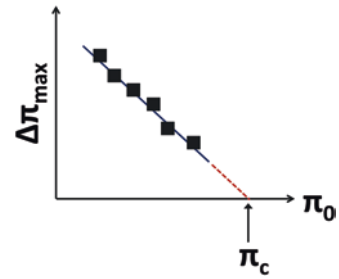

Fig. 7 Graphical determination of the critical pressure of insertion. Cholesterol monolayers are prepared at several distinct surface pressures (usually 10–30 mN/m). For each monolayer, the maximal surface pressure increase $\Delta\pi_{max}$ induced by the peptide (or the protein) is plotted against the initial surface pressure π_0. The critical pressure of insertion π_c is extrapolated as the theoretical value of π_0 at $\Delta\pi_{max} = 0$

mutual induced-fit mode of interaction, i.e., the conformational flexibility of both partners (protein and ligand). In our experience, the binding of cholesterol to a membrane protein generally proceeds through such mechanisms [3]. Since our method may lead to the characterization of several distinct cholesterol–protein complexes resulting from distinct starting conditions, it is of high interest to evaluate the affinity of each complex. The "ligand energy inspector" (Tools menu) of the Molegro Molecular Viewer software is a simple way to assess and compare the predicted energy of interaction of a series of molecular complexes. For each complex, the data are presented as a list of amino acid residues that physically interact with each atom of cholesterol [13, 14]. Finally, an important issue to consider is the environment of the ligand and the protein. The docking may be performed in vacuum to speed up the process, yet the introduction of water and lipid molecules is of course preferred, even if it will considerably increase the time of simulation, even at the docking step.

4.2 Consensus Cholesterol-Binding Motifs

In some cases, the membrane-spanning domain displays a consensus cholesterol-binding motif such as the CARC motif defined by the linear array (K,R)–X_{1-5}–(Y,F)–X_{1-5}–(L,V) according to Baier et al. [13]. The CARC motif is oriented in such a way that the OH group of cholesterol faces the cationic group of the basic residue (either Lys or Arg) of CARC, consistent with the establishment of a hydrogen bond [3, 12]. The aromatic residue may interact with one of the sterane rings of cholesterol through a CH-π bond (Fig. 3). Finally, the branched aliphatic residue of CARC (Leu or Val) may contact the iso-octyl chain of cholesterol, which could further stabilize the complex by a series of van der Waals interactions [3]. Overall, the basic principles that govern cholesterol binding to transmembrane domains fully apply to

CARC–cholesterol interactions. The search for a fit between cholesterol and a CARC motif is thus a good approach for testing in silico the biochemical logic of protein–cholesterol interactions, especially for membrane proteins.

4.3 Lipid Monolayer Assay

The Langmuir system has several advantages over other methods for studying lipid–protein interactions. On one hand, the actual molar ratio of lipids in the monolayer can be easily controlled. Accordingly, mixed monolayers containing several lipid species can be prepared. This point is important because in other reconstituted membrane lipid systems (e.g., liposomes or black lipid membranes), the lipid distribution in each monolayer is generally not determined. On the other hand, Langmuir monolayers can be probed with low protein amounts (nM–μM range) that may reflect in vivo conditions. Combined with in silico approaches, the Langmuir setup provides a robust and reliable method for studying lipid–protein interactions [12].

Acknowledgments

We would like to thank Henri Chahinian, Francisco Barrantes, and Nouara Yahi for their constant support and encouragement, and for valuable discussions.

References

1. Fantini J, Barrantes FJ (2009) Sphingolipid/cholesterol regulation of neurotransmitter receptor conformation and function. Biochim Biophys Acta 1788:2345–2361
2. Rose IA, Hanson KR, Wilkinson KD, Wimmer MJ (1980) A suggestion for naming faces of ring compounds. Proc Natl Acad Sci U S A 77:2439–2441
3. Fantini J, Barrantes FJ (2013) How cholesterol interacts with membrane proteins: an exploration of cholesterol-binding sites including CRAC, CARC, and tilted domains. Front Physiol 4:31
4. Di Scala C, Chahinian H, Yahi N, Garmy N, Fantini J (2014) Interaction of Alzheimer's beta-amyloid peptides with cholesterol: mechanistic insights into amyloid poreformation. Biochemistry 53:4489–4502
5. Fantini J, Di Scala C, Evans LS, Williamson PT, Barrantes F (2016) A mirror code for protein–cholesterol interactions in the two leaflets of biological membranes. Sci Rep 6:21907
6. Hammache D, Pieroni G, Maresca M, Ivaldi S, Yahi N, Fantini J (2000) Reconstitution of sphingolipid-cholesterol plasma membrane microdomains for studies of virus-glycolipid interactions. Methods Enzymol 312:495–506
7. Hanson MA, Cherezov V, Griffith MT, Roth CB, Jaakola VP, Chien EY et al (2008) A specific cholesterol binding site is established by the 2.8 A structure of the human beta2-adrenergic receptor. Structure 16:897–905
8. Nishio M, Umezawa Y, Fantini J, Weiss MS, Chakrabarti P (2014) CH–π hydrogen bonds in biological macromolecules. Phys Chem Chem Phys 16:12648–12683
9. Fantini J, Carlus D, Yahi N (2011) The fusogenic tilted peptide (67–78) of alpha-synuclein is a cholesterol binding domain. Biochim Biophys Acta 1808:2343–2351
10. Chen YC (2015) Beware of docking! Trends Pharmacol Sci 36:78–95
11. Di Scala C, Yahi N, Lelievre C, Garmy N, Chahinian H, Fantini J (2013) Biochemical identification of a linear cholesterol-binding domain within Alzheimer's beta amyloid peptide. ACS Chem Nerosci 4:509–517
12. Fantini J, Yahi N (2015) Brain lipids in synaptic function and neurological disease: clues to

innovative therapeutic strategies for brain disorders. Elsevier Academic Press, San Francisco

13. Baier CJ, Fantini J, Barrantes FJ (2011) Disclosure of cholesterol recognition motifs in transmembrane domains of the human nicotinic acetylcholine receptor. Sci Rep 1:69
14. Di Scala C, Troadec JD, Lelievre C, Garmy N, Fantini J, Chahinian H (2014) Mechanism of cholesterol-assisted oligomeric channel formation by a short Alzheimer beta-amyloid peptide. J Neurochem 128: 186–195

Chapter 3

Structural Stringency of Cholesterol for Membrane Protein Function Utilizing Stereoisomers as Novel Tools: A Review

Md. Jafurulla and Amitabha Chattopadhyay

Abstract

Cholesterol is an important lipid in the context of membrane protein function. The function of a number of membrane proteins, including G protein-coupled receptors (GPCRs) and ion channels, has been shown to be dependent on membrane cholesterol. However, the molecular mechanism underlying such regulation is still being explored. In some cases, specific interaction between cholesterol and the protein has been implicated. In other cases, the effect of cholesterol on the membrane properties has been attributed for the regulation of protein function. In this article, we have provided an overview of experimental approaches that are useful for determining the degree of structural stringency of cholesterol for membrane protein function. In the process, we have highlighted the role of immediate precursors in cholesterol biosynthetic pathway in the function of membrane proteins. Special emphasis has been given to the application of stereoisomers of cholesterol in deciphering the structural stringency required for regulation of membrane protein function. A comprehensive examination of these processes would help in understanding the molecular basis of cholesterol regulation of membrane proteins in subtle details.

Key words Cholesterol, Cholesterol-binding motif, *ent*-Cholesterol, *epi*-Cholesterol, GPCRs, Ion channels, Stereoisomers, Stereospecificity

1 Introduction

Biological membranes exhibit a vast degree of functional and compositional heterogeneity and provide an ideal environment for the function of a variety of membrane lipids and proteins. A comprehensive understanding of diverse membrane functions requires deciphering molecular details of interactions between membrane components. Work from a number of groups has led to our current understanding of the requirement of specific lipids in the function of membrane proteins [1]. An important membrane lipid in this context is cholesterol, which exhibits heterogeneous (nonrandom) distribution in membranes and has been shown to modulate functions of several membrane proteins [1–8]. In this context, two important classes of membrane proteins studied are seven transmembrane domain G protein-coupled receptors (GPCRs) and ion

Ingrid C. Gelissen and Andrew J. Brown (eds.), *Cholesterol Homeostasis: Methods and Protocols*, Methods in Molecular Biology, vol. 1583, DOI 10.1007/978-1-4939-6875-6_3,

channels. GPCRs constitute an important superfamily of proteins that mediate a variety of physiological processes and serve as major drug targets in all clinical areas [9] (*see* below). Ion channels, on the other hand, are transmembrane proteins that regulate ionic permeability across cell membranes.

Although the cholesterol-dependent function for several proteins and peptides has been reported, the molecular details and specificity of their interaction are still emerging. Recent technical advancements, and ready availability of multiple agents for modulation of membrane cholesterol and close structural analogs of cholesterol, have made it possible to delineate the structural stringency associated with the interaction of cholesterol with membrane proteins and receptors. In this article, we provide an overview of the approaches, particularly utilizing structural analogs of cholesterol, for addressing structural stringency of cholesterol for the function of membrane proteins, with special emphasis on stereoisomers of cholesterol.

2 Requirement of Cholesterol for the Function of Membrane Proteins

The detailed mechanism underlying the modulation of the structure and function of membrane proteins and receptors by membrane cholesterol is not completely understood and appears to be complex [5, 10, 11]. It has been proposed that cholesterol could modulate the function of membrane receptors by a direct (specific) interaction, which could induce conformational change(s) in the receptor, or by altering the physical properties of the membrane in which the receptor is embedded. Yet another possibility could be a combination of both. Importantly, the concept of "nonannular"-binding sites of lipids in membrane proteins has been proposed as specific interaction sites [11, 12]. These sites are characterized by lack of accessibility to the annular lipids, i.e., annular lipids cannot compete and displace the lipids at these sites [13, 14].

Work from our laboratory and others has comprehensively demonstrated the role of membrane cholesterol in the organization, dynamics, function, and stability of GPCRs (reviewed in refs. [2–7, 9]). For example, cholesterol has been shown to play an important role in the function and stability of the serotonin$_{1A}$ receptor [15–17], β_2-adrenergic receptor [18–20], cholecystokinin receptor [21], serotonin$_{7a}$ receptor [22], oxytocin receptor [23, 24], and human type-1 cannabinoid receptor [25]. In addition, cholesterol has been shown to play a crucial role in the function and organization of several ion channels [8]. For example, the specific role of cholesterol in the activation, trafficking, and desensitization of the nicotinic acetylcholine receptor has been previously reported [26–31]. Cholesterol has been shown to modulate the agonist effectiveness of $GABA_A$ receptors and an optimal

requirement of cholesterol for the channel function has been reported [32–35]. In addition, membrane cholesterol has been shown to modulate the function of multiple types of K^+ channels (reviewed in refs. [8, 36], *see* below), the channel opening probability (lifetime), and the rate of desensitization of NMDA receptors [37].

As mentioned above, previous work from our laboratory has shown an absolute requirement of membrane cholesterol in the function of the serotonin$_{1A}$ receptor (reviewed in refs. [3, 5, 7]). We employed several approaches to explore the specific role of membrane cholesterol in the organization, dynamics, and function of the serotonin$_{1A}$ receptor. These approaches include: (1) acute modulation of membrane cholesterol using MβCD; (2) complexation of membrane cholesterol (without physical depletion) by agents such as nystatin and digitonin; (3) chemical modification of cholesterol to cholestenone using cholesterol oxidase; and (4) use of metabolic inhibitors of cholesterol biosynthesis such as statins and AY 9944. Interestingly, we utilized the loss in membrane cholesterol associated with receptor solubilization [38, 39] as an effective strategy to explore specific cholesterol effects on receptor function. We will discuss some of these approaches in detail later in the review.

Several structural features of proteins believed to assist preferential association with cholesterol have been recently reported [5, 7, 40, 41]. Prominent sites among them are CRAC (cholesterol recognition/interaction amino acid consensus) motif [41–44], CCM (cholesterol consensus motif) [45], SSD (sterol-sensing domain) [46, 47], and CARC (inverse CRAC) motif [41, 48, 49]. These cholesterol-binding sequences or motifs have been proposed to contain an aromatic amino acid that could interact with the near planar ring structure of cholesterol [45, 50], and a positively charged residue capable of participating in electrostatic interactions with the 3β-hydroxyl group of cholesterol [43, 50, 51]. In this context, it is important to note that the proposed "nonannular"-binding sites of lipids in membrane proteins could be considered specific interaction sites [11, 12] with possible locations at inter or intramolecular (interhelical) protein interfaces. Detailed analysis of the role of individual amino acids in these putative cholesterol interaction sites could help us understand the specific requirement of cholesterol observed for the function, organization, dynamics, and signaling of membrane proteins.

3 Approaches for Altering the Content and Availability of Membrane Cholesterol

A convenient way of exploring the structural stringency of lipids for the function of integral membrane proteins is to replace or modifty the lipid of interest to close structural analogs and examine the protein function. It therefore becomes important to look for specific tools to modulate or exchange the lipid of interest with its

close structural analogs. In many instances, enzymes that modify specific sites of lipids have been utilized for this purpose. The role of membrane cholesterol in the function of membrane proteins has been studied by a number of groups using a variety of agents to modulate the availability of membrane cholesterol. These include inhibitors of cholesterol biosynthesis (e.g., statins, triparanol, AY9944), cholesterol oxidase that oxidizes membrane cholesterol, agents physically modulating the cholesterol content (e.g., methyl-β-cyclodextrin (MβCD)), and cholesterol sequestering compounds (e.g., amphotericin B, digitonin, nystatin, filipin). We discuss some of these approaches in detail below.

3.1 Specific Carriers of Membrane Cholesterol

Acute and specific depletion of membrane cholesterol is possible due to the development of cyclodextrins that act as effective catalysts of cholesterol efflux from membranes [52]. Among a variety of cyclodextrins available with broad specificity for membrane lipids, the oligomer with seven methylated-glucose residues (MβCD) displays higher specificity for cholesterol relative to phospholipids (*see* Fig. 1a). The polar nature and small size of cyclodextrins compared to other lipid carriers, allow them to come close to the membrane without partitioning and favor efficient efflux of cholesterol. MβCD has therefore been extensively utilized and has evolved as a convenient tool to selectively and efficiently modulate membrane cholesterol by incorporating it in a central nonpolar cavity [53–56]. The stoichiometry of 1:2 (mol/mol) has been reported for such cholesterol-cyclodextrin complexes [56–58].

3.2 Cholesterol Complexing Agents

Complexation of membrane cholesterol, which effectively reduces the availability of cholesterol without physical depletion, represents a strategy to minimize any nonspecific effects associated with cholesterol depletion from membranes. When used at appropriate concentrations, cholesterol complexing agents partition into membranes and sequester cholesterol. These agents include digitonin, filipin, nystatin, and amphotericin B. Digitonin is a plant glycoalkaloid saponin detergent known to form water-insoluble 1:1 complex with cholesterol [59–61]. Nystatin [55, 62–65] and amphotericin B [62, 63, 66–70] are sterol-binding antifungal polyene antibiotics that are known to sequester membrane cholesterol (*see* Fig. 1). They effectively partition into membranes and sequester cholesterol (1:1 (mol/mol) complex) and form channels in the membrane. On the other hand, filipin is a fluorescent sterol-binding antifungal polyene antibiotic, often utilized to stain free cholesterol in fixed cells [54, 63]. These agents reduce the availability of cholesterol for its interaction with membrane receptors.

3.3 Inhibitors of Cholesterol Biosynthesis

A chronic and more physiological way of reducing membrane cholesterol content is by inhibiting cholesterol biosynthesis. A number of cholesterol biosynthesis inhibitors have been used for reducing

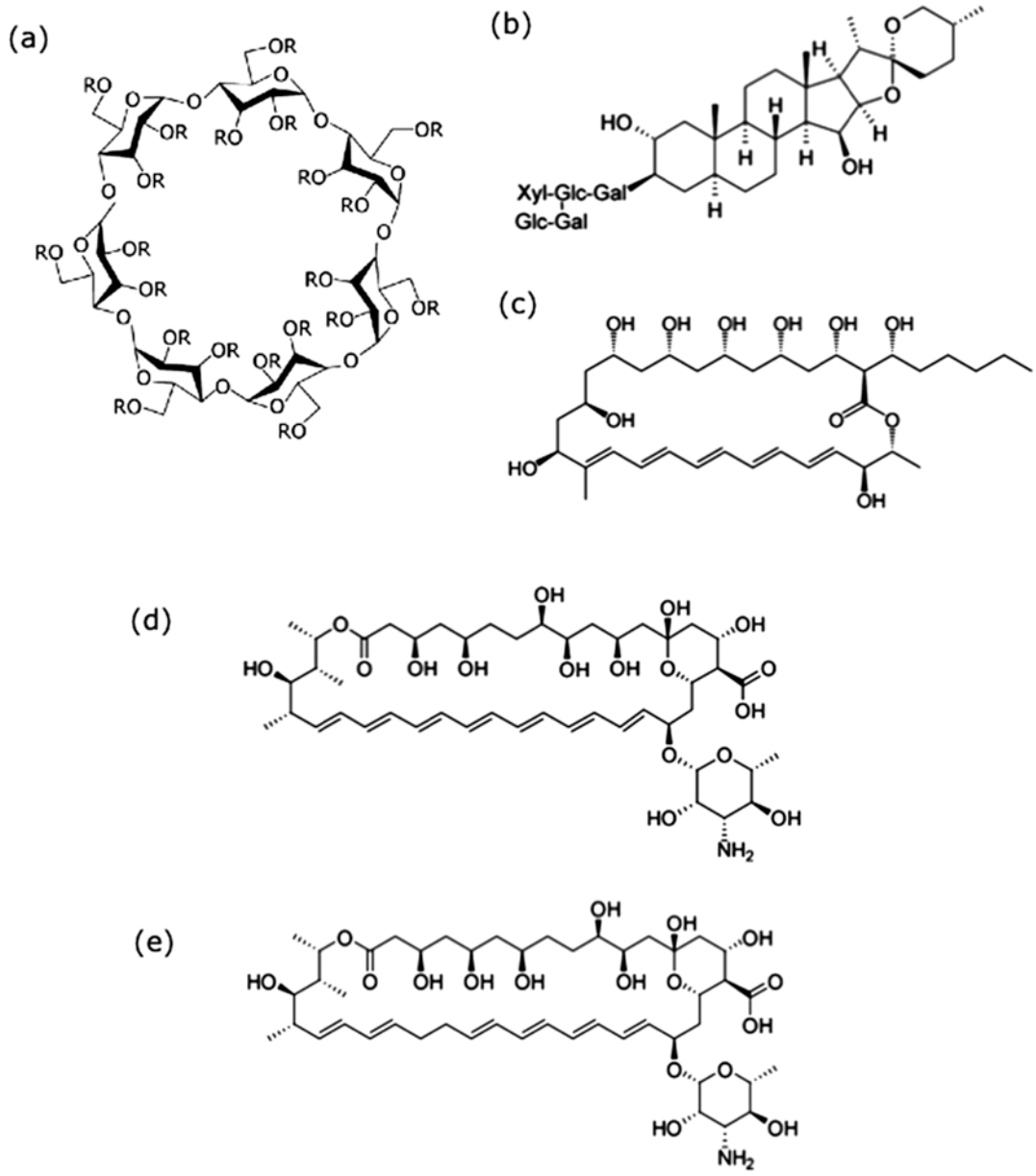

Fig. 1 Compounds that modulate availability of membrane cholesterol. (**a**) The chemical structure of β-cyclodextrin (containing seven glucose residues). Cyclodextrins can solubilize a variety of hydrophobic compounds by trapping them in their inner cavity. The oligomer with seven methylated-glucose residues (MβCD, where R denotes a methyl group) displays higher specificity for cholesterol relative to phospholipids. The stoichiometry of 1:2 (mol/mol) has been reported for such cholesterol-cyclodextrin complex. The chemical structures of cholesterol complexing agents such as (**b**) digitonin, (**c**) filipin, (**d**) amphotericin B, and (**e**) nystatin. Digitonin is a plant glycoalkaloid saponin detergent, while filipin, amphotericin B, and nystatin belong to the group of sterol-binding antifungal polyene antibiotics. Complexation of membrane cholesterol, which effectively reduces the availability of cholesterol without physical depletion, has been utilized as a strategy to minimize any nonspecific effects associated with use of MβCD to remove membrane cholesterol. Cholesterol complexing agents partition into membranes and sequester cholesterol. See text for more details

membrane cholesterol in metabolically active cells. For example, statins are a group of globally best selling drugs that are widely used for reducing membrane cholesterol. They act as competitive inhibitors of 3-hydroxy-3-methylglutaryl coenzyme A (HMG-CoA) reductase, a key rate-limiting enzyme in early cholesterol biosynthesis [71–73]. In addition, several distal inhibitors of cholesterol biosynthesis have been utilized. For example, AY9944 and BM15766 inhibit 7-dehydrocholesterol reductase (7-DHCR), an enzyme that catalyzes the last step in the Kandutsch-Russell pathway [74], and results in the accumulation of 7-dehydrocholesterol (7-DHC). This mimics one of the most serious autosomal recessive disease conditions called Smith-Lemli-Opitz Syndrome (SLOS) [75–79]. On the other hand, triparanol, another distal inhibitor of cholesterol biosynthesis, acts on 24-dehydrocholesterol reductase (24-DHCR), which catalyzes the last step in the Bloch pathway of cholesterol biosynthesis [80]. This results in accumulation of desmosterol which mimics another autosomal recessive disorder called desmosterolosis [78, 79, 81–84]. The use of these distal cholesterol biosynthesis inhibitors (AY9944, BM15766 and triparanol) has been limited because of severe effects resulting from accumulation of cholesterol precursors [85].

3.4 Enzymatic Oxidation of Cholesterol

Oxidation of membrane cholesterol by the enzyme cholesterol oxidase is yet another approach to modify the chemistry of cholesterol within the membrane without physical depletion. Cholesterol oxidase is a water-soluble enzyme that catalyzes the oxidation of cholesterol to cholestenone (cholest-4-en-3-one) at the membrane interface [86, 87]. The impact of oxidation of hydroxyl group of cholesterol appears to be relatively mild on membrane physical properties, and thereby is thought to minimize the nonspecific effects of cholesterol modulation.

4 Structural Analogs Utilized for Deciphering Stringency of Membrane Cholesterol in Protein Function

An efficient and quick way to explore structural stringency of cholesterol for a given process is to replace cholesterol with its close structural analogs. This is often conveniently achieved by depleting cholesterol using MβCD or metabolic inhibitors, and replacing it with its structural analogs either by utilizing a preformed sterol-MβCD complex, or by supplementation in reconstituted LDL particles in the culture medium of cells. Yet another convenient approach to explore the structural stringency of cholesterol for protein function is membrane solubilization using appropriate detergents [88, 89]. Membrane solubilization is often associated with delipidation (loss of lipids), and results in differential extents of lipid solubilization [38, 39]. Since membrane lipids play an

important role in maintaining the function of membrane proteins and receptors, such delipidation upon solubilization often results in loss of protein function. This phenomenon has been effectively utilized to explore molecular details of specific lipid requirements for the function of membrane proteins [90, 91] and has been recently reviewed [89].

As mentioned above, work from our laboratory and others has shown the crucial role of membrane cholesterol in the organization, dynamics, function, and stability of GPCRs [2–7, 9]. Availability of the above-mentioned agents and structural analogs of cholesterol (*see* sections 4.1 and 4.2) has made it possible to examine the structural stringency of cholesterol necessary for the function of several membrane proteins and peptides. These include ion channels, GPCRs, model peptides such as gramicidin and toxins such as *Vibrio cholerae* cytolysin and streptococcal streptolysin O. We discuss below some of the close structural analogs of cholesterol that have been utilized for exploring the stringent requirement of cholesterol in the function of membrane proteins and peptides.

4.1 Biosynthetic Precursors of Cholesterol: 7-DHC and Desmosterol

7-DHC and desmosterol are two close structural analogs of cholesterol, which differ with cholesterol merely in an additional double bond at the 7th position in the sterol ring and the 24th position in alkyl side chain, respectively (*see* Fig. 2b, c). 7-DHC and desmosterol are immediate biosynthetic precursors of cholesterol in the Kandutsch-Russell and Bloch pathways, respectively. Malfunctioning of enzymes that catalyze the conversion of 7-DHC and desmosterol to cholesterol (7-DHCR and 24-DHCR) results in low levels of serum cholesterol and accumulation (high levels) of the respective immediate precursors. This leads to fatal neurological disorders such as the Smith-Lemli-Opitz Syndrome (SLOS) and desmosterolosis [78, 79]. Availability of these structural analogs of cholesterol in relatively pure form has been useful to address the underlying mechanism of malfunctioning of proteins under such disease conditions.

Work from our laboratory and others has utilized these structural analogs to explore the function of important membrane proteins such as ion channels and GPCRs. For example, previous work from our laboratory has explored whether 7-DHC or desmosterol could replace cholesterol in supporting the function of the serotonin$_{1A}$ receptor, an important neurotransmitter receptor [92, 93]. An interesting aspect of our results is that the requirement of cholesterol for the function of the serotonin$_{1A}$ receptor was shown to be considerably stringent. Our results showed that while desmosterol could support the receptor function [84], 7-DHC could not [77, 94, 95]. In addition, cholesterol has been shown to inhibit the activity of a prokaryotic Kir (KirBac1.1) channel, while replacement with desmosterol has been reported to enhance channel activity [96]. In contrast, it has been shown that replacement of cholesterol

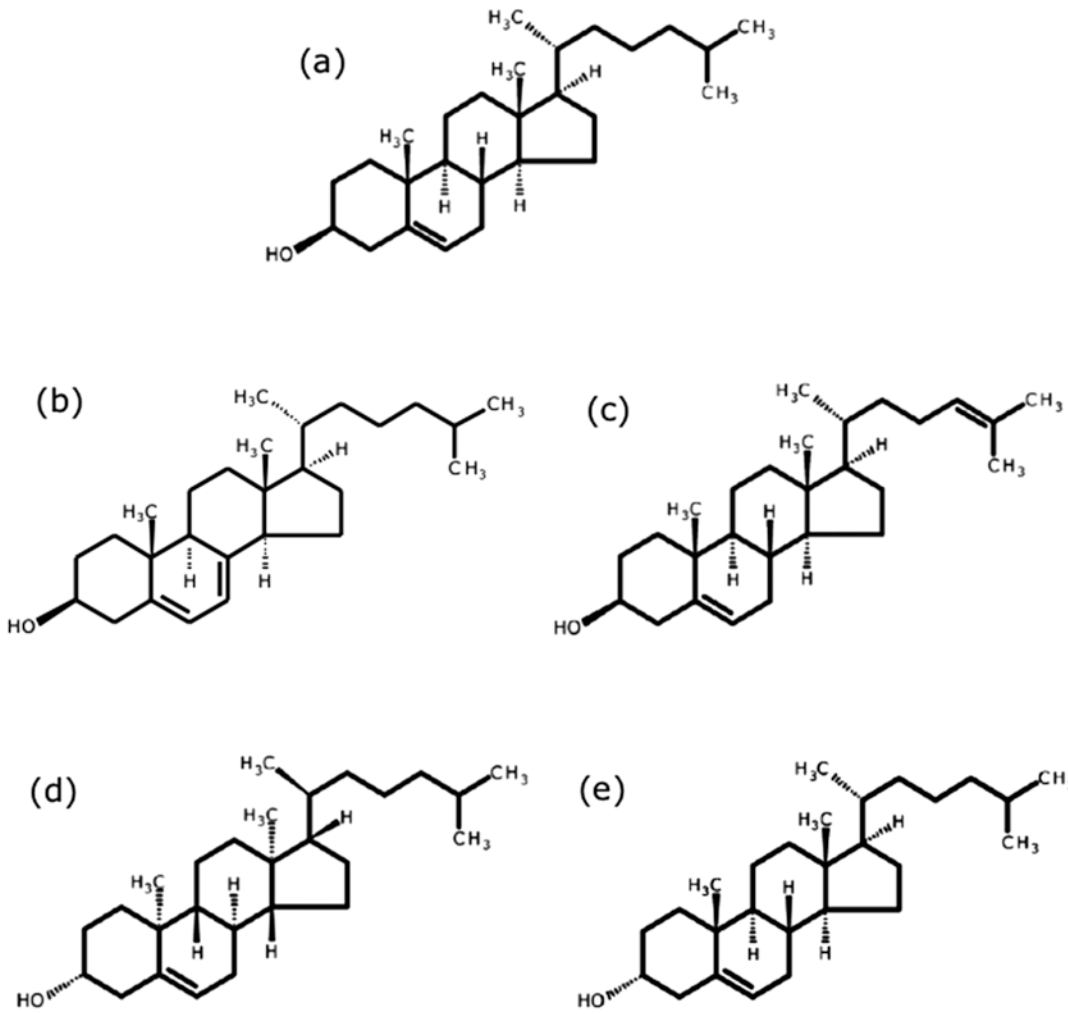

Fig. 2 Chemical structures of (**a**) cholesterol, and its structural analogs; (**b**) 7-dehydrocholesterol (7-DHC) and (**c**) desmosterol are immediate biosynthetic precursors of cholesterol in the Kandutsch-Russell and Bloch pathways, respectively, which differ with cholesterol merely in an additional double bond at the 7th position in the sterol ring and the 24th position in the alkyl side chain; (**d**) *ent*-cholesterol and (**e**) *epi*-cholesterol are stereoisomers of cholesterol. The enantiomer of cholesterol (*ent*-cholesterol) is the nonsuperimposable mirror image of natural cholesterol and exhibits similar physicochemical properties. *epi*-Cholesterol, on the other hand, is a diastereomer of cholesterol, that differs with cholesterol only in the orientation of the hydroxyl group at carbon-3, which is inverted relative to natural cholesterol. Adapted from ref. 89. See text for more details

with 7-DHC or desmosterol has relatively mild effect on the function of two structurally related peptide receptors, the oxytocin receptor and the cholecystokinin receptor [23].

4.2 Stereoisomers of Cholesterol

Stereoisomers of cholesterol such as enantiomer of cholesterol (*ent*-cholesterol) and *epi*-cholesterol (a diastereomer of cholesterol) have been developed as novel tools to differentiate the specific and

general effect of cholesterol in protein function. *ent*-Cholesterol is the nonsuperimposable mirror image of natural cholesterol (*see* Fig. 2d) and exhibits similar biophysical properties in the membrane (such as compressibility, phase behavior, and dipole potential) as natural cholesterol [97–99]. In addition, *ent*-cholesterol has been shown to support normal growth of a mutant mammalian cell line similar to its natural counterpart [100]. *epi*-Cholesterol, on the other hand, is a diastereomer of cholesterol that differs with cholesterol only in the orientation of the hydroxyl group at carbon-3, which is inverted relative to natural cholesterol (Fig. 2e). *epi*-Cholesterol has been shown to exhibit differences in membrane biophysical properties (such as condensing ability, tilt angles, and phase transition) relative to natural cholesterol (reviewed in refs. [97, 98]). *ent*-Cholesterol is often utilized to distinguish whether the effect of cholesterol observed is due to specific interaction with membrane components such as proteins and peptides, or due to general membrane (nonspecific) effects [97–103]. The selectivity of natural cholesterol and its enantiomer on the function of several peptides and proteins has been studied in detail. We discuss some of these examples below.

4.2.1 G Protein-Coupled Receptors

G protein-coupled receptors (GPCRs) are important superfamily of transmembrane proteins that primarily transduce signals from outside the cell to the cellular interior [104–106]. GPCRs mediate a vast variety of physiological processes and therefore serve as major drug targets in all clinical areas [9, 107–109]. Recent work from our laboratory has addressed the stereospecific requirement of cholesterol utilizing *ent*-cholesterol and *epi*-cholesterol for the function of the serotonin$_{1A}$ receptor. In order to determine the structural stringency of cholesterol, we replenished solubilized membranes (which contain significantly less cholesterol compared to native membranes [38, 39]) with *ent*-cholesterol or *epi*-cholesterol and examined if they could support receptor function. Our results showed that *ent*-cholesterol behaved similarly to native cholesterol in supporting the function of the serotonin$_{1A}$ receptor, although *epi*-cholesterol could not support receptor function [110] (*see* Fig. 3). Our results therefore point out the requirement of membrane cholesterol for the serotonin$_{1A}$ receptor function to be diastereospecific, yet not enantiospecific. These results also highlighted the *equatorial* configuration of the 3-hydroxyl group of cholesterol as a key structural feature for its ability to support the serotonin$_{1A}$ receptor function. These results, along with our previous observations with other close structural analogs of cholesterol [77, 84, 94, 95], extended our understanding of the degree of specificity of interaction of membrane cholesterol with the serotonin$_{1A}$ receptor. In an earlier study, it has been shown that *epi*-cholesterol could not support the specific ligand binding to the oxytocin receptor (a peptide binding GPCR for which the specific

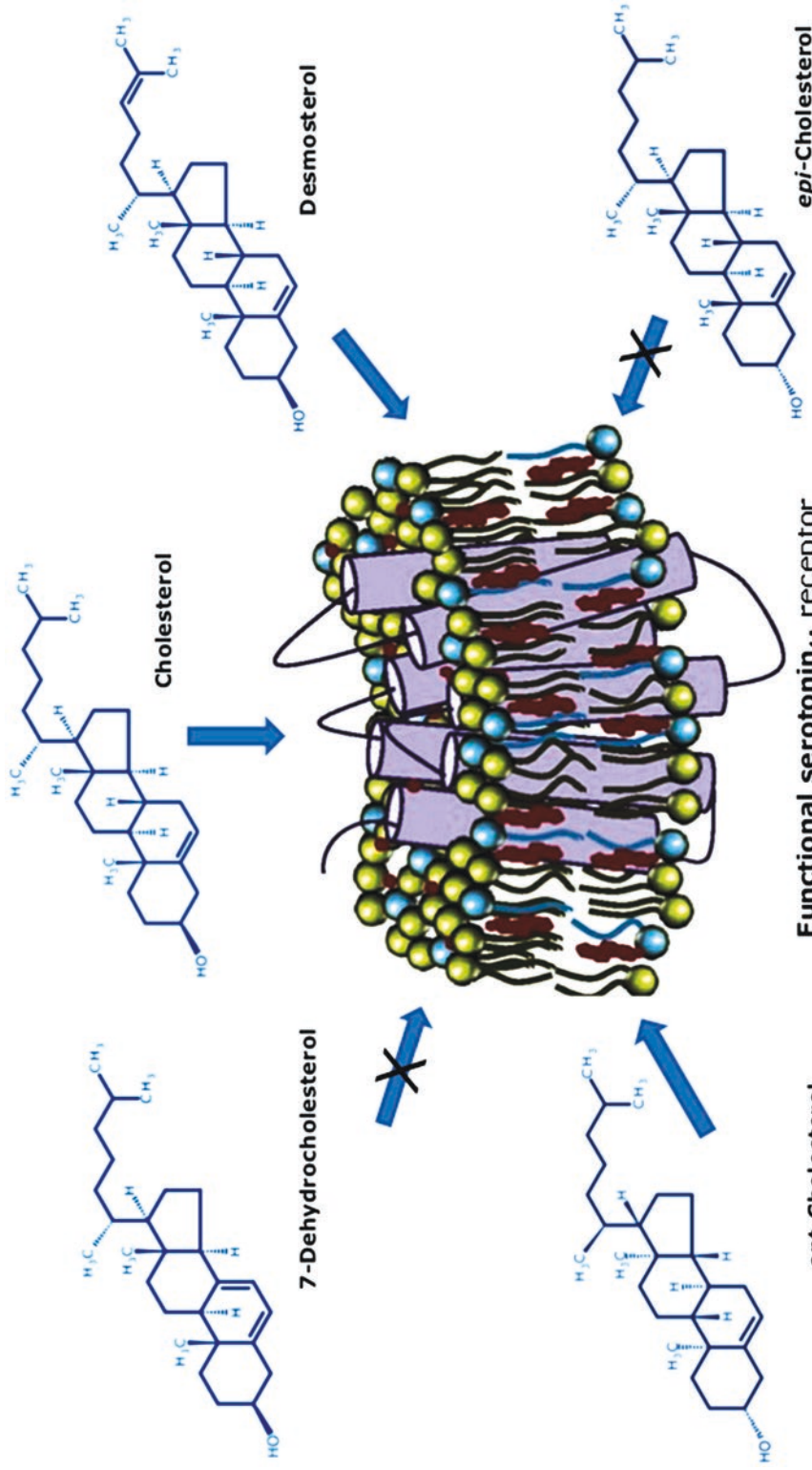

Fig. 3 Exploring the structural stringency of cholesterol required for the function of a representative GPCR, the serotonin$_{1A}$ receptor. Replenishment of solubilized hippocampal membranes containing the serotonin$_{1A}$ receptor with cholesterol and its close structural analogs allows us to effectively explore the stringency of cholesterol structure in receptor function. The schematic shows that cholesterol, desmosterol, and *ent*-cholesterol could support the function of the serotonin$_{1A}$ receptor, whereas 7-dehydrocholesterol and *epi*-cholesterol could not. The serotonin$_{1A}$ receptor is shown in purple, and the replenished sterol molecules are shown in maroon. The underlying message here is that even subtle changes in sterol structure may be crucial for receptor function, thereby reinforcing the stringency associated with receptor-cholesterol interaction. Adapted from ref. 89. See text for more details

requirement of membrane cholesterol for its function has been demonstrated [23]). Taken together, these results demonstrate the stringent requirement of cholesterol structure for the function of GPCRs.

4.2.2 Ion Channels

Ion channels are transmembrane proteins that regulate ionic permeability across cell membranes and are crucial for normal functioning of cells. Malfunctioning of ion channels has been implicated in a number of diseases collectively known as "channelopathies" [111]. Membrane cholesterol has been shown to modulate the function of several ion channels, such as multiple types of K^+ channels, including inwardly rectifying, Ca^{2+}-sensitive and voltage-gated K^+ channels, voltage-gated Na^+ and Ca^{2+} channels, volume-regulated anion channels (reviewed in ref. 8). In many cases, cholesterol inhibited the channel function either by decreasing the channel opening probability (lifetime) or the number of active channels. In contrast, cholesterol is observed to be essential for the function of the nicotinic acetylcholine receptor (nAChR) [27, 30] and $GABA_A$ receptors [32–34]. Although cholesterol has been shown to modulate the function of a number of ion channels, the structural stringency of cholesterol (stereospecificity in particular) and details of molecular interaction have been explored only in a few cases. For example, the enantioselectivity of cholesterol for the function of inward rectifier K^+ channels from bacteria (KirBac1.1 and KirBac3.1) and human (Kir2.1) has been studied. While natural cholesterol is known to inhibit these channels, its enantiomer, *ent*-cholesterol, does not inhibit the channel function. It was therefore concluded that the regulation of channel function by the membrane cholesterol is through possible direct channel-cholesterol interaction [102]. In addition, the stereoselectivity of cholesterol in the function of inward rectifier K^+ channels has been previously explored utilizing the diastereomer of cholesterol (*epi*-cholesterol) [112]. Similarly, *epi*-cholesterol has been shown to be significantly less efficient than natural cholesterol in inhibiting the activity of prokaryotic Kir (KirBac1.1) channels [96]. These results show an absolute requirement of cholesterol for maintaining channel function with possible direct interaction with the protein.

In contrast, the cholesterol dependence of agonist stimulated channel conductance of the nicotinic acetylcholine receptor has been shown to be supported by both *ent*-cholesterol and *epi*-cholesterol [113]. In yet another study, channel formation of gramicidin in the presence of stereoisomers of cholesterol was studied. Gramicidin is a 15-residue linear antimicrobial peptide that forms prototypical ion channels specific for monovalent cations and serves as an excellent model for studying the organization, dynamics, and function of membrane-spanning channels [114–116]. Both natural and *ent*-cholesterol were observed to support the formation of identical gramicidin ion channels [101]. The results with the nicotinic

acetylcholine receptor and gramicidin channels were therefore attributed to a nonspecific mode of regulation of protein function by membrane cholesterol (i.e., through influence on membrane physical properties).

4.2.3 Regulators of Cholesterol Homeostasis

Cholesterol homeostasis in cells is stringently maintained through interaction of key proteins that sense membrane cholesterol levels. Among the proteins involved, sterol regulatory element-binding protein 2 (SREBP-2) and SREBP cleavage-activating protein (Scap) play important roles in cholesterol homeostasis. Cellular cholesterol regulates its own synthesis by modulating the activation of SREBP-2 transcription factors [117]. When in excess, cholesterol in the endoplasmic reticulum (ER) is sensed by Scap which upon conformational change assists binding of Insig, a protein that tethers the SREBP-Scap complex at ER in inactive form [118–120]. When cholesterol levels fall below a certain threshold, SREBP-2 is transported to the Golgi by Scap and is activated upon proteolytic cleavage. The activated (cleaved) fragment gets translocated to nucleus that induces expression of proteins involved in biosynthesis and uptake of cholesterol.

In a recent study, cholesterol enantioselecivity for proteins involved in cholesterol homeostasis was explored [103]. This study showed that activation of SREBP-2, the master transcriptional regulator of cholesterol metabolism, is suppressed by *ent*-cholesterol with similar efficiency as natural cholesterol. In agreement with this, the expression of target genes of SREBP-2 such as *LDLR* (LDL receptor), *HMGCR* (HMG-CoA reductase), and *SQLE* (Squalene epoxidase/monooxygenase) is suppressed by *ent*-cholesterol, similar to natural cholesterol. Importantly, *ent*-cholesterol induced the conformational change in the cholesterol-sensing protein Scap like its natural counterpart, which would result in retention of SREBP-2 in ER. Taken together, these results show that *ent*-cholesterol exhibits similarly homeostatic responses as natural cholesterol. On this basis, it has been suggested that cholesterol could also maintain its homeostasis through alterations in membrane properties beyond those specific cholesterol–protein interactions currently recognized [103].

4.2.4 Enzymes

Enantioselectivity of some of the enzymes involved in cholesterol metabolism has been previously examined. Cholesterol oxidase that catalyzes oxidation of cholesterol is one of the well-studied and extensively utilized enzymes. Cholesterol oxidase is a water-soluble enzyme that catalyzes the oxidation of cholesterol to cholestenone (cholest-4-en-3-one) at the membrane interface [86]. The stereospecificity of cholesterol recognition by cholesterol oxidase has been explored earlier [121]. Results showed that while *ent*-cholesterol serves as a substrate for cholesterol oxidase, the kinetics of oxidation is slower and oxidation was incomplete as

compared to its natural analog. In another study, acyl CoA cholesterol acyltransferase (ACAT), an ER resident enzyme that catalyzes cholesterol esterification, has been shown to be enantioselective for cholesterol, with *ent*-cholesterol being a poor substrate [122]. In contrast, proteasomal degradation of squalene monooxygenase, a key enzyme in cholesterol biosynthesis, has been shown to be accelerated by *ent*-cholesterol similarly to natural cholesterol, although to a lesser extent [103]. While enzyme substrate interaction is thought to be very stringent, studies with close structural analogs, especially the stereoisomers help broaden our understanding of stringency of their interaction.

4.2.5 Bacterial Toxins

The mechanism of action of several pore-forming toxins to selectively permeabilize host membranes is explained by their specific interaction with sterols in eukaryotic membranes, and cholesterol in particular, in higher eukaryotes. The requirement of cholesterol for the activity of bacterial pore-forming toxins such as *Vibrio cholerae* cytolysin [123] and streptococcal streptolysin O [124] has been reported earlier. In the case of *Vibrio cholerae* cytolysin, cholesterol has been shown to be required for membrane permeabilization, and cytolysin could not permeabilize membranes when cholesterol was replaced with *ent*-cholesterol [125]. These results highlight the enantioselectivity of cholesterol for its function. On the other hand, cholesterol has been shown to be essential for the membrane binding of streptococcal streptolysin O, which exhibited permeabilization of membranes in the presence of *ent*-cholesterol, albeit with less potency [125]. Bacterial toxins such as *Staphylococcus aureus* α-hemolysin and *Streptococcus agalactiae* CAMP factor, whose erythrocyte lysis is dependent on membrane cholesterol, did not exhibit enantioselectivity [126]. These results suggest a lower degree of structural specificity in toxin-sterol interactions, and the change in cholesterol-dependent membrane properties, but not direct interaction, could affect the function of these bacterial toxins.

It is important to mention here that in all the above-mentioned examples where the stereospecificity of cholesterol has been explored, *ent*-cholesterol has been particularly utilized to differentiate the specific and general role of cholesterol in protein function. The crucial assumption in these studies is that the specific cholesterol binding site would be geometrically stringent enough that it could differentiate the enantiomers. While such stringency would require more than two specific interactions between the ligand and the receptor, at least four geometrical constraints are proposed to be required to distinguish the enantiomers [97, 98]. However, in a protein that is non-rigid, defining such geometrical constraints would be difficult. Interestingly, a possibility of a non-enantioselective pattern of binding in a non-geometrically constrained protein cleft (such as a non-annular lipid binding site, as discussed above) has been earlier

proposed [97, 98]. It is therefore important to keep this caveat in mind when interpreting a finding of lack of enantioselectivity.

5 Conclusion and Future Perspectives

Advances in techniques to modulate the accessibility of membrane cholesterol, along with the availability of close structural analogs of cholesterol, have made it possible to delineate the structural stringency of cholesterol required for maintaining the optimum function of several membrane proteins such as GPCRs and ion channels. In particular, the stereoisomers of cholesterol have been useful in examining the specific effect of cholesterol from its general effects on membrane properties. Taken together, these approaches have helped us address the molecular details of regulation of membrane protein function by cholesterol. Insights from such studies could help us understand details of functioning of important membrane proteins in healthy and diseased conditions with impaired cholesterol metabolism.

Acknowledgments

Work in A.C.'s laboratory was supported by the Council of Scientific and Industrial Research (Govt. of India) Network project BSC0115. A.C. is an Adjunct Professor of Tata Institute of Fundamental Research (Mumbai), RMIT University (Melbourne, Australia), Indian Institute of Technology (Kanpur), and Indian Institute of Science Education and Research (Mohali). A.C. gratefully acknowledges J.C. Bose Fellowship (Dept. of Science and Technology, Govt. of India). Some of the work described in this article was carried out by former members of A.C.'s research group whose contributions are gratefully acknowledged. We thank G. Aditya Kumar for help in making figures, and members of the Chattopadhyay laboratory for critically reading the manuscript.

References

1. Lee AG (2011) Lipid–protein interactions. Biochem Soc Trans 39:761–766
2. Burger K, Gimpl G, Fahrenholz F (2000) Regulation of receptor function by cholesterol. Cell Mol Life Sci 57:1577–1592
3. Pucadyil TJ, Chattopadhyay A (2006) Role of cholesterol in the function and organization of G-protein coupled receptors. Prog Lipid Res 45:295–333
4. Fantini J, Barrantes FJ (2009) Sphingolipid/cholesterol regulation of neurotransmitter receptor conformation and function. Biochim Biophys Acta 1788:2345–2361
5. Paila YD, Chattopadhyay A (2010) Membrane cholesterol in the function and organization

of G-protein coupled receptors. Subcell Biochem 51:439–466

6. Oates J, Watts A (2011) Uncovering the intimate relationship between lipids, cholesterol and GPCR activation. Curr Opin Struct Biol 21:802–807
7. Jafurulla M, Chattopadhyay A (2013) Membrane lipids in the function of serotonin and adrenergic receptors. Curr Med Chem 20:47–55
8. Levitan I, Singh DK, Rosenhouse-Dantsker A (2014) Cholesterol binding to ion channels. Front Physiol 5:65
9. Chattopadhyay A (2014) GPCRs: lipid-dependent membrane receptors that act as drug targets. Adv Biol 2014:143023
10. Paila YD, Chattopadhyay A (2009) The function of G-protein coupled receptors and membrane cholesterol: specific or general interaction? Glycoconj J 26:711–720
11. Lee AG (2011) Biological membranes: the importance of molecular detail. Trends Biochem Sci 36:493–500
12. Paila YD, Tiwari S, Chattopadhyay A (2009) Are specific nonannular cholesterol binding sites present in G-protein coupled receptors? Biochim Biophys Acta 1788:295–302
13. Simmonds AC, East JM, Jones OT, Rooney EK, McWhirter J, Lee AG (1982) Annular and non-annular binding sites on the (Ca^{2+} + Mg^{2+})-ATPase. Biochim Biophys Acta 693:398–406
14. Jones OT, McNamee MG (1988) Annular and nonannular binding sites for cholesterol associated with the nicotinic acetylcholine receptor. Biochemistry 27:2364–2374
15. Pucadyil TJ, Chattopadhyay A (2004) Cholesterol modulates ligand binding and G-protein coupling to serotonin$_{1A}$ receptors from bovine hippocampus. Biochim Biophys Acta 1663:188–200
16. Saxena R, Chattopadhyay A (2012) Membrane cholesterol stabilizes the human serotonin$_{1A}$ receptor. Biochim Biophys Acta 1818:2936–2942
17. Patra SM, Chakraborty S, Shahane G, Prasanna X, Sengupta D, Maiti PK, Chattopadhyay A (2015) Differential dynamics of the serotonin$_{1A}$ receptor in membrane bilayers of varying cholesterol content revealed by all atom molecular dynamics simulation. Mol Membr Biol 32:127–137
18. Yao Z, Kobilka BK (2005) Using synthetic lipids to stabilize purified β_2 adrenoceptor in detergent micelles. Anal Biochem 343:344–346
19. Zocher M, Zhang C, Rasmussen SGF, Kobilka BK, Müller DJ (2012) Cholesterol increases kinetic, energetic, and mechanical stability of the human β_2-adrenergic receptor. Proc Natl Acad Sci U S A 109:E3463–E3472
20. Paila YD, Jindal E, Goswami SK, Chattopadhyay A (2011) Cholesterol depletion enhances adrenergic signaling in cardiac myocytes. Biochim Biophys Acta 1808:461–465
21. Harikumar KG, Puri V, Singh RD, Hanada K, Pagano RE, Miller LJ (2005) Differential effects of modification of membrane cholesterol and sphingolipids on the conformation, function, and trafficking of the G protein-coupled cholecystokinin receptor. J Biol Chem 280:2176–2185
22. Sjögren B, Hamblin MW, Svenningsson P (2006) Cholesterol depletion reduces serotonin binding and signaling via human 5-HT$_{7(a)}$ receptors. Eur J Pharmacol 552:1–10
23. Gimpl G, Burger K, Fahrenholz F (1997) Cholesterol as modulator of receptor function. Biochemistry 36:10959–10974
24. Gimpl G, Fahrenholz F (2002) Cholesterol as stabilizer of the oxytocin receptor. Biochim Biophys Acta 1564:384–392
25. Oddi S, Dainese E, Fezza F, Lanuti M, Barcaroli D, De Laurenzi V, Centonze D, Maccarrone M (2011) Functional characterization of putative cholesterol binding sequence (CRAC) in human type-1 cannabinoid receptor. J Neurochem 116:858–865
26. Criado M, Eibl H, Barrantes FJ (1982) Effects of lipids on acetylcholine receptor. Essential need of cholesterol for maintenance of agonist-induced state transitions in lipid vesicles. Biochemistry 21:3622–3629
27. Fong TM, McNamee MG (1986) Correlation between acetylcholine receptor function and structural properties of membranes. Biochemistry 25:830–840
28. Santiago J, Guzmán GR, Rojas LV, Marti R, Asmar-Rovira GA, Santana LF, McNamee M, Lasalde-Dominicci JA (2001) Probing the effects of membrane cholesterol in the *Torpedo californica* acetylcholine receptor and the novel lipid-exposed mutation αC418W in *Xenopus* oocytes. J Biol Chem 276:46523–46532
29. Borroni V, Baier CJ, Lang T, Bonini I, White MM, Garbus I, Barrantes FJ (2007) Cholesterol depletion activates rapid internalization of submicron-sized acetylcholine receptor domains at the cell membrane. Mol Membr Biol 24:1–15

30. Barrantes FJ (2007) Cholesterol effects on nicotinic acetylcholine receptor. J Neurochem 103(Supp 1):72–80
31. Borroni V, Barrantes FJ (2011) Cholesterol modulates the rate and mechanism of acetylcholine receptor internalization. J Biol Chem 286:17122–17132
32. Sooksawate T, Simmonds MA (1998) Increased membrane cholesterol reduces the potentiation of $GABA_A$ currents by neurosteroids in dissociated hippocampal neurones. Neuropharmacology 37:1103–1110
33. Sooksawate T, Simmonds MA (2001) Influence of membrane cholesterol on modulation of the $GABA_A$ receptor by neuroactive steroids and other potentiators. Br J Pharmacol 134:1303–1311
34. Sooksawate T, Simmonds MA (2001) Effects of membrane cholesterol on the sensitivity of the $GABA_A$ receptor to GABA in acutely dissociated rat hippocampal neurones. Neuropharmacology 40:178–184
35. Nothdurfter C, Tanasic S, Di Benedetto B, Uhr M, Wagner E-M, Gilling KE, Parsons CG, Rein T, Holsboer F, Rupprecht R, Rammes G (2013) Lipid raft integrity affects $GABA_A$ receptor, but not NMDA receptor modulation by psychopharmacological compounds. Int J Neuropsychopharmacol 16:1361–1371
36. Rosenhouse-Dantsker A, Levitan I (2012) Insights into structural determinants of cholesterol sensitivity of Kir channels. In: Levitan I, Barrantes F (eds) Cholesterol regulation of ion channels and receptors. John Wiley, NJ, pp 47–67
37. Korinek M, Vyklicky V, Borovska J, Lichnerova K, Kaniakova M, Krausova B, Krusek J, Balik A, Smejkalova T, Horak M, Vyklicky L (2015) Cholesterol modulates open probability and desensitization of NMDA receptors. J Physiol 593:2279–2293
38. Banerjee P, Joo JB, Buse JT, Dawson G (1995) Differential solubilization of lipids along with membrane proteins by different classes of detergents. Chem Phys Lipids 77:65–78
39. Chattopadhyay A, Jafurulla M, Kalipatnapu S, Pucadyil TJ, Harikumar KG (2005) Role of cholesterol in ligand binding and G-protein coupling of $serotonin_{1A}$ receptors solubilized from bovine hippocampus. Biochem Biophys Res Commun 327:1036–1041
40. Gimpl G (2010) Cholesterol-protein interaction: methods and cholesterol reporter molecules. Subcell Biochem 51:1–45
41. Fantini J, Barrantes FJ (2013) How cholesterol interacts with membrane proteins: an exploration of cholesterol-binding sites including CRAC, CARC, and tilted domains. Front Physiol 4:31
42. Li H, Papadopoulos V (1998) Peripheral-type benzodiazepine receptor function in cholesterol transport. Identification of a putative cholesterol recognition/interaction amino acid sequence and consensus pattern. Endocrinology 139:4991–4997
43. Epand RM (2006) Cholesterol and the interaction of proteins with membrane domains. Prog Lipid Res 45:279–294
44. Jafurulla M, Tiwari S, Chattopadhyay A (2011) Identification of cholesterol recognition amino acid consensus (CRAC) motif in G-protein coupled receptors. Biochem Biophys Res Commun 404:569–573
45. Hanson MA, Cherezov V, Griffith MT, Roth CB, Jaakola V-P, Chien EYT, Velasquez J, Kuhn P, Stevens RC (2008) A specific cholesterol binding site is established by the 2.8 Å structure of the human β_2-adrenergic receptor. Structure 16:897–905
46. Brown MS, Goldstein JL (1999) A proteolytic pathway that controls the cholesterol content of membranes, cells, and blood. Proc Natl Acad Sci U S A 96:11041–11048
47. Kuwabara PE, Labouesse M (2002) The sterol-sensing domain: multiple families, a unique role? Trends Genet 18:193–201
48. Baier CJ, Fantini J, Barrantes FJ (2011) Disclosure of cholesterol recognition motifs in transmembrane domains of the human nicotinic acetylcholine receptor. Sci Rep 1:69
49. Fantini J, Di Scala C, Evans LS, Williamson PTF, Barrantes FJ (2016) A mirror code for protein-cholesterol interactions in the two leaflets of biological membranes. Sci Rep 6:21907
50. Jamin N, Neumann J-M, Ostuni MA, Vu TKN, Yao Z-X, Murail S, Robert J-C, Giatzakis C, Papadopoulos V, Lacapère J-J (2005) Characterization of the cholesterol recognition amino acid consensus sequence of the peripheral-type benzodiazepine receptor. Mol Endocrinol 19:588–594
51. Epand RF, Thomas A, Brasseur R, Vishwanathan SA, Hunter E, Epand RM (2006) Juxtamembrane protein segments that contribute to recruitment of cholesterol into domains. Biochemistry 45:6105–6114
52. Härtel S, Diehl HA, Ojeda F (1998) Methyl-*β*-cyclodextrins and liposomes as water-soluble carriers for cholesterol incorporation into membranes and its evaluation by a microenzymatic fluorescence assay and membrane

fluidity-sensitive dyes. Anal Biochem 258:277–284

53. Zidovetzki R, Levitan I (2007) Use of cyclodextrins to manipulate plasma membrane cholesterol content: evidence, misconceptions and control strategies. Biochim Biophys Acta 1768:1311–1324
54. Gimpl G, Gehrig-Burger K (2011) Probes for studying cholesterol binding and cell biology. Steroids 76:216–231
55. Chattopadhyay A, Jafurulla M (2012) Role of membrane cholesterol in leishmanial infection. Adv Exp Med Biol 749:201–213
56. López CA, de Vries AH, Marrink SJ (2013) Computational microscopy of cyclodextrin mediated cholesterol extraction from lipid model membranes. Sci Rep 3:2071
57. Breslow R, Zhang B (1996) Cholesterol recognition and binding by cyclodextrin dimers. J Am Chem Soc 118:8495–8496
58. Tsamaloukas A, Szadkowska H, Slotte JP, Heerklotz H (2005) Interactions of cholesterol with lipid membranes and cyclodextrin characterized by calorimetry. Biophys J 89:1109–1119
59. Elias PM, Goerke J, Friend DS, Brown BE (1978) Freeze-fracture identification of sterol-digitonin complexes in cell and liposome membranes. J Cell Biol 78:577–596
60. Nishikawa M, Nojima S, Akiyama T, Sankawa U, Inoue K (1984) Interaction of digitonin and its analogs with membrane cholesterol. J Biochem 96:1231–1239
61. Paila YD, Pucadyil TJ, Chattopadhyay A (2005) The cholesterol-complexing agent digitonin modulates ligand binding of the bovine hippocampal serotonin$_{1A}$ receptor. Mol Membr Biol 22:241–249
62. Holz RW (1974) The effects of the polyene antibiotics nystatin and amphotericin B on thin lipid membranes. Ann N Y Acad Sci 235:469–479
63. Bolard J (1986) How do the polyene macrolide antibiotics affect the cellular membrane properties? Biochim Biophys Acta 864: 257–304
64. Coutinho A, Prieto M (2003) Cooperative partition model of nystatin interaction with phospholipid vesicles. Biophys J 84:3061–3078
65. Pucadyil TJ, Shrivastava S, Chattopadhyay A (2004) The sterol-binding antibiotic nystatin differentially modulates ligand binding of the bovine hippocampal serotonin$_{1A}$ receptor. Biochem Biophys Res Commun 320:557–562
66. Readio JD, Bittman R (1982) Equilibrium binding of amphotericin B and its methyl ester and borate complex to sterols. Biochim Biophys Acta 685:219–224
67. Mouri R, Konoki K, Matsumori N, Oishi T, Murata M (2008) Complex formation of amphotericin B in sterol-containing membranes as evidenced by surface plasmon resonance. Biochemistry 47:7807–7815
68. Paila YD, Saha B, Chattopadhyay A (2010) Amphotericin B inhibits entry of *Leishmania donovani* into primary macrophages. Biochem Biophys Res Commun 399:429–433
69. Chattopadhyay A, Jafurulla M (2011) A novel mechanism for an old drug: amphotericin B in the treatment of visceral leishmaniasis. Biochem Biophys Res Commun 416:7–12
70. Kamiński DM (2014) Recent progress in the study of the interactions of amphotericin B with cholesterol and ergosterol in lipid environments. Eur Biophys J 43:453–467
71. Istvan ES, Deisenhofer J (2001) Structural mechanism for statin inhibition of HMG-CoA reductase. Science 292:1160–1164
72. Shrivastava S, Pucadyil TJ, Paila YD, Ganguly S, Chattopadhyay A (2010) Chronic cholesterol depletion using statin impairs the function and dynamics of human serotonin$_{1A}$ receptors. Biochemistry 49:5426–5435
73. Singh P, Saxena R, Srinivas G, Pande G, Chattopadhyay A (2013) Cholesterol biosynthesis and homeostasis in regulation of the cell cycle. PLoS One 8:e58833
74. Kandutsch AA, Russell AE (1960) Preputial gland tumor sterols: III A metabolic pathway from lanosterol to cholesterol. J Biol Chem 235:2256–2261
75. Smith DW, Lemli L, Opitz JM (1964) A newly recognized syndrome of multiple congenital anomalies. J Pediatr 64:210–217
76. Waterham HR, Wanders RJA (2000) Biochemical and genetic aspects of 7-dehydrocholesterol reductase and Smith-Lemli-Opitz syndrome. Biochim Biophys Acta 1529:340–356
77. Paila YD, Murty MRVS, Vairamani M, Chattopadhyay A (2008) Signaling by the human serotonin$_{1A}$ receptor is impaired in cellular model of Smith-Lemli-Opitz Syndrome. Biochim Biophys Acta 1778: 1508–1516
78. Porter FD, Herman GE (2011) Malformation syndromes caused by disorders of cholesterol synthesis. J Lipid Res 52:6–34
79. Kanungo S, Soares N, He M, Steiner RD (2013) Sterol metabolism disorders and neurodevelopment-an update. Dev Disabil Res Rev 17:197–210

80. Bloch KE (1983) Sterol structure and membrane function. CRC Crit Rev Biochem 14:47–92
81. Clayton P, Mills K, Keeling J, FitzPatrick D (1996) Desmosterolosis: a new inborn error of cholesterol biosynthesis. Lancet 348:404
82. FitzPatrick DR, Keeling JW, Evans MJ, Kan AE, Bell JE, Porteous MEM, Mills K, Winter RM, Clayton PT (1998) Clinical phenotype of desmosterolosis. Am J Med Genet 75: 145–152
83. Waterham HR, Koster J, Romeijn GJ, Hennekam RCM, Vreken P, Andersson HC, FitzPatrick DR, Kelley RI, Wanders RJA (2001) Mutations in the 3β-hydroxysterol Δ^{24}-reductase gene cause desmosterolosis, an autosomal recessive disorder of cholesterol biosynthesis. Am J Hum Genet 69:685–694
84. Singh P, Jafurulla M, Paila YD, Chattopadhyay A (2011) Desmosterol replaces cholesterol for ligand binding function of the serotonin$_{1A}$ receptor in solubilized hippocampal membranes: support for nonannular binding sites for cholesterol? Biochim Biophys Acta 1808:2428–2434
85. Roux C, Wolf C, Mulliez N, Gaoua W, Cormier V, Chevy F, Citadelle D (2000) Role of cholesterol in embryonic development. Am J Clin Nutr 71(5 Suppl):1270S–1279S
86. Sampson NS, Vrielink A (2003) Cholesterol oxidases: a study of nature's approach to protein design. Acc Chem Res 36:713–722
87. Pucadyil TJ, Shrivastava S, Chattopadhyay A (2005) Membrane cholesterol oxidation inhibits ligand binding function of hippocampal serotonin$_{1A}$ receptors. Biochem Biophys Res Commun 331:422–427
88. Kalipatnapu S, Chattopadhyay A (2005) Membrane protein solubilization: recent advances and challenges in solubilization of serotonin$_{1A}$ receptors. IUBMB Life 57:505–512
89. Chattopadhyay A, Rao BD, Jafurulla M (2015) Solubilization of G protein-coupled receptors: a convenient strategy to explore lipid-receptor interaction. Methods Enzymol 557:117–134
90. Jones OT, Eubanks JH, Earnest JP, McNamee MG (1988) A minimum number of lipids are required to support the functional properties of the nicotinic acetylcholine receptor. Biochemistry 27:3733–3742
91. Kirilovsky J, Schramm M (1983) Delipidation of a β-adrenergic receptor preparation and reconstitution by specific lipids. J Biol Chem 258:6841–6849
92. Pucadyil TJ, Kalipatnapu S, Chattopadhyay A (2005) The serotonin$_{1A}$ receptor: a representative member of the serotonin receptor family. Cell Mol Neurobiol 25:553–580
93. Kalipatnapu S, Chattopadhyay A (2007) Membrane organization and function of the serotonin$_{1A}$ receptor. Cell Mol Neurobiol 27:1097–1116
94. Singh P, Paila YD, Chattopadhyay A (2007) Differential effects of cholesterol and 7-dehydrocholesterol on the ligand binding activity of the hippocampal serotonin$_{1A}$ receptors: implications in SLOS. Biochem Biophys Res Commun 358:495–499
95. Chattopadhyay A, Paila YD, Jafurulla M, Chaudhuri A, Singh P, Murty MRVS, Vairamani M (2007) Differential effects of cholesterol and 7- dehydrocholesterol on ligand binding of solubilized hippocampal serotonin$_{1A}$ receptors: implications in SLOS. Biochem Biophys Res Commun 363:800–805
96. Singh DK, Rosenhouse-Dantsker A, Nichols CG, Enkvetchakul D, Levitan I (2009) Direct regulation of prokaryotic Kir channel by cholesterol. J Biol Chem 284:30727–30736
97. Westover EJ, Covey DF (2004) The enantiomer of cholesterol. J Membr Biol 202:61–72
98. Covey DF (2009) *ent*-Steroids: novel tools for studies of signaling pathways. Steroids 74:577–585
99. Bandari S, Chakraborty H, Covey DF, Chattopadhyay A (2014) Membrane dipole potential is sensitive to cholesterol stereospecificity: implications for receptor function. Chem Phys Lipids 184:25–29
100. Xu F, Rychnovsky SD, Belani JD, Hobbs HH, Cohen JC, Rawson RB (2005) Dual roles for cholesterol in mammalian cells. Proc Natl Acad Sci U S A 102:14551–14556
101. Mickus DE, Levitt DG, Rychnovsky SD (1992) Enantiomeric cholesterol as a probe of ion-channel structure. J Am Chem Soc 114:359–360
102. D'Avanzo N, Hyrc K, Enkvetchakul D, Covey DF, Nichols CG (2011) Enantioselective protein-sterol interactions mediate regulation of both prokaryotic and eukaryotic inward rectifier K^+ channels by cholesterol. PLoS One 6:e19393
103. Kristiana I, Luu W, Stevenson J, Cartland S, Jessup W, Belani JD, Rychnovsky SD, Brown AJ (2012) Cholesterol through the looking glass: ability of its enantiomer also to elicit homeostatic responses. J Biol Chem 287: 33897–33904

104. Pierce KL, Premont RT, Lefkowitz RJ (2002) Seven-transmembrane receptors. Nat Rev Mol Cell Biol 3:639–650
105. Rosenbaum DM, Rasmussen SGF, Kobilka BK (2009) The structure and function of G-protein-coupled receptors. Nature 459:356–363
106. Granier S, Kobilka B (2012) A new era of GPCR structural and chemical biology. Nat Chem Biol 8:670–673
107. Heng BC, Aubel D, Fussenegger M (2013) An overview of the diverse roles of G-protein coupled receptors (GPCRs) in the pathophysiology of various human diseases. Biotechnol Adv 31:1676–1694
108. Jacobson KA (2015) New paradigms in GPCR drug discovery. Biochem Pharmacol 98:541–555
109. Tautermann CS (2014) GPCR structures in drug design, emerging opportunities with new structures. Bioorg Med Chem Lett 24:4073–4079
110. Jafurulla M, Rao BD, Sreedevi S, Ruysschaert J-M, Covey DF, Chattopadhyay A (2014) Stereospecific requirement of cholesterol in the function of the serotonin$_{1A}$ receptor. Biochim Biophys Acta 1838:158–163
111. Jentsch TJ, Hübner CA, Fuhrmann JC (2004) Ion channels: function unravelled by dysfunction. Nat Cell Biol 6:1039–1047
112. Romanenko VG, Rothblat GH, Levitan I (2002) Modulation of endothelial inward-rectifier K^+ current by optical isomers of cholesterol. Biophys J 83:3211–3222
113. Addona GH, Sandermann H Jr, Kloczewiak MA, Miller KW (2003) Low chemical specificity of the nicotinic acetylcholine receptor sterol activation site. Biochim Biophys Acta 1609:177–182
114. Killian JA (1992) Gramicidin and gramicidin–lipid interactions. Biochim Biophys Acta 1113:391–425
115. Koeppe RE II, Andersen OS (1996) Engineering the gramicidin channel. Annu Rev Biophys Biomol Struct 25:231–258
116. Kelkar DA, Chattopadhyay A (2007) The gramicidin ion channel: a model membrane protein. Biochim Biophys Acta 1768: 2011–2025
117. Brown MS, Goldstein JL (2009) Cholesterol feedback: from Schoenheimer's bottle to Scap's MELADL. J Lipid Res 50:S15–S27
118. Brown AJ, Sun L, Feramisco JD, Brown MS, Goldstein JL (2002) Cholesterol addition to ER membranes alters conformation of SCAP, the SREBP escort protein that regulates cholesterol metabolism. Mol Cell 10:237–245
119. Adams CM, Goldstein JL, Brown MS (2003) Cholesterol-induced conformational change in SCAP enhanced by Insig proteins and mimicked by cationic amphiphiles. Proc Natl Acad Sci U S A 100:10647–10652
120. Radhakrishnan A, Goldstein JL, McDonald JG, Brown MS (2008) Switch-like control of SREBP-2 transport triggered by small changes in ER cholesterol: a delicate balance. Cell Metab 8:512–521
121. Luker GD, Pica CM, Kumar AS, Covey DF, Piwnica-Worms D (2000) Effects of cholesterol and enantiomeric cholesterol on P-glycoprotein localization and function in low-density membrane domains. Biochemistry 39:7651–7661
122. Liu J, Chang CCY, Westover EJ, Covey DF, Chang T-Y (2005) Investigating the allosterism of acyl-CoA:cholesterol acyltransferase (ACAT) by using various sterols: *in vitro* and intact cell studies. Biochem J 391:389–397
123. Ikigai H, Akatsuka A, Tsujiyama H, Nakae T, Shimamura T (1996) Mechanism of membrane damage by El Tor hemolysin of *Vibrio cholerae* O1. Infect Immun 64:2968–2973
124. Bhakdi S, Tranum-Jensen J, Sziegoleit A (1985) Mechanism of membrane damage by streptolysin-O. Infect Immun 47:52–60
125. Zitzer A, Westover EJ, Covey DF, Palmer M (2003) Differential interaction of the two cholesterol-dependent, membrane-damaging toxins, streptolysin O and *Vibrio cholerae* cytolysin, with enantiomeric cholesterol. FEBS Lett 553:229–231
126. Palmer M (2004) Cholesterol and the activity of bacterial toxins. FEMS Microbiol Lett 238:281–289

Chapter 4

Manipulating Cholesterol Status Within Cells

Winnie Luu, Ingrid C. Gelissen, and Andrew J. Brown

Abstract

Cellular cholesterol levels are intricately controlled to maintain homeostasis. Here, we describe ways in which cellular cholesterol status can be manipulated for the study of cholesterol homeostasis, including sterol starvation (by culturing cells in lipoprotein-deficient serum and pretreating/treating with the cholesterol-lowering drug, statin) and sterol enrichment (using cholesterol complexed to cyclodextrin, and low-density lipoprotein). We also describe how to prepare lipoprotein-deficient serum and complex cholesterol to cyclodextrin.

Key words Cholesterol, Lipoprotein-deficient serum, Statins, Chinese hamster ovary cells, LDL

1 Introduction

Cholesterol homeostasis is maintained by balancing cholesterol uptake, synthesis, and efflux (Fig. 1). Cholesterol can be synthesized by enzymes largely under the control of the major transcription factor, sterol-regulatory element-binding protein (SREBP)-2. SREBP-2 is produced in the endoplasmic reticulum (ER) as an inactive protein, complexed with SREBP-cleavage-activating protein (Scap). When cholesterol levels in the cell are low or insufficient, Scap escorts SREBP-2 to the Golgi to be activated. In the Golgi, SREBP-2 becomes proteolytically cleaved by site-1 and -2 protease (S1P/S2P), releasing the active N-terminal fragment to the nucleus to upregulate a set of genes to promote cholesterol synthesis [e.g., 3-hydroxy-3-methylglutaryl coenzyme A reductase (HMGCR); the classical rate-limiting enzyme of cholesterol synthesis] and uptake via the low-density lipoprotein (LDL) receptor. When cholesterol levels are sufficient or in excess, Scap is retained in the ER by the Insig retention protein, preventing the activation of SREBP-2 and hence inhibiting the activation of cholesterogenic target genes. Excess cholesterol upregulates genes involved in cholesterol export via the nuclear receptors, liver X receptor/retinoic acid receptor. This is a classic example of feedback regulation in

Ingrid C. Gelissen and Andrew J. Brown (eds.), *Cholesterol Homeostasis: Methods and Protocols*, Methods in Molecular Biology, vol. 1583, DOI 10.1007/978-1-4939-6875-6_4,

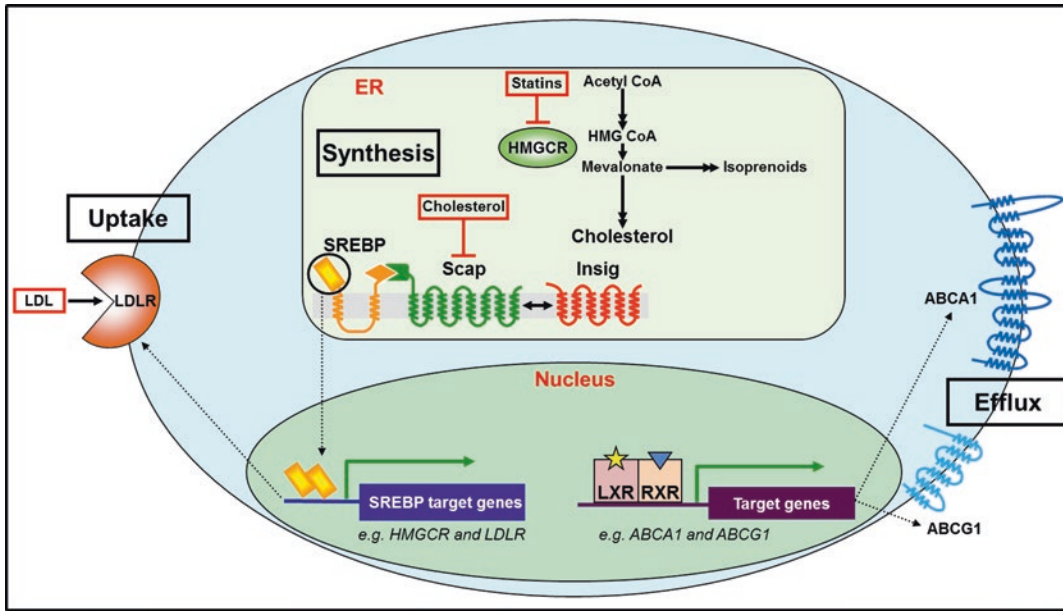

Fig. 1 Methods to manipulate cellular cholesterol homeostasis. Cellular cholesterol is balanced by cholesterol synthesis, uptake, and efflux. Cholesterol status can be lowered by treating cells with statins (HMGCR inhibitors), cyclodextrins, and LPDS. On the other hand, cells can be enriched in cholesterol by treating with Chol/CD, LDL, and in full serum. Please see text for more information. Adapted from [8]

that excess cellular cholesterol inhibits SREBP-2 activation, inhibiting cholesterol synthesis and uptake, and promoting efflux.

In this chapter, we describe ways in which cellular cholesterol status can be manipulated in cell culture studies for the study of cholesterol homeostasis, including sterol starvation and sterol enrichment. Cellular cholesterol levels can be manipulated in several ways (described in Subheading 3.3); for example, lowering basal cellular cholesterol status before a treatment to upregulate the expression of cholesterol synthesis genes. One way to do this is to pretreat and/or treat cells with a class of drugs that target HMGCR called the statins. As statins competitively inhibit a very early step in the mevalonate pathway, they also inhibit the formation of essential non-sterol products such as isoprenoids. Thus, a small amount of mevalonate (the product of HMGCR) is added to allow for the production of these products [1]. Statin pretreatment/treatment is usually performed in low cholesterol medium using lipoprotein-deficient serum (LPDS; Subheading 3.1) to decrease basal cholesterol levels. Cellular cholesterol can also be depleted using cyclodextrins, including methyl-β-cyclodextrin (MBCD) and (2-hydroxypropyl)-β-cyclodextrin (HPCD) [2]. To increase cholesterol status, cells can be treated with cholesterol (delivered to cells complexed to MBCD; Chol/CD; Subheading 3.2) or LDL, and this can be performed in media containing full serum, further enhancing cholesterol levels. Sterols can also be

depleted (e.g., by statin pretreatment) to lower basal levels before treating with Chol/CD or LDL to maximize effects.

Cell types suited for studying the regulation of cholesterol homeostasis can vary, depending on the genes of interest or research questions. We routinely use a subline of Chinese hamster ovary (CHO) cells, CHO-7, which were adapted from CHO-K1 cells to grow in LPDS medium so their basal cellular cholesterol remains low and therefore easy to manipulate, making them an ideal cell line for studying cholesterol metabolism (e.g., [3, 4]). Genetically manipulated CHO sub-lines such as sterol-regulatory deficient (SRD) cells, revealed different roles of the cholesterol homeostatic machinery [5], and can be employed in cholesterol studies. For example, SRD1 cells express high levels of active (nuclear) SREBP-2 and thus lack transcriptional regulation, and therefore can be used to exclude the possibility of transcriptional involvement in posttranscriptional effects. Table 1 highlights some useful CHO cell lines for the study of cholesterol metabolism, including the growth media and special characteristics.

Table 1
Cell lines generally used to study cholesterol homeostasis (generated by the Dallas laboratory of Michael Brown and Joseph Goldstein)

CHO sub-lines	Growth media[a]	Special characteristics	Reference
CHO-K1	10 % (v/v) FCS/Ham's F12	Parental CHO cells	
CHO-7	5 % (v/v) NCLPDS/DMEM/F12	Adapted to grow in LPDS	[10]
CHO/pGFP-Scap	5 % (v/v) NCLPDS/DMEM/F12	Stably expresses pGFP-Scap useful for fluorescence microscopy	[11]
SRD1	5 % (v/v) NCLPDS/DMEM/F12 supplemented with 1 μg/mL 25HC	Express high levels of nuclear SREBP	[10]
SRD2	5 % (v/v) NCLPDS/DMEM/F12 supplemented with 1 μg/mL 25HC		[10]
SRD3	5 % (v/v) NCLPDS/DMEM/F12 supplemented with 2 μg/mL 25HC		[12]
SRD4	5 % (v/v) NCLPDS/DMEM/F12 supplemented with 1 μg/mL 25HC	Mutation in Scap	[13]
SRD5	5 % (v/v) FCLPDS/DMEM/F12 supplemented with 1 μg/mL 25HC	Mutation in Scap	[14]
SRD6	5 % FCS/DMEM/F12 supplemented with 5 μg/mL cholesterol, 1 mM mevalonate	Express low levels of nuclear SREBP	[15]
SRD8	5 % (v/v) NCLPDS/DMEM/F12 supplemented with 1 μg/mL 25HC	Mutation in Scap	[16]

(continued)

Table 1
(continued)

CHO sub-lines	Growth media[a]	Special characteristics	Reference
SRD9	5 % (v/v) NCLPDS/DMEM/F12 supplemented with 1 μg/mL 25HC	Mutation in Scap	[17]
SRD12A/B	5 % FCS/DMEM/F12 supplemented with 5 μg/mL cholesterol, 1 mM mevalonate, 20 μM sodium oleate	Lacks S1P	[18]
SRD13A	5 % (v/v) NCS/DMEM/F12 supplemented with 5 μg/mL cholesterol, 1 mM mevalonate, 20 μM sodium oleate	A sterol-regulatory deficient CHO cell line lacking Scap	[19]
SRD14	5 % (v/v) NCLPDS/DMEM/F12 supplemented with 500 μg/mL G418	Lacks Insig-1	[20]
SRD15	5 % (v/v) FCS/DMEM/F12 supplemented with 5 μg/mL cholesterol, 1 mM mevalonate, 20 μM sodium oleate, 500 μg/mL G418	Lacks Insig-1 and -2	[21]

[a]Other media may also be suitable for various cell lines (e.g., CHO-K1 can also be maintained in F-12K medium)

2 Materials

2.1 General Reagents

1. Cell lines of interest, such as SRD1 cells.
2. Lipoprotein-deficient serum (LPDS) (described in Subheading 3.1).
3. Cholesterol complexed to MBCD [Chol/CD; commercially available, or can be prepared in-house (described in Subheading 3.2)].
4. LDL (commercially available, or can be isolated in-house as described in [6]).
5. Statin (e.g., 10 mM mevastatin, also called compactin, in DMSO).
6. Mevalonate (0.5 M in 100 % ethanol).

2.2 Preparation of NCLPDS or FCLPDS

1. Serum: newborn calf serum to make newborn calf lipoprotein-deficient serum (NCLPDS) and fetal calf serum to make fetal calf lipoprotein-deficient serum (FCLPDS).
2. Potassium bromide (KBr).
3. Dialysis tubing cellulose membrane (25 mm; typical molecular weight cutoff of 14,000).
4. 150 mM sodium chloride (NaCl) (*see* **Note 1**).
5. Protein assay (e.g., bicinchoninic acid assay).

6. 0.22 μm sterile syringe filters.
7. Ultracentrifuge.
8. Fixed-angle rotor (e.g., Hitachi P70AT, Beckman Type 70 Ti) or equivalent.
9. Ultracentrifuge tubes (*see* **Note 2**).
10. Heat sealer and heat sealing caps.
11. 14G, 18G, and 27½G needles and syringes.

2.3 Preparation of Chol/CD

1. Cholesterol stock (15 mg/mL in 100 % ethanol).
2. 5 % (w/v) MBCD in ultrapure water.
3. Stirring heat block.
4. Micro magnetic stir bars (5 mm × 2 mm).
5. Vacuum centrifuge or freeze dryer to lyophilize the Chol/CD.

3 Methods

3.1 Preparation of LPDS

This method has been adapted from [7]. Please *see* Fig. 2 for an overview of the method.

3.1.1 Serum Heat-Inactivation

1. Thaw frozen serum at room temperature, or in the fridge overnight (*see* **Note 3**).
2. Set the waterbath to 56 °C and allow the temperature to equilibrate (*see* **Note 4**).
3. When the temperature is steady, place serum in waterbath for 30 min, swirling the bottle every 5 min to allow even heat distribution.
4. Cool on ice (*see* **Note 5**) and aliquot serum into sterile tissue culture tubes for storage at −20 °C, or further processing under Subheading 3.1.2.

3.1.2 Density Adjustment and Ultracentrifugation

1. Transfer 300 mL of serum into a beaker.
2. Adjust the density of serum to 1.215 g/mL with KBr by adding 101 g per 300 mL serum.
3. Stir at room temperature until the KBr is dissolved.
4. Allow the serum solution to reach room temperature before loading into the ultracentrifuge tubes (*see* **Note 6**).
5. Draw serum solution into a 50 mL syringe fitted with a 14G needle, and load 8 ultracentrifuge tubes with ~40 mL serum solution (*see* **Note 7**).
6. Weigh each tube (including its ultracentrifuge cap) and balance each pair according to the ultracentrifuge specification (e.g., within 0.002 × *g*).

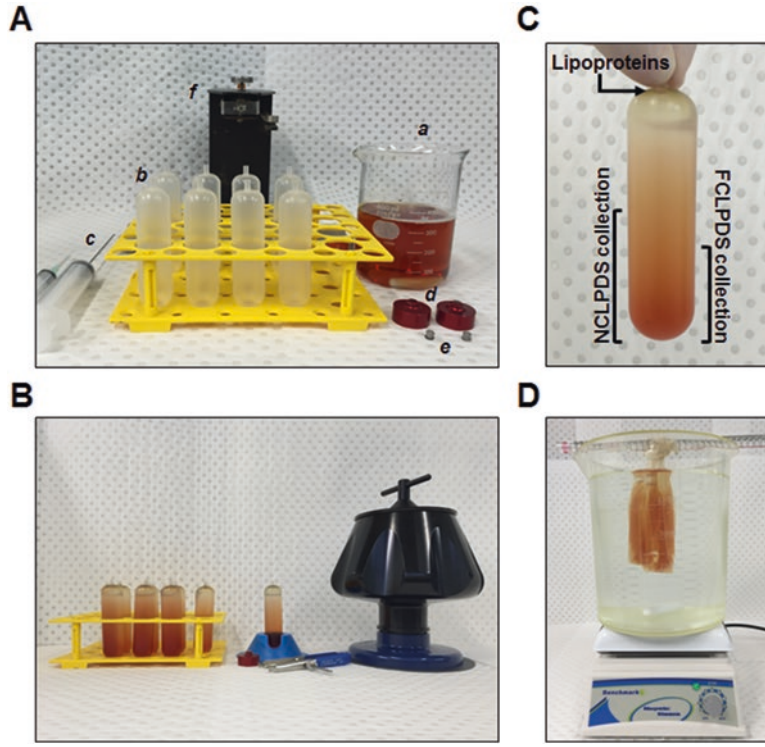

Fig. 2 Preparation of LPDS. (**a**) Heat-inactivated serum was density-adjusted with potassium bromide (*a*), and transferred into ultracentrifuge tubes (*b*) with a syringe fitted with a 14G needle (*c*). Ultracentrifuge tubes were weighed with the ultracentrifuge caps (*d*), fitted with heat-sealing caps (*e*) for heat-sealing (*f*), and then ultracentrifuged. (**b**, **c**) After centrifugation, 2 fractions should be observed: top fraction containing lipoproteins, and bottom fraction containing LPDS (*brown*). (**d**) The pooled LPDS fraction was dialyzed against five changes of sodium chloride solution. Please see text for more information

7. Heat-seal the tubes and check for leaks before reweighing and placing the tubes into the ultracentrifuge rotor (*see* **Note 8**).
8. Spin the tubes using the following ultracentrifugation settings:
   - Time: 22–24 h.
   - Speed: 250,000 × *g*, acceleration fast, deceleration slow.
   - Temperature: 10 °C.
9. Turn on the vacuum, and start the centrifugation.
10. After the centrifuge has stopped, release the vacuum.
11. Remove the tubes from the ultracentrifuge (*see* **Note 9**). Two fractions should be observed; the top fraction containing lipoproteins, and the bottom containing LPDS (Fig. 2b, c).
12. Carefully puncture the top of the tubes using a 27½ G needle to introduce an air hole (*see* **Note 10**).

13. Clean the bottom of the tube with ethanol, and then puncture one or two holes on the bottom side of the tube with a sharp 18G needle (*see* **Notes 11** and **12**).
14. For each tube, collect approximately two-thirds of the NCLPDS fraction, or approximately half of the FCLPDS fraction, allowing the LPDS fraction to drip into one clean beaker (Fig. 2c).

3.1.3 Dialysis of LPDS

1. Cut approximately ~2 m of dialysis tubing, and boil by microwaving in a 1 L beaker of ultrapure water for 10 min to soften the tubing.
2. Rinse three times with ultrapure water and drain.
3. Tie one end securely and run approximately 5 mL of LPDS through the tubing to ensure there are no leaks (*see* **Note 13**).
4. Fill the tubing with the full volume of LPDS, leaving a lot of empty space for tying the tube and liquid expansion.
5. Tie the tubing securely at the end and check the tubing for leaks.
6. Fold the tubing over a stirring rod, and suspend in a beaker containing 5 L of 150 mM NaCl, ensuring that the LPDS is fully covered by the NaCl solution (Fig. 2d).
7. Dialyze by gently stirring at 4 °C, ensuring that the stirrer does not hit the bottom of the tubing.
8. Change the dialysis solution (5 L of 150 mM NaCl) four more times. Dialysis should be against five changes of NaCl solution over 48–72 h (*see* **Note 14**).
9. After dialysis, cut the tubing at one end and empty the LPDS into a beaker (*see* **Note 15**).
10. Take an aliquot to measure protein concentration (*see* **Note 16**).
11. Adjust LPDS to a protein concentration of 50 mg/mL for NCLPDS, and 30 mg/mL for FCLPDS, using 150 mM NaCl (*see* **Note 17**).
12. Filter-sterilize the LPDS through a 0.22 μm syringe filter, and store in suitable aliquots at −20 °C.
13. Use the Amplex red assay to verify that the total cholesterol content of the LPDS is <5 % of the level in whole serum.

3.2 Preparation of Chol/CD

1. Prepare 1.5 mL tubes each containing 500 μL of 5 % (w/v) MBCD in ultrapure water.
2. Clean micro magnetic stir bars by washing and vortexing in ethanol three times, and place into the tubes containing the MBCD solution.
3. Set the stirring heat block to 80 °C.
4. Fill the heating block holes with water for better heat transfer, and place tubes in the heating block and stir.

5. Add 10 μL of 15 mg/mL cholesterol stock into each tube, and stir gently until the cholesterol has dissolved (*see* **Notes 18** and **19**).
6. Repeat **step 5** until a total of 50 μL of cholesterol stock has been added to each tube.
7. Stir at 80 °C for another 30 min, or until the cholesterol is stably incorporated into MBCD solution (i.e., when solution looks clear).
8. Spin tubes at 1000 × *g* for 30 s, and remove the micro magnetic stir bar from the tubes.
9. Snap freeze the solution using liquid nitrogen or dry ice for 2 min (*see* **Note 20**).
10. Lyophilize (using a Speedvac system) the frozen cholesterol/MBCD overnight, or until all liquid is evaporated and a white fluffy powder remains.
11. Store Chol/CD aliquots at −20 °C until use.
12. Immediately before use, add 375 μL of ultrapure water into the tube, vortex well until the complex is dissolved (*see* **Note 21**). Under sterile conditions, filter the Chol/CD into new sterile tubes with 0.22 μm syringe filter (*see* **Note 22**).

3.3 Treatment of Cells to Manipulate Cholesterol Content

Below is an example method to first decrease cellular cholesterol status, and then increase it to maximize the difference in cholesterol status, and potentially increase observed effects. For details of further manipulations, please *see* Table 2.

1. Seed SRD1 cells at 60–80 % confluence in 5 % (v/v) NCLPDS/DMEM/F12.
2. Pretreat cells overnight in 5 % (v/v) NCLPDS/DMEM/F12 containing 5 μM mevastatin and 50 μM mevalonate.
3. Treat cells in 5 % (v/v) NCLPDS/DMEM/F12 containing 5 μM mevastatin and 50 μM mevalonate, with or without 20 μg/mL Chol/CD for up to 8 h.
4. Measure desired output. For an example of endogenous squalene monooxygenase protein degradation in SRD1 cells, please *see* Fig. 3.

4 Notes

1. If preparing the 150 mM NaCl solution in advance, this should be stored at 4 °C to avoid contamination of the LPDS.
2. Purchase Polyallomer Quick-Seal Centrifuge Tubes specific to the rotor used.

Table 2
Ways to manipulate cellular cholesterol status

Effect	Method	Conditions	Comments
Lower cholesterol status	Statin treatment	Use 5 μM mevastatin as a pretreatment (e.g., overnight) and/or in the treatment[a]	• Statins inhibit HMGCR, decreasing cholesterol synthesis, which in turn upregulates SREBP-2 target genes (e.g., HMGCR) • Pretreating/treating cells with statins is done in the presence of 50 μM mevalonate to allow for adequate isoprenoid synthesis (but not enough for the mevalonate to reenter the cholesterol synthesis pathway)
	Inhibitors of the cholesterol synthesis enzymes	For example, treating cells with inhibitors of squalene synthase (e.g., Zaragozic acid A trisodium salt at 150 μM),squalene monooxygenase (e.g., GR144000X at 10 μM), or lanosterol synthase (R048-8071 at 10 μM) for up to 8 h [3]	• Similar effects to statin treatment
	LPDS	Use LPDS instead of full serum in the pretreatment and/or treatment medium	
	Cyclodextrin	Treat cells with 5 % (w/v) MBCD or 1 % (w/v) HPCD for up to 8 h	• Treating with cyclodextrin extracts plasma membrane cholesterol, which lowers the overall cellular cholesterol status
Increase cholesterol status	Chol/CD	Treat cells with 20 μg/mL Chol/CD for up to 8 h, or 5 μg/mL for longer incubations, to avoid cellular toxicity	• A reductionist way of delivering cholesterol without adding other lipids • A less physiological way of delivering cholesterol
	LDL	Treat cells with 50 μg/mL LDL for up to 16 h	• A more physiological way of delivering cholesterol • However, there are lipids other than cholesterol in LDL
	Full serum	Use in cell culture medium, or in pretreatment and/or treatment medium	

[a]Concentrations and times of inhibitors and treatments listed are examples used in our lab or references quoted and should be optimized for each specific cell type

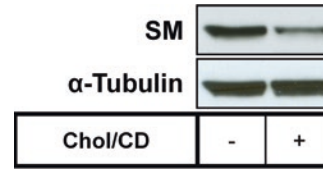

Fig. 3 Chol/CD treatment accelerates squalene monooxygenase degradation. SRD1 cells were pretreated with 5 μM mevastatin and 50 μM mevalonate in LPDS containing media overnight, and then treated with 5 μM mevastatin and 50 μM mevalonate, with or without Chol/CD, for 8 h. Cell lysates were subjected to SDS-PAGE and blotted for endogenous squalene monooxygenase (SM) and the housekeeping protein, α-tubulin. Cholesterol treatment accelerates SM degradation, as seen in [3, 9]

3. Thawing serum in a 37 °C waterbath may result in proteins and lipids concentrating at the bottom of the bottle and appearing as white globules.
4. To equilibrate the temperature to 56 °C, insert a thermometer into a similar container filled with water (same volume as the serum).
5. Heat-inactivated serum can be stored at −20 °C long term, at this step.
6. Allowing the chilled solution to warm up to room temperature avoids condensation that can form on the outside of the tube, which can affect the weight of the tube.
7. After drawing the serum into the syringe, wipe the needle with lint-free wipe before ejecting into the tube to avoid wetting the neck of the tube, as this would reduce spillage while the tube is filled. Be careful not to introduce air bubbles by slowly ejecting the serum to the side of the tube. If they are introduced, add more solution until the air bubbles are pushed out. Wipe off any residue on the tube with ethanol.
8. Small pieces of sticky tape can be added to the bottom of the tubes to increase their weight.
9. Be careful not to bump the tubes as lipoproteins at the top can easily contaminate the pure LPDS at the bottom.
10. Place a lint-free wipe near the top of the tube while puncturing the tube to avoid spillage.
11. Ensure different needles are used for the top (lipoprotein fraction) and bottom (LPDS fraction) of the tube to avoid contaminating the LPDS with lipoproteins.
12. Puncturing the bottom side of the tube rather than at the bottom of the tube avoids the salt pellet, which is discarded.

13. Dry the tubing using paper towel to make checking for leaks easier.
14. Preparation of LPDS can be performed in one working week. We recommend/suggest the following working schedule for this protocol:
    - Day 1: Serum preparation and ultracentrifugation (Subheadings 3.1.1 and 3.1.2).
    - Day 2: Harvest LPDS (Subheading 3.1.2, steps 10–14), and start dialysis #1 overnight (Subheading 3.1.3, steps 1–7).
    - Day 3: Perform dialysis #2 from morning to afternoon, and dialysis #3 overnight.
    - Day 4: Perform dialysis #4 from morning to afternoon, and dialysis #5 overnight.
    - Day 5: Adjust LPDS protein concentration, and filter-sterilize (Subheading 3.1.3, **steps 9–13**).
15. LPDS can be stored in the fridge for a few days if needed, but needs to be frozen at −20 °C for long-term storage.
16. When measuring protein concentration of LPDS, perform several dilutions (e.g., 1:100, 1:200, 1:300, 1:400, and 1:500) of the LPDS to ensure an accurate determination.
17. The FCLPDS has lower protein content than NCLPDS. These estimations are based on the fact that approximately 30 mg/mL was the maximum amount we could consistently achieve in our lab using the conditions described.
18. This protocol can also be used to complex other sterols to MBCD.
19. To avoid ethanol evaporation, minimize opening of the tube, and wet the pipette tip with cholesterol/ethanol stock several times before dispensing it into the MBCD.
20. Snap frozen Chol/CD can be stored at −20 °C overnight if necessary.
21. Alternatively, Chol/CD can be reconstituted into the required cell culture media.
22. Final concentration of Chol/CD is 2 mg/mL, and can be stored at 4 °C up to 1 month.

Acknowledgments

We thank Dr. Laura J. Sharpe, Anika V. Prabhu, and Vicky Howe for critically reviewing the manuscript. The Brown Lab is supported by a UNSW Goldstar Award and a grant from the National Health and Medical Research Council (1060515).

References

1. Nakanishi M, Goldstein JL, Brown MS (1988) Multivalent control of 3-hydroxy-3-methylglutaryl coenzyme A reductase. Mevalonate-derived product inhibits translation of mRNA and accelerates degradation of enzyme. J Biol Chem 263(18):8929–8937
2. Zidovetzki R, Levitan I (2007) Use of cyclodextrins to manipulate plasma membrane cholesterol content: evidence, misconceptions and control strategies. Biochim Biophys Acta 1768(6):1311–1324
3. Gill S, Stevenson J, Kristiana I, Brown AJ (2011) Cholesterol-dependent degradation of squalene monooxygenase, a control point in cholesterol synthesis beyond HMG-CoA reductase. Cell Metab 13(3):260–273
4. Prabhu AV, Luu W, Sharpe LJ, Brown AJ (2016) Cholesterol-mediated degradation of 7-dehydrocholesterol reductase switches the balance from cholesterol to vitamin D synthesis. J Biol Chem 291(16):8363–8373
5. Goldstein JL, Rawson RB, Brown MS (2002) Mutant mammalian cells as tools to delineate the sterol regulatory element-binding protein pathway for feedback regulation of lipid synthesis. Arch Biochem Biophys 397(2):139–148
6. Schumaker VN, Puppione DL (1986) Sequential flotation ultracentrifugation. Meth Enzymol 128:155–170
7. Goldstein JL, Basu SK, Brown MS (1983) Receptor-mediated endocytosis of low-density lipoprotein in cultured cells. Meth Enzymol 98:241–260
8. Luu W, Sharpe LJ, Gelissen IC, Brown AJ (2013) The role of signalling in cellular cholesterol homeostasis. IUBMB Life 65(8):675–684
9. Zelcer N, Sharpe LJ, Loregger A, Kristiana I, Cook EC, Phan L, Stevenson J, Brown AJ (2014) The E3 ubiquitin ligase MARCH6 degrades squalene monooxygenase and affects 3-hydroxy-3-methyl-glutaryl coenzyme A reductase and the cholesterol synthesis pathway. Mol Cell Biol 34(7):1262–1270
10. Metherall JE, Goldstein JL, Luskey KL, Brown MS (1989) Loss of transcriptional repression of three sterol-regulated genes in mutant hamster cells. J Biol Chem 264(26):15634–15641
11. Nohturfft A, Yabe D, Goldstein JL, Brown MS, Espenshade PJ (2000) Regulated step in cholesterol feedback localized to budding of SCAP from ER membranes. Cell 102(3):315–323
12. Dawson PA, Metherall JE, Ridgway ND, Brown MS, Goldstein JL (1991) Genetic distinction between sterol-mediated transcriptional and posttranscriptional control of 3-hydroxy-3-methylglutaryl-coenzyme A reductase. J Biol Chem 266(14):9128–9134
13. Metherall JE, Ridgway ND, Dawson PA, Goldstein JL, Brown MS (1991) A 25-hydroxycholesterol-resistant cell line deficient in acyl-CoA: cholesterol acyltransferase. J Biol Chem 266(19):12734–12740
14. Yabe D, Xia ZP, Adams CM, Rawson RB (2002) Three mutations in sterol-sensing domain of SCAP block interaction with insig and render SREBP cleavage insensitive to sterols. PNAS 99(26):16672–16677
15. Evans MJ, Metherall JE (1993) Loss of transcriptional activation of three sterol-regulated genes in mutant hamster cells. Mol Cell Biol 13(9):5175–5185
16. Nohturfft A, Hua X, Brown MS, Goldstein JL (1996) Recurrent G-to-A substitution in a single codon of SREBP cleavage-activating protein causes sterol resistance in three mutant Chinese hamster ovary cell lines. PNAS 93(24):13709–13714
17. Nohturfft A, Brown MS, Goldstein JL (1998) Sterols regulate processing of carbohydrate chains of wild-type SREBP cleavage-activating protein (SCAP), but not sterol-resistant mutants Y298C or D443N. PNAS 95(22):12848–12853
18. Rawson RB, Cheng D, Brown MS, Goldstein JL (1998) Isolation of cholesterol-requiring mutant Chinese hamster ovary cells with defects in cleavage of sterol regulatory element-binding proteins at site 1. J Biol Chem 273(43):28261–28269
19. Rawson RB, DeBose-Boyd R, Goldstein JL, Brown MS (1999) Failure to cleave sterol regulatory element-binding proteins (SREBPs) causes cholesterol auxotrophy in Chinese hamster ovary cells with genetic absence of SREBP cleavage-activating protein. J Biol Chem 274(40):28549–28556
20. Sever N, Lee PC, Song BL, Rawson RB, Debose-Boyd RA (2004) Isolation of mutant cells lacking Insig-1 through selection with SR-12813, an agent that stimulates degradation of 3-hydroxy-3-methylglutaryl-coenzyme A reductase. J Biol Chem 279(41):43136–43147
21. Lee PC, Sever N, Debose-Boyd RA (2005) Isolation of sterol-resistant Chinese hamster ovary cells with genetic deficiencies in both Insig-1 and Insig-2. J Biol Chem 280(26): 25242–25249

Chapter 5

Assaying Low-Density-Lipoprotein (LDL) Uptake into Cells

Anke Loregger, Jessica K. Nelson, and Noam Zelcer

Abstract

Determination of LDL particle uptake into cells is a valuable technique in the field of cholesterol metabolism. This allows assessment of LDL uptake capacity in different adherent and non-adherent cells types, as well as the effect of cellular, genetic, or pharmacological perturbations on this process. Here, we detail a general procedure that describes the production of fluorescently-labeled LDL particles and quantitative and non-quantitative assays for determining cellular LDL uptake.

Key words Cholesterol metabolism, LDL, LDLR, Endocytosis

1 Introduction

Cholesterol is vital for mammalian life [1]. Apart from its important function as an integral component of cellular membranes, cholesterol is essential for diverse cellular processes and signaling pathways. However, cholesterol's physiochemical properties, particularly its inherent insolubility in water, pose a challenge when it comes to transporting this molecule throughout the body. For this reason, cholesterol and other lipids are packaged into lipoprotein particles, which are trafficked systemically. Lipoproteins are particles that contain triacylglycerol, phospholipids, cholesterol, and amphipathic proteins called apolipoproteins (for a detailed review of lipoproteins see Hegele et al. [2]). The four major classes of lipoproteins are chylomicrons, very low-density lipoprotein (VLDL), low-density lipoprotein (LDL), and high-density lipoprotein (HDL), which vary in their triacylglycerol, phospholipid, cholesterol, and protein composition. Amongst these, LDL constitutes ~50% of the total lipoprotein mass in the plasma. It contains a single protein, $ApoB_{100}$, and lipids (~25 and ~75% of mass, respectively), the latter consisting of ~6–8% free cholesterol, ~45–50% cholesteryl ester, ~18–24% phospholipid, and ~4–8% triacylglycerols [2]. LDL is a major carrier of cholesterol to peripheral cells, accounting for over 60% of the total cholesterol in plasma.

Ingrid C. Gelissen and Andrew J. Brown (eds.), *Cholesterol Homeostasis: Methods and Protocols*, Methods in Molecular Biology, vol. 1583, DOI 10.1007/978-1-4939-6875-6_5,

Extensive epidemiological studies have shown that elevated levels of circulating LDL-cholesterol is a well-established risk factor for atherosclerosis, which is the primary cause for coronary artery disease and ensuing cardiovascular complications that account for ~25% of world-wide deaths [3]. As such, the transport and uptake of LDL to hepatic and non-hepatic tissues is extensively coordinated and is an important determinant of LDL levels in the circulation. Endocytosis of LDL depends on the interactions of the sole protein in LDL, $ApoB_{100}$ with a dedicated plasma membrane receptor, the LDL receptor (LDLR) [4]. The LDLR-LDL complex is internalized from the plasma membrane by clathrin-mediated endocytosis where it dissociates as a result of the decreasing pH in the endosomal transport system. Subsequently, the LDL particle is delivered to lysosomes from which cholesterol can be salvaged for cellular use, whereas the receptor is recycled back to the cell surface for a new round of uptake.

Hepatic LDLR activity is a central determinant of circulating levels of LDL. Accordingly, mutations in the *LDLR* are the leading cause of autosomal dominant hypercholesterolemia [5]. In line with its crucial function in cholesterol homeostasis, LDLR abundance is tightly regulated at the transcriptional as well as post-transcriptional level. Transcriptional levels of the *LDLR* are primarily determined by the sterol response element-binding protein (SREBP) transcription factors [6]. On a post-translational level, the SREBP target gene proprotein convertase subtilisin/kexin 9 (PCSK9) and the Liver X receptors (LXR) target gene inducible degrader of the LDLR (IDOL) control LDLR abundance [7–10]. While both PCSK9 and IDOL increase lysosomal degradation of the LDLR, the underlying mechanism they use for doing so is distinct [8]. Acting as an E3 ubiquitin ligase, IDOL promotes ubiquitination of the intracellular tail of LDLR, thereby targeting it for lysosomal degradation. In contrast, PCSK9 is a secreted protein that binds to the extracellular domain of LDLR, and after internalization prevents receptor recycling back to the plasma membrane, thereby increasing its lysosomal degradation. These pathways are also of clinical relevance. Recently, antibodies that target PCSK9 and thereby increase hepatic LDLR levels and LDL clearance have shown strong LDL-lowering potency [11, 12], and are being currently introduced into clinical practice [13]. Strategies to pharmacologically inhibit IDOL activity with small molecules are also being investigated, but are at an earlier phase of development.

To study the activity of the LDLR we describe below a general approach to determine LDL uptake into cells, using fluorescently-labeled LDL. Originally, studies of LDLR function were carried out using radioactive assays based on the measurement of binding,

uptake and degradation of ^{125}I-labeled LDL. Although radioactive assays have the advantage of being very sensitive, iodination of LDL is expensive, requires specific expertise and equipment, and handling radioactive material is subject to strict regulations. In contrast, performing these assays using fluorescently-labeled LDL, as described below, is an inexpensive and simple alternative that is suitable for both adherent and non-adherent cells and can be used to provide qualitative or quantitative information.

2 Materials

Prepare all solutions using ultrapure water (dH_2O) and analytical grade reagents and follow all waste disposal regulations when disposing of waste materials.

2.1 Isolation of Human LDL

Human LDL can be purchased from different commercial suppliers. Alternatively, the isolation procedure is included in this Chapter and reagents required listed below.

1. EDTA stock solution 0.5 M (pH 8.0): 186.1 g of disodium EDTA (Na_2EDTA) in 800 mL dH_2O; adjust the pH to 8.0 with NaOH (~50 mL): bring volume to 1 L with dH_2O; stir vigorously on a magnetic stirrer (*see* **Note 1**).
2. NaCl/EDTA solution (0.9% (w/v) NaCl/1 mM EDTA): Dissolve 9 g NaCl in 900 mL dH_2O, add 2 mL of 0.5 M EDTA stock and bring volume to 1 L with dH_2O.
3. Make density solutions with KBr (1.225 and 1.100 g/mL) in NaCl/EDTA solution.
4. EDTA-containing blood collection tubes.
5. Beckman L-70 ultracentrifuge with a SW-40 rotor or equivalent equipment.
6. Suitable ultracentrifuge tubes.

2.2 Labeling LDL

1. DyLight 488 NHS-Ester can be purchased. Alternatively, other DyLight Dyes, with absorption spectra ranging from 350 to 770 nm are commercially available and can be substituted. Dissolve reagent in DMF to 10 mg/mL.
2. PBS: To prepare 1 L of 1× PBS, dissolve 8 g NaCl, 0.2 g KCl, 1.44 g Na_2HPO_4 and 0.24 g KH_2PO_4 in 800 mL of dH_2O. Adjust the pH to 7.4 with HCl, and add dH_2O to a final volume of 1 L.
3. Dialysis tubing or dialysis slides with a molecular weight cutoff of 14 kDa.

2.3 LDL-Cholesterol Uptake Assay

1. Simvastatin stock solution 5 mg/mL: Dilute commercially available simvastatin sodium salt in DMSO. Use as 2000× solution (final concentration: 2.5 μg/mL).
2. 200 mM mevalonic acid: Dissolve 1 g of mevalonolactone in 20 mL of 1 N NaOH. Stir overnight at RT and then transfer to 50 mL conical tube. Add 385 μL of 2 M HEPES (pH 7.4). Adjust the pH to 7.4 by drop-wise addition of concentrated HCl. Incubate at 37 °C overnight maintaining the pH at 7.4. Bring the volume to 38.4 mL with dH_2O, then sterilize by filtration. Aliquot and store at −20 °C. Use as 2000× solution (final concentration: 100 μM).
3. Sterol-depletion medium: Culture medium supplemented with 10% (v/v) lipoprotein-deficient FCS (*see* **Note 2**), 2.5 μg/mL simvastatin and 100 μM mevalonic acid.
4. DMEM-BSA (0.5% (w/v)): Dissolve 0.5 g BSA per 100 mL DMEM.
5. PBS-BSA (0.5% (w/v)): Dissolve 0.5 g BSA per 100 mL PBS.

2.4 Quantification of LDL-Cholesterol Uptake in Total Cell Lysates

1. RIPA (radioimmunoprecipitation assay) buffer: 150 mM NaCl, 1% (w/v) NP-40, 0.5% (w/v) SDS (sodium dodecyl sulphate), 50 mM Tris–HCl; pH 8.0. Protease inhibitors should be added freshly before use.
2. Fluorescence microplate reader: Typhoon FLA-9500 imager or equivalent.
3. Black 384-well microplates with a flat and transparent bottom or equivalent.
4. BCA protein assay kit.

2.5 Quantification of LDL-Cholesterol Uptake Using Fluorescence Assisted Cell Sorting (FACS)

1. FACS buffer: 2 mM EDTA, 0.5% (w/v) BSA (added freshly) in PBS; pH 7.4.
2. Non-enzymatic dissociation reagent to release the cells from the cell surface, for example Trypsin or Trypsin-EDTA.
3. FACS machine: Any FACS equipped with a laser capable of excitation at 488 nm and emission filters at 518 nm (for DyLight 488) can be used.

2.6 Imaging of Cellular LDL-Cholesterol Uptake

1. 4% paraformaldehyde: Dilute 16% paraformaldehyde (w/v; Methanol-free; commercially available) with PBS.
2. Mounting medium with DAPI (4′,6-diamidino-2-phenylindole; commercially available) (*see* **Note 3**).
3. Glass coverslips.
4. Fluorescent microscope with compatible filters or a confocal laser-scanning microscope, equipped with a 488-nm laser (for DyLight 488-labeled LDL) and a 405-nm laser (for DAPI).

3 Methods

3.1 Isolation of Human LDL

Serum lipoproteins comprise a heterogeneous population of lipid–protein complexes that can be grouped into different classes: very low (VLDL), low (LDL), and high (HDL) density, each having a different protein and lipid composition as also reflected in their density. The density of VLDL is <1.006 g/mL, of LDL 1.019–1.063 g/mL, and that of HDL is 1.063–1.21 g/mL. This difference in density can be used to specifically isolate any given lipoprotein. To isolate human LDL (d 1.019–1.063 g/mL) from plasma, a one-step ultracentrifugation procedure [14] is described here. *Important*: As human plasma is potentially a source of blood-borne disease, wear gloves and eye protection during the whole procedure.

1. Draw blood from a normolipidemic adult volunteer, and collect blood into EDTA-containing tubes.
2. Separate plasma from whole blood by centrifugation at 1000 × *g* for 20 min at 4 °C and use freshly. Alternatively, purchase human plasma.
3. Add 2.695 g KBr to 7 mL of plasma (final density of 1.25 g/L).
4. Transfer 3.5 mL density-adjusted plasma to a centrifuge tube. Gently overlay this with KBr solutions (Subheading 2.1, **item 3**) as follows: Add first 2 mL of 1.225 g/mL solution, followed by 4 mL of 1.100 g/mL solution, and then 3 mL of NaCl/EDTA solution (Subheading 2.1, **item 2**).
5. Centrifuge the gradient using a swing-out bucket rotor (SW-40) at 105,000 × *g* for 20 h at 10 °C (with brakes set to "off") in a Beckman L-70 ultracentrifuge (or equivalent).
6. After centrifugation, collect the LDL fraction by slicing the tube using a tube slicer (*see* **Note 4**). To do so, firmly position the tube between two rubber rings and with care make a cut between the LDL fraction (above) and the HDL fraction (below) (Fig. 1). Subsequently, from the cut tube collect the LDL band with a pipette.
7. To confirm whether one-step ultracentrifugation provides LDL of acceptable purity, one can subject the isolated LDL fraction to high-performance gel-permeation chromatography (HPGC). To do so, run 60 μL of isolated LDL on a Superose 6 HR 10/30 column [15].
8. Determine the LDL concentration by measuring ApoB using a commercially available nephelometric assay on an auto-analyzer system. ApoB is the only protein constituent of LDL and its levels can be directly used to standardize the uptake assay

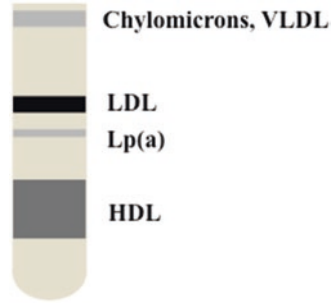

Fig. 1 Schematic diagram of lipoprotein-subclass separation after gradient density centrifugation

according to the equivalent number of LDL particles. Alternatively, use a BCA assay to determine the protein content of the isolated LDL and use this to standardize the uptake assay.

9. LDL can be stored at 4 °C for up to 1 month. However, it is preferable to directly continue with the LDL labeling procedure.

3.2 Fluorescent Labeling of Isolated LDL

DyLight 488-labeled LDL can be produced as previously described [16].

1. Mix 1–10 mg of purified LDL with DyLight 488 NHS-Ester in a volume of 100 μL–1 mL. The amount of fluorescent-labeling reagent to use for each reaction depends on the amount of protein in the LDL fraction. Follow the manufacturer's instructions and calculate the appropriate amount of fluorophore needed. For example, we label ~1 mg of LDL (as determined by ApoB mass) with ~20 μg of the DyLight 488 NHS-Ester in a total volume of 1 mL.
2. Mix well by inverting the tube and incubate the reaction at room temperature for 1 h in the dark. Mix regularly. Do not vortex the tube as this can lead to LDL aggregation.
3. Subsequently, to remove excess non-reacted dye, dialyze the reaction mixture 4 h for at least four times against 1 L PBS.
4. Store DyLight488-labeled LDL in a light-protective tube in the dark at 4 °C for up to 1 month. Discard when formation of precipitates is observed.

3.3 Cellular LDL-Cholesterol Uptake Assay

We describe a general strategy for conducting the LDL uptake assay. Depending on the specific experiment, the cell type, number of cells, well size, and other experimental parameters may be adjusted. After performing the assay, several readouts to evaluate LDL uptake are available.

Day 1

1. Seed cells in a 12-well plate and allow them to reach 70% confluency (e.g. for human hepatic HepG2 cells, seed 250,000 cells per well).

Day 2

1. Wash cells twice with pre-warmed PBS.
2. When grown in standard growth medium containing 10% (v/v) serum, most cells have low LDLR levels and low basal LDL uptake activity. Therefore, to increase LDLR abundance, cells should be incubated in sterol-depletion medium for 16–24 h (*see* **Note 5**).

Day 3

1. Wash cells twice with pre-warmed PBS.
2. Incubate cells with 5 μg/mL DyLight488-labeled LDL in DMEM-BSA for 1 h at 37 °C. As controls, include cells that are treated as above, but with addition of excess (100 μg/mL) unlabeled LDL, and cells incubated with DMEM-BSA only. These controls can be later used to determine the specific LDL uptake into cells.
3. To terminate the assay, wash cells twice with ice-cold PBS-BSA followed by one wash with ice-cold PBS (*see* **Note 6**).

At this point, cellular LDL uptake can be assessed as described under Subheadings 3.4–3.6, either by determining (readout 1) fluorescence in total cell lysates, (readout 2) cellular fluorescence by FACS, (readout 3) cellular fluorescence by imaging. Note that the first two readouts are quantitative, whereas the latter is qualitative in nature.

3.4 Quantification of LDL-Cholesterol Uptake in Total Cell Lysates

Perform the LDL-uptake assay as described in Subheading 3.3.

1. To cells from **step 6**, add ice-cold RIPA buffer (1 mL per 5×10^6 cells) supplemented with protease inhibitors (*see* **Note 7**).
2. Gently rock plate for 30 min at 4 °C in the dark to facilitate cell lysis.
3. Collect total cell lysates by quantitatively transferring the lysate to a pre-chilled microcentrifuge tube.
4. Centrifuge the tube at 4 °C for 10 min at 14,000 × *g* to remove cell debris.
5. Transfer the supernatant to a fresh pre-chilled tube on ice and discard the original tube.
6. The fluorescent signal in the total cell lysate can now be measured. Transfer 30 μL of each lysate to a well of a black 384-well microplate with a flat and transparent bottom (*see* **Note 8**).

7. To measure fluorescence on the Typhoon imager, set excitation to 473 nm and filter LPB. Determine the scan area, sensitivity, and resolution and scan plate. Once scan is completed, save the associated image for further analysis.
8. Using image analysis software (e.g. Image J) to quantify the fluorescent signal in each well. Keep the size and position of the measured area consistent between wells. Preferably, use a grid-based measurement procedure. For each measured value, subtract the background (i.e. fluorescence measured from cells that have been incubated with an excess of non-labeled LDL).
9. For each cell lysate, determine protein concentration using a BCA kit following the manufacturer's instructions. Normalize the corrected fluorescence signal to protein level, and plot averages (*see* **Note 9**).

3.5 Quantification of Cellular LDL-Cholesterol Uptake by Fluorescence Activated Cell Sorting (FACS)

Perform the LDL-uptake assay as described in Subheading 3.3.

1. To cells from **step 6**, add a non-enzymatic dissociation reagent to release the cells from the cell surface. Note that dissociation of some cell types may require the use of Trypsin or Trypsin-EDTA (*see* **Note 10**). Cover the cell monolayer and incubate at 37 °C until cells detach from the surface.
2. Add 1 mL FACS-buffer to dissociated cells. If using trypsin, add medium containing serum to the cell suspension to inhibit further trypsinisation, which may damage cells. Alternatively, when culturing in serum-free conditions, soybean trypsin inhibitor can be used to stop trypsinisation.
3. Transfer cell suspension to a microcentrifuge tube. From this point on, keep cells and all solutions cold.
4. Centrifuge cells at 500 × *g* for 5 min at 4 °C.
5. Wash cells once with cold FACS buffer.
6. Resuspend cells in FACS buffer to a density of 1–3 × 10^6 cells per mL (typically 200–400 μL of buffer is required).
7. Transfer cells to a FACS compatible tube and measure the fluorescent signal in the cells by FACS (Fig. 2).

3.6 Imaging of Cellular LDL-Uptake

If a qualitative assessment of LDL uptake in cells is sufficient, imaging can be used instead of the quantitative assessments described under Subheadings 3.4 and 3.5 (*see* **Note 11**).

1. Grow cells on glass coverslips to a confluence of approximately 70%.
2. Perform the LDL-uptake assay as described above in Subheading 3.3.

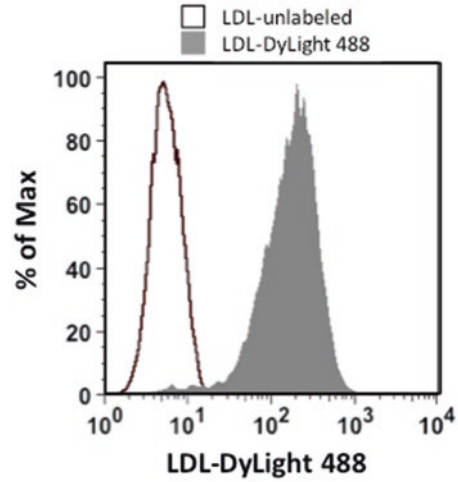

Fig. 2 FACS analysis of LDL uptake in A431 cells. Cells were cultured in sterol-depletion medium for 16 h to induce expression of the LDLR. Subsequently, cells were incubated with 5 μg/mL LDL-DyLight 488 (*grey*) or unlabeled LDL (*white*) for 1 h at 37 °C, after which cells were washed and prepared for FACS analysis as described in the text. Note the large increase in cellular LDL content following uptake of DyLight488-labeled LDL

3. Following the wash steps, fix the cells with 4% (w/v) paraformaldehyde in PBS for 20 min at room temperature in the dark.
4. Wash the fixed cells three times with PBS.
5. For long-term storage and visualization of the nucleus, mount the cells on microscope slides using mounting medium containing DAPI (fluorescence excitation/emission maxima: 358/461 nm).
6. Examine the uptake of DyLight 488-labeled LDL into cells using a fluorescent microscope with compatible filters. Alternatively, a confocal laser scanning microscope equipped with a 488-nm laser (for DyLight 488-labeled LDL) and a 405-nm laser (for DAPI) can be used (Fig. 3).
7. Store microscope slides at 4 °C in the dark.

4 Notes

1. The di-sodium salt of EDTA will not dissolve until the pH of the solution is adjusted to 8.0 by addition of NaOH.
2. Lipoprotein-deficient FCS is commercially available or can be prepared following the procedure described by Redgrave et al. [17].
3. DAPI fluoresces when bound to DNA and is used as a nuclear counterstain.

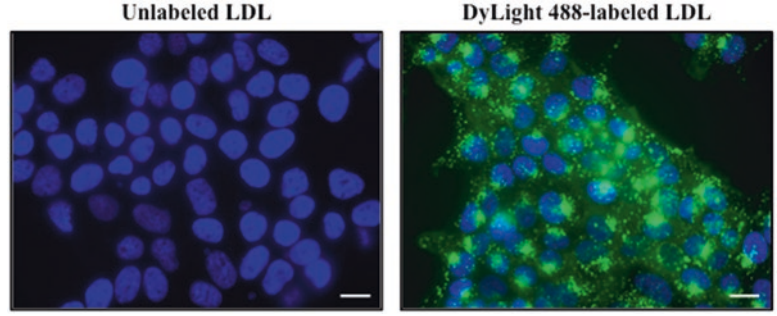

Fig. 3 Imaging of fluorescent LDL uptake in A431 cells. Cells were grown on glass coverslips and cultured for 16 h in sterol-depletion medium to induce expression of the LDLR. Subsequently, cells were incubated with 5 μg/mL LDL-DyLight 488 or unlabeled LDL for 1 h at 37 °C, washed, fixed and prepared for fluorescent microscopy. Size bar is 10 μm

4. If a tube slicer is not available, the LDL band can be drawn out with a syringe and fine needle. Ensure that the ultracentrifugation tube has been pierced with a small needle at the top for air to be drawn in when the LDL band is removed.
5. Dependent on the cell type, cells can be cultured in sterol-depletion medium for 12 to 30 h. This should be determined for each cell type.
6. To assess LDL binding to cells (i.e. a proxy for LDL-LDLR association at the cell surface), LDL uptake assays can be conducted at 4 °C, as this will prevent subsequent endocytosis of LDL. Keep buffers cold as well.
7. Other lysis buffers are compatible with this protocol. The advantage of using RIPA is that this buffer allows protein extraction of cytoplasmic, membrane and nuclear proteins and is compatible with many downstream applications, including immunoblotting.
8. Any instrument compatible with measuring DyLight 488 (excitation: 493 nm; emission: 518 nm) can be used. We use a Typhoon FLA-9500 imager (GE Healthcare), a laser scanner with multiple imaging applications including sensitive and quantitative measurements of fluorescence. Subheading 3.4, **steps 7** and **8** can be adjusted when using other instruments.
9. Culturing cells in sterol-depletion medium should increase LDL uptake several fold. Treatment of cells with recombinant PCSK9 or with an IDOL-inducing LXR agonist (e.g. GW3695) will result in decreased LDLR abundance and LDL uptake. If required, these treatments can be included as controls in LDL uptake experiments.
10. Trypsin solutions can range from 0.025 to 0.5% (w/v). Different cell lines require varying trypsin concentrations and

incubation times for detachment. These parameters should be determined for each cell line. If trypsin must be used to dissociate the cells, limit the treatment to the minimum required time.

11. In parallel, immunofluorescence staining can be performed in order to immune-localize additional proteins of interest (e.g., LDLR).

Acknowledgment

We thank Dr. Geesje M. Dallinga-Thie (AMC, The Netherlands) for her advice and comments. AL is supported by a Dekker grant from the Dutch Heart Foundation (2016T015). NZ is an Established Investigator of the Dutch Heart Foundation (2013T111) and is supported by an ERC Consolidator grant (617376) from the European Research Council.

References

1. Maxfield FR, van Meer G (2010) Cholesterol, the central lipid of mammalian cells. Curr Opin Cell Biol 22:422–429
2. Hegele RA (2009) Plasma lipoproteins: genetic influences and clinical implications. Nat Rev Genet 10:109–121
3. Mozaffarian D et al (2015) Heart disease and stroke statistics--2015 update: a report from the American Heart Association. Circulation 131:e29–322
4. Brown MS, Goldstein JL (1986) A receptor-mediated pathway for cholesterol homeostasis. Science 232:34–47
5. Hobbs HH, Russell DW, Brown MS, Goldstein JL (1990) The LDL receptor locus in familial hypercholesterolemia: mutational analysis of a membrane protein. Annu Rev Genet 24:133–170
6. Goldstein JL, DeBose-Boyd RA, Brown MS (2006) Protein sensors for membrane sterols. Cell 124:35–46
7. Zelcer N, Hong C, Boyadjian R, Tontonoz P (2009) LXR regulates cholesterol uptake through Idol-dependent ubiquitination of the LDL receptor. Science 325:100–104
8. Sorrentino V, Zelcer N (2012) Post-transcriptional regulation of lipoprotein receptors by the E3-ubiquitin ligase inducible degrader of the low-density lipoprotein receptor. Curr Opin Lipidol 23: 213–219
9. Abifadel M et al (2003) Mutations in PCSK9 cause autosomal dominant hypercholesterolemia. Nat Genet 34:154–156
10. Cohen J et al (2005) Low LDL cholesterol in individuals of African descent resulting from frequent nonsense mutations in PCSK9. Nat Genet 37:161–165
11. Blom DJ et al (2014) A 52-week placebo-controlled trial of evolocumab in hyperlipidemia. N Engl J Med 370:1809–1819
12. Stein EA et al (2012) Effect of a monoclonal antibody to PCSK9 on LDL cholesterol. N Engl J Med 366:1108–1118
13. Stein EA, Raal F (2014) Reduction of low-density lipoprotein cholesterol by monoclonal antibody inhibition of PCSK9. Annu Rev Med 65:417–431
14. Kleinveld HA, Duif PF, Pekelharing HL, van Rijn HJ (1996) Oxidation of lipoprotein(a) and low density lipoprotein containing density gradient ultracentrifugation fractions. Biochim Biophys Acta 1303:15–21
15. Levels JHM, Lemaire LCJM, van den Ende AE, van Deventer SJH, van Lanschot JJB (2003) Lipid composition and lipopolysaccharide binding capacity of lipoproteins in plasma and lymph of patients with systemic inflammatory response syndrome and multiple organ failure. Crit Care Med 31:1647–1653
16. Motazacker MM et al (2012) Advances in genetics show the need for extending screening strategies for autosomal dominant hypercholesterolaemia. Eur Heart J 33:1360–1366
17. Redgrave TG, Roberts DC, West CE (1975) Separation of plasma lipoproteins by density-gradient ultracentrifugation. Anal Biochem 65:42–49

Chapter 6

The Use of L-sIDOL Transgenic Mice as a Murine Model to Study Hypercholesterolemia and Atherosclerosis

Eser J. Zerenturk and Anna C. Calkin

Abstract

There are many advantages to the use of mice as a model to study the regulation of cholesterol metabolism. Common models of hypercholesterolemia include low-density lipoprotein receptor deficient (LDLR −/−) mice and apolipoprotein E deficient (ApoE) −/− mice. Herein, we describe the recently generated mouse model, L-sIDOL Tg mice, which express a dominant active form of Inducible Degrader Of the Low-density lipoprotein receptor (IDOL) in a liver-specific manner. This murine model offers significant advantages over previously established models for the study of hypercholesterolemia and atherosclerosis.

Key words Hypercholesterolemia, Atherosclerosis, Mouse model, LDL cholesterol, Liver, Transgenic, IDOL, LDLR

1 Introduction

Studies in mice have made a significant contribution to our understanding of the mechanisms that regulate cholesterol metabolism [1–5]. Mice provide considerable advantages in terms of ease of breeding, timeframe to generate litters, maintenance cost, and their ability to be genetically manipulated. However, mice are intrinsically resistant to the development of hypercholesterolemia and atherosclerosis, and their lipoprotein profile differs from that seen in humans, in part due to the lack of cholesterol ester transfer protein (CETP). This has been somewhat overcome by novel gene manipulations which have led to mouse models with lipoprotein profiles that more closely resemble that seen in humans, with concomitant atherosclerotic lesion development. Commonly utilized mouse models of hypercholesterolemia and atherosclerosis include low-density lipoprotein receptor deficient (LDLR −/−) mice, apolipoprotein E deficient (ApoE −/−) mice and ApoE*3 Leiden mice [6–10]. Herein, we describe our recently developed novel mouse model of hypercholesterolemia and

Ingrid C. Gelissen and Andrew J. Brown (eds.), *Cholesterol Homeostasis: Methods and Protocols*, Methods in Molecular Biology, vol. 1583, DOI 10.1007/978-1-4939-6875-6_6,

diet-induced atherosclerosis, which has distinct advantages over the abovementioned models, for the study of cholesterol metabolism and atherosclerosis.

Liver specific sIDOL transgenic (L-sIDOL Tg) mice express a dominant-active form of Inducible Degrader Of the LDLR (IDOL) termed "sIDOL" in a liver specific manner via the albumin promoter [11, 12]. IDOL is an E3 ligase linked to the regulation of plasma cholesterol levels in humans [13–16]. IDOL-mediated degradation of hepatic LDLR in these mice results in reduced uptake of LDL cholesterol via the liver, leading to an elevation in plasma cholesterol levels. Hypercholesterolemia is exacerbated on a western diet in a time-dependent manner in these mice, and is associated with the development of atherosclerotic lesions [12]. Significant advantages of this mouse model over other available models include their susceptibility to lesion development on a western diet without the need for specialized diets such as those with added cholate. With respect to breeding strategy, these mice have the distinct advantage of being a monoallelic transgenic model. This makes the breeding strategy to generate a compound mutant to investigate a given gene of interest simpler and thus more time and cost effective. Moreover, wild type littermates are generated in a 1:1 ratio with L-sIDOL Tg mice, making the generation of experimental cohorts an efficient process. L-sIDOL Tg mice exhibit a lipid profile which mimics that seen in humans, with the majority of their cholesterol in the LDL fraction. This is in contrast to ApoE−/− and ApoE*3 Leiden mice, which carry much of their cholesterol in the very-low-density lipoprotein (VLDL) fraction. Finally, L-sIDOL mice are an uncomplicated model of hypercholesterolemia as this model exclusively targets IDOL-mediated LDLR degradation in the liver. This is in contrast to the widely used LDLR−/− mice, which harbor a global deletion of LDLR. Currently, the relative contribution of specific tissues to the phenotype of LDLR−/− mice is unclear, making this a complex model with which to study cholesterol metabolism. This can be a potentially confounding factor dependent upon the mechanisms of cholesterol metabolism to be studied. Furthermore, the presence of residual LDLR levels in L-sIDOL Tg mice affords investigators the potential to study effects on this pathway.

2 Materials

2.1 Mice

1. L-sIDOL Tg mice (Jackson Laboratories).
2. Wild type C57Bl/6J mice (Jackson Laboratories).
3. Genetic model of interest (e.g., knockout or transgenic) as required.

2.2 Genotyping Reagents

1. Ear punch/tail clipper.
2. Standard DNA isolation/PCR genotyping kit(s).
3. Primers (For 5′-GCC AGG AGG GCT CTG TAC A-3′; Rev 5′ GAA TAG AAT GAC ACC TAC TCA GAC AAT-3′).
4. Agarose.
5. Tris–acetate–EDTA (TAE) buffer. 50× TAE stock: 242 g Tris base, 57.1 mL acetate, 100 mL of 0.5 M EDTA, to 1 L with deionized H_2O (dH_2O).
6. Nucleic acid stain.
7. Deionized water.
8. Gel casting tray and comb.
9. Electrophoresis tank.
10. DNA ladder standard.
11. Gel imaging apparatus.

2.3 Diets

1. Chow diet.
2. Western diet.

3 Methods

3.1 Breeding Strategy

1. Breed mice to heterozygosity by mating L-sIDOL Tg mice with wild type C57Bl/6J mice (*see* **Notes 1–3**).
2. To generate a compound mutant where the gene of interest is a single transgene model (*Tg), simply cross L-sIDOL Tg mice with your model of interest. This will generate all the required genotypes (wild type, L-sIDOL Tg, *Tg and L-sIDOL/* double Tg) in a 1:1:1:1 ratio (*see* **Note 4**).
3. To generate a compound L-sIDOL Tg mutant, where the model of interest is a homozygous knockout (Gene X −/−), requires a multistep breeding process. Homozygous knockout mice should first be crossed with L-sIDOL Tg mice, which will generate mice all heterozygous for the deletion of the gene of interest, of which 50% will carry the sIDOL transgene, based on Mendelian ratios (Table 1, cross 1). The second breeding step requires breeding homozygous knockout mice with L-sIDOL Tg mice heterozygote for the gene of interest. This will generate 50% of mice heterozygous for deletion of the gene of interest and 50% homozygous knockout for the gene of interest (Table 1, cross 2). Of these mice, 50% will carry the sIDOL transgene in a 1:1:1:1 ratio. Thus, this step generates the specific genotype of interest, a mouse homozygous negative for the gene of interest, which carries the sIDOL transgene (25%). Breeding of this genotype to knockout mice will generate the

Table 1
Breeding Strategy to generate a compound L-sIDOL Tg mutant mouse where the model of interest is a knockout mouse

Cross	Mice generated	Ratios
1. Gene X (−/−) L-sIDOL WT × Gene X (+/+) L-sIDOL Tg	Gene X (+/−), L-sIDOL WT Gene X (+/−), L-sIDOL Tg	1:1
2. Gene X (−/−) L-sIDOL WT × Gene X (+/−), L-sIDOL Tg	Gene X (+/−) L-sIDOL WT Gene X (+/−) L-sIDOL Tg Gene X (−/−) L-sIDOL WT Gene X (−/−) L-sIDOL Tg	1:1:1:1
3. Gene X (−/−) L-sIDOL WT × Gene X (−/−) L-sIDOL Tg	Gene X (−/−) L-sIDOL WT Gene X (−/−) L-sIDOL Tg	1:1

two specific genotypes of interest as littermates in a 1:1 ratio (Table 1, cross 3), (*see* **Note 4**).

3.2 Genotyping Strategy

1. Take a tail or ear clipping from mice, preferably at 2 weeks of age (*see* **Note 5**).
2. Isolate DNA from tail/ear tissue samples according to the manufacturer's instructions.
3. Undertake genotyping PCR according to the manufacturer's instructions using the abovementioned primer set.
4. Prepare 1× TAE Buffer from 50× stock by adding 20 mL of 50× stock to 980 mL of dH_2O.
5. Prepare 2% (w/v) agarose gel by adding 2 g of agarose to 100 mL of 1× TAE buffer. Heat until dissolved. Cool until ~37 °C, then add the nucleic acid stain (*see* **Note 6**). Pour into casting tray and add comb (*see* **Note 7**).
6. Once gel is set, place in an electrophoresis tank. Fill tank with 1× TAE buffer until it completely covers the gel.
7. Load samples into gel as well as a DNA ladder standard.
8. Run gel for ~20 min at 100 V.
9. Image gel. A band will appear at ~550 base pairs to indicate the presence of the sIDOL transgene. This band will be absent in wild type mice.

3.3 Experimental Design

1. At 6–8 weeks of age, place mice on a western diet.
2. Run experiment to the desired level of hypercholesterolemia and/or atherosclerosis. Figure 1 demonstrates the level of hypercholesterolemia achieved with a Western Diet containing 21% (w/w) fat and 0.21% (w/w) cholesterol after 20 or 30 weeks. The concomitant deposition of atherosclerotic lesions observed at these time points is shown in Fig. 2 (*see* **Note 8**).

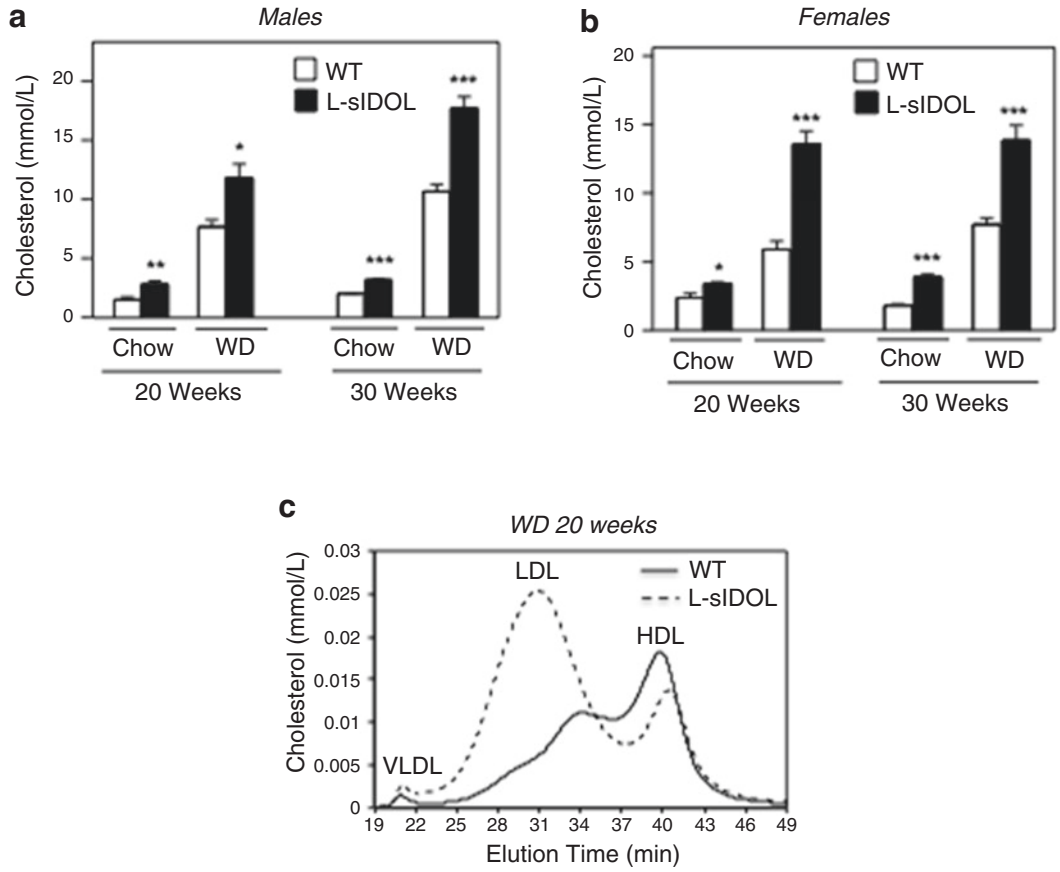

Fig. 1 Plasma Cholesterol levels in L-sIDOL Tg mice. Plasma cholesterol levels in wild type (WT) and L-sIDOL Tg mice following chow and western diet (WD) feeding for 20 or 30 weeks in male (**a**) and female (**b**) mice; high performance liquid chromatography (HPLC) chromatogram of plasma cholesterol after 20 weeks on WD (**c**). Data are expressed as mean ± SEM (**a**, **b**); $*p < 0.05$, $**p < 0.01$; $***p < 0.001$ vs. matched WT. Adapted from Calkin et al. [12]

4 Notes

1. Crossing wild type mice with L-sIDOL Tg mice should result in Mendelian ratios of 50% wild type and 50% transgenic. It is not recommended to breed mice to homozygosity as the sIDOL transgene is randomly inserted into the DNA. Any phenotype attributed to this random insertion could become markedly more apparent in the presence of two alleles. Furthermore, the abovementioned genotyping strategy is not designed to distinguish whether one or two copies of the transgene are present.

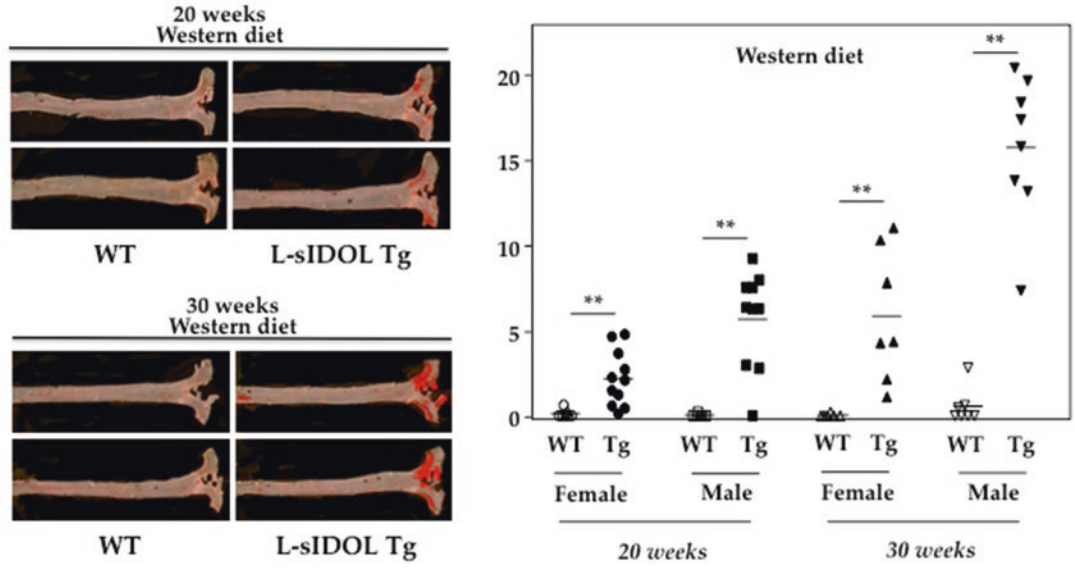

Fig. 2 *En face* analysis of lesion deposition in L-sIDOL Tg mice. Representative images of *en face* assessment of atherosclerotic lesions (Sudan IV) in wild type (WT) and L-sIDOL transgenic (Tg) mice after 20 and 30 weeks of western diet, *left*; quantitation of *en face* lesion deposition in mice as detailed, *right*. Data are expressed as mean ± SEM; $^{**}p < 0.01$ vs. matched WT; Adapted from Calkin *et al.* [12]

2. L-sIDOL Tg mice were generated on a C57Bl/6J background. To avoid any confounding factors due to strain variation, it is recommended to cross mice with "wild type" C57Bl/6J mice.
3. If mice are not breeding, then separate them for ~1 week, before placing them back together.
4. Ensure that the genetically modified mouse model of interest is of the same background strain (C57Bl/6J).
5. If mice are ear clipped at 2 weeks of age, required genotypes can be confirmed prior to weaning which can save on agistment costs.
6. As an alternative to adding the nucleic acid stain to the agarose gel itself, it can be added to the samples at the time of electrophoresis.
7. If bubbles appear when pouring agarose gel, use a pipette tip to burst bubble or drag it away to the side.
8. Dependent upon the level of hypercholesterolemia and/or atherosclerosis required, the content of cholesterol in the diet can be varied to modulate this. Alternatively, cholate can be added to the diet to further potentiate hypercholesterolemia and atherosclerosis.

Acknowledgements

This work was supported in part by the Victorian Government's Operational Infrastructure Support Program. Anna C. Calkin is supported by a National Heart Foundation of Australia Future Leader Fellowship (100067). Eser J. Zerenturk is supported by a National Heart Foundation of Australia Post-doctoral Fellowship (101275).

References

1. Jiang XC, Masucci-Magoulas L, Mar J, Lin M, Walsh A, Breslow JL, Tall A (1993) Down-regulation of mRNA for the low density lipoprotein receptor in transgenic mice containing the gene for human cholesteryl ester transfer protein. Mechanism to explain accumulation of lipoprotein B particles. J Biol Chem 268:27406–27412
2. Su K, Sabeva NS, Wang Y, Liu X, Lester JD, Liu J, Liang S, Graf GA (2014) Acceleration of biliary cholesterol secretion restores glycemic control and alleviates hypertriglyceridemia in obese db/db mice. Arterioscler Thromb Vasc Biol 34:26–33
3. Van Rooyen DM, Gan LT, Yeh MM, Haigh WG, Larter CZ, Ioannou G, Teoh NC, Farrell GC (2013) Pharmacological cholesterol lowering reverses fibrotic NASH in obese, diabetic mice with metabolic syndrome. J Hepatol 59:144–152
4. Matsuda M, Korn BS, Hammer RE, Moon YA, Komuro R, Horton JD, Goldstein JL, Brown MS, Shimomura I (2001) SREBP cleavage-activating protein (SCAP) is required for increased lipid synthesis in liver induced by cholesterol deprivation and insulin elevation. Genes Dev 15:1206–1216
5. Engelking LJ, Kuriyama H, Hammer RE, Horton JD, Brown MS, Goldstein JL, Liang G (2004) Overexpression of Insig-1 in the livers of transgenic mice inhibits SREBP processing and reduces insulin-stimulated lipogenesis. J Clin Invest 113:1168–1175
6. Ishibashi S, Brown MS, Goldstein JL, Gerard RD, Hammer RE, Herz J (1993) Hypercholesterolemia in low density lipoprotein receptor knockout mice and its reversal by adenovirus-mediated gene delivery. J Clin Invest 92:883–893
7. Ishibashi S, Goldstein JL, Brown MS, Herz J, Burns DK (1994) Massive xanthomatosis and atherosclerosis in cholesterol-fed low density lipoprotein receptor-negative mice. J Clin Invest 93:1885–1893
8. Plump AS, Smith JD, Hayek T, Aalto-Setala K, Walsh A, Verstuyft JG, Rubin EM, Breslow JL (1992) Severe hypercholesterolemia and atherosclerosis in apolipoprotein E-deficient mice created by homologous recombination in ES cells. Cell 71:343–353
9. Zhang SH, Reddick RL, Piedrahita JA, Maeda N (1992) Spontaneous hypercholesterolemia and arterial lesions in mice lacking apolipoprotein E. Science 258:468–471
10. van Vlijmen BJ, van't Hof HB, Mol MJ, van der Boom H, van der Zee A, Frants RR, Hofker MH, Havekes LM (1996) Modulation of very low density lipoprotein production and clearance contributes to age- and gender-dependent hyperlipoproteinemia in apolipoprotein E3-Leiden transgenic mice. J Clin Invest 97:1184–1192
11. Calkin AC, Goult BT, Zhang L, Fairall L, Hong C, Schwabe JW, Tontonoz P (2011) FERM-dependent E3 ligase recognition is a conserved mechanism for targeted degradation of lipoprotein receptors. Proc Natl Acad Sci U S A 108:20107–20112
12. Calkin AC, Lee SD, Kim J, Van Stijn CM, Wu XH, Lusis AJ, Hong C, Tangirala RI, Tontonoz P (2014) Transgenic expression of dominant-active IDOL in liver causes diet-induced hypercholesterolemia and atherosclerosis in mice. Circ Res 115:442–449
13. Chasman DI, Pare G, Mora S, Hopewell JC, Peloso G, Clarke R, Cupples LA, Hamsten A, Kathiresan S, Malarstig A et al (2009) Forty-three loci associated with plasma lipoprotein size, concentration, and cholesterol content in genome-wide analysis. PLoS Genet 5:e1000730
14. Sorrentino V, Fouchier SW, Motazacker MM, Nelson JK, Defesche JC, Dallinga-Thie GM, Kastelein JJ, Kees Hovingh G, Zelcer N (2013) Identification of a loss-of-function inducible degrader of the low-density lipoprotein receptor variant in individuals with low circulating low-density lipoprotein. Eur Heart J 34:1292–1297

15. Weissglas-Volkov D, Calkin AC, Tusie-Luna T, Sinsheimer JS, Zelcer N, Riba L, Tino AM, Ordonez-Sanchez ML, Cruz-Bautista I, Aguilar-Salinas CA et al (2011) The N342S MYLIP polymorphism is associated with high total cholesterol and increased LDL receptor degradation in humans. J Clin Invest 121:3062–3071
16. Zelcer N, Hong C, Boyadjian R, Tontonoz P (2009) LXR regulates cholesterol uptake through Idol-dependent ubiquitination of the LDL receptor. Science 325:100–104

Chapter 7

CRISPR/Cas9-Mediated Generation of Niemann–Pick C1 Knockout Cell Line

Ximing Du, Ivan Lukmantara, and Hongyuan Yang

Abstract

Generating a cholesterol storage phenotype of Niemann–Pick Type C (NPC) disease is important for investigating the mechanisms of intracellular cholesterol trafficking, as well as screening drugs for potential treatment of NPC disease. The use of the CRISPR/Cas9 technology to knockout specific genes within the genome of mammals has become routine in the past few years. Here, we describe a protocol for producing a cellular NPC cholesterol storage phenotype in HeLa cells using the CRISPR-Cas9 system to disrupt the *NPC1* gene. The protocol details the steps for single guide RNA oligo cloning, cell colony selection, and cell line verification by filipin staining and immunoblotting.

Key words Cholesterol, NPC1, CRISPR, Cas9, sgRNA, Filipin

1 Introduction

Niemann–Pick type C1 protein (NPC1) is a large membrane protein localized to late endosomes and lysosomes. Loss-of-function mutations in NPC1 cause NPC disease, characterized by abnormal cholesterol storage in late endosomes and lysosomes [1, 2]. Reproducing the cholesterol storage phenotype in NPC1-deficient cells is pivotal for studying intracellular cholesterol trafficking and homeostasis, understanding the molecular mechanisms of NPC1, and testing drugs for possible treatment of NPC disease. U18666A, a cationic amphiphile that blocks NPC1 function [3], and small-interference RNA or small-hairpin RNA that target the *NPC1* gene have been widely used to generate the NPC cholesterol storage phenotype in cell models, albeit mostly in a transient manner. In the past few years, the use of the Clustered Regularly Interspaced Short Palindromic Repeats (CRISPR)-Cas9 genome editing technology has exploded and made it possible to generate stable NPC1-deficient cell lines, reproducing cholesterol storage phenotype in a permanent state.

Ingrid C. Gelissen and Andrew J. Brown (eds.), *Cholesterol Homeostasis: Methods and Protocols*, Methods in Molecular Biology, vol. 1583, DOI 10.1007/978-1-4939-6875-6_7,

The CRISPR-Cas9 system is an adaptive immune system used by select microbes to defend themselves against invading viruses. Remarkably, this system has now been engineered and become a popular technique suitable for numerous applications, including genome editing in living cells of mammals and other organisms, generating animal models of human-inherited disorders, and specifically turning on or off the genes of interest [4]. Cas9 is an RNA-guided nuclease that is capable of binding to a target DNA, thereby introducing a double strand break (DSB) in a sequence specific manner [5]. The specificity of Cas9 is determined by a single guide RNA (sgRNA) that recognizes the complementary 20-nucleotide genomic sequence with a downstream protospacer-adjacent motif (PAM) sequence [6, 7]. Guided by sgRNA, Cas9 introduces DSBs approximately three nucleotides upstream of the PAM sequence [8]. DSBs are then repaired by the host DNA damage repair mechanisms. This can be accomplished by using either the homology-directed repair (HDR) pathway that precisely modifies a specific gene in the presence of a donor double-stranded or single-stranded DNA template, or the error-prone non-homologous end-joining (NHEJ) pathway, which gives rise to small insertions and deletions, essentially knocking out a specific gene [9].

This chapter describes a protocol for employing the CRISPR-Cas9 system to disrupt the *NPC1* gene in HeLa cells. The protocol consists of three main sections: cloning of a sgRNA oligo duplex into a Cas9 expression vector, selection of HeLa cells transfected with the sgRNA/Cas9 co-expression plasmid for single cell clones, and verification of the *NPC1* gene disruption by immunoblotting and filipin staining.

2 Materials

2.1 Molecular Cloning

1. Cas9 expression plasmid: PX459 (pSpCas9-2A-Puro V2.0; Addgene).
2. DNA oligos (standard desalted) for sgRNA constructions (*see* **Note 1**).
3. Cloning enzymes: FastDigest BbsI (BpiI) (Thermo Scientific/Fermentas), T4 Polynucleotide kinase (PNK) and T4 DNA ligase (New England BioLabs).
4. 10× T4 PNK buffer (New England BioLabs).
5. 10× T4 DNA ligase buffer (New England BioLabs).
6. 10× Tango buffer (Thermo Scientic/Fermentas).
7. 10 mM adenosine 5′-triphosphate (ATP).
8. Ultrapure water (RNAse/DNAse-free).

9. One Shot Stbl3 chemically competent *E. coli* (Life Technologies).
10. Ampicillin sodium salt powder.
11. Luria Broth (LB) medium.
12. LB agar plates (LB medium supplemented with 2 % (w/v) of agar and 100 μg/mL of ampicillin).
13. QIAprep spin miniprep kit (Qiagen).
14. PureLink® PCR Purification Kit (Life Technologies).
15. NucleoBond® Xtra Midi kits (Macherey-Nagel GmbH & Co. KG).
16. Sequencing primer: GAGGGCCTATTTCCCATGATTCC.

2.2 Cell Culture

1. HeLa cell line.
2. Dulbecco's Modified Eagle's Medium (DMEM), high glucose.
3. Fetal bovine serum (FBS).
4. Penicillin–streptomycin–glutamine (100×).
5. Opti-MEM® Reduced Serum Medium.
6. TrypLE™ Express Enzyme (1×), no phenol red (Gibco™).
7. Lipofectamine® LTX Reagent with PLUS™ Reagent (Invitrogen™) or equivalent transfection reagent.
8. Puromycin dihydrochloride.
9. DPBS, no calcium, no magnesium.
10. Cell culture dish (6-cm), 6-, 12-, and 96-well cell culture plates.
11. Nunc Lab-Tek Chamber Slide system 8 wells, glass slide.

2.3 Filipin Staining

1. Filipin complex from *Streptomyces filipinensis*, approximately 50 μg/mL in PBS: For a quick preparation of the filipin solution, dip a yellow tip in the original stock of filipin powder, then quickly dip the yellow tip with the filipin powder attached into a microcentrifuge tube containing 15 μL of DMSO for dissolving. Dilute further in 9 mL of PBS for staining.
2. 4 % Paraformaldehyde in PBS: In a fume hood, add 1 ampule (10 mL) of 16 % (w/v) paraformaldehyde solution (commercially available) to 30 mL of PBS in a 50 mL falcon centrifuge tube. Make fresh on the day.
3. ProLong® Gold Antifade Mountant (Life Technologies).
4. Leica wide-field microscope (CTR5500) equipped with an EL6000 fluorescent lamp and a DFC300 FX digital camera (360/40-nm excitation and 470/50-nm band-pass emission) or equivalent microscope.

2.4 Western Blotting

1. TGX™ FastCast™ Acrylamide Solutions (10 % w/v) (Bio-Rad).
2. 1× running buffer for Tris-Glycine SDS-PAGE.
3. 1× Tris-Glycine Transfer Buffer.
4. Nitrocellulose transfer membrane.
5. Anti-NPC1 antibody (ab36983; Abcam).
6. Donkey anti rabbit IgG (H+L) secondary antibody (Jackson ImmunoResearch Laboratories).
7. Protease Inhibitor Cocktail.
8. Laemmli 2× Sample Buffer (Sigma-Aldrich).
9. Bicinchoninic Acid (BCA) Kit for Protein Determination.
10. Cell lysis buffer: 50 mM Tris, pH 7.8, 100 mM NaCl, 1 % Triton X-100.
11. Protease inhibitors.

3 Methods

3.1 Cloning of NPC1 sgRNA into PX459 Vector

Ultrapure water is used for all the reactions. All reagents are kept on ice and reactions are carried out at room temperature unless otherwise indicated.

1. Dilute sgRNA oligos with water to 10 μM (*see* **Note 2**).
2. Set up kinase treatment reaction in 200 μL PCR tubes to add phosphate group to the 5′ end of the oligos (*see* Table 1 for reaction components).
3. Incubate at 37 °C for 45 min.
4. Anneal the Forward and Reverse sgRNA oligos: combine forward and reverse reactions into one tube after a brief centrifugation. Incubate the combined forward and reverse reaction mixture at 100 °C for 5 min, then allow it to cool slowly to room temperature (*see* **Note 3**).

Table 1
Kinase treatment reaction of sgRNA oligos

Components	Forward (μL)	Reverse (μL)
Oligo (10 μM)	1	1
10× PNK buffer	1	1
H_2O	6	6
ATP (10 mM)	1	1
Total volume	10	10

5. Digest PX459 backbone plasmid with BbsI for 2 h at 37 °C (*see* **Note 4**). Set up a reaction as shown in Table 2.
6. Purify digested PX459 plasmid using PCR purification column and elute in 30 μL of H_2O.
7. Set up ligation as shown in Table 3. Incubate at room temperature for 1 h (*see* **Note 5**).
8. Transform One Shot Stbl3 chemically competent *E. coli* cells (*see* **Note 6**) with 5 μL ligation mixture following the manufacturer's instruction. Spread cells onto LB agar plates containing 100 μg/mL ampicillin, and incubate the plates at 37 °C overnight.
9. Check the plate after overnight incubation. The plate should normally have over tens to hundreds of colonies. Pick 10 colonies and inoculate individual colonies into 5 mL LB broth containing 100 μg/mL of ampicillin. Incubate and shake the LB culture at 37 °C overnight. Extract plasmid DNA using QIAprep spin miniprep kit according to manufacturer's instruction.
10. Verify positive clones by sequencing with a forward primer (GAGGGCCTATTTCCCATGATTCC) located within the

Table 2
BbsI digestion reaction of PX459 backbone plasmid

Components	Amount
BbsI (10 U/μi)	2 μL
10× digestion buffer	4 μL
PX459	2 μg
H_2O	32 μL
Total volume	40 μL

Table 3
Ligation of NPC1 sgRNA oligos with digested PX459 plasmid

Components	Amount (μL)
Annealed sgRNA oligos	1
Digested PX458	1
T4 ligase	1
10× ligase buffer	1
H_2O	6
Total volume	10

human U6 promoter of the PX459 vector. Prepare the verified clones with the successful insertion of NPC1 sgRNA sequences between BbsI sites (PX459-NPC1-sgRNA) using NucleoBond® Xtra Midi kits for HeLa cell transfection (*see* **Note 7**).

3.2 HeLa Cell Transfection and Selection

1. HeLa cells are grown in DMEM medium supplemented with 10 % (v/v) FBS, 100 units/mL of potassium penicillin and 100 μg/mL of streptomycin sulfate, and maintained in a 37 °C incubator with 5 % CO_2 supply. Change medium every 2–3 days and passage the cells before they reach full confluence.
2. On the day of transfection, seed 10^6 cells/dish into two 6-cm culture dishes containing 3 mL of medium.
3. Prepare transfection complex as follows: Dilute the targeting plasmid (PX459-NPC1-sgRNA) in one microcentrifuge tube by adding 3 μg of DNA into 500 μL of Opti-MEM Reduced Serum Medium. Add 3 μL of PLUS Reagent to the diluted DNA. Dilute Lipofectamine LTX Reagent in another microcentrifuge tube by adding 6 μL of the reagent into 500 μL Opti-MEM Reduced Serum Medium. Mix both tubes by inversion and incubate at room temperature for 5–10 min. Transfer all Lipofectamine LTX-Opti-MEM dilutions to the tube containing the diluted plasmid–Opti-MEM mixture. Mix well and incubate the mixture for 15–20 min at room temperature.
4. Add the transfection complex dropwise to one newly seeded dish of cells. Leave another dish of cells non-transfected as a blank control. Replace the transfection medium with 4 mL of fresh medium 24 h post transfection.
5. Two to 3 days post transfection, replace the medium on both the transfected cells and non-transfected cells with selection medium, containing DMEM medium supplemented with 10 % (w/v) FBS, 100 units/mL of potassium penicillin, 100 μg/mL of streptomycin sulfate, and 2 μg/mL of puromycin (*see* **Note 8**). Replace the medium with fresh selection medium every second day. Typically, in the non-transfected dish, all cells are killed by puromycin 2–3 days post selection, while in the transfected dish, there are numerous cells surviving selection at this stage depending on the transfection efficiency. Keep culturing the surviving cells in selection medium until no more dead cells are seen floating in the medium and distinct cell colonies are formed.
6. The surviving cells are subjected to limited dilution as follows: Rinse cells in transfected dish with 4 mL of PBS, and add 0.25 mL of TrypLE Express enzyme to the dish. Gently swirl the dish to let the enzyme cover all cells. Aspirate excessive

liquid and allow trypinization at room temperature for 3–5 min. Gently resuspend the cells with 4 mL of medium, and count using a hemocytometer or an automated cell counter. Dilute 500 cells in 50 mL DMEM medium supplemented with 10 % (w/v) FBS, 100 units/mL of potassium penicillin, and 100 μg/mL of streptomycin sulfate in a sterile tissue culture tube. Transfer 100 μL/well to five 96-well plates using an 8-channel pipette. Incubate the plates in a 37 °C incubator and change medium every 3–4 days (*see* **Note 9**). Examine the plates regularly over a period of 2 weeks after seeding and label the wells that have single cell colonies.

3.3 Cell Colony Expansion and Verification

1. Rinse single cell colonies in labeled wells of the 96-well plates with 100 μL of PBS, add 10 μL of TrypLE Express enzyme to the wells, and allow cells to be trypinized at room temperature for 3–5 min. Gently resuspend the cells in 100 μL of DMEM medium supplemented with 10 % (w/v) FBS, 100 units/mL of potassium penicillin, 100 μg/mL of streptomycin sulfate, and 2 μg/mL of puromycin. Transfer trypsinized cells to the individual well of a 12-well plates containing 900 μL of medium per each well.
2. Allow cells to grow to 70–80 % confluence in the 12-well plates. Rinse each well with 1 mL of PBS. Add 100 μL of TrypLE Express enzyme to the wells, and allow cells to be trypinized at room temperature for 3–5 min. Gently resuspend the cells with 1 mL of medium. Transfer 250 μL of trypsinized cells to the individual well of Nunc Lab-Tek 8-well Chamber Slide. Transfer the residual cells to a 12-well plate to continue expansion, making sure that corresponding cell lines on the chamber slide are numbered identically in the 12-well plate.
3. Aspirate the medium from the 8-well chamber 24–48 h post seeding, add 100 μL of 4 % paraformaldehyde (freshly prepared from 16 % w/v stock) and fix cells for 30 min at room temperature. Remove the paraformaldehyde and rinse the wells with 200 μL of PBS for three times. Add 100 μL of filipin solution (approx. 50 μg/mL in PBS) to the wells and stain the cells in the dark for 30 min at room temperature. Remove the filipin solution and rinse the wells three times with 200 μL of PBS. Remove the chamber wall according to the manufacturer's instruction. Apply the Antifade Mountant on top of the cells and cover with cover slip. Image the stained cells using a suitable microscope. In our lab, we use a Leica wide-field microscope (CTR5500) equipped with an EL6000 fluorescent lamp and a DFC300 FX digital camera (360/40-nm excitation and 470/50-nm band-pass emission) [10].
4. Filipin staining results (Fig. 1) will indicate which cell clones grown in the 12-well plates are potentially NPC1-deficient,

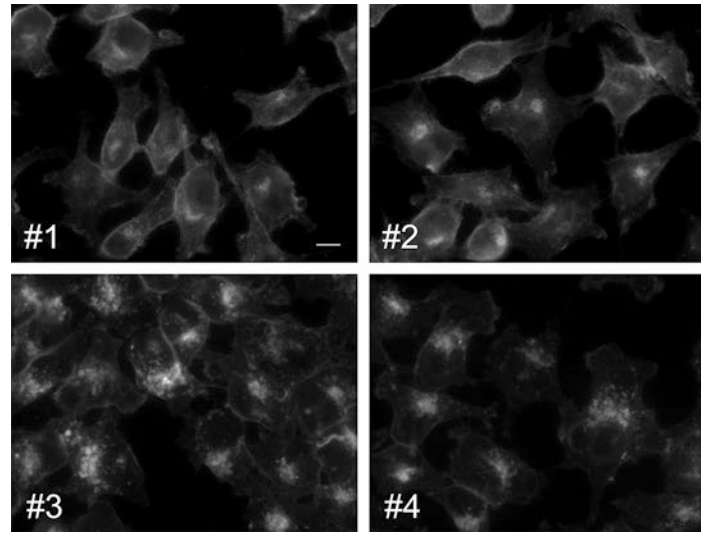

Fig. 1 Filipin staining for screening of positive NPC1-deficient cell clones mediated by CRISPR/Cas9. HeLa cells derived from single cell clones were grown in 8-well chamber slides and fixed with 4 % paraformaldehyde for 30 min at room temperature. After washing, cells were stained with 50 μg/mL of filipin in PBS for 30 min at room temperature. The stained cells were mounted, covered, and imaged using a Leica wide-field microscope with a UV filter set. Representative images designated as clone #1-4 are shown. Note that the #3 and #4 show a punctate cholesterol staining pattern and are indicative of positive NPC1-deficient clones

which is mediated by the CRISPR/Cas9 system. This can be further verified by immunoblotting using a NPC1 antibody as follows.

5. Grow the individual cell lines, expanded under Subheading 3.3, **step 2**, in a 12-well dish. When 70–80 % confluent, wash wells with 1 mL of PBS, add 100 μL of TrypLE Express enzyme to the wells, and allow cells to be trypinized at room temperature for 3–5 min. Gently resuspend the cells with 1 mL of medium, transfer 750 μL of trypsinized cells to the individual well of the 6-well plates (for screening), and pipette the remaining cells to the individual well of the new 12-well plates (to keep expanding). Add 1.25 and 0.75 mL of medium to the 6-well plates and 12-well plates, respectively. Return the plates to the incubator and grow cells for 24–48 h.
6. Remove medium from the 6-well plate. Scrape cells in 1 mL of PBS. Transfer cells to microcentrifuge tubes, and spin down at 2000 × *g* for 5 min. Resuspend the cell pellets using 30 μL of cell lysis buffer (*see* **Note 10**) supplemented with protease inhibitors, and incubate the tubes on ice for 30 min. Spin down lysed cells at 18,000 × *g* for 15 min at 4 °C. Transfer 22 μL of the supernatant (i.e., the cell lysates) to chilled microcentrifuge

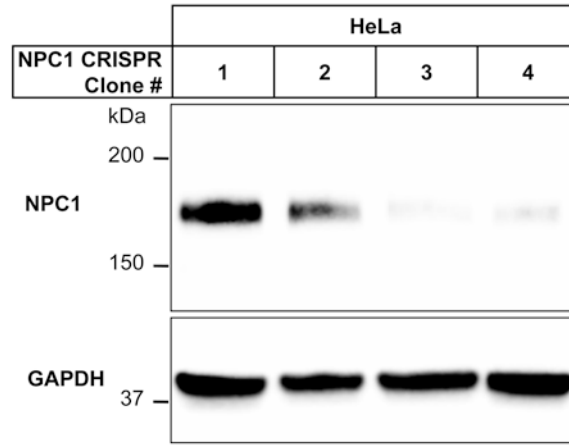

Fig. 2 Western blotting analysis of cell lysates prepared from NPC1 CRISPR clone #1-4 using a polyclonal anti-NPC1 antibody. Anti-GAPDH was blotted as a loading control. Note that while NPC1 is abundant in clone #1 and #2, its levels are significantly lower in the other two clones, especially in clone #3, indicating a successful *NPC1* gene disruption mediated by CRISPR/Cas9

tubes on ice. Determine protein concentration of the lysates using the BCA assay from 2 × 1 μL aliquots. Add 20 μL of 2× laemmli buffer to the remaining cell lysates and mix well. Load a total of 30 μg of cell lysate protein on a 10 % TGX FastCast gel, and transfer the gel to a nitrocellulose membrane, followed by blocking with 5 % skim milk diluted in TBST. Incubate the membrane with 1 μg/mL of NPC1 polyclonal antibody in TBST at 4 °C overnight. After incubating with the secondary antibody for 1 h at room temperature, image the NPC1 blot using a Gel Doc XR system (Bio-Rad) (Fig. 2).

4 Notes

1. For sgRNA designing, we normally go to https://genome.ucsc.edu/ and search for the genomic sequences of the genes to be deleted. Select around 200 bp nucleotides within either of the first few exons of the *NPC1* gene, and proceed to http://crispr.mit.edu/ to acquire sgRNA sequence. Choose the sgRNA sequence with highest score. Design oligo with 5′ end overlap using the following design template to add in BbsI sites at both 5′ and 3′ ends:
   5′-CACCGNNNNNNNNNNNNNNNNNNN-3′
   3′-CNNNNNNNNNNNNNNNNNNNCAAA-5′
2. Use ultrapure water to prepare 100 μM oligo stock. Prepare 10 μM oligo by adding 10 μL of the oligo stock to 90 μL of water.

3. Set up a heating block at 100 °C first. After incubation, turn off the heating block but keep incubating the tubes until the temperature decreases to room temperature. Briefly centrifuge the tubes during the cooling process.
4. The plasmid can also be digested at 37 °C overnight to ensure a complete digestion.
5. Ligation reaction can also be carried out at 4 °C overnight.
6. Common competent cells such as the DH5α strain can also be used. We found no significant decrease in terms of transformation efficiency for this step.
7. In most cases, a mini-prep with good quality DNA may be enough for the subsequent experiments.
8. To define an optimal puromycin concentration, a killing curve of puromycin for different cell lines needs to be generated prior to selection. The lowest concentration potent enough to kill all non-resistant cells should be used. For HeLa cells, we found 1–2 μg/mL of puromycin is sufficient to kill non-transfected cells with 2–3 days.
9. From this point onwards, it is essential that care is taken to avoid cross-contamination of individual cell lines. For example, when changing the medium in the 96-well plate, it is essential that each well is aspirated with a separate pipette tip to avoid cross-contaminating wells that contain individual cell lines. This may seem laborious but is an essential part of making single clonal cell lines.
10. For the lysis buffer, other detergents such as sodium dodecyl sulfate can be used instead of Triton X-100.

Acknowledgments

This work is supported by a research grant (#1041301) from the National Health and Medical Research Council (NHMRC) of Australia. H.Y. is a Senior Research Fellow of the NHMRC.

References

1. Davies JP, Ioannou YA (2000) Topological analysis of Niemann-Pick C1 protein reveals that the membrane orientation of the putative sterol-sensing domain is identical to those of 3-hydroxy-3-methylglutaryl-CoA reductase and sterol regulatory element binding protein cleavage-activating protein. J Biol Chem 275:24367–24374
2. Carstea ED, Morris JA, Coleman KG, Loftus SK, Zhang D, Cummings C, Gu J et al (1997) Niemann-Pick C1 disease gene: homology to mediators of cholesterol homeostasis. Science 277:228–231
3. Lu F, Liang Q, Abi-Mosleh L, Das A, De Brabander JK, Goldstein JL, Brown MS (2015) Identification of NPC1 as the target of U18666A, an inhibitor of lysosomal cholesterol export and Ebola infection. Elife 4:e12177
4. Lander ES (2016) The Heroes of CRISPR. Cell 164:8–28

5. Jinek M, Chylinski K, Fonfara I, Hauer M, Doudna JA, Charpentier E (2012) A programmable dual-RNA-guided DNA endonuclease in adaptive bacterial immunity. Science 337: 816–821
6. Gilbert LA, Larson MH, Morsut L, Liu Z, Brar GA, Torres SE, Stern-Ginossar N et al (2013) CRISPR-mediated modular RNA-guided regulation of transcription in eukaryotes. Cell 154:442–451
7. Mali P, Yang L, Esvelt KM, Aach J, Guell M, DiCarlo JE, Norville JE et al (2013) RNA-guided human genome engineering via Cas9. Science 339:823–826
8. Hsu PD, Lander ES, Zhang F (2014) Development and applications of CRISPR-Cas9 for genome engineering. Cell 157:1262–1278
9. Maresca M, Lin VG, Guo N, Yang Y (2013) Obligate ligation-gated recombination (ObLiGaRe): custom-designed nuclease-mediated targeted integration through non-homologous end joining. Genome Res 23:539–546
10. Du X, Kumar J, Ferguson C, Schulz TA, Ong YS, Hong W, Prinz WA et al (2011) A role for oxysterol-binding protein-related protein 5 in endosomal cholesterol trafficking. J Cell Biol 192:121–135

Chapter 8

Quantitative Measurement of Cholesterol in Cell Populations Using Flow Cytometry and Fluorescent Perfringolysin O*

Jian Li[$], Peter L. Lee[$], and Suzanne R. Pfeffer

Abstract

Methods to quantify intracellular cholesterol are valuable for the study of its trafficking and storage in normal cells and in lysosomal storage disorders. Traditionally, cholesterol has been tracked using the small molecule, filipin. Filipin can be difficult to visualize and visualization can be cytotoxic as it requires UV illumination. Here we describe a method to measure cholesterol using a fluorescently labeled, mutant form of Perfringolysin O, a soluble protein toxin that binds cholesterol specifically. This approach has been used to measure the impact of NPC1 deficiency on lysosomal cholesterol levels and monitor the rescue of cholesterol export under conditions that reduce the thickness of the lysosomal glycocalyx.

Key words Lysosome, Cholesterol, Perfringolysin O, Niemann Pick type C

1 Introduction

Cholesterol plays an important role in cell physiology as both a component of cellular membranes and a precursor of numerous biomolecules [1, 2]. Mammalian cells can synthesize cholesterol but also acquire it exogenously through the blood [3]. Exogenous cholesterol is acquired through the endocytic uptake of low density lipoprotein (LDL) molecules by LDL-receptor mediated endocytosis [4]. Cholesterol esters that comprise the core of LDL are trafficked through the endocytic pathway to late endosomes and lysosomes, where they are hydrolyzed by lysosomal acid lipases [5]. Upon hydrolysis, it is thought that the protein NPC2 binds cholesterol in the lysosomal lumen and presents it to NPC1's N-terminal domain after binding to its luminal domain 2 [6]. NPC1 then transports the cholesterol out of lysosomes to the endoplasmic reticulum, plasma membrane and/or peroxisomes [7].

[$]These authors contributed equally to this work.

Ingrid C. Gelissen and Andrew J. Brown (eds.), *Cholesterol Homeostasis: Methods and Protocols*, Methods in Molecular Biology, vol. 1583, DOI 10.1007/978-1-4939-6875-6_8,

The importance of lysosomal cholesterol export is demonstrated clearly in diseases such as Niemann–Pick Type C, in which mutations in NPC1 or NPC2 cause cholesterol and glycosphingolipids to accumulate in lysosomes [8, 9]. Being able to follow and detect cholesterol accumulation is thus important for the diagnosis of cholesterol transport defects, and for in depth characterization of intracellular cholesterol transport pathways. The small molecule filipin, which binds to free cholesterol, has long been used to detect the intracellular localization and cellular content of cholesterol. However, filipin staining is challenging as it is prone to photo bleaching, requires UV light excitation which makes it difficult to visualize, and can be cytotoxic.

Perfringolysin O (PFO) is a *Clostridium perfringens* derived, soluble toxin that forms large, homo-oligomeric pore complexes capable of binding to cholesterol-containing membranes. Because of its specificity for cholesterol, PFO has been used to label intracellular cholesterol, specifically as a biotinylated derivative BCθ [10]. However, as PFO is cytolytic, one disadvantage of BCθ is its toxicity to cells. To alleviate BCθ's cytotoxic properties, a mutant form of PFO, PFO*, was constructed; PFO* cannot insert its β-hairpins into the membrane and as such, does not form a pore at 4 °C [11]. PFO* has been used successfully to label plasma membrane-associated cholesterol after ^{125}I labeling [11]. Here we describe the alternative use of fluorescently labeled PFO* to measure the accumulation of cholesterol within cells. This approach has been used to demonstrate the role of lysosomal membrane protein glycosylation in the transport and accumulation of cholesterol in lysosomes of Chinese hamster ovary cells [11]. It is essential to verify the localization of the fluorescent staining in a given cell type to fully understand the significance of any changes that may seen in flow cytometry experiments. CHO cells work especially well with this method.

2 Materials

2.1 PFO* Plasmid Transformation

1. PFO* plasmid constructed and provided by Arun Radhakrishnan (University of Texas Southwestern Medical School, Dallas, USA) and amplified in DH5α bacterial cells.
2. Rosetta 2 (DE3) chemically competent cells.
3. Selective LB agar Miller plates: 100 μg/mL carbenicillin, 25 μg/mL chloramphenicol, 10 g/L peptone, 5 g/L yeast extract, 10 g/L NaCl, 12 g/L agar.
4. T7 primer—TAATACGACTCACTATAGG.

2.2 PFO* Expression in Rosetta 2 Cells

1. Selective LB Miller broth: 100 μg/mL carbenicillin, 25 μg/mL chloramphenicol, 10 g/L peptone, 5 g/L yeast extract, 10 g/L NaCl.
2. 1 M isopropyl β-*p*-thiogalactopyranoside in sterile water.

2.3 PFO* Purification

1. Phosphate Buffered Saline (PBS): 137 mM NaCl, 2.7 mM KCl, 10 mM Na_2HPO_4, 2 mM KH_2PO_4.
2. Lysis buffer: PBS with 10 % glycerol (v/v).
3. Protease inhibitor stock solutions: 0.1 M phenylmethanesulfonyl fluoride (PMSF) dissolved in isopropanol (100×); 0.1 mg/mL aprotinin dissolved in double distilled water (100×); 0.1 mg/mL leupeptin dissolved in double distilled water (100×); 1 mg/mL pepstatin dissolved in methanol (1000×).
4. Wash buffer: lysis buffer with 50 mM imidazole.
5. Elution buffer: lysis buffer with 300 mM imidazole.
6. EDTA.
7. Ni-NTA resin.
8. 18 mL Kontes FLEX column (15 mm × 100 mm).
9. LABQUAKE shaker Rotisserie Mixer with Clips or equivalent instrument.
10. Emulsiflex C-5 homogenizer.
11. Amicon Ultra-4 10-kDa cutoff centrifugal filters.
12. PD-10 desalting columns.
13. Advanced Protein Assay (Cytoskeleton, Aurora, CO) or equivalent protein assay.

2.4 PFO*-Dye Conjugation and Flow Cytometry

1. Alexa Fluor 647 NHS Ester (*N*-hydroxy Succinimidyl Ester).
2. NanoDrop 2000 UV-Vis Spectrophotometer.
3. 7 % (w/v) paraformaldehyde (PFA) working solution: Dissolve 0.92 g of PFA in 11 mL sterile water; three drops (around 50 μL per drop) of 1 M KOH are added and heated at 50 °C for 15 min. Vortex gently for a few times during heating. Add 1.33 mL 10× PBS buffer (pH 7.4), mix and filter-sterilize the solution. Store at room temperature until use.
4. PBS containing 0.1 % (w/v) Triton X-100.
5. 1 % (w/v) Bovine Serum Albumin (BSA) in PBS.
6. 10 mm Tris–HCl (pH 7.4).
7. PD-10 desalting columns.
8. FACScan Analyzer or equivalent flow cytometer.

2.5 Cell Culture

CHO (Chinese Hamster Ovary) ldl-D cells were from Bill Balch (The Scripps Research Institute, San Diego).

1. NPC1−/− CHO ldl-D clones were generated using the CRISPR technique.
2. HeLa cells.

3. Minimum Essential Medium alpha (MEM alpha) and Dulbecco's Modified Eagle Medium (DMEM).
4. Fetal Bovine Serum (FBS) and LPDS (Lipoprotein Deficient Serum from fetal bovine).
5. Penicillin/Streptomycin, 10,000 U/mL.
6. 0.05 % (w/v) trypsin, 5 mM EDTA in PBS.
7. *N*-acetylgalactosamine and d (+) galactose, dissolved in sterile water to make 100 mM and 8 mM stocks, respectively. Stocks are aliquoted and stored in −20 °C.

3 Methods

Procedures are carried out aseptically at room temperature, unless otherwise noted.

3.1 PFO* Plasmid Transformation

1. Plasmid (50 ng) encoding bacterially expressed His-tagged PFO* is mixed with 50 μL Rosetta 2 (DE3) cells on ice and incubated for 30 min.
2. Cells are then placed in a 42 °C circulating water bath for 30 s and chilled on ice for 2 min.
3. Transformed cells are plated on selective LB agar Miller plates and incubated for 16 h at 37 °C (*see* **Note 1**).
4. Single colonies are selected and screened by sequencing using T7 primer to check for the presence of the PFO* plasmid.

3.2 PFO* Expression in Rosetta 2 Cells

1. A single PFO* positive colony is inoculated into 10 mL of selective LB Miller Broth and incubated 16 h with 200 rpm oscillation at 37 °C.
2. The culture is transferred to 1 L selective LB Miller Broth and incubated with 200 rpm oscillation at 37 °C until the culture reached OD_{600} = 0.5–0.6 (*see* **Note 2**).
3. Following incubation, cells are induced with 1:1000 ratio of isopropyl β-*p*-thiogalactopyranoside stock solution (1 mM final concentration) and incubated at 37 °C, orbitally oscillating at 200 rpm for 4 h.
4. Cells are spun down at 4500 × G (max) for 15 min at 4 °C, using a swinging bucket JS-4.2A centrifuge. Pellets are washed once with cold distilled water and can be stored at −20 °C prior to purification.

3.3 PFO* Purification

1. The pellet from the 1 L culture is suspended in 40 mL ice-cold lysis buffer with the addition of protease inhibitors at the following concentrations: 1 mM PMSF, 1 μg/mL leupeptin, 1 μg/mL aprotinin, and 1 μg/mL pepstatin A. After ensuring

that the pellet was evenly suspended, the suspension is passed twice through an Emulsiflex C-5 homogenizer to lyse the cells. After lysis, the suspension will appear clearer. Be sure to keep the lysate on ice during homogenization. The lysate should be approximately 42.5 mL at this stage (*see* **Note 3**).

2. The lysate is clarified by dividing into two 50 mL FALCON tubes and centrifuging at 13,000 rpm (19,650 × *g*) for 15 min at 4 °C for two cycles, keeping the supernatant and disposing of the pellet each time. We use a J2-HS centrifuge with a Faberlite F15-8x50c rotor.
3. While the lysate is being clarified, wash 2 mL Ni-NTA resin (to remove any ethanol in the slurry) with 10 mL lysis buffer in a 50 mL Falcon tube by spinning down the resin at 700 × *g* for 2 min at 4 °C in an Allegra X-15R centrifuge or equivalent instrument, discarding the supernatant.
4. Continue washing the Ni-NTA resin by repeating **step 3** two additional times.
5. Add the clarified lysate from **step 2** to the washed resin and gently invert the tube 3–4 times to mix resin and cell lysate.
6. Continue mixing the resin and lysate on a LABQUAKE shaker for 1 h at 4 °C to allow for Ni-NTA binding to equilibrate with the His-tagged PFO*.
7. Once the incubation is complete, collect the beads in an 18 mL Kontes FLEX column. It is recommended to keep the flow-through material at this stage to check the efficiency of Ni-NTA binding, and for later use in the rare event that initial binding is unsuccessful.
8. Wash the collected resin five times with 8 mL wash buffer.
9. Elute the protein four times with 2 mL elution buffer containing 1 mM EDTA (final concentration). Allow the last wash to complete before adding the initial elution volume. For subsequent elutions, allow the previous elution buffer to enter the bed completely before adding additional elution buffer (*see* **Note 4**).
10. Concentrate the purified protein with an Amicon Ultra-4 10-kDa cutoff centrifugal filter First rinse the filter with 1 mL lysis buffer and add 4 mL eluted protein to the filter, centrifuge at 3500 × *g* for 15 min at 4 °C, in a swinging bucket Allegra X-15R centrifuge or equivalent instrument.
11. Remove the flow-through (about 3 mL) and add the remainder of the purified protein (4 mL) to the filter reservoir containing the concentrated protein. Mix the reservoir well to ensure homogenous distribution of protein and centrifuge again as described in **step 10**.
12. Transfer the concentrated protein to a new 15 mL falcon tube (around 2 mL) and store on ice.

13. Equilibrate a PD-10 desalting column four times with 6 mL lysis buffer with 1 mM EDTA.
14. Apply the concentrated protein from **step 12** to the equilibrated PD-10 column and allow the protein to enter column completely.
15. Add 0.5 mL additional lysis buffer with 1 mM EDTA to the column in order to adjust the total volume to 2.5 mL and discard the flow-through.
16. Elute the desalted protein from the PD-10 column with 3.5 mL of lysis buffer with 1 mM EDTA.
17. Measure the protein concentration of the final product. In our lab, we mix 2 μL of concentrated protein with 1 mL 1× Advanced Protein Assay and measuring OD_{600}. On average we obtain ~10 mg total (3.5 mL of 3 mg/mL) protein from 1 L bacteria. Store protein at 4 °C until use. Figure 1 shows an SDS-PAGE of the purified protein.

3.4 PFO*-Dye Conjugation

1. For dye conjugation, make 1.25 mL of 1 mg/mL purified PFO* by diluting the concentrated, purified protein with lysis buffer with 1 mM EDTA. Store the protein on ice prior to conjugation.
2. Dissolve 100 μg NHS-647 dye with 50 μL DMSO to make a 1.54 mM dye solution. Mix the dye well. In a 1.5 mL Eppendorf tube, add 49 μL dye to 1.201 mL lysis buffer (60 μM in 1.25 mL), invert immediately 3–4 times to completely dissolve the dye. Wrap the tube with aluminum foil to limit exposure to light.
3. Mix the protein solution from **step 1** with the dye solution in a 1:1 volume ratio (3:1 dye to protein ratio) and incubate at room temperature for 1 h (*see* **Note 5**).

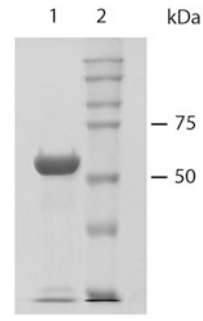

Fig. 1 Coomassie stained SDS-PAGE of purified PFO*. Purified PFO* (7 μg) was loaded onto a 10 % (w/v) gel and stained with Coomassie Blue R-250. *Lane 1*, purified PFO*; *lane 2*, protein molecular weight markers

4. While the NHS-activated dye is conjugating to the PFO*, equilibrate a PD-10 desalting column four times with 6 mL lysis buffer with 1 mM EDTA and 10 mM Tris–HCl (pH 7.4) (*see* **Note 6**). Allow each equilibration volume to enter the packed bed completely. Add 1 mL equilibration buffer to the column and cap the bottom until use.
5. Uncap the column, allow equilibration buffer to flow through the column, and add the PFO*-dye conjugate. Allow sample to completely enter the column.
6. Elute protein with 3.5 mL lysis buffer with 1 mM EDTA and 10 mM Tris–HCl (pH 7.4) and collect the eluate into a 15 mL Falcon tube. Cover the tube with aluminum foil and store at 4 ° C (*see* **Note 7**).
7. Protein and dye concentrations of the conjugate are measured by a NanoDrop 2000 UV-Vis Spectrophotometer, using Extinction Coefficients of 72,770 M^{-1} cm^{-1} for PFO* and 239,000 M^{-1} cm^{-1} for Alexa Fluor 647 respectively. Most preparations will yield approximately 4 μM PFO* and 8 μM dye (*see* **Note 8**).

3.5 PFO* Labelling for Flow Cytometry

1. 2×10^5 CHO ldl-D (WT) and NPC1 −/− CHO ldlD cells are seeded in 10 cm dishes and grown in MEM alpha medium supplemented with 7.5 % (v/v) FBS, 100 U/mL Penicillin, 100 U/mL Streptomycin, 100 μM *N*-acetyl-galactosamine and 8 μM d (+) galactose (full medium). 5×10^5 HeLa cells are plated in 10 cm dishes and cultured in DMEM medium supplemented with 7.5 % (v/v) FBS, 100 U/mL Penicilin, 100 U/mL Streptomycin. After 24 h, cells are switched to the same medium with 5 % (v/v) LPDS (*see* **Note 9**) [12].
2. After 72 h for CHO ldlD cells (WT or NPC1 −/−) and 24 h for HeLa cells, cells are washed once with 4 mL PBS; 2 mL 0.05 % trypsin, 5 mM EDTA in PBS buffer is slowly added to each dish to cover the cell monolayer. Remove trypsin and incubate cells in the incubator. Check cells every 30 s until they round up under the microscope, gently tap dishes so that cells completely lift off from the dish. Resuspend cells in 10 mL full medium as used in **step 1**, transfer to 15 mL FALCON tubes, and pellet by centrifugation (5 min, 300 × *g* at 4 °C).
3. 500 μL PBS is added to the cell pellets and cells are resuspended so that no visible clumps are detected. After resuspending cells, transfer to a 1.5 mL Eppendorf tube.
4. Add 500 μL 7 % (w/v) PFA solution to cells so that the final PFA concentration is 3.5 %; gently invert tubes a few times to resuspend cells completely (*see* **Note 10**).
5. Rotate on a LABQUAKE shaker for 20 min.

6. Pellet cells via centrifugation (5 min, 300 × *g*), remove the supernatant and add 1 mL PBS to each tube to resuspend cells completely.
7. Pellet cells again via centrifugation (5 min, 300 × *g*), aspirate the supernatant and resuspend with 1 mL PBS containing 0.1 % (w/vol) Triton X-100 to permeabilize cells.
8. Rotate tubes on a LABQUAKE shaker for 5 min.
9. Pellet cells, remove the supernatant and add 1 mL 1 % BSA (w/v) in PBS.
10. Resuspend cells completely and rotate on a LABQUAKE shaker for 15 min.
11. Pellet cells again via centrifugation (5 min, 300 × *g*). Remove supernatant and add 1 mL, 10 μg/mL PFO*-AF647, diluted in 1 % (w/v) BSA PBS (*see* **Note 11**).
12. Resuspend cells completely, wrap with aluminum foil and rotate on a LABQUAKE shaker for 45 min.
13. Pellet cells again via centrifugation (5 min, 300 × *g*). Wash once with 1 mL PBS as in **step 6**.
14. Resuspend cells in 0.5 mL PBS, transfer to 5 mL FALCON Polystyrene Round-Bottom tubes (12 × 75 mm) and analyze by FACScan Analyzer as shown in Fig. 2.

4 Notes

1. Carbenicillin is used to maintain the transformed PFO* plasmid while chloramphenicol maintains the rare tRNA plasmids supplied with the Rosetta 2 cells. Carbenicillin-only agar plates can be used if chloramphenicol (250 μg/10 mL LB agar Miller plate) is spread and allowed to dry before the addition of the transformed cells. If chloramphenicol is added on top of plates, colonies closer to the center of the plate should be selected to increase the chance that cells contain both the tRNA and PFO* plasmids.
2. OD_{600} = 0.5–0.6 is optimal for expression and expression was sensitive to OD_{600}. Care should be taken to avoid inducing the culture at OD_{600} > 0.8 as this may reduce the protein yield. Given the 1:100-fold inoculation, the culture usually reaches OD_{600} = 0.55 in 3–3.5 h.
3. If other methods are used to lyse the cells, the volume of the resuspended cells should be adjusted accordingly. PMSF, leupeptin, aprotinin, and pepstatin A are added to minimize PFO* degradation by inhibiting endogenous bacterial proteases. The efficiency of cell lysis can be approximated from the OD_{600} of the suspension before and after lysis.

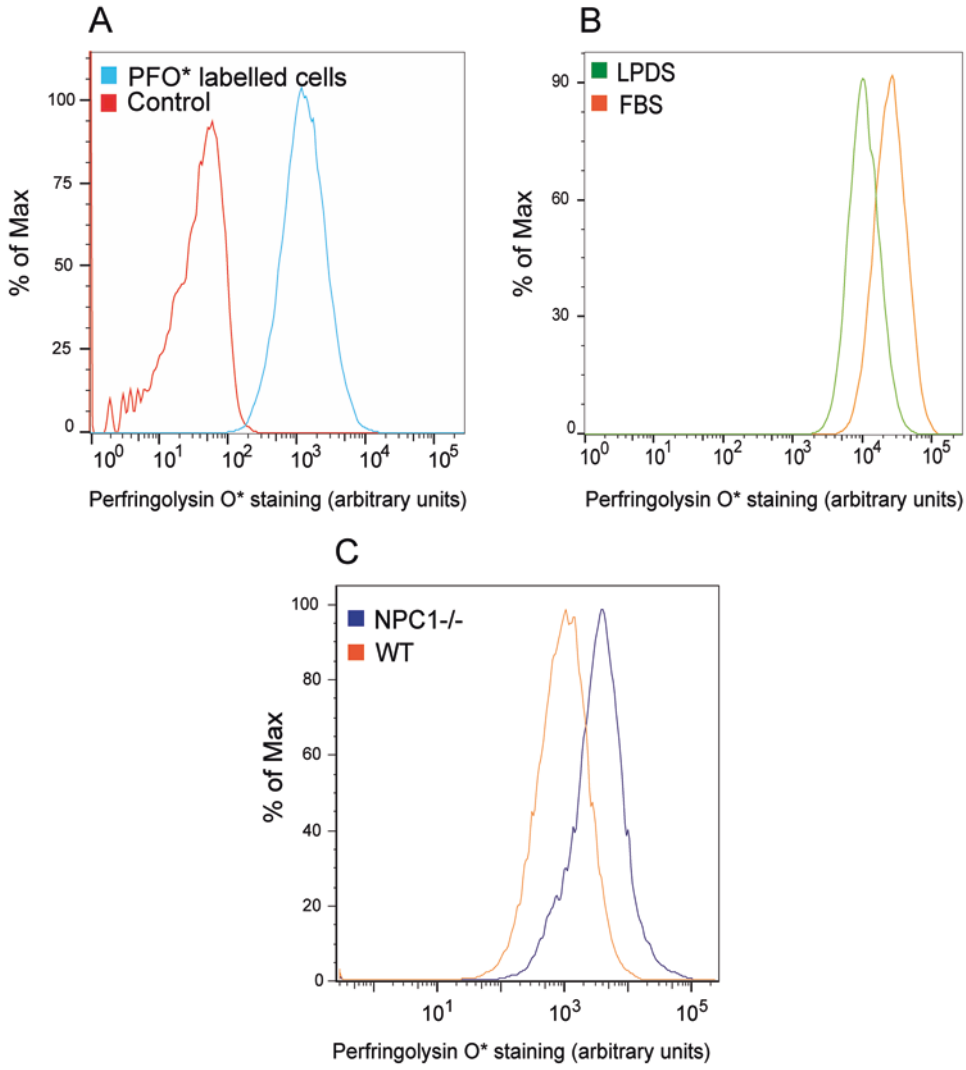

Fig. 2 Flow cytometry analysis of cells stained by PFO*-AF647. A representative flow cytometry analysis of CHO ldl-D cells grown in FBS medium (**A**), HeLa cells grown in FBS or LPDS medium (**B**) and WT and NPC1−/− CHO ldl-D cells grown in FBS medium (**C**), stained with (**B**, **C**) or without (**Control in A**) 10 μg/mL PFO*-AF647. Over 4000 cells were analyzed for each sample

4. After purification, PFO* protein will crash out and precipitate quickly in the absence of 1 mM EDTA and as such, addition of 1 mM EDTA to the elution buffer is crucial. Additionally, the protein should be kept in 1 mM EDTA containing buffer in all steps following elution from the Ni-NTA column. Glycerol may help stabilize purified PFO* and can be added to prolong storage at 4 °C. In the event that PFO* has precipitated in a noncompatible buffer, 1 mM EDTA can be added to rescue and solubilize the protein.

5. The dye–protein ratio should be kept at around 3:1 to achieve an eventual 2:1 stoichiometry of labeling. A higher dye–protein ratio can result in fluorescence quenching and occlude PFO*'s ability to bind cholesterol. In contrast, lower dye–protein ratio may result in lower signal. In CHO cells, staining is primarily lysosomal; in other cell types, this should be verified by light microscopy and if needed, a lower ratio of dye to protein can be utilized.
6. The 10 mM Tris added to the equilibration and elution buffers will quench unconjugated NHS-647 dye due to the presence of Tris's primary amines.
7. AF647-labeled PFO* can be stored at 4 °C up to 1 month. Longer storage will result in loss of cellular cholesterol staining capacity.
8. Theoretical Extinction Coefficient of PFO* was obtained using "ProtParam tool" (expasy.org). To obtain protein and dye concentration, the conjugate was analyzed by the built-in program "Protein&Label" according to the manufacturer of NanoDrop 2000 UV-Vis Spectrophotometer.
9. CHO (Chinese Hamster Ovary) ldl-D cells are defective in UDP-Gal/UDP-GalNAc 4-epimerase, leading to less N- and O-linked glycosylation in cells. *N*-acetyl-galactosamine and d (+) galactose were added back to medium so that cellular N- and O-linked glycosylation can be partially or fully restored. Other cell types can be used depending on the experimental design. LPDS medium treatment is optional.
10. Resuspending cells directly in 3.5 % PFA solution causes aggregration of cells and subsequent loss of cells for flow cytometry, as they stick to each other and to the walls of the tubes. Resuspending cells in PBS first followed by adding the same volume of 7 % (w/v) PFA (final PFA concentration is 3.5 %) dramatically decreases cell loss.
11. 1 μg/mL and 100 μg/mL PFO*-AF647 were also tried. In our hands, we found that 10 μg/mL yielded similar signal as 100 μg/mL and much higher than 1 μg/mL. Depending on cell types and permeabilization methods, optimization might be required to determine the concentration of PFO*-AF647 that gives the best signal and resolution.

References

1. Hanukoglu I (1992) Steroidogenic enzymes: structure, function, and role in regulation of steroid hormone biosynthesis. J Steroid Biochem Mol Biol 43:779–804
2. Javitt NB (1994) Bile acid synthesis from cholesterol: regulatory and auxiliary pathways. FASEB J 8:1308–1311
3. Ikonen E (2008) Cellular cholesterol trafficking and compartmentalization. Nat Rev Mol Cell Biol 9:125–138
4. Brown MS, Goldstein JL (1974) Familial hypercholesterolemia: defective binding of lipoproteins to cultured fibroblasts associated with impaired regulation of 3-hydroxy-3-

methylglutaryl coenzyme a reductase activity. Proc Natl Acad Sci U S A 71:788–792

5. Brown MS, Goldstein JL (1986) A receptor-mediated pathway for cholesterol homeostasis. Science 232:34–47
6. Deffieu MS, Pfeffer SR (2011) Niemann-Pick type C1 function requires lumenal domain residues that mediate cholesterol-dependent NPC2 binding. Proc Natl Acad Sci U S A 108:18932–18936
7. Underwood KW, Jacobs NL, Howley A, Liscum LJ (1998) Evidence for a cholesterol transport pathway from lysosomes to endoplasmic reticulum that is independent of the plasma membrane. J Biol Chem 273:4266–4274
8. Carstea ED, Morris JA, Coleman KG, Loftus SK, Zhang D, Cummings C et al (1997) Niemann-Pick C1 disease gene: homology to mediators of cholesterol homeostasis. Science 277:228–231
9. Naureckiene S, Sleat DE, Lackland H, Fensom A, Vanier MT, Wattiaux R et al (2000) Identification of HE1 as the second gene of Niemann–Pick C disease. Science 290:2298–2301
10. Sugii S, Reid PC, Ohgami N, Shimada Y, Maue RA, Ninomiya H et al (2003) Biotinylated θ-toxin derivative as a probe to examine intracellular cholesterol-rich domains in normal and Niemann-Pick type C1 cells. J Lipid Res 44:1033–1041
11. Das A, Goldstein JL, Anderson DD, Brown MS, Radhakrishnan A (2013) Use of mutant 125I-perfringolysin O to probe transport and organization of cholesterol in membranes of animal cells. Proc Natl Acad Sci U S A 110:10580–10585
12. Li J, Deffieu MS, Lee PL, Saha P, Pfeffer SR (2015) Glycosylation inhibition reduces cholesterol accumulation in NPC1 protein-deficient cells. Proc Natl Acad Sci U S A 112:14876–14881

Chapter 9

Transport Assays for Sterol-Binding Proteins: Stopped-Flow Fluorescence Methods for Investigating Intracellular Cholesterol Transport Mechanisms of NPC2 Protein

Leslie A. McCauliff and Judith Storch

Abstract

In this chapter we describe the use of stopped flow fluorescence spectroscopy to analyze the kinetic mechanisms of protein mediated cholesterol transfer to, from, and between model membranes. These assays allow for the detection of protein–membrane interactions that may occur during cholesterol transfer by simply modifying donor or acceptor concentrations, membrane composition, or buffer properties, and analyzing resultant transfer rates.

Key words Collisional transfer, Diffusional transfer, Cholesterol, Cholesterol trafficking, FRET, Stopped flow, Fluorescence, Model membranes, Small unilamellar vesicles

1 Introduction

Much is currently known about cholesterol synthesis and metabolism, about its extracellular transport in plasma lipoproteins and about the uptake of cholesterol-rich low density lipoprotein (LDL) via receptor-mediated endocytosis of the LDL receptor. Intracellular trafficking of cholesterol is crucial for maintaining cholesterol homeostasis, yet many questions remain regarding the mechanisms of intracellular cholesterol transport.

Cholesterol is extremely hydrophobic, and its transport has been shown to occur via vesicular and protein mediated mechanisms [1]. Several of the processes involved in intracellular sterol transport, however, are still unclear. The lysosomal storage disorder Niemann Pick type C (NPC) disease presents a valuable model for understanding some of these processes, specifically with regards to the egress of LDL-derived cholesterol from the endosomal/lysosomal system. In NPC disease, LDL-derived cholesterol accumulates in the late endosomal/lysosomal (LE/LY) compartment,

Ingrid C. Gelissen and Andrew J. Brown (eds.), *Cholesterol Homeostasis: Methods and Protocols*, Methods in Molecular Biology, vol. 1583, DOI 10.1007/978-1-4939-6875-6_9,

leading to lysosomal and cellular dysfunction. Studies have identified two endo/lysosomal proteins, NPC1 and NPC2, which are necessary for normal transport of cholesterol out of the LE/LY compartment. Questions remain, however, regarding the mechanism(s) by which these proteins mediate LE/LY cholesterol egress. Given the critical nature of normal LE/LY cholesterol egress in maintaining cellular and whole-body cholesterol homeostasis, elucidating the mechanism(s) by which this transport occurs is of great fundamental importance.

In the present chapter, we describe an in vitro approach that utilizes purified NPC2 protein and model membranes to determine whether the mechanism of protein mediated cholesterol transport involves protein–membrane interactions. Two of the three assays described utilize the intrinsic fluorescence of tryptophan residues in the cholesterol-binding NPC2 protein to monitor movement of cholesterol from the protein to membranes, and from membranes to the protein. The third approach detailed below employs the fluorescent cholesterol analog dehydroergosterol (DHE) and its fluorescence resonance energy transfer (FRET) partner dansyl, as part of dansyl-phosphatidylethanolamine (Dansyl-PE), in two independent vesicle populations for determining the mechanism of protein-mediated cholesterol transport *between* membranes. All three approaches can also be utilized to elucidate the transport mechanism of sterol binding proteins other than NPC2, however it is important to note that variations in the protocols may be necessary. In particular, if cholesterol binding does not modulate the intrinsic tryptophan fluorescence of the protein of interest, fluorescent cholesterol analogs such as DHE or cholestatrienol (CTE) can be instead utilized in a FRET pairing to monitor cholesterol transport, in lieu of changes in tryptophan fluorescence.

The basis of the three assays is similar; all are used to distinguish between the presence of a diffusional versus collisional mechanism of cholesterol transport. In short, if transfer involves the diffusion of sterol through an aqueous medium, the rate limiting step is dissociation of sterol from protein or membrane (Fig. 1a), which is unaffected by the acceptor. Thus, no change in the rate of sterol transfer would be observed as the concentration of donor or acceptor (either protein or membrane) increases [2, 3]. In contrast, the rate of sterol transfer for a collisional mechanism is proportional to the frequency of collisions between the protein and membrane (Fig. 1b), which is determined by the donor and acceptor concentrations [2, 3]. Therefore, if protein–membrane interactions are integral to the transfer of cholesterol between protein and membrane, the rate of transfer will increase as either the concentration of protein or the concentration of model membranes increases.

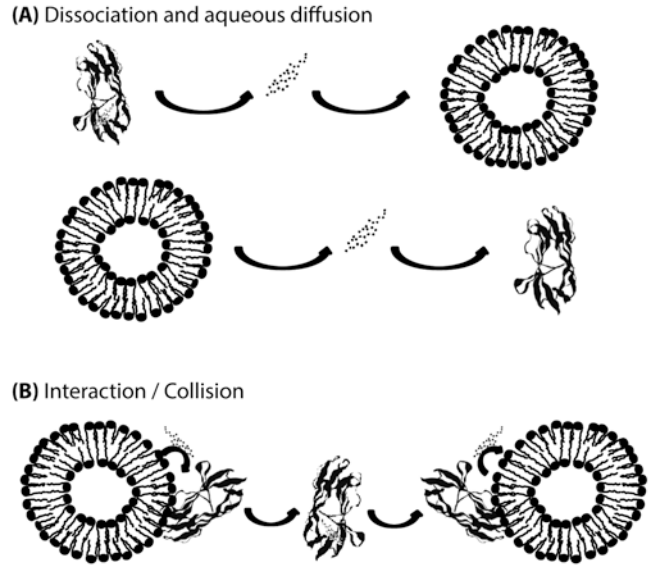

Fig. 1 Potential mechanisms of cholesterol transport between protein and membranes. (**a**) Aqueous diffusion of cholesterol between protein and membrane, in which the rate of sterol transfer is limited by the dissociation of cholesterol from the protein or membrane. (**b**) In a collisional mechanism, the rate of sterol transfer is proportional to the number of interactions between protein and membrane

Factors beyond donor and acceptor concentration can also elicit changes in sterol transfer rates, and these properties can be exploited in the outlined assays as an additional means of distinguishing between collisional versus diffusional mechanisms of cholesterol transport. One such property is the phospholipid composition of membranes; if changes in sterol transfer rates are observed between membranes with varying phospholipid compositions, it is likely that the protein is directly interacting with membranes to transfer sterol. In the case of NPC2, as shown below, rates of sterol transfer from the protein to membranes increase dramatically with the incorporation of lyso-bis phosphatidic acid (LBPA), a unique LE/LY phospholipid, in zwitterionic phosphatidylcholine acceptor membranes, supporting a collisional transfer mechanism [4, 5]. Buffer properties like pH and ionic strength can also affect rates of diffusional sterol transfer by proteins. For instance, the solubility of hydrophobic compounds decreases as ionic strength of the aqueous medium increase. Thus, sterol transfer rates would decrease as the salt concentration of the buffer increases for a diffusional, but not a collisional transfer mechanism [4, 6].

There are important advantages to utilizing stopped flow mixing in determining mechanisms of sterol transfer by proteins. First, rates of sterol transfer between protein and membranes can be quite rapid and may otherwise be undetectable in instances where either manual mixing is used, or with instrumentation that has

considerable dead time prior to data acquisition. Methods that require physical separation of protein from membrane, such as centrifugation or column separation, are also unlikely to be able to detect rates of sterol movement; rather, these methods provide only the equilibrium distribution of the sterol between the protein and the membrane, i.e., the *amount* of ligand that can transfer given certain concentrations of protein and membranes, but not the *rate* at which the ligand transfers. Using stopped-flow mixing, on the other hand, we have for example been able to detect cholesterol transfer rates from the NPC2 protein to membranes containing LBPA of approximately 5.0 s^{-1} (half-time of about 0.14 s) [4]. In the case of NPC2, we are able to use unmodified protein (e.g., no tags or labels) and the native ligand, cholesterol, thereby obtaining rates of sterol transfer that are likely to be physiologically relevant. Thus, in contrast to the stopped flow-based assays outlined in this chapter, equilibrium methods cannot be used to determine the mechanism(s) by which a sterol binding protein transfers ligand.

2 Materials

1. Sodium citrate buffer: 20 mM sodium citrate, 150 mM NaCl, pH 5.0 (*see* **Note 1**).
2. Delipidated protein (*see* **Note 2**).
3. Cholesterol (> 98% purity). Resuspend in DMSO to a concentration between 500 μM and 2 mM, and store at −20 °C protected from light. (*see* **Note 3**).
4. Egg phosphatidylcholine (EPC) (>99% purity) in chloroform at a concentration between 10 and 25 mg/mL. Store at −20 °C.
5. Dehydroergosterol (DHE) (>99% purity). Resuspend in chloroform to a concentration of 1 mg/mL and store at −20 °C protected from light.
6. Dansyl-phosphatidylethanolamine (Dansyl-PE) in chloroform at 1 mg/mL (Avanti Polar Lipids, Alabaster, AL, USA). Protect from light and store at −20 °C.
7. Nitrogen evaporator.
8. Lyophilizer.
9. Water bath.
10. Sonicator equipped with a half inch (127 mm) diameter tapped bio horn (probe) with a removal flat tip.
11. Ultracentrifuge and fixed angle rotor.
12. Stopped flow spectrofluorometer and accompanying software.

13. 299 nm long pass filter for detection of tryptophan fluorescence (used with excitation wavelength of 280 nm).
14. 370 nm narrow band filter for detection of DHE fluorescence (used with excitation wavelength of 323 nm).
15. 515 nm long pass filter for detection of Dansyl-PE fluorescence (used in a FRET pair with the DHE excitation wavelength of 323 nm).
16. A suitable assay for determining phospholipid concentration of vesicles via quantification of inorganic phosphate [7].

3 Methods

All procedures are performed at room temperature unless otherwise noted.

3.1 Membrane Vesicle Preparation

1. In a clean, dry, glass tube, prepare 1 mL of a 3 mM lipid solution in chloroform. Refer to the specific transfer assay for necessary phospholipid compositions.
2. Dry the preparation under nitrogen.
3. Lyophilize overnight to remove trace solvent.
4. Hydrate the dried film in 3 mL buffer (citrate buffer or other, *see* Subheading 2) to generate a 1 mM suspension of phospholipid.
5. Sonicate under nitrogen using a half inch (127 mm) diameter flat tip probe for 45 min at 4 °C in order to avoid overheating, and thus degradation, of the lipid suspension. (On a Branson Sonifier 450, set the duty cycle to 70% and output control to 3) (*see* **Note 4**).
6. Ultracentrifuge the sonicated supernatant at 105,000 × *g* for 45 min in order to remove titanium residue and any remaining multilamellar vesicles (MLVs).
7. Carefully remove the supernatant containing the SUVs and transfer to a brown vial. Keep on ice for immediate use or store at 4 °C for up to 1 week (for EPC vesicles).
8. Determine phospholipid concentration of vesicles via quantification of inorganic phosphate (*see* **Note 5**).

3.2 Cholesterol Transfer from Protein to Membranes

Transfer assays are performed using an SX20 Stopped Flow Spectrofluorometer (Applied Photophysics, UK), with a 20 μL SF cell volume and 1.1 ms deadtime, equipped with a water bath chamber. Settings may need to be adjusted if alternate equipment is used.

1. Prepare 100 mol% EPC SUVs (or other compositions, as desired) as per Subheading 3.1.
2. Turn on stopped flow lamp and allow it to warm up.

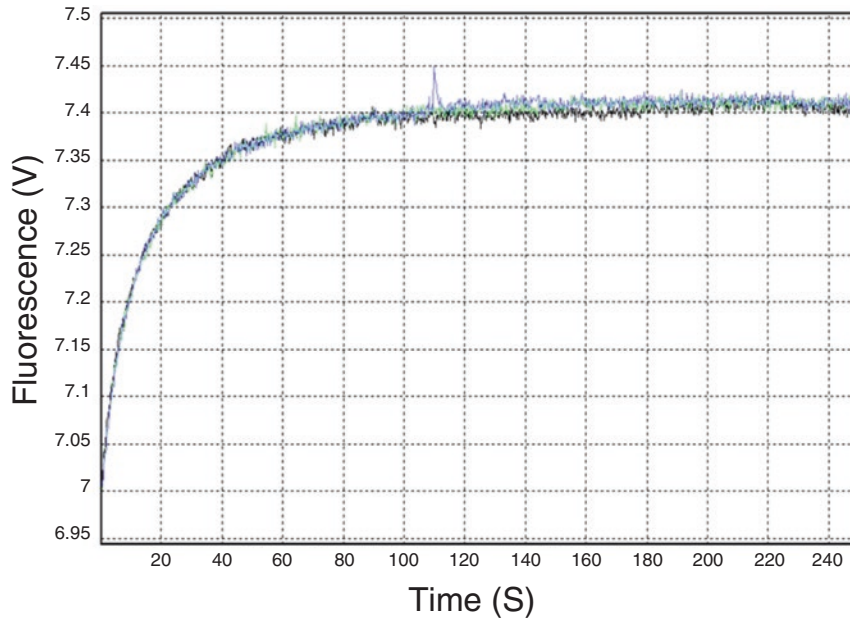

Fig. 2 Transfer of cholesterol from NPC2 to membranes. Example acquisition, in triplicate, monitoring tryptophan dequenching over time as 1 μM cholesterol is transferred from 1 μM NPC2 to 250 μM EPC SUVs. Curves were fitted with a single exponential function

3. Set water bath to 25 °C or desired temperature, and allow temperature to equilibrate.
4. Set the excitation wavelength on the stopped flow to 280 nm and equip with a 299 nm long pass filter. Initially, set the monochromator slits to 0.5/0.5.
5. Prepare 2 mL samples of 100, 200, and 500 μM EPC SUVs in buffer (*see* **Note 6**). Keep on ice while not in use.
6. Prepare 4 mL of a 5 μM holo-protein sample by incubating 5 μM protein in buffer with 5 μM cholesterol (final concentration) using the DMSO stock solution, for at least 20 min at room temperature. Final DMSO level should always be kept at less than 1% (v/v). Keep on ice while not in use.
7. Load holo-protein preparation (donor) and buffer into the sample syringes in order to obtain blank readings (*see* **Note 7**).
8. Trigger mixing of the donor with the buffer solutions. Acquire tryptophan fluorescence readings (arbitrary units) in triplicate over a period of 200 s. Adjust instrument settings to ensure absence of photobleaching (*see* **Note 8**).
9. Load holo-protein preparation (donor) and SUVs (acceptor) into the sample syringes.
10. Trigger mixing. Acquire tryptophan fluorescence readings in triplicate over a period of 200 s (Fig. 2).

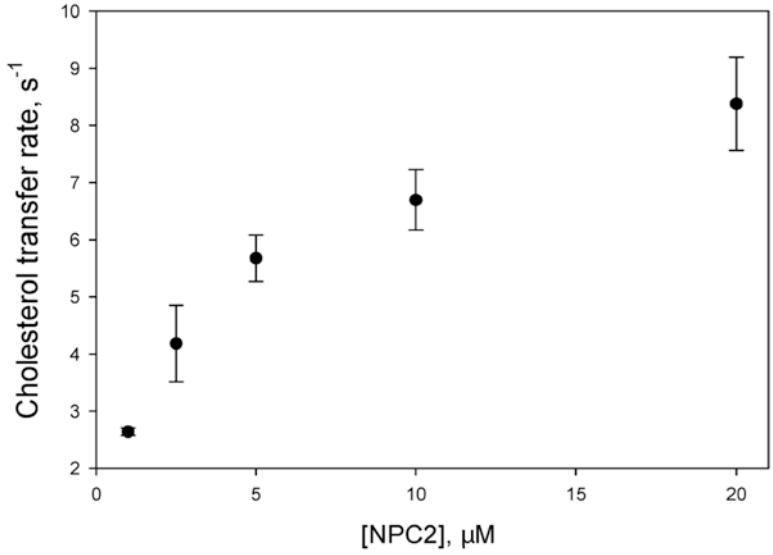

Fig. 3 Transfer of cholesterol from membranes to NPC2. Rates of NPC2 tryptophan quenching were determined for the transfer of 2.5 μM cholesterol from 250 μM SUVs to increasing concentrations of apo-NPC2 protein. The observed increase in transfer rate from donor membranes to NPC2 as the protein acceptor concentration increases indicates the presence of protein-membrane interactions. Reprinted with permission from [5] Copyright 2016 American Chemical Society

11. Average the readings and fit curves using a single exponential function. If unavoidable photobleaching remained during blank readings, be sure to subtract these curves prior to obtaining transfer rates via curve fitting.
12. Repeat **steps 9–11** using increasing concentrations of acceptor SUVs. If the rate of transfer increases as the concentration of acceptor increases, as in Fig. 3, the protein is likely directly interacting with membranes to transfer sterol, as the rate of collisional transfer is proportional to the product of the donor and acceptor concentration [2, 3]. If instead the rate of transfer remains constant as the concentration of acceptor SUVs increases, the protein is likely utilizing a diffusional mechanism, as the rate limiting step in this mode of transfer is the off rate of the cholesterol from the protein [2, 3] into the aqueous phase.

3.3 Cholesterol Transfer from Membranes to Protein

1. Prepare 90 mol% EPC, 10 mol% cholesterol SUVs (or other sterol compositions, as desired) as per Subheading 3.1.
2. Turn on stopped flow lamp and allow it to warm up.
3. Set water bath to 25 °C or desired temperature, and allow temperature to equilibrate.

4. Set the excitation wavelength on the stopped flow to 280 nm and equip with a 299 nm long pass filter
5. Prepare 2 mL samples of your delipidated protein (apo protein) at 1, 2, 5, 10, and 20 μM in buffer (*see* **Note 6**). Keep on ice while not in use.
6. Prepare 6 mL of a 200 μM EPC/cholesterol SUV sample in buffer (*see* **Note 9**). Keep on ice while not in use.
7. Load apo-protein preparation (acceptor) and buffer into the sample syringes in order to obtain blank readings. (*see* **Note 7**)
8. Trigger mixing. Acquire tryptophan fluorescence readings (arbitrary units) in triplicate over a period of at least 200 s. Adjust instrument settings to ensure absence of photobleaching (*see* **Note 8**).
9. Load cholesterol containing SUVs (donor) and apo-protein (acceptor) into the sample syringes.
10. Trigger mixing. Acquire fluorescence readings in triplicate over a period of at least 200 s.
11. Average the readings and fit curves using exponential fitting (*see* **Note 10**). If photobleaching was unavoidable during blank readings be sure to subtract these curves prior to obtaining transfer rates via curve fitting.
12. Repeat **steps 9–11** with increasing concentrations of donor SUVs; evaluate the results as described above (under Subheading 3.2, **step 12**), to determine whether a collisional mechanism or diffusional mechanism of transfer is employed by the protein to extract cholesterol from membranes.

3.4 Intermembrane Transfer of Sterol

1. Prepare two populations of SUVs as per Subheading 3.1; donor vesicles contain 75 mol% EPC and 25 mol% DHE; acceptor vesicles contain 97 mol% EPC and 3 mol% Dansyl-PE, serving as an energy transfer quencher of DHE fluorescence.
2. Turn on stopped flow lamp and allow it to warm up.
3. Set water bath to 25 °C or desired temperature, and allow temperature to equilibrate.
4. Set the excitation wavelength on the stopped flow to 323 nm and equip with a 370 nm narrow band filter.
5. Prepare a 10 mL sample of 100 μM DHE-containing (donor) SUVs in buffer (*see* **Note 6**). Keep on ice while not in use.
6. Prepare 2 mL samples of Dansyl-PE containing (acceptor) SUVs at 100 μM, 200 μM, and 500 μM in buffer. Keep on ice while not in use.
7. Prepare at least three additional 2 mL samples of the 100, 200, and 500 μM Dansyl-PE containing (acceptor) SUVs with 2 μM apo-protein.

8. Finally, prepare at least three additional 2 mL samples of 500 μM Dansyl-PE containing (acceptor) SUVs with 2, 5, and 10 μM apo-protein.
9. Load DHE containing (donor) SUVs and buffer into the sample syringes in order to obtain blank readings.
10. Trigger mixing. Acquire relative DHE fluorescence readings (arbitrary units) in triplicate over a period of at least 200 s and up to 1000 s. Adjust instrument settings to ensure absence of DHE photobleaching (*see* **Note 11**).
11. Rinse drive syringes and sample chamber well with buffer. Change to a 515 nm cut on filter.
12. Load Dansyl-PE containing (acceptor) SUVs and buffer into the sample syringes in order to obtain blank readings.
13. Trigger mixing. Acquire relative Dansyl fluorescence readings (arbitrary units) in triplicate over a period of at least 200 s and up to 1000 s. Further adjust instrument settings if necessary to ensure absence of Dansyl photobleaching.
14. Load DHE containing (donor) SUVs and Dansyl-PE containing (acceptor) SUVs into the sample syringes in order to determine spontaneous rates of DHE (cholesterol) transfer between membranes, i.e., in the absence of protein.
15. Trigger mixing and acquire relative Dansyl fluorescence readings in triplicate over a period of at least 200 s and up to 1000 s (*see* **Note 12**).
16. Average the readings and fit curves using exponential fitting. If photobleaching was unavoidably present during blank readings, be sure to subtract these curves prior to obtaining transfer rates via curve fitting. (*see* **Note 13**).
17. Repeat **steps 14–16** with increasing concentrations of acceptor vesicles. The spontaneous rate of DHE transfer between membranes occurs via a diffusional mechanism and therefore should not change as acceptor vesicle concentration increases (Fig. 4a) [5, 8, 9].
18. Load DHE containing (donor) SUVs and 100 μM Dansyl-PE containing (acceptor) SUVs, together with 2 μM apo-protein into the sample syringes.
19. Trigger mixing. Acquire Dansyl fluorescence readings in triplicate over a period of at least 200 s.
20. Average the readings and fit curves using exponential fitting (*see* **Note 10**). If photobleaching was unavoidable during blank readings be sure to subtract theses curves prior to obtaining transfer rates via curve fitting.
21. Repeat **steps 18–20** with increasing concentrations of Dansyl-PE (acceptor) SUVs, each containing 2 μM apo-protein, to determine whether protein-membrane interactions are present during transfer (Fig. 4a).

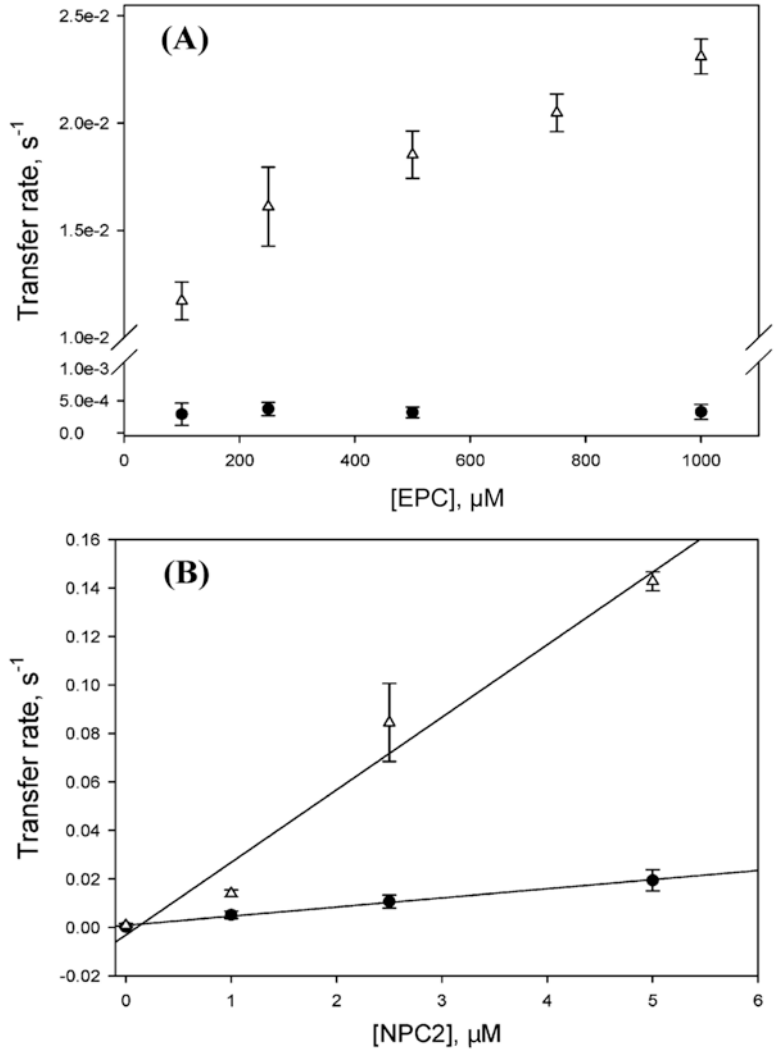

Fig. 4 Transfer of DHE between two membrane populations. (**A**) Transfer of DHE from 50 μM donor SUVs (75/25 EPC/DHE) to increasing concentrations of acceptor SUVs (97/3 EPC/Dansyl-PE) in the presence (*open triangle*) of 1 μM NPC2 suggests a collisional mechanism of transfer. In the absence (*filled circle*) of NPC2, no change in transfer rates is observed, demonstrating the characteristics of a diffusional transfer mechanism. (**B**) Variable transfer rates of DHE from 50 μM donor SUV (50/25/25 EPC/LBPA/DHE) to 250 μM Dansyl-PE containing acceptor SUV with (*open triangle*) or without (*filled circle*) LBPA in the presence of increasing concentrations of NPC2 is indicative of a collisional transfer mechanism. Reprinted with permission from [5] Copyright 2016 American Chemical Society

22. Rinse drive syringes and sample chamber well with buffer.
23. Load DHE containing (donor) SUVs and Dansyl-PE containing (acceptor) SUVs, together with 2 μM protein into the sample syringes.
24. Trigger mixing. Acquire relative Dansyl fluorescence readings in triplicate over a period of at least 200 s.

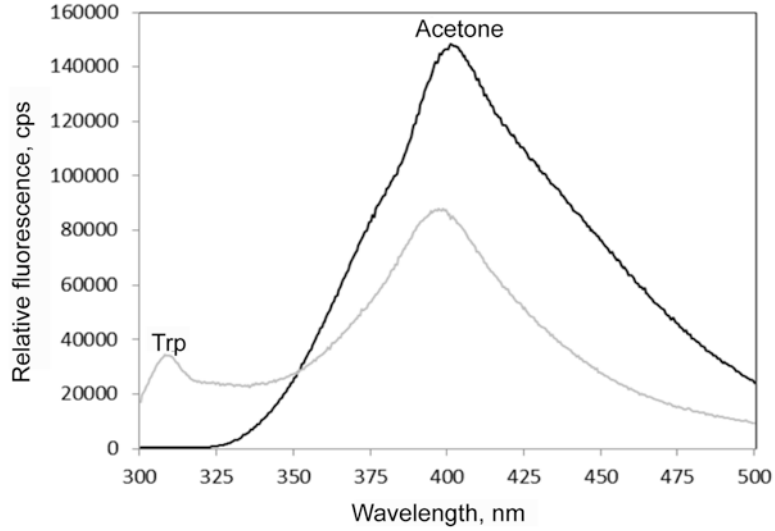

Fig. 5 Acetone contamination in delipidated protein sample. Pure acetone (*black* trace) and a delipidated NPC2 protein sample in buffer (*gray* trace) were excited at 280 nm and emission spectrum were acquired. Acetone contamination in the protein sample indicates insufficient drying of the protein pellet following precipitation

25. Average the readings and fit curves using exponential fitting (*see* **Note 10**). If photobleaching was unavoidable during blank readings, be sure to subtract these curves prior to obtaining transfer rates via curve fitting.
26. Repeat **steps 23–25** with Dansyl-PE (acceptor) SUVs containing increasing concentrations of protein to determine whether a collisional mechanism or diffusional mechanism of transfer is employed by the protein to transport sterol between membranes. (Fig. 4b) (*see* **Note 14**).

4 Notes

1. Sodium citrate buffer was employed in our studies to mimic the pH of the endo/lysosomal system, where the soluble NPC2 protein resides. Modify the buffer as necessary to reflect the pH of the inherent cellular compartment of the protein of interest.
2. Acetone precipitation is an effective way to delipidate purified NPC2 protein samples [10]. Avoid acetone contamination of your sample, which can be detected by a peak at approximately 400 nm (Fig. 5), by ensuring the sample has been sufficiently dried. Conversely, be careful not to overdry the pellet prior to resuspending in buffer, or it will be difficult to solubilize the

protein. Further note that we tended to experience significant losses in protein yield following precipitation. Thus, in instances where little purified protein is available it may be possible to bypass this step; we did observe similar kinetics between samples that were and were not delipidated following purification.

3. The suggested cholesterol stock concentration of 500 μM to 2 mM is based on maintaining a final DMSO concentration of at least <1% (v/v) in holo-protein preparations. Thus, the stock concentration of cholesterol will need to be determined based on the concentrations of holo-protein to be used in transfer assays, most notably the membrane to protein assays where increasing concentrations of protein are utilized.
4. When sonicating the lipid suspension for production of SUVs, the suspension needs to be kept at a temperature that is higher than the phase transition temperature of the membrane lipid component with the lowest melting point. If this cannot be achieved with probe sonication, a water bath sonicator may also be used. Ultracentrifugation will still be necessary in order to remove multilamellar vesicles (MLVs).
5. If reusing an SUV preparation after several days of storage at 4 °C, it is advisable to ultracentrifuge the sample and repeat the phospholipid quantification assay to account for aggregation of some of the vesicles.
6. The total volume of sample needed for each assay will depend, in part, upon the drive volume setting on your stopped flow. We kept the drive volume between 75 and 100 μL per syringe for all the transfer studies outlined in the chapter, and primed the sample handling unit between experimental conditions by driving the samples through three times (no data acquired). Thus, in order to acquire transfer data in triplicate, a minimum sample volume of approximately 450–600 μL was required for each condition in our transfer assays. The other factors to consider when determining required volumes are the number of conditions the sample will be used in, including blank readings, and the number of replicates desired.
7. Although we acquire blank readings for both donor and acceptor, it is especially critical to ensure that tryptophan fluorescence of the protein alone remains steady over the assay period.
8. If photobleaching is present, first reduce the monochromator slits; we have acquired data successfully at 0.1/0.1 settings. Alternatively, we have also experienced success by modifying the excitation wavelength by up to 10 nm. If some decrease in signal intensity over time remains after adjustments have been made, be sure to subtract these curves from the final data sets prior to determining transfer rates.

9. When using the protein as an acceptor (i.e., when assaying the rate of sterol transfer from membrane to protein), it is crucial to measure the equilibrium distribution of sterol between protein and phospholipid membranes *prior* to deciding on the concentrations of membranes and protein to be used in the transfer assays. The relative partition coefficient will indicate the amount of acceptor protein needed to obtain the minimum 1:1 relative partition ratio of membrane (donor) to protein (acceptor). A relative partition of 1:1 (and 1: >1) is required to ensure that unidirectional movement of sterol is monitored in the transfer assays. If relative partition is not determined and insufficient acceptor protein is used in the transfer assay, it is possible that back-transfer will obscure the true rate of sterol movement from membrane to protein [5, 11, 12, 13].
10. When cholesterol or DHE are incorporated into donor membranes, it may be necessary to use a double exponential function to fit curves due to flip-flop of the sterol in membranes. This flip-flop will be observed as the k_{slow} while actual transfer of sterol from donor to acceptor will be the k_{fast} [3].
11. We tended to experience photobleaching often with DHE, and have had success by reducing the excitation wavelength to between 270 and 300 nm, in addition to reducing the monochromator slits.
12. Intermembrane transfer of DHE can either be measured by DHE quenching or by the sensitized emission of Dansyl fluorescence, as described. To monitor the former, replace the 370 nm narrow band filter and repeat the assay. Rates of transfer should be the same regardless of the fluorescence monitored.
13. The spontaneous rate of sterol transfer between membranes is slow; reported rates are in the range of 0.0003 s^{-1} [5, 8, 9].
14. In instances of limited protein supply, we have instead kept the concentration of protein in the assay constant while increasing the concentration of acceptor Dansyl-PE containing vesicles, as previously outlined in the protocol.

Acknowledgments

This work was supported by the Ara Parseghian Medical Research Foundation (J.S.), the American Heart Association (L.M. and J.S.), and the National Institute of Health (J.S.) (GM 115866).

References

1. Soccio RE, Breslow JL (2004) Intracellular cholesterol transport. Arterioscler Thromb Vasc Biol 24(7):1150–1160
2. Roseman MA, Thompson TE (1980) Mechanism of the spontaneous transfer of phospholipids between bilayers. Biochemistry 19(3): 439–444
3. Storch J, Kleinfeld AM (1986) Transfer of long-chain fluorescent free fatty acids between unilamellar vesicles. Biochemistry 25(7):1717–1726
4. Cheruku S, Xu Z, Dutia R et al (2006) Mechanisms of cholesterol transfer from the Niemann-Pick Type C2 protein to model membranes supports a role in lysosomal cholesterol transport. J Biol Chem 281(42): 31594–31604
5. Xu Z, Farver W, Kodukula S, Storch J (2008) Regulation of sterol transport between membranes and NPC2. Biochemistry 47(42): 11134–11143
6. Kim HK, Stoch J (1992) Free fatty acid transfer from rat liver fatty acid-binding protein to phospholipid vesicles. J Biol Chem 267(1): 77–82
7. Gomori G (1942) A modification of colorimetric phosphorus determination for use with photoelectric colorimeter. J Lab Clin Med 27:955
8. Backer JM, Dawidowicz EA (1981) Mechanism of cholesterol exchange between phospholipid vesicles. Biochemistry 20:3805–3810
9. Neufeld EB, Cooney AM, Pitha J et al (1996) Intracellular trafficking of cholesterol monitored with a cyclodextrin. J Biol Chem 271: 21604–21613
10. Liou HL, Dixit SS, Xu S et al (2006) NPC2, the protein deficient in Niemann–Pick C2 disease, consists of multiple glycoforms that bind a variety of sterols. J Biol Chem 281(48): 36710–36723
11. Nichols JW, Pagano RE (1981) Kinetics of soluble lipid monomer diffusion between vesicles. Biochemistry 20(10):2783–2789
12. Storch J, Bass NM (1990) Transfer of fluorescent fatty acids from liver and heart fatty acid-binding proteins to model membranes. J Biol Chem 265:7827–7831
13. Herr FM, Li E, Weinberg RB et al (1999) Differential mechanisms of retinoid transfer from cellular retinol binding proteins types I and II to phospholipid membranes. J Biol Chem 274(14):9556–9563

Chapter 10

Synthesis and Live-Cell Imaging of Fluorescent Sterols for Analysis of Intracellular Cholesterol Transport

Maciej Modzel*, Frederik W. Lund*, and Daniel Wüstner

Abstract

Cellular cholesterol homeostasis relies on precise control of the sterol content of organelle membranes. Obtaining insight into cholesterol trafficking pathways and kinetics by live-cell imaging relies on two conditions. First, one needs to develop suitable analogs that resemble cholesterol as closely as possible with respect to their biophysical and biochemical properties. Second, the cholesterol analogs should have good fluorescence properties. This interferes, however, often with the first requirement, such that the imaging instrumentation must be optimized to collect photons from suboptimal fluorophores, but good cholesterol mimics, such as the intrinsically fluorescent sterols, cholestatrienol (CTL) or dehydroergosterol (DHE). CTL differs from cholesterol only in having two additional double bonds in the ring system, which is why it is slightly fluorescent in the ultraviolet (UV). In the first part of this protocol, we describe how to synthesize and image CTL in living cells relative to caveolin, a structural component of caveolae. In the second part, we explain in detail how to perform time-lapse experiments of commercially available BODIPY-tagged cholesterol (TopFluor-cholesterol®; TF-Chol) in comparison to DHE. Finally, using two-photon time-lapse imaging data of TF-Chol, we demonstrate how to use our imaging toolbox SpatTrack for tracking sterol rich vesicles in living cells over time.

Key words Cholesterol trafficking, Fluorescent sterols, Life-cell imaging, SpatTrack

1 Introduction

Fluorescence microscopy is one of the few methods that allows for studying the distribution of compounds at subcellular level and the only one that allows for tracking their transport in living cells. As cholesterol itself is not fluorescent, its analogs must be used to track it. While there are many extrinsically fluorescent analogs commercially available, their properties differ—sometimes strongly—from these of cholesterol itself. An alternative approach is to use

*These authors contributed equally to this work.

Electronic supplementary material: Supplementary material is available in the online version of this chapter at 10.1007/978-1-4939-6875-6_10. Videos can also be accessed at http://www.springerimages.com/videos/978-1-4939-6873-2.

Ingrid C. Gelissen and Andrew J. Brown (eds.), *Cholesterol Homeostasis: Methods and Protocols*, Methods in Molecular Biology, vol. 1583, DOI 10.1007/978-1-4939-6875-6_10, © Springer Science+Business Media LLC 2017

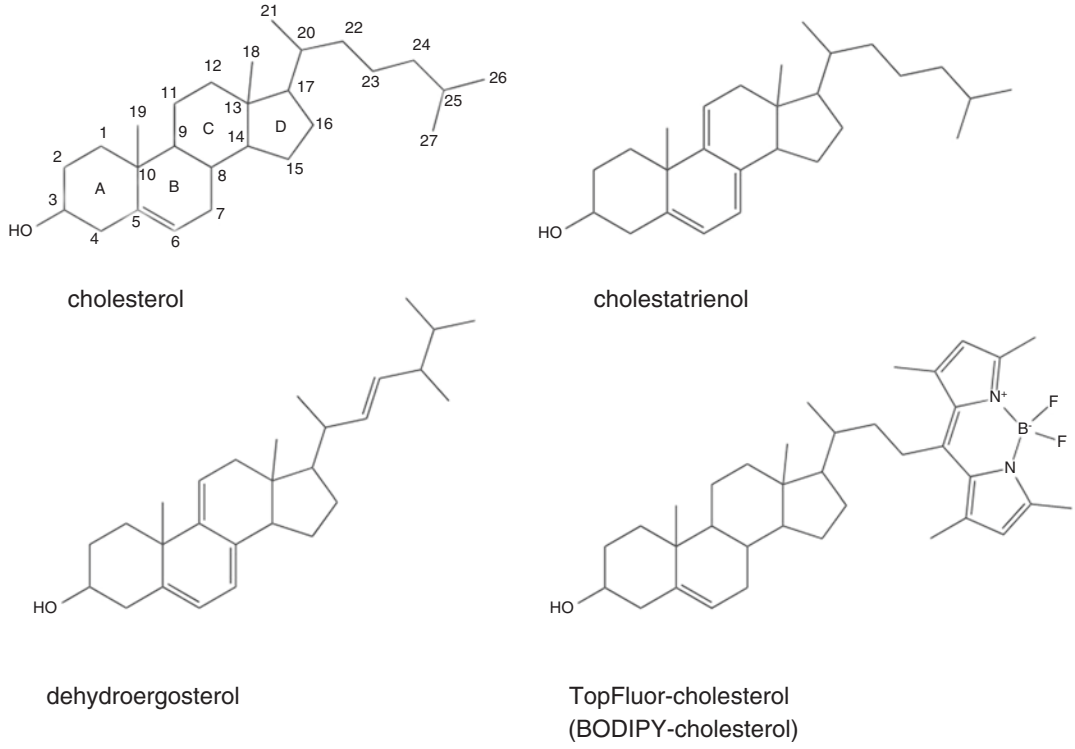

Fig. 1 Structure of cholesterol and its fluorescent analogs. *Upper left*, cholesterol, *upper right*, cholestatrienol (CTL), *lower left*, dehydroergosterol (DHE), *lower right*, TopFluor-cholesterol (TF-Chol) or BODIPY-cholesterol

intrinsically fluorescent sterols—usually sterols containing a system of conjugated double bonds. While some of them—like dehydroergosterol (DHE)—are commercially available, others, like cholestatrienol (CTL, Fig. 1), which is the closest structural analog of cholesterol, are not. Therefore, in order to indirectly image cholesterol using the fluorescent analogs, these must first be synthesized. Alternatively, one can employ dye-tagged cholesterol analogs in which the attached fluorophore alters the properties of the cholesterol probe as little as possible. In this approach, one can perform more advanced and prolonged imaging experiments, as the photostability and brightness of such analogs is superior to CTL or DHE. However, one must accept that the resemblance of cholesterol is affected [1]. One such analog with minimized alteration of cholesterol's properties is the commercially available TopFluor-cholesterol (i.e., cholesterol tagged with the BODIPY fluorophore at carbon 24, Fig. 1; TF-Chol). The physico-chemical properties of this cholesterol analog, its intracellular dynamics, applications in cell research and its limitations due to the attached fluorophore have been recently reviewed [2].

Single particle tracking (SPT) is commonly used to follow the dynamics of fluorescently labeled membrane proteins, but has also been applied to follow the motion of intracellular vesicles. For example, SPT has been used to study the dynamics of GLUT4 containing vesicles in adipose cells [3, 4] or the entry of hepatitis B virus-like vesicles in cells [5]. We used SPT to analyze the motion of intracellular vesicles containing TopFluor-cholesterol, which showed that the vesicular motion was largely dictated by the dynamics of the cytoskeleton with intermittent periods of active transport along cytoskeleton filaments [6]. Chen et al. found that cholesterol depletion with methyl-β-cyclodextrin increased the mobility of cholesterol containing endosomes in human carcinoma KB cells [7]. In contrast to this, cholesterol loading appears to reduce vesicle mobility. Niemann-Pick disease type C (NPC) is a neurodegenerative disease caused by loss-of-function mutations in either protein NPC1 or NPC2. The hallmark of NPC is the accumulation of cholesterol and other lipids in late endosomes and lysosomes (LE/LYSs) [8–11]. Eventually a perinuclear lysosomal storage organelle, consisting of largely immobile LE/LYSs, is formed in the perinuclear area of the cell [12, 13]. Using SPT we showed that restoring cholesterol efflux from LE/LYs in NPC2$^{-/-}$ cells increased the mobility of LE/LYs containing functional NPC2 protein supporting that cholesterol loading reduces the mobility of endosomes [14].

A great number of particle tracking algorithms have been developed and implemented in different software suites. Here we describe the typical workflow in SpatTrack; a software suite we developed for spatial and temporal analysis of vesicle like structures in fluorescence microscopy images of cells. The advantage of SpatTrack is that it combines particle tracking and subsequent trajectory analysis by the click of a mouse. However, the method described here should be broadly applicable to other particle tracking studies. Furthermore, since SpatTrack is made up of separate modules it is possible to import the particle trajectories from another tracking algorithm and do the trajectory analysis in SpatTrack.

There are two main elements to consider when acquiring images for SPT, (1) how fast the molecule of interest moves, and (2) the precision of the detected particle coordinates. Thompson et al. [15] showed that the error of the determined particle coordinates is described by:

$$\left\langle x^2 \right\rangle = \frac{s^2}{N} + \frac{a^2}{12N} + \frac{8\pi s^4 b^2}{a^2 N^2}, \tag{1}$$

where N is the number of photons collected, s is the standard deviation of the point spread function (PSF), a is the pixel size, and b is the background noise including autofluorescence and noise of

the detector. The number of detected photons primarily depends on frame rate of acquisition (determined by the pixel dwell time of the scanning microscope) and on the laser intensity. Finding the optimum frame rate depends on the mobility of the molecule of interest. For rapidly moving molecules such as proteins or lipids in the PM, a frame rate on the millisecond scale may be required. On the other hand intracellular vesicles move significantly slower and a frame rate of 2–3 images per second may be sufficient. In order to connect the trajectories in time, the frame rate should be such that the particle displacement from one frame to the next is small. On the other hand, living cells are sensitive to high intensity laser light so acquiring images at too high a rate may introduce unnecessary photodamage. Furthermore, increasing the frame rate may cause photobleaching of the fluorophore and will also result in a decreased number of detected photons and thereby reduce the precision of the tracking algorithm as seen in Eq. 1. Increasing the laser power improves the signal-to-noise ratio but also causes photodamage, therefore, if possible, the detector gain should be increased before the laser power. As shown in Eq. 1, the error of the detected particle locations increases with increasing standard deviation of the PSF. Thus, an objective lens with a high numerical aperture is recommended. The pixel size affects the detection precision due to pixel noise. That is, due to the finite size of the pixel it is not possible to determine where the photon arrived. Therefore, it is recommended that the pixel size is about equal to the standard deviation of the PSF.

2 Materials

2.1 Synthesis and Purification of CTL

1. 7-dehydrocholesterol (purity at least 95 %).
2. Methanol.
3. Ethanol.
4. Hexane.
5. Mercury acetate.
6. Dichloromethane.
7. Acetic acid.
8. Acetic anhydride.
9. 5 % (w/v) NaCl in distilled water.
10. 10 % (w/v) sodium hydroxide in ethanol.
11. 1:1 (v:v) ethanol–acetone.
12. Eluent for chromatography (20 % (v/v) ethyl acetate in hexane): Mix 100 mL of ethyl acetate and 400 mL of hexane (measured with a graduated cylinder) in a bottle. Store in a tightly closed bottle in a ventilated cabinet.

13. TLC visualization reagent: In a beaker, mix 3.5 mL of 85 % (v/v) ortophosphoric acid with 16.5 mL of distilled water (remember to add water first and then slowly pour in the acid). Add 3 g of CuSO4 and mix thoroughly.
14. TLC plates (aluminum, coated with silica gel 60): Put the plates on a cutting board, with the silica layer facing down. Cut with a sharp knife to a size of approximately 3 × 5 cm.
15. Silica gel preparation: Put silica gel (pore size 60 Å, 70–230 mesh) in a beaker, adjusting the amount used to the size of the column, and add the eluent (**item 12**) until its level is about 1 cm above the level of the gel. Mix thoroughly to remove all the air bubbles. Prepare immediately before using.
16. Saturated solution of sodium bicarbonate: Weigh 10 g of sodium bicarbonate in a beaker. Add 100 mL of distilled water and mix thoroughly.
17. Heat gun.
18. Gravitational chromatography column (tap at the bottom).
19. Cotton.
20. Filter paper.
21. Separating funnel—250 mL.
22. Rotary evaporator.

2.2 Generation of Fluorescent Endocytotic Probes and Labeling Solutions

1. Fatty acid-depleted BSA.
2. Buffer medium contained 150 mM NaCl, 5 mM KCl, 1 mM $CaCl_2$, 1 mM $MgCl_2$, 5 mM glucose, and 20 mM HEPES (pH 7.4).
3. Methyl-β-cyclodextrin (MβCD) solution: 30 mM MβCD dissolved in buffer medium with 0.1 % (w/v) BSA.
4. Rhodamine-labeled dextran (Rh-dextran; 70 kDa), and 1,1′-didodecyl-3,3,3′,3′-tetramethylindocarbocyanine perchlorate (DiIC12(3)) can be purchased from Molecular Probes (Eugene, Oregon, USA).
5. The succimidyl ester of Alexa 546 (purchased as a protein labeling kit from Molecular probes/Invitrogen, Thermo Fisher Scientific, Waltham, MA, USA).
6. Dialysis tubing or slides.

2.3 Transfection, Culture, and Imaging of Cells

1. Cell culture supplies: Fetal calf serum (FCS), DMEM, Ham's F12 medium (4.5 g/L glucose), and antibiotics/supplements.
2. Chinese hamster ovarian (CHO) cells or other cell line of interest.
3. Enhanced green fluorescein tagged caveolin 1 (Cav1-eGFP; a generous gift from Prof. Bo van Deurs, University of Copenhagen).

4. Transfection reagent such as Lipofectamine (Invitrogen A/S, Taastrup, Denmark).
5. Glass coverslips, pre-coated with poly-d-lysine as inlet to microscope dishes.
6. Microscopy equipment.

3 Methods

3.1 Synthesis and Purification of CTL

The overall strategy of CTL synthesis is outlined in Fig. 2a. 7-Dehydrocholesterol containing two double bonds instead of one, as in cholesterol, is the start compound [1]. First, the 3β-hydroxygroup is protected by acetylation with acetic anhydride to produce 7-dehydrocholesterol acetate [2]. This is followed by oxidation using mercury (II) acetate as catalyst to obtain cholestatrienol acetate [3] and finally by hydrolysis (or deacetylation) using NaOH to produce CTL [4]. By this procedure, we typically reach a reaction yield of 30–40 % and a product stable for several months.

Crucial steps during the synthesis are the analysis of products of each step using thin layer chromatography (TLC) and the purification of the synthesized sterol using gel chromatography. Both steps are therefore described in detail first (Subheadings 3.1.1 and 3.1.2). This is followed by a description of the actual synthesis in detail (Subheading 3.1.3).

3.1.1 TLC

1. Draw a start line (with a pencil) parallel to the shorter side of the plate, about 5 mm above it.
2. Place a drop of the solution to be analyzed on the starting line with a capillary or a pipette tip. Evaporate the solvent and, if the solution is diluted, repeat the procedure several times. If several solutions are to be analyzed in parallel, they can be placed on the same starting line, as long as the spots made by the drops are well separated.
3. Place the plate in a beaker containing the eluent (*see* Subheading 2.1, **item 12**) such that the lower part—below the starting line—is immersed. This usually corresponds to 3–4 mm of the eluent in the beaker. Cover the beaker with a glass or plastic lid (Fig. 2b).
4. When the eluent covered approximately 95 % of the plate's surface, take the plate out, dry it, drench with the visualization reagent (*see* Subheading 2.1, **item 13**) and heat with a heat gun set to 300 °C.

3.1.2 Column Chromatography

1. Place a gravitational chromatography column upright in a holder.
2. Place a bud of cotton in the bottom, narrow part of the column.

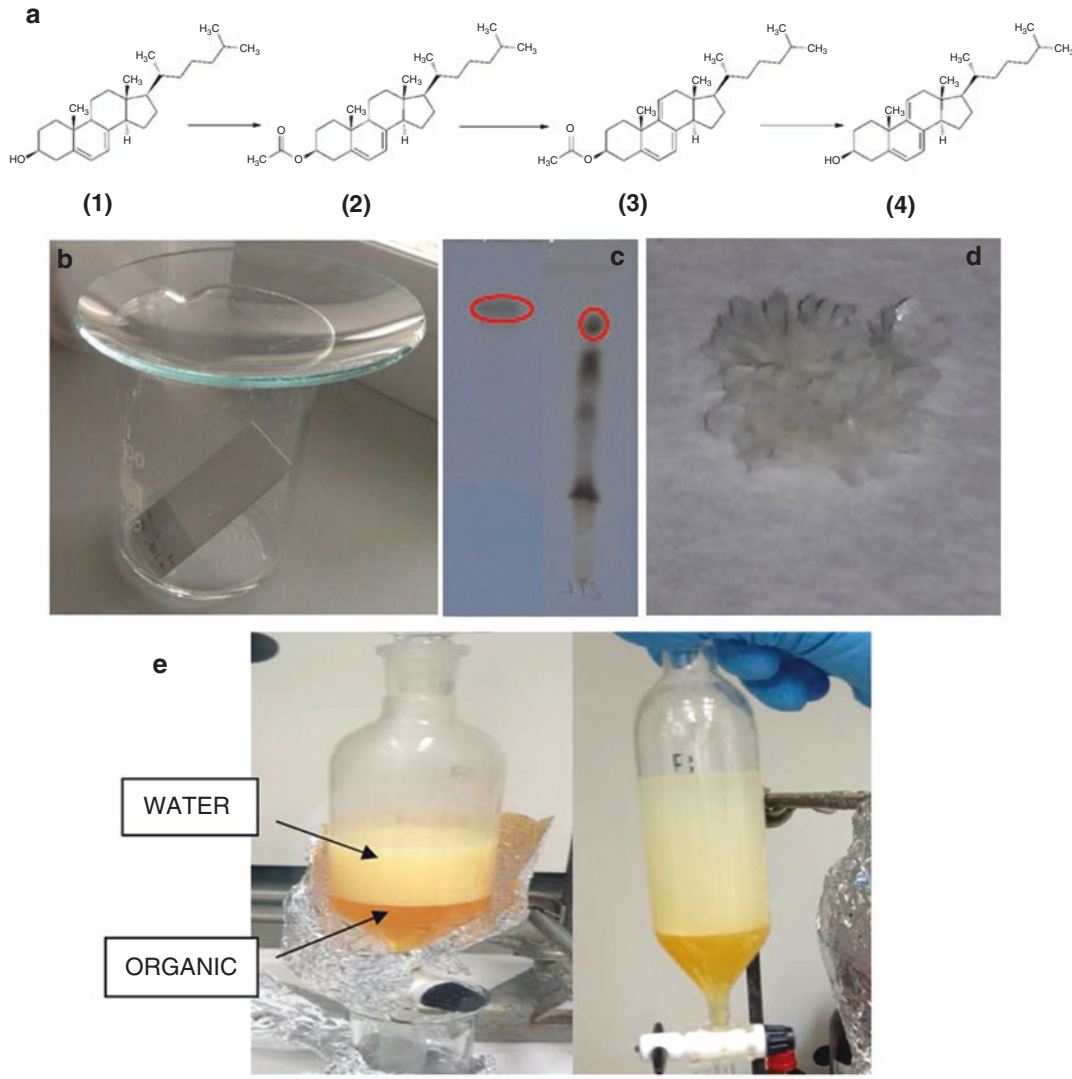

Fig. 2 Illustration of CTL synthesis. (**a**) Scheme of CTL synthesis; starting from 7-dehydrocholesterol having two double bonds [1], one protects the hydroxyl group against the subsequent oxidation reaction by acetylation to obtain 7-dehydrocholesterol acetate [2], oxidizes this sterol with mercury (II) acetate to CTL acetate [3] followed by deacylation to obtain CTL [4]. Panel (**b**) shows the setup for TLC analysis; panel (**c**) shows TLC plates of more (*left*) and less (*right*) pure CTL acetate—the *red oval* shows which fraction should be collected. Panel (**d**) shows a sample crystal of CTL (the final product). Panel (**e**) shows the separatory funnel with two phases: the organic one containing the sterol at the bottom, and the aqueous one with the mercury leftovers above (two funnels of different sizes are shown)

3. Pour the gel (prepared as described above) into the column.
4. Allow the gel to deposit—if necessary another aliquot can be added, so that finally the gel takes about 2/3 of the column's volume. Rinse it thoroughly with the eluent and allow it to stabilize (with the tap closed) for about 15 min.

5. Open the tap again to allow the eluent to drip out, so that its surface is barely above the surface of the gel. Then add a solution of the substance to be purified—so that its layer is no more than 3–5 mm thick. When it is absorbed on the gel, add more eluent.
6. Collect the liquid flowing from the column to test tubes (*see* **Note 1**).
7. If the column is to be used again, in order to purge it rinse it with pure methanol (two volumes of the column), then with the eluent again (3 volumes of the column)—discarding the solvent afterwards, and repeat from **step 5**.

3.1.3 Chemical Synthesis of CTL

Acetylation

1. Suspend 7-dehydrocholesterol (2 g) in acetic acid (20 mL) in a flask. Add 5 mL of acetic anhydride and a magnetic stirring bar. Heat the mixture to 80 °C and stir for 6 h using a magnetic stirrer with a heater.
2. Cool the mixture to room temperature and neutralize the acid with a saturated aqueous solution of sodium bicarbonate. Add the solution slowly until no more bubbles are formed (*see* **Note 2**).
3. Extract 7-dehydrocholesterol acetate with hexane. Evaporate the solvent in a stream of dry nitrogen.
4. Purify the product by gravitational column chromatography (*see* Subheading 3.1.2).
5. Analyze all the fractions by TLC (*see* Subheading 3.1.1)—collect those containing pure 7-dehydrocholesterol acetate (the top spot on the TLC plate—*see* Fig. 2c), join them together and evaporate the solvent in a stream of dry nitrogen.

Oxidation

1. Dissolve 7-dehydrocholesterol acetate (1.4 g) in 30 mL of ethanol with 6 mL of dichloromethane (DCM) in a dark glass bottle. Add a magnetic stirring bar and stir.
2. Prepare a suspension of 4 g of mercury acetate in 40 mL of ethanol with 1.5 mL of acetic acid in a glass beaker and add dropwise to the stirred solution of 7-dehydrocholesterol acetate (*see* **Note 3**).
3. Close the bottle tightly and stir the solution on a magnetic stirrer for 48 h.
4. Filter the solution through a filter paper and wash the filtrate cake with DCM until the solvent after washing is colorless. Add the solvent used for washing to the filtrate.
5. Wash the filtrate five times with 5 % (w/v) NaCl in distilled water to remove any traces of mercury. The volume of the 5 % (w/v) NaCl solution used for each rinse should be approximately three

times the volume of the organic phase. Mix the phases thoroughly in a separating funnel. At regular intervals invert the funnel and open the tap to depressurize it. After approximately 2 min of mixing, leave the funnel in an upright position for 15 min for the phases to separate. Cover the funnel with aluminum foil during this time to protect it from light. After each wash, return the lower organic phase to the separating funnel, while discarding the upper aqueous phase to a mercury waste container (Fig. 2e). If an off-white precipitate appears in the organic phase in the separating funnel, remove the precipitate by using filter paper and wash the precipitate thoroughly with DCM. Discard the precipitate as mercury containing waste (*see* **Note 4**).

6. Remove DCM by rotary evaporation (*see* **Note 5**).
7. Purify the crude product, i.e., CTL acetate by gravitational column chromatography, eluting with 20 % ethyl acetate in hexane.
8. Join the fractions containing CTL acetate together and evaporate the solvent in a stream of dry nitrogen.

Hydrolysis

1. Dissolve CTL acetate in 5 mL of 10 % (w/v) NaOH in ethanol in a dark glass bottle. Add a magnetic stirring bar and close the bottle tightly. Heat the solution to 50 °C and stir for 2 h using a magnetic stirrer with heater.
2. Evaporate the solvent in a stream of dry nitrogen. Dissolve the product, i.e., free CTL, with DCM, filter it through a filter paper into a dark glass vial and evaporate the solvent using a stream of dry nitrogen.
3. Dissolve the dry product, with heating, in a minimal amount of 1:1 (v:v) mixture of ethanol and acetone. Close the vessel tightly and allow the mixture to cool to room temperature, then leave in a freezer overnight. Filter off the crystals of CTL (Fig. 2d) through a filter paper, and store under nitrogen at −80 °C without access to light (*see* **Note 6**).

3.2 Generation of Fluorescent Endocytotic Probes and Fluorescent Sterol Labeling Solutions

3.2.1 Endocytic Probes

1. Transferrin (Tf) iron loading and labeled with Alexa 546 to get Alexa 546-Tf has been previously described [16, 17]. Briefly, iron is loaded onto Tf by incubating with Ammonium iron(III) citrate for 20 min at 37 °C after vortexing. The Fe_2Tf is purified over an S300 column followed by dialysis overnight and concentration by centrifugation at 1300 × *g* on a Sorvall T-6000D centrifuge. The loading efficiency can be determined by measuring absorption of the protein at 280 and 465 nm, respectively.
2. Dissolve appropriate amounts of DiIC12 in ethanol and inject into a buffer solution (PBS or buffer medium) containing fatty acid-depleted BSA (0.1 % w/v) while vortexing

for 5 min [18, 19]. Dialyze the solution against PBS and store at 4 °C under nitrogen until use.

3. Freshly prepare labeling solutions of Rh-dextran and Alexa 546-Tf in buffer medium (which contains glucose to meet energy demand and ensure normal membrane traffic) from respective stock solutions (in PBS) to get a final concentration of 5 mg/mL for Rh-dextran and 20 μg/mL for Alexa 546-Tf, respectively.

3.2.2 Sterol Labeling Solutions

1. For cell labeling, CTL is first loaded onto methyl-β-cyclodextrin (MβCD) as previously described for DHE. Crystals of synthesized CTL are dissolved in ethanol to obtain a 5 mM stock solution. Transfer 750 μL of this stock solution into a glass tube, and evaporate off the ethanol under nitrogen (*see* **Note 7**).
2. Add 1000 μL of the 30 mM MβCD solution in buffer medium (with 0.1 % (w/v) BSA) to get a MβCD/CTL-ratio of 8:1 (mol/mol). Carefully suspend the solution by vortexing and bath-sonicating the solution (*see* **Note 8**).
3. After centrifugation at 20,000 × *g* for 20 min, the supernatant CTL/MβCD solution should be carefully collected and stored at 4 °C under nitrogen.
4. Check the properties of the labeling solution and reproducibility of the loading procedure routinely by measuring its fluorescence excitation and emission spectra using an appropriate spectrofluorometer (in our case an ISS Chronos spectrofluorometer, Laboratory of Fluorescence Dynamics, Urbana Campaign, IL, USA) (*see* **Note 9**).
5. To make a labeling solution containing two different fluorescent sterols (i.e., DHE and TF-Chol), the same procedure as described above can be followed. That is, DHE and TF-Chol were added in appropriate amounts from an ethanol stock solution in a glass vial, evaporated together and suspended in 1 mL of the 30 mM MβCD solution in buffer medium (with 0.1 % (w/v) BSA). The final concentrations of DHE and TF-Chol in the MβCD complexes were 3.75 mM and 3.75–6 μM, respectively. Thus, DHE in this case was at least in 600-fold excess compared with TF-Chol.
6. To make a labeling solution containing only TF-Chol, dissolve this sterol probe in ethanol and follow the procedure described above, except that 100-fold less MβCD is used.

3.3 Transfection, Culture and Imaging of CHO Cells

3.3.1 Culture and Transfection of CHO Cells

1. For imaging, CHO cells are routinely seeded on glass coverslips as inlet to microscope dishes, which are pre-coated with poly-d-lysine as described [20].
2. Transfect cells with Cav1-eGFP plasmid using Lipofectamine or an equivalent transfection reagent according to the manufacturer's instructions. Allow cells to settle for 24 h, then wash and pulse-label with CTL/MβCD for 2 min at 37 °C. After labeling, wash the cells and chase in buffer medium.

3.3.2 Imaging of CTL Relative to Endocytic Probes and eGFP-Caveolin in CHO Cells

In our laboratory, we utilize a DMIRBE inverted wide field microscope equipped with a 63 × 1.4 NA oil immersion fluotar objective (Leica Lasertechnik GmbH) with a Lambda SC smart-shutter (Sutter Instrument Company) as illumination control. Images are acquired with a Hamamatsu Orca BT512 4-stage peltier and water cooled (−80 °C) CCD camera (Hamamatsu Photonics Inc., HamamatsuCity, Japan) driven by ImagePro Plus and ScopePro (Media Cybernetics, Inc., Silver Spring, MD, USA) or with an Andor Ixon^{EM} blue EMCCD camera operated at −75 °C and driven by the Solis software supplied with the camera. CTL can be imaged in the UV using a specially designed filter cube obtained from Chroma Technology Corp. with 335-nm (20-nm bandpass) excitation filter, 365-nm dichromatic mirror, and 405-nm (40-nm bandpass) emission filter. The eGFP-caveolin can be imaged using a standard fluorescein filter set [470-nm, (20-nm bandpass) excitation filter, 510-nm longpass dichromatic filter, and 537-nm (23-nm bandpass) emission filter]. In both channels, we usually acquire 10–12 images along the optical axis with a distance of 0.5 μm between subsequent frames. The microscope stage is controlled with a z-stepping motor (Merzhäuser, Germany).

3.3.3 Assessment of and Correction for Chromatic Aberration

To detect colocalization of CTL and Cav1-eGFP or any other green probe (as TF-Chol) or red-emitting fluorescent molecule (as Rh-dextran), the axial and lateral chromatic aberration of the microscope in the UV channel compared to green and red channels has to be taken into account [21]. To this end, serial focal plane images of 0.1 μm TetraSpec fluorescent beads (Molecular Probes) mounted in gelvatol on a glass coverslip are acquired as described [22]. Lateral chromatic shift between corresponding bead images are corrected using the TurboReg plugin of ImageJ software written by Dr. Thevenaz (Swiss Federal Insitute of Technology, Lausanne, Switzerland). Hereby, a rigid body transformation is applied to spatially register corresponding planes of CTL vs. Cav1-eGFP, DiIC12, Rh-dextran, and Alexa 546-Tf or of DHE vs. TF-Chol [23]. Axial chromatic aberration is measured by determining the in-focus position in the UV and red channel from obtained bead images, respectively. The point spread function (PSF) of the microscope has its intensity maximum at the in-focus position with some side-maxima given particular shape of the PSF. The in-focus position is also characterized by a peak maximum in combination with a half-width minimum of the autocorrelation function of the PSF having a Gaussian shape. Thus, the in-focus position can be determined by these criteria from the autocorrelation function of the PSF as described [22].

3.3.4 Sterol Trafficking from the PM to the ERC Is Independent of Caveolin 1

Intrinsically fluorescent polyene-sterols as DHE or CTL have been shown previously to traffic mostly by non-vesicular transport from the plasma membrane (PM) to the endocytic recycling compartment

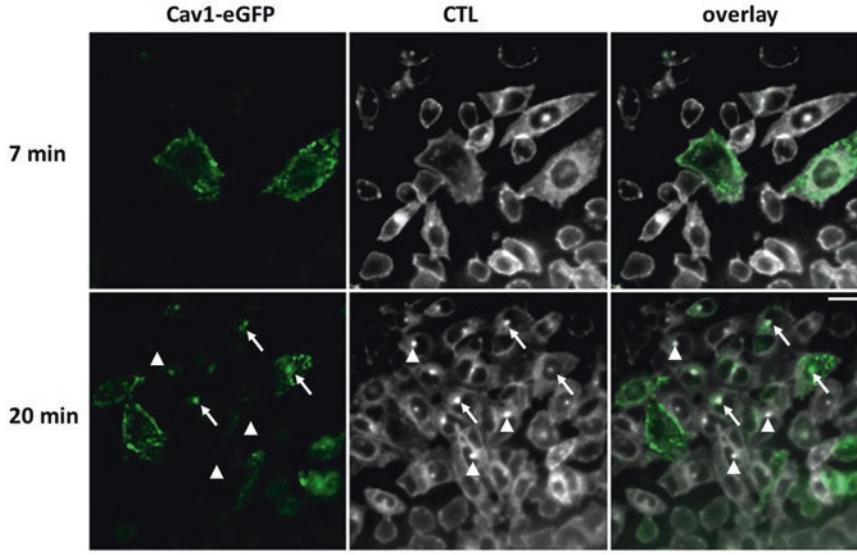

Fig. 3 Transport of CTL from the plasma membrane in cells expressing Cav1-eGFP. CHO cells were transiently transfected with the plasmid coding for Cav1-eGFP followed by labeling with CTL/MβCD for 2 min at 37 °C. Cells were washed and incubated in buffer medium for either 7 min (*upper panels*) or 20 min (*lower panels*) at 37 °C followed by imaging on a UV-sensitive wide field microscope, as described in the main text. CTL and Cav1-eGFP co-localize in the perinuclear region (resembling mostly the ERC) in some cells (*arrows*) but CTL reaches this region also in cells not expressing Cav1-eGFP (*arrowheads*). Bar, 10 μm

(ERC) in CHO cells [24, 25]. This transport is enhanced upon overexpressing the soluble sterol carrier protein StARD4 and results in enrichment of DHE in the cytoplasmic leaflets of the ERC and PM, respectively [25, 26]. On the other hand, significant vesicular sterol trafficking can be found in time-lapse imaging of DHE and TF-Chol (see below and [27]). Also, recycling of DHE from the ERC back to the PM was strongly reduced in a CHO mutant cell line expressing a mutated Rme-1/EHD domain protein, a known regulator of recycling of Tf from the ERC [24, 28]. Thus, both vesicular and non-vesicular trafficking modes contribute to sterol exchange between PM and ERC in mammalian cells. Caveolin consists of three isoforms which play a crucial structural role in establishing and maintaining submicroscopic PM invaginations in certain cell types, named caveolae [29]. Caveolin has also been implicated in the regulation of cellular cholesterol balance, while trafficking and alterations in cellular cholesterol content affect transport of caveolins [29, 30]. In addition, mutations in caveolin have been suggested to affect cellular cholesterol distribution [31].

Using the setup and tools described above, we set out experiments to study trafficking of CTL from the PM to the ERC in CHO cells transiently transfected with Cav1-eGFP (Fig. 3). We found that cells expressing Cav1-eGFP showed similar transport

dynamics of CTL from the PM to the ERC compared to cells not expressing caveolins (CHO cells do not contain caveolins in the first place). Some Cav1-eGFP co-localized with CTL in the perinuclear ERC/Golgi region after 20 min chase (arrows in Fig. 3), but CTL accumulated in the ERC also in cells not expressing Cav1-eGFP (arrowheads in Fig. 3). Thus, caveolins or at least caveolin 1 does not seem to have a controlling effect on sterol trafficking between PM and ERC.

Next, we used the instrumentation and tools described above to look for endocytic events, i.e., for co-internalization of caveolin and PM sterol (Fig. 4). CHO cells transiently expressing Cav1-eGFP were pulse-labeled for 2 min at 37 °C with CTL/MβCD, washed and chased for 5 min in the presence of 20 μg/mL Alexa 546-Tf in buffer medium. Labeled cells were imaged on a UV-sensitive wide field microscope, as described above (Subheadings 3.3.2 and 3.3.3). Even though CHO cells are less efficient in Tf uptake compared to TRVb-1 cells expressing the human Tf-receptor, we frequently observed fluorescent endosomes containing Alexa 546-Tf (Fig. 4a) [24]. Those endosomes also contained CTL and sometimes Cav1-eGFP (arrows in Fig. 4a), indicating that a portion of caveolin 1 is internalized by endocytosis together with sterol. In a separate experiment, cells were pre-labeled with Rh-dextran for 5 min, washed and labeled with CTL/MβCD, and imaged as described above. While occasionally, endosomes containing Rh-dextran and Cav1-eGFP were found, co-localization of such vesicles with CTL was rarely found (Fig. 4b). Thus, very little CTL seems to be transported to dextran containing endosomes following our protocol in CHO cells.

Finally, one can also label the PM using another lipid probe, as the lipophilic red emitting carbocyanine derivatives, as DiIC12, DiIC16, or DiIC18 (the number in the name indicates the length of the two aliphatic membrane anchoring chains on these probes, while the fluorophore forms the "head group"). These lipid analogs have a long tradition in membrane biophysics, as they show characteristic phase preference in model membranes in dependence on the degree of host lipid unsaturation and membrane cholesterol content [32, 33]. While DiIC12 is a fluid-preferring probe, DiIC16 and even more DiIC18 partition preferentially into phases or domains with saturated phospho- or sphingolipids. DiIC18 is also often used as a lipophilic probe in lipoproteins for uptake and trafficking studies [34–36]. We showed previously that DiIC12 segregates almost completely from DHE in giant unilamellar vesicles (GUVs) made of dipalmitoylphosphatidylcholine (DPPC), dioleoylphosphatidylcholine (DOPC) and DHE, while TF-Chol showed only a slight segregation from DiIC12 in a similar GUV system [17, 37]. DiIC12 and DiIC16 have also been used in endocytic trafficking studies, where they were found to segregate in CHO-derived TRVb1 cells; DiIC12 co-localized with fluorescent

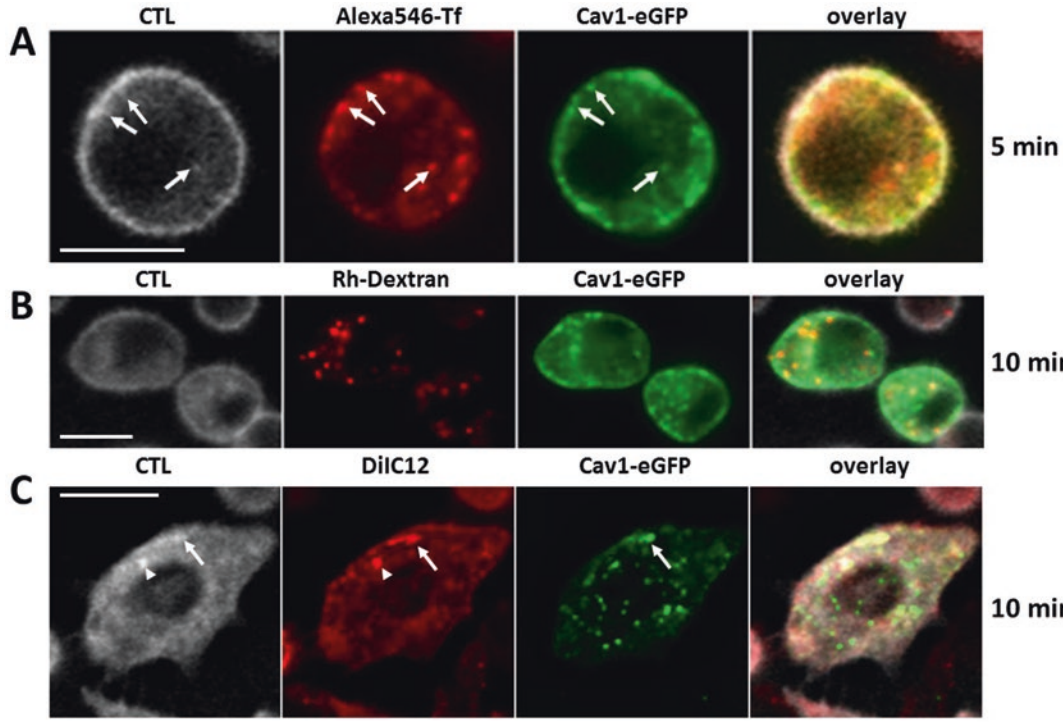

Fig. 4 Co-localization of CTL with Cav1-eGFP and endocytic markers. CHO cells were transiently transfected with the plasmid coding for Cav1-eGFP followed by labeling with CTL/MβCD for 2 min at 37 °C. (**a**) Cells were washed and incubated in buffer medium containing 20 μg/mL Alexa 546-Tf for 5 min at 37 °C followed by imaging on a UV-sensitive wide field microscope, as described in the main text. Individual endocytic vesicles containing CTL, Alexa 546-Tf and Cav1-eGFP were found underneath the PM and towards the cell center (*arrows* in panel **a**). (**b**) Cells were incubated with 5 mg/mL Rh-dextran for 5 min before labeling with CTL/MβCD. Cells were washed and incubated in buffer medium for 10 min at 37 °C followed by imaging as described above. (**c**) Cells were labeled with CTL/MβCD for 2 min at 37 °C, washed and labeled in the same way with DiIC12, washed and further incubated with in buffer medium for 10 min at 37 °C. Some endocytic vesicles containing CTL, DiIC12 and Cav1-eGFP (*arrows*) or only CTL and DiIC12 (*arrowheads*) were found close to the PM. Bar, 10 μm

Tf in the sterol-rich ERC, while DiIC16 was sorted to LE/LYSs [18]. Upon cholesterol depletion or increased membrane unsaturation, DiIC16 also accumulated in the ERC in these cells [38]. These effects seem to be cell-type dependent, as DiIC12 and DiIC16 co-localize with fluorescent Tf in basolateral and subapical early/recycling endosomes in polarized hepatic HepG2 cells [19]. When CHO cells transiently expressing Cav1-eGFP were pulse-labeled with CTL/MβCD followed by a brief labeling with DiIC12 and chase for 10 min at 37 °C, we found co-localization of all three probes in the PM and in PM derived vesicles or surface invaginations (arrows in Fig. 4). Overall, the co-localization of CTL and DiIC12 was higher than that of any of these probes with Cav1-eGFP, as often double-labeled vesicles having CTL and DiIC12 but no Cav1-eGFP were found (arrowheads in Fig. 4).

Co-localization of CTL and DiIC12 with Cav1-eGFP in CHO cells is not related to the phase preference of both lipid probes or to particular physicochemical properties of caveolae or caveolin-containing vesicles, as CTL and DiIC12 show opposite phase preference in model membranes [37]. Together, using the labeling strategy explained above, we can show that trafficking of fluorescent caveolin 1 overlaps with that of PM derived CTL, a close mimic of cholesterol. However, caveolin 1 does not seem to be required for sterol trafficking, nor is sterol particularly enriched in caveolar structures involving Cav1-eGFP at the cell surface. All these conclusions are in line with our earlier results [39, 40]. We cannot exclude, though, that the protocol we used for transient expression of Cav1-eGFP causes trafficking artifacts. To rule this out, one should employ cells with genome-edited expression of fluorescent caveolin in future studies [41].

3.3.5 Labeling of CHO Cells with TF-Chol and Time-Lapse Imaging of Sterols

TF-Chol is fluorescent in the visible spectrum and is significantly more photostable than DHE or CTL. Therefore, it is possible to acquire images of TF-Chol on a confocal or a multiphoton microscope without special optics. TF-Chol's excitation and emission maxima are at 495 and 507 nm, respectively. Consequently, on confocal microscope, the 488 nm laser line should be used to excite the fluorophore while the emission may be detected using for example a 510 ± 20 nm bandpass filter. Initially, we aimed to verify that TF-Chol can supplement sterol trafficking studies performed with polyene-sterols such as CTL or DHE. Therefore, we co-labeled CHO cells with DHE and TF-Chol, both loaded onto cyclodextrin as described in Subheading 3.2.2 above and in [17]. After 2-min pulse labeling, cells were washed and chased in buffer medium for 30 min at 37 °C. TF-Chol and DHE show almost perfect co-localization in CHO cells under these culture conditions (Fig. 5a). This is in contrast to cells cultured under conditions of excess fat storage, in which TF-Chol partitions artificially into lipid droplets in addition to its co-trafficking with DHE through endosomes [17, 42, 43]. Similarly, in HeLa cells which form abundant droplets under standard culture conditions, TF-Chol is mistargeted partially to droplets, while DHE or the cholesterol-binding polyene filipin indicate low abundance of non-esterified cholesterol in these organelles [17, 42]. However, we verified that in CHO cells under standard cell culture conditions, TF-Chol is a reliable marker of endosomal cholesterol distribution (*see* **Note 10**).

On the same wide field setup, we performed time-lapse imaging experiments of double-sterol labeled cells, first in the UV channel to follow the dynamics of DHE until it is more or less bleached (100 ms acquisition time with electron multiplication (EM) factor 50), followed by acquisition in the green channel to follow TF-Chol (50 ms without EM; Fig. 5b, b′). While both sterols label the same

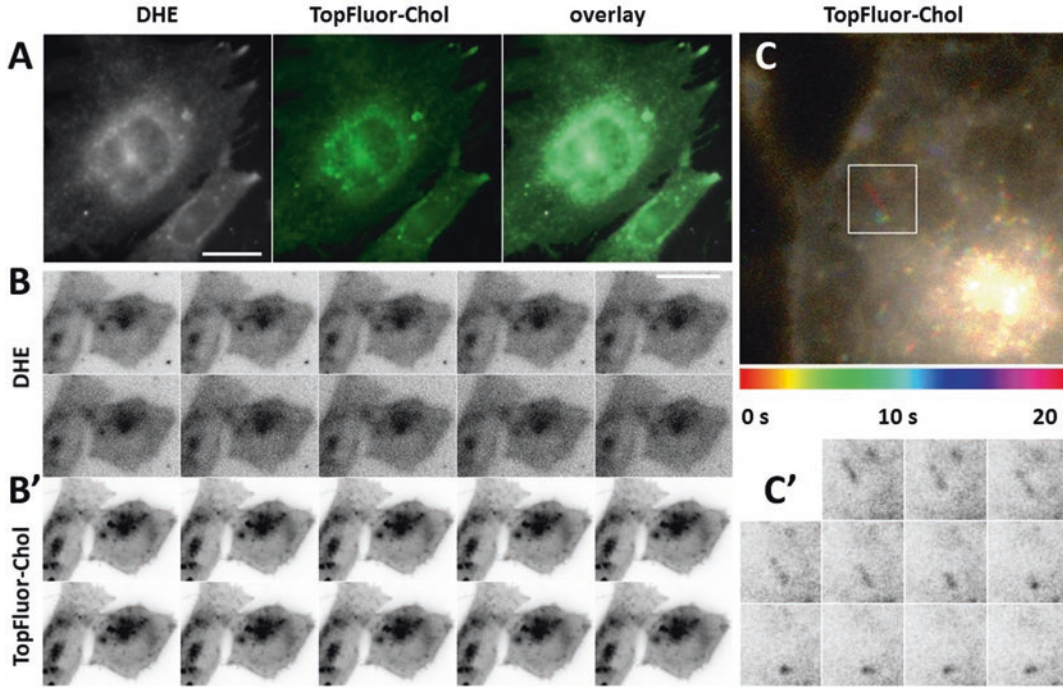

Fig. 5 Time-lapse imaging of DHE and TF-Chol in CHO cells. (**a**, **b**) Cells were co-labeled with DHE and TF-Chol from a complex with cyclodextrin for 2 min at 37 °C, washed and incubated in buffer medium for additional 30 min at 37 °C. Cells were imaged on a UV-sensitive wide field microscope, as described in the main text. (**a**) High co-localization of both sterol probes is found in CHO cells under these conditions (**b**), on the same system, double-labeled cells were repeatedly imaged, first in the UV channel to follow the dynamics of DHE (**b**) followed by imaging in the green channel to follow TF-Chol (**b′**), both at 2 Hz acquisition rate. Little dynamics but strong bleaching is found for DHE, while for TF-Chol no bleaching but significant vesicle movement in the cell periphery could be discerned (see also Supplemental Video 1). (**c**) In a separate experiment CHO cells were labeled only with TF-Chol and imaged another wide field setup equipped with a 150× NA 1.4 objective with an acquisition rate of 2 Hz. Directed movement of sterol containing vesicles in the cell periphery was found. (**c′**) Shows selected frames of the zoom box in panel (**c**) with inverted LUT for better visibility of vesicle movement from the *upper left* to the lower part of the image. The vesicle is stretched in the beginning indicating active pulling by cytoskeleton-assisted motor proteins. Bar, 10 μm

vesicles in these cells, tiny peripheral vesicles in the DHE channel are hardly discernable and can therefore not be tracked. The DHE-rich perinuclear, large vesicles and the ERC, however, do not move significantly during this experiment. Dim peripheral vesicles can however be clearly seen in the subsequently acquired video sequence for TF-Chol from the same field of view (see also a side-by-side comparison in the Supplemental Video 1). This result illustrates clearly the potential of TF-Chol for tracking of sterol-rich endosomes in living cells, thereby complementing studies performed with DHE or CTL.

In what follows, we focus on time-lapse imaging and tracking of TF-Chol in CHO cells. Further wide field time-lapse imaging was carried out on an Olympus IX70 microscope equipped with an

Andor camera and a 150× objective with NA = 1.4 (Fig. 5c). In this high-resolution imaging modality, we could observe extensive trafficking of vesicles containing TF-Chol, as indicated in the motional color coding in Fig. 5c. In particular, we found vesicles moving directionally, i.e., along a straight line and with significant elongation into tubes parallel to the movement direction (Fig. 5c box, enlarged in Fig. 5c′). Such vesicles move actively by specific motors along cytoskeleton tracks as microtubule or actin, as we have shown for TF-Chol in CHO cells [6]. In the same setup and identical recording, TF-Chol bleaches with a half-time of about 64 frames (see Supplemental Material in [6]). In contrast, when time-lapse imaging is performed on a multiphoton microscope with an excitation wavelength of 930 nm, photobleaching of TF-Chol in CHO cells was virtually absent [6]. Fluorescence time-lapse measurements of TF-Chol were performed using a custom-built setup based on an Olympus IX70 microscope. The objective used was a 60× water immersion objective with a NA of 1.2. The excitation light source was a femtosecond Ti:Sa laser (Broadband Mai Tai XF W25 with a 10W Millennia pump laser, 80 MHz pulse-frequency, tunable excitation range 710–980 nm, Spectra Physics, Mountain View, CA). To collect TF-Chol's emission, a 540 ± 25 nm filter was used (Bright-Line HC). The light was detected by a photomultiplier tube (Hamamatsu H7422P-40), operated in the photon counting mode. The data were acquired using simFCS software developed by the Laboratory for Fluorescence Dynamics, University of California, Irvine. Tracking of vesicles containing TF-Chol in CHO cells is based on the data gathered on this microscope and further discussed below.

3.3.6 Image Optimization for Particle Detection

Image denoising in SpatTrack is based on a bandpass filtering method first described by Crocker and Grier [44] which we found to be the best denoising algorithm for fluorescent particles in a comparison between different denoising algorithms for particle tracking [45]. First, two low-pass images are generated; (1) an image convolved by a Gaussian blur with a variance of one pixel to suppress image noise and (2) an image convolved with a boxcar filter with extent $2w+1$, where w is an integer larger than the average radius of the particles but smaller than the smallest inter-sphere separation. The denoised image is generated by subtracting the boxcar filtered image from the Gaussian blurred image. Finally, all pixels with intensities below a given threshold are set equal to zero. The threshold is based on the average fluorescence of the denoised image. For example, when the intensity threshold is set to 5, all pixels with an intensity below 5× the average intensity of the image are set to zero. To account for possible photobleaching during the image acquisition (absent in multiphoton imaging but present in wide field imaging of TF-Chol, CTL and DHE), the threshold is calculated for each frame in the time-lapse image sequence.

The Image-denoiser GUI of SpatTrack along with an image of a CHO cell labeled with TF-Chol and imaged by multiphoton microscopy as described above is shown in Fig. 6a. The right panel in this GUI shows the corresponding denoised image.

3.4 Tracking of Vesicles Containing TF-Chol

Once the image sequence has been optimized for particle tracking, open the tracking GUI from the main SpatTrack window. Particle tracking in SpatTrack 2.0 has been considerably upgraded compared to the earlier version, since we have implemented an improved tracking algorithm based on the Hungarian (Munkres') algorithm to optimize the nearest neighbor distances between coordinates in one frame and the next [46]. This implementation is approximately 10 times faster than the linking algorithm used in SpatTrack 1.0 [14, 45]. Additionally, the tracking algorithm now allows for relinking of shorter trajectories caused by particle merging or splitting (*see* **Note 11**).

Particle tracking in SpatTrack is performed in three steps (1) particle detection, where the particles are located in each frame and the coordinates are refined to sub-pixel precision, (2) trajectory linking, where the detected coordinates are linked from one frame to the next and (3) trajectory merging, where the algorithm attempts to relink remaining short trajectories.

1. *Particle Detection*. Particle detection requires two parameters (a) an intensity threshold and (b) a particle location diameter. If the fluorophore bleaches during image acquisition, the particles will be dimmer in the last frame than in the first frame. Therefore, the intensity threshold is calculated for each frame in the image stack based on the user input. Specifically, the intensity threshold is given by a percentage of pixel intensities. For example, if the threshold is set to 92, the detection algorithm will ignore all but the 8 % brightest pixels in the respective frame of the image stack. The particle location diameter ensures that only one particle coordinate is found within a particle. In a noisy image a particle could potentially contain more than one bright pixel which might be considered a particle coordinate. Thus, the "Location Diameter" should ideally be set to a value larger than the estimated particle size but smaller than the distance between two neighbor particles. However, for particles undergoing merging or splitting, two particle centroids may actually be within one "Location Diameter." Therefore, the "Location Diameter" should be set according to the expected behavior of the particles.
2. *Trajectory Linking*. Frame-to-frame linking is performed by the simpletracker MatLab function developed by Jean-Yves Tinevez and available on the MatLab File Exchange at http://www.mathworks.com/matlabcentral/fileexchange/34040-simple-tracker. Initially, the Euclidean distance is calculated for

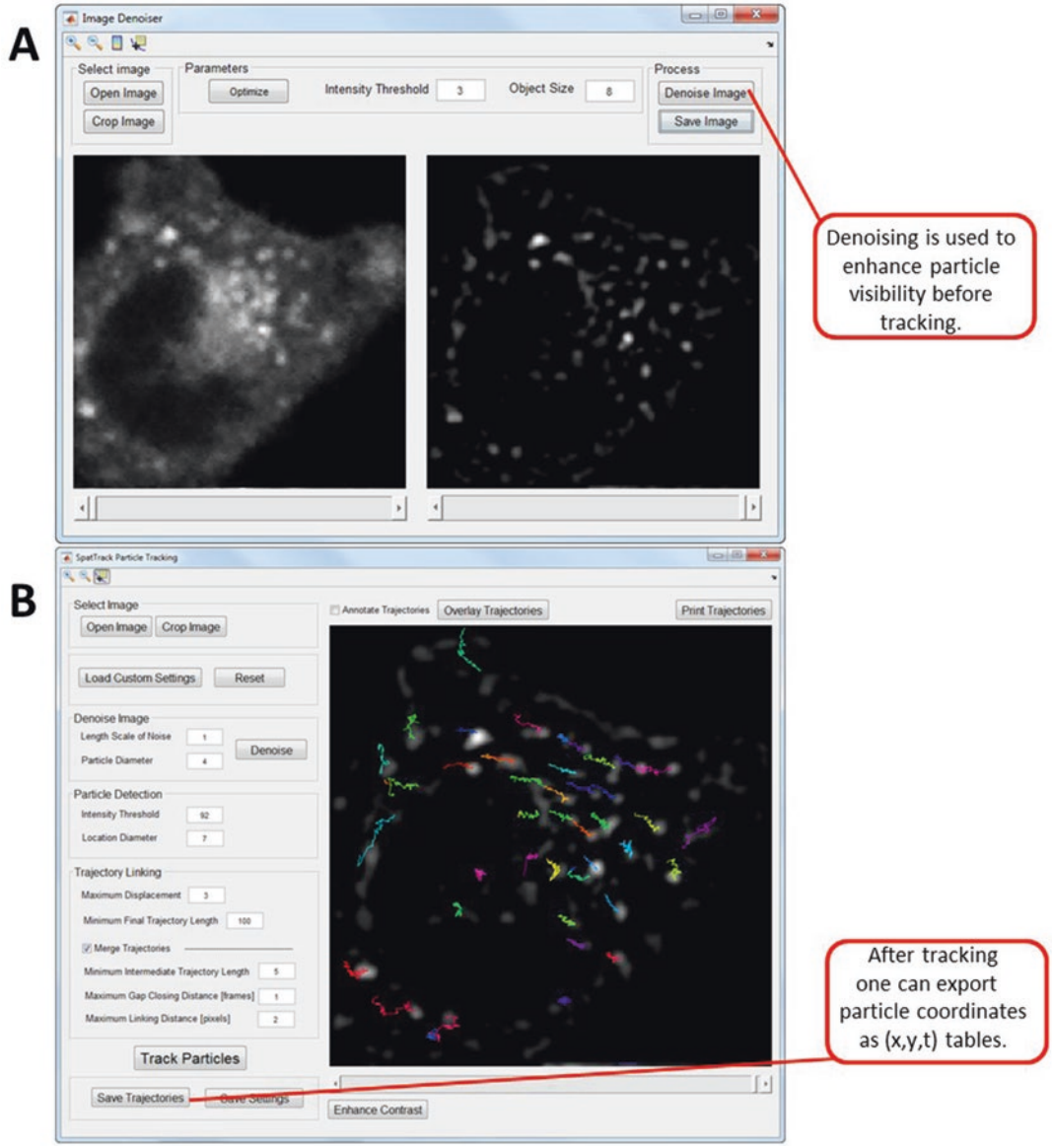

Fig. 6 Overview of the image denoising GUI of SpatTrack. (**a**) Multiphoton image sequence of a TF-Chol containing CHO cell shown in the left panel and the denoised image is shown in the right hand panel. Image denoising was performed with an estimated object size of 8 pixels and with an intensity threshold of 90 % of all pixel intensities in the intermediate denoised image. (**b**) Example of particle tracking in SpatTrack in the denoised image of a cell labeled with TF-Chol. Particle tracking was performed with an intensity threshold of 92 %, a location diameter of 7 pixels, a maximum displacement of 3 pixels, a minimum intermediate trajectory length of 5 pixels, a maximum gap closing distance of 1 frame and a maximum linking distance of 2 pixels. The minimum final trajectory length was set to 100 frames

all particle coordinates in frame i with respect to all particle coordinates in frame i+1. Subsequently, the sum of particle-particle distances is minimized by the Hungarian algorithm, such that each particle in frame i is connected to the nearest neighbor in frame i+1. To avoid unrealistically large link-distances, the user must supply the "Maximum Displacement" allowed in the "Trajectory Linking" panel of the tracking GUI (*see* Fig. 6b). Typically, the "Linking Distance" should be no larger than the particle size. If this is not possible, one might consider acquiring the time-lapse image sequence at a higher frame rate.

3. *Trajectory Merging.* At this stage, there are likely a large number of trajectories that are shorter than the number of frames in the image series. These may arise from particles moving into or out of the focal plane or alternatively due to merging or splitting particles. SpatTrack includes the possibility to relink these incomplete trajectories. To do this, the "Merge Trajectories" box must be checked. Relinking requires three parameters. The "Minimum Intermediate Trajectory Link" which determines the shortest trajectory that the algorithm will consider for relinking. For example, it is very likely that a particle coordinate detected in only a single frame is due to noise rather than a true particle. Typically, we set the "Minimum Intermediate Trajectory Link" to 5 frames. Thus, all trajectories consisting of less than 5 steps are discarded prior to relinking. The second parameter is the "Maximum Gap Closing Distance." This is the maximum number of frames allowed for linking the end of one trajectory to the start of another. Finally, the algorithm requires a "Maximum Linking Distance," which is the largest distance, in pixels, over which two trajectories can be linked. For a more elaborate description of the linking algorithm, *see* **Note 11**.
4. *Minimum Final Trajectory Length.* After the trajectory merging step, there are still likely a number of trajectories of intermediate length. Thus, setting this to less than the full length of the number of frames in the time-lapse image sequence will often result in more trajectories. On the other hand, the statistical power of the mean squared displacement (MSD) analysis decreases with trajectory length. Hence, it is up to the judgement of the experimentalist to determine the minimum allowed trajectory length.
5. *Saving the Results.* Finally, the trajectories can be saved as three separate .csv files containing the x- and y-coordinates for each trajectory as well as the particle intensities in each frame. Similarly, the tracking parameters can be saved so they may be reused in a later experiment.

3.5 Trajectory Analysis

3.5.1 Introduction to Trajectory Analysis

Within the Trajectory-Analysis GUI, SpatTrack allows the user to easily calculate the MSD of the trajectories and to determine the most likely diffusive process underlying the observed motion (Fig. 7). The type of motion is reflected in the particle trajectory, which essentially consists of a number of particle steps with a step length and direction determined by the type of motion. For normal (Brownian) diffusion the step lengths are distributed according to a Gaussian distribution. In other words, the probability density function (PDF) or diffusion propagator for normal diffusion is:

$$P(r,t) = \frac{1}{\sqrt{\pi\sigma}} \exp\left(-r^2 / \sigma\right), \tag{2}$$

where r is the step length and σ is the variance of the Gaussian function. For purely random motion the average of the Gaussian function is zero. However, the variance, which is also called the MSD, increases linearly with time. The variance is given by $\sigma = 2dDt$, where d is the dimensionality of the motion. Thus, for two-dimensional diffusion:

$$MSD(t) = 4Dt, \tag{3}$$

where D is the diffusion constant of the particle. For a particle moving by a combination of diffusion and flow the MSD is given by:

$$MSD(t) = 4Dt + v^2t^2, \tag{4}$$

where v is the flow speed. Intracellular motion is often anomalous either due to active transport of hindered diffusion. Both cases can be described by fractional Brownian motion where the MSD is given by:

$$MSD(t) = 4D_\alpha t^\alpha, \tag{5}$$

where α is the anomalous exponent. For anomalous sub-diffusion $0 < \alpha < 1$ and a plot of the MSD as a function of time shows a downwards curvature (Fig. 8b). In contrast to this, we have $1 < \alpha < 2$ for anomalous super-diffusion, which is recognized by an upwards curved MSD vs time plot. We observed that intracellular diffusion often is a mixture of different types of diffusion. Therefore, we implemented a model for anomalous sub-diffusion plus flow in SpatTrack. This model may either be used to describe the MSD of a trajectory switching between the two types of motion or more commonly for a population of particles where one sub-population moves by diffusion plus flow while the other population moves by hindered diffusion. The MSD for the mixed diffusion is given by:

$$MSD(t) = 4D_\alpha t^\alpha + v^2t^2. \tag{6}$$

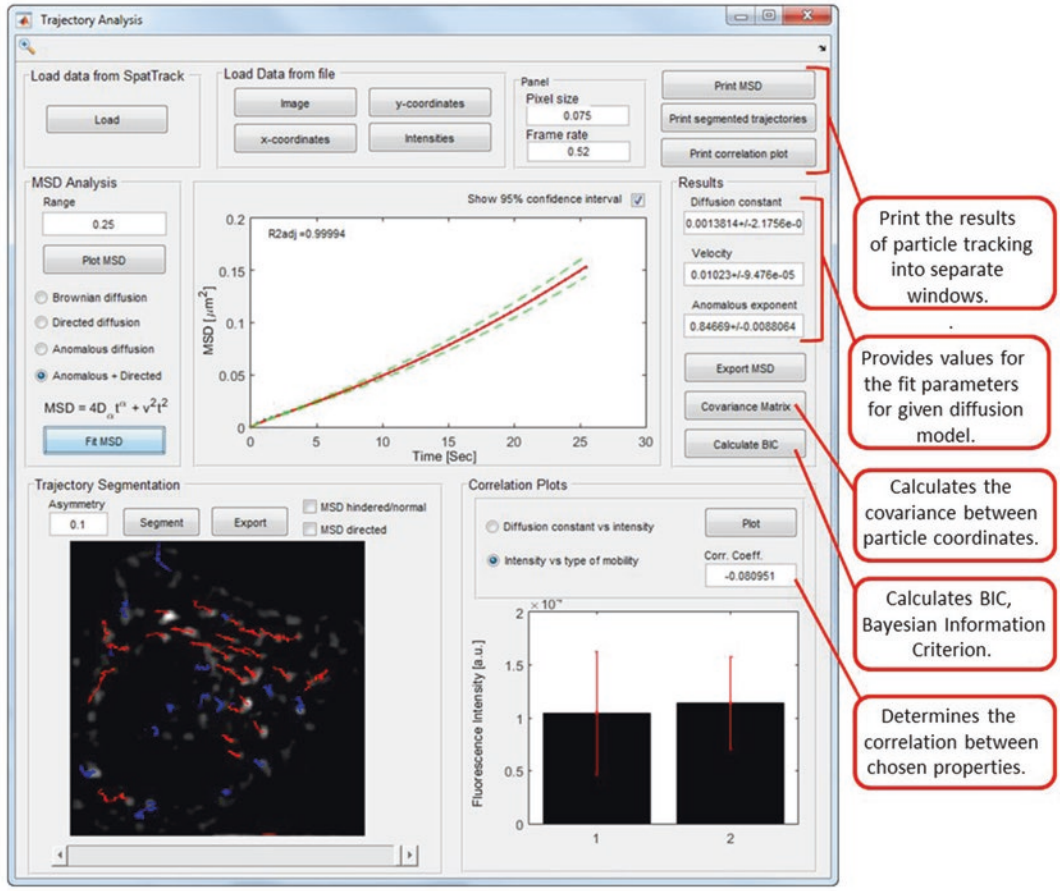

Fig. 7 Overview of the trajectory analysis GUI of SpatTrack. Here the MSD for 53 vesicles containing TF-Chol was calculated in the 1/4th range and fitted to the model for anomalous subdiffusion plus flow yielding a diffusion constant of $D\alpha = 1.4 \times 10^{-3}$ μm²/sα, $v = 1.0 \times 10^{-2}$ μm/s and $\alpha = 0.85$. The lower left panel shows trajectories classified as directed plotted in *red* and trajectories classified as hindered/normal plotted in *blue*. Finally, the bar plot in the lower right corner shows that the two types of trajectories have the same average fluorescence intensity

Rather than determining the second moment of the distribution of step sizes, the MSD is typically calculated as:

$$MSD(t) = \frac{1}{N-n}\sum_{t=1}^{N-n} d^2\left(\boldsymbol{P}_t, \boldsymbol{P}_{t+vt}\right), \tag{7}$$

where $d^2(\mathrm{P}t, \mathrm{P}t_{+\Delta}t)$ is the distance traveled from time t to time $t + \Delta t$ squared (*see* **Note 12**).

3.5.2 Trajectory Analysis in SpatTrack

1. *Loading the trajectories.* The Trajectory-Analysis GUI is shown in Fig. 7 and can be opened from the main SpatTrack menu. The trajectories can either be loaded directly from the tracking GUI or from the .txt files containing the *x*- and *y*-coordinates

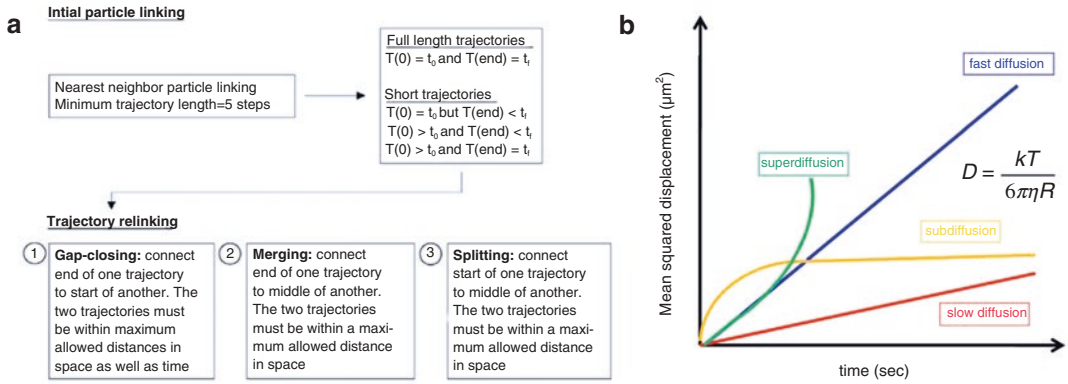

Fig. 8 Diffusion analysis in SpatTrack. (**a**) Schematic description of the trajectory relinking process; (**b**) scheme of possible diffusion processes and the resulting mean square displacement (MSD) of particles. The MSD is the second moment of the probability density function (PDF) of the underlying stochastic process. For Brownian motion (i.e., normal diffusion), the MSD grows linearly with time, and the slope is proportional to the diffusion coefficient, *D*. Thus, slow (normal) diffusion has a small slope (*red curve*) and fast (normal) diffusion has a larger slope (*blue curve*). In case of anomalous diffusion, the MSD changes with time as MSD ~$t\alpha$ with $0 < \alpha < 1$ for subdiffusion (*yellow curve*) and $\alpha > 1$ for superdiffusion (*green curve*). See text for further explanations

and the particle intensities. To load the data directly from the tracking GUI open the Trajectory Analysis GUI and click on the load button. Alternatively, the data may be loaded from files. The advantage of this approach is that one can pool the trajectories from several cells in one experiment and, thus, increase the statistical power of the MSD analysis. Additionally, loading the trajectories from files allows one to use a different tracking algorithm provided that the files are organized correctly. For more information on the file format, see the SpatTrack user guide (*see* **Note 13**).

2. *Calculating and Fitting the MSD.* Once the trajectories have been loaded, set the pixel size and the frame rate. Additionally, the MSD analysis requires the range in which to calculate the MSD. As described in **Note 12**, the rule of thumb is to set the range to ¼ of the full MSD. Thus, set the range to 0.25. SpatTrack includes analytical expressions for four different types of diffusional motion (a) Normal diffusion, (b) diffusion plus flow, (c) anomalous diffusion and (d) anomalous diffusion plus flow. The latter was developed to describe the motion of endosomes which showed anomalous sub-diffusion on short time scales and directed diffusion on longer time scales [6]. However, it may also be useful where some particles are moving by anomalous sub-diffusion while other move by directed diffusion. To determine the best model to fit the MSD to, we suggest using the decision tree described in Fig. 2 of Lund et al. [14]. Importantly, the algorithm implemented in SpatTrack can calculate the MSD for trajectories that are not of

the same length, do not start at the same time or have missing coordinates (i.e., gaps). The MSD for the 53 TF-Chol containing vesicles found in the tracking section above was best fitted to the model for anomalous diffusion plus flow which yielded $D\alpha = 1.4 \times 10^{-3}$ μm^2/sα, $v = 1.0 \times 10^{-2}$ μm^2/s and an anomalous coefficient $\alpha = 0.85$ (Fig. 7).

3. *Trajectory segmentation*. In the Trajectory Analysis GUI, it is possible to separate trajectories of particles moving by diffusion plus flow from trajectories of particles moving by normal or hindered subdiffusion. Trajectory separation is based on the asymmetry of each trajectory which is calculated from the radius of gyration (RoG) [47, 48]. The asymmetry is calculated as $a_2 = R_2^2 / R_1^2$, where R_1 and R_2 are the larger and smaller principal radii of the RoG. For a circular trajectory $R_1 = R_2$ and, consequently, $a_2 = 1$. On the other hand for a linear trajectory $R_2 = 0$ and, thus, $a_2 = 0$. Based on simulated trajectories, Saxton showed that the most probable a_2 value for Brownian diffusion = 0.12. Thus, to separate directed trajectories from normal/hindered trajectories, we set the asymmetry to 0.1. The image in the lower left shows a frame of the TF-Chol vesicles overlaid with directed trajectories in red and normal/hindered trajectories in blue. Once the trajectories have been separated, the MSDs can be analyzed separately for the directed and the normal/hindered trajectories. For the directed trajectories this yielded a diffusion constant $D = 9.1 \times 10^{-4}$ μm^2/s and a speed of the directed motion, $v = 9.9 \times 10^{-3}$ μm/s (data not shown). The MSD for the normal/hindered fraction of trajectories was best fitted to the model for normal diffusion with a diffusion constant of $D = 1.4 \times 10^{-3}$ μm^2/s (data not shown).

4 Notes

1. It is advisable to change the tubes often—every 15 s or so—in particular when you expect your product to be eluted.
2. Drip the bicarbonate slowly as the reaction can be violent.
3. Weigh mercury acetate in a fume hood. When working with mercury (both acetate and mercury-containing waste), be sure to wear two layers of gloves.
4. Several washings may be necessary. When you add DCM, mix the precipitate with it thoroughly. The precipitate is mercury (I) acetate, which is insoluble in water and the majority of organic solvents.
5. Refer to the evaporator's manual for the conditions under which it should be removed.

6. Preferably use dark glass vials.
7. Evaporate the solvent slowly by gently rotating the glass tube manually during the evaporation process. In this way, you maintain the solution temperature and obtain at the same time a thin even film of the fluorescent sterol on the wall of the glass vial. Such a film makes the subsequent loading step onto cyclodextrin more efficient.
8. While the sterol-cyclodextrin solution is typically turbid right after dissolving the sterol from the ethanol-evaporated lipid film, it should become opalescent after sonication. This is a good indication for successful loading of CTL (or DHE) onto MβCD. Hold the glass tube against a ceiling light and watch the slight coloring when moving the tube slightly back and forth.
9. Polyene-sterols such as DHE or CTL show three characteristic peaks in their emission spectrum, and the one at lowest energy (i.e., highest wavelength centered around 410 nm) shows a characteristic increase upon loading the sterol onto MβCD (not shown but see [49] for an example spectrum with DHE).
10. We recommend assessing the extent of mistargeting of TF-Chol to lipid droplets prior to any live-cell imaging application of this cholesterol analog. Lipid droplets are mostly rich in triacylglycerols (e.g., when feeding fibroblast cell cultures with oleic acid from an albumin complex or when adipocytes form after inducing differentiation of suitable fibroblast-like cells [17], [22]). Such droplets contain only little cholesterol in its non-esterified form in the phospholipid monolayer surrounding the droplets [22, 42, 50]. In contrast, specialized cell types that esterify primarily cholesterol, such as macrophages, contain also significant non-esterified cholesterol in their droplets [51–53]. This is likely because the cholesteryl-ester rich core can also accommodate some cholesterol, in contrast to the triacylglycerol-rich emulsions forming the core of droplets in most of the cultured cells [54, 55]. The BODIPY group is a prominent marker of droplets, which in most cells are rich in triacylglycerols [56, 57]. Thus, it is very important to check the extent of mistargeting of TF-Chol due to passive partitioning into these organelles. This can be conveniently done using infrared droplet markers in multi-color imaging (as DeepRed-LipidTox®) together with DHE or CTL as a reference cholesterol probe [17]. Alternatively, one can use filipin staining as a reference to assess the extent of mistargeting of TF-Chol [58]. Additional labeling with Alexa 546-Tf would allow one to highlight the ERC in parallel. Image analysis protocols for quantification of sterol content in droplets relative to the ERC can be found in our previous publications [17, 22, 59].

11. Relinking incomplete trajectories (*see* Fig. 8a): As described above the initial tracking process may lead to several incomplete trajectories (i.e., trajectories with a lower number of steps than the number of frames in the time-lapse image sequence). Incomplete trajectories could be due to a particle entering or leaving the focal plane during image acquisition but could also be caused by merging or splitting particles. Since a "trajectory" consisting of a single coordinate in a single frame is likely due to noise, the first step in the relinking algorithm is to remove very short trajectories. Commonly, we remove any trajectories shorter than five steps. Subsequently, the incomplete trajectories can be divided into three subclasses (a) trajectories which start at the first frame but end before the last frame, (b) trajectories which start later than the first frame and ends before the last frame, and (c) trajectories which start later than the first frame and ends at the last frame. Trajectory relinking proceeds in three steps. The first step is gap closing which attempts to connect the end of one trajectory to the beginning of another trajectory within an allowed pixel wise distance and number of frames. In practice, the spatial and temporal allowed distances are given by the "Maximum Linking Distance [pixels]" and the "Maximum Gap Closing Distance [frames]" in the tracking GUI. From all possible trajectories fulfilling these criteria, the link is made between the two trajectories which minimize the Euclidean end-to-start distance but such that no end is connected to more than one start and *vice versa*. After this step the trajectory is still incomplete. In order for the trajectory to be complete the missing coordinates must be filled with coordinates from another trajectory within the allowed spatial linking distance in the same frames. Otherwise, the trajectory is eventually discarded. Particle merging is performed by linking the end of a trajectory that ends at time t to the middle of trajectory at time t+1. Similarly, particle splitting is performed by connecting the beginning of a trajectory at time t+1 to the middle of a trajectory at time t. Common to both trajectory merging and splitting, the trajectories must be within the "Maximum Linking Distance [pixels]."
12. Statistical Power of the MSD Calculation: From Eq. (7) it follows that the statistical reliability of the MSD decreases with increasing lag-time [60]. For example, for a trajectory of 100 steps and a lag-time of 2 steps, the MSD is averaged over 100–2 = 98 trajectory segments while a lag-time of 98 steps the MSD is averaged over 2 segments. This raises two questions (a) which lag-time yields the most accurate result and (b) how many steps should the trajectory consist of to reliably

determine the diffusional parameters. Based on simulated trajectories of 1024 steps, Saxton showed that including all 1024 points of the MSD resulted in a very broad distribution of diffusion constants while including only 8 or 4 time points narrowed the distribution of diffusion constants significantly [60]. Recently, this has been reexamined for a large set of real, microscopy based trajectories, which showed that determining the diffusion constant from the first 4 points in the MSD (excluding the point at $t = 0$) yielded an accuracy of 25 % for a trajectory of 100 steps which increased to 10 % for trajectories of 1000 steps [61]. Unfortunately, it is often not possible to obtain 1000 or more frames of a biological system due to photobleaching or particles leaving the focal plane. Moreover, for such an image sequence the effect of phototoxicity should be considered [46, 62]. Therefore, most trajectories from a biological system will likely consist of a few hundred steps. One way to improve the result is to calculate the ensemble average of several MSDs [60, 63]. However, doing so may hide subpopulations with different types of motion [64]. Furthermore, even for an ensemble averaged MSD, the statistical significance decreases with increasing lag-time. Hence, a rule of thumb is to fit the first 1/4th of the time points in the MSD [60].

13. Along with this publication comes an improved version of SpatTrack compared to our original publication [14]. In SpatTrack 2.0, we have implemented an improved tracking algorithm, which implements the simpletracker frame linking algorithm developed by Jean-Yves Tinevez and freely available at the MatLab File Exchange (http://www.mathworks.com/matlabcentral/fileexchange/34040-simple-tracker) Simpletracker uses the Hungarian algorithm to optimize the nearest neighbor distances between coordinates in one frame and the next and is approximately 10 times faster than the linking algorithm implemented in SpatTrack 1.0 [14, 45]. The MSD algorithm can now calculate the average MSD of several trajectories where some of the particle coordinates are missing. You can download SpatTrack 2.0 together with an updated User Guide and sample images described in the text as standalone version at www.sdu.dk/bmb/spattrack. Please note that MatLab is not required to run the program, but the MatLab Runtime environment (version 8.5 2015a 64-bit for Windows available at http://www.mathworks.com/products/compiler/mcr/) must be installed in the same folder as the main program. Further download instructions can be found in the User Guide.

References

1. Solanko KA, Modzel M, Solanko LM, Wüstner D (2016) Fluorescent sterols and cholesteryl esters as probes for intracellular cholesterol transport. Lipid Insights 8(Suppl 1):95–114
2. Wüstner D, Lund FW, Röhrl C, Stangl H (2015) Potential of BODIPY-cholesterol for analysis of cholesterol transport and diffusion in living cells. Chem Phys Lipids 194:12–28
3. Li CH, Bai L, Li DD, Xia S, Xu T (2004) Dynamic tracking and mobility analysis of single GLUT4 storage vesicle in live 3T3-L1 cells. Cell Res 14(6):480–486
4. Lizunov VA, Stenkula K, Troy A, Cushman SW, Zimmerberg J (2013) Insulin regulates Glut 4 confinement in plasma membrane clusters in adipose cells. PLoS One 8(3):e57559
5. Hao X, Shang X, Wu J, Shan Y, Cai M, Jiang J et al (2011) Single-particle tracking of hepatitis B virus-like vesicle entry into cells. Small 7(9):1212–1218
6. Lund FW, Lomholt MA, Solanko LM, Bittman R, Wüstner D (2012) Two-photon time-lapse microscopy of BODIPY-cholesterol reveals anomalous sterol diffusion in chinese hamster ovary cells. BMC Biophys 18:5–20
7. Chen H, Yang J, Low PS, Cheng JX (2008) Cholesterol level regulates endosome motility via Rab proteins. Biophys J 94(4):1508–1520
8. Pentchev PG, Comly ME, Kruth HS, Tokoro T, Butler J, Sokol J et al (1987) Group C Niemann-Pick disease: faulty regulation of low-density lipoprotein uptake and cholesterol storage in cultured fibroblasts. FASEB J 1(1): 40–45
9. Liscum L, Ruggiero RM, Faust JR (1989) The intracellular transport of low density lipoprotein-derived cholesterol is defective in Niemann-Pick type C fibroblasts. J Cell Biol 108(5): 1625–1636
10. Lloyd-Evans E, Morgan AJ, He X, Smith DA, Elliot-Smith E, Sillence DJ et al (2008) Niemann-Pick disease type C1 is a sphingosine storage disease that causes deregulation of lysosomal calcium. Nat Med 14(11):1247–1255
11. Zervas M, Dobrenis K, Walkley SU (2001) Neurons in Niemann-Pick disease type C accumulate gangliosides as well as unesterified cholesterol and undergo dendritic and axonal alterations. J Neuropathol Exp Neurol 60(1):49–64
12. Sleat DE, Wiseman JA, El-Banna M, Price SM, Verot L, Shen MM et al (2004) Genetic evidence for nonredundant functional cooperativity between NPC1 and NPC2 in lipid transport. Proc Natl Acad Sci U S A 101(16): 5886–5891
13. Vanier MT, Millat G (2003) Niemann-Pick disease type C. Clin Genet 64(4):269–281
14. Lund FW, Jensen ML, Christensen T, Nielsen GK, Heegaard CW, Wustner D (2014) SpatTrack: an imaging toolbox for analysis of vesicle motility and distribution in living cells. Traffic 15(12):1406–1429
15. Thompson RE, Larson DR, Webb WW (2002) Precise nanometer localization analysis for individual fluorescent probes. Biophys J 82(5): 2775–2783
16. Yamashiro DJ, Tycko B, Fluss SR, Maxfield FR (1984) Segregation of transferrin to a mildly acidic (pH 6.5) para-Golgi compartment in the recycling pathway. Cell 37:789–800
17. Wüstner D, Solanko LM, Sokol E, Lund FW, Garvik O, Li Z et al (2011) Quantitative assessment of sterol traffic in living cells by dual labeling with dehydroergosterol and BODIPY-cholesterol. Chem Phys Lipids 164(3): 221–235
18. Mukherjee S, Soe TT, Maxfield FR (1999) Endocytic sorting of lipid analogues differing solely in the chemistry of their hydrophobic tails. J Cell Biol 144:1271–1284
19. Wüstner D (2006) Quantification of polarized trafficking of transferrin and comparison with bulk membrane transport in hepatic cells. Biochem J 400:267–280
20. Salzmann NH, Maxfield FR (1989) Fusion accessibility of endocytic compartments along the recycling and lysosomal endocytic pathways in intact cells. J Cell Biol 109:2097–2104
21. Wüstner D, Herrmann A, Hao M, Maxfield FR (2002) Rapid nonvesicular transport of sterol between the plasma membrane domains of polarized hepatic cells. J Biol Chem 277: 30325–30336
22. Wüstner D, Færgeman NJ (2008) Chromatic aberration correction and deconvolution for UV sensitive imaging of fluorescent sterols in cytoplasmic lipid droplets. Cytometry A 73(8): 727–744
23. Thevenaz P, Ruttimann UE, Unser E (1998) A pyramid approach to subpixel registration based on intensity. IEEE Trans Image Process 7:27–41
24. Hao M, Lin SX, Karylowski OJ, Wüstner D, McGraw TE, Maxfield FR (2002) Vesicular and non-vesicular sterol transport in living cells. The endocytic recycling compartment is a major sterol storage organelle. J Biol Chem 277:609–617
25. Mondal M, Mesmin B, Mukherjee S, Maxfield FR (2009) Sterols are mainly in the cytoplas-

mic leaflet of the plasma membrane and the endocytic recycling compartment in CHO cells. Mol Biol Cell 20(2):581–588

26. Mesmin B, Pipalia NH, Lund FW, Ramlall TF, Sokolov A, Eliezer D et al (2011) STARD4 abundance regulates sterol transport and sensing. Mol Biol Cell 22(21):4004–4015
27. Lund FW, Lomholt MA, Solanko LM, Wüstner D (2012) Two-photon time-lapse microscopy of BODIPY-cholesterol reveals anomalous sterol diffusion in Chinese hamster ovary cells. BMC Biophys 5:20
28. Lin SX, Grant B, Hirsh D, Maxfield FR (2001) Rme-1 regulates the distribution and function of the endocytic recycling compartment in mammalian cells. Nat Cell Biol 3:567–572
29. Ikonen E, Parton RG (2000) Caveolins and cellular cholesterol balance. Traffic 1:212–217
30. Sharma DK, Brown JC, Choudhury A, Peterson TE, Holicky E, Marks DL et al (2004) Selective stimulation of caveolar endocytosis by glycosphingolipids and cholesterol. Mol Biol Cell 15:3114–3122
31. Pol A, Luetterforst R, Lindsay M, Heino S, Ikonen E, Parton RG (2001) A caveolin dominant negative mutant associates with lipid bodies and induces intracellular cholesterol imbalance. J Cell Biol 152:1057–1070
32. Baumgart T, Hunt G, Farkas ER, Webb WW, Feigenson GW (2007) Fluorescence probe partitioning between Lo/Ld phases in lipid membranes. Biochim Biophys Acta 1768(9): 2182–2194
33. Spink CH, Yeager MD, Feigenson GW (1990) Partitioning behavior of indocarbocyanine probes between coexisting gel and fluid phases in model membranes. Biochim Biophys Acta 1023:25–33
34. Pitas RE, Innerarity TL, Weinstein JN, Mahley RW (1981) Acetoacetylated lipoproteins used to distinguish fibroblasts from macrophages in vitro by fluorescence microscopy. Arteriosclerosis 1:177–185
35. Tabas I, Lim S, Xu XX, Maxfield FR (1990) Endocytosed beta-VLDL and LDL are delivered to different intracellular vesicles in mouse peritoneal macrophages. J Cell Biol 111: 929–940
36. Ghosh RN, Webb WW (1994) Automated detection and tracking of individual and clustered cell surface low density lipoprotein receptor molecules. Biophys J 66(5):1301–1318
37. Garvik O, Benediktson P, Simonsen AC, Ipsen JH, Wüstner D (2009) The fluorescent cholesterol analog dehydroergosterol induces liquid-ordered domains in model membranes. Chem Phys Lipids 159(2):114–118
38. Hao M, Mukherjee S, Sun Y, Maxfield FR (2004) Effects of cholesterol depletion and increased lipid unsaturation on the properties of endocytic membranes. J Biol Chem 279: 14171–14178
39. Wüstner D, Færgeman NJ (2008) Spatio-temporal analysis of endocytosis and membrane distribution of fluorescent sterols in living cells. Histochem Cell Biol 130(5): 891–908
40. Wüstner D (2007) Plasma membrane sterol distribution resembles the surface topography of living cells. Mol Biol Cell 18:211–228
41. Shvets E, Bitsikas V, Howard G, Hansen CG, Nichols BJ (2015) Dynamic caveolae exclude bulk membrane proteins and are required for sorting of excess glycosphingolipids. Nat Commun 6:6867
42. Du X, Kumar J, Ferguson C, Schulz TA, Ong YS, Hong W et al (2011) A role for oxysterol-binding protein-related protein 5 in endosomal cholesterol trafficking. J Cell Biol 192(1): 121–135
43. Lee HJ, Zhang W, Zhang D, Yang Y, Liu B, Barker EL et al (2015) Assessing cholesterol storage in live cells and *C. elegans* by stimulated Raman scattering imaging of phenyl-Diyne cholesterol. Sci Rep 5:7930
44. Crocker JC, Grier DG (1996) Methods of digital video microscopy for colloidal studies. J Colloid Interface Sci 179:298–311
45. Lund FW, Wustner D (2013) A comparison of single particle tracking and temporal image correlation spectroscopy for quantitative analysis of endosome motility. J Microsc 252(2):169–188
46. Dixit R, Cyr R (2003) Cell damage and reactive oxygen species production induced by fluorescence microscopy: effect on mitosis and guidelines for non-invasive fluorescence microscopy. Plant J 36(2):280–290
47. Saxton MJ (1993) Lateral diffusion in an archipelago. Single-particle diffusion. Biophys J 64: 1766–1780
48. Rudnick J, Gaspari G (1987) The shapes of random walks. Science 237(4813):384–389
49. Wüstner D (2005) Improved visualization and quantitative analysis of fluorescent membrane sterol in polarized hepatic cells. J Microsc 220: 47–64
50. Prattes S, Horl G, Hammer A, Blaschitz A, Graier WF, Sattler W, Zechner R, Steyrer E (2000) Intracellular distribution and mobilization of unesterified cholesterol in adipocytes: triglyceride droplets are surrounded by cholesterol-rich ER-like surface layer structures. J Cell Sci 113:2977–2989

51. McGookey DJ, Anderson RW (1983) Morphological characterization of the cholesteryl ester cycle in cultured mouse macrophage foam cells. J Cell Biol 97:1156–1168
52. Brown MS, Goldstein JL, Krieger M, Ho YK, Anderson RG (1979) Reversible accumulation of cholesteryl esters in macrophages incubated with acetylated lipoproteins. J Cell Biol 82:597–613
53. Wüstner D, Mondal M, Tabas I, Maxfield FR (2005) Direct observation of rapid internalization and intracellular transport of sterol by macrophage foam cells. Traffic 6:396–412
54. Li Q-T, Sawyer WH (1993) Effect of cholesteryl ester on the distribution of fluorescent cholesterol analogues in triacylglycerol-rich emulsions. Biochim Biophys Acta 1166:145–153
55. Saito H, Minamida T, Arimoto I, Handa T, Miyajima K (1996) Physical states of surface and core lipids in lipid emulsions and apolipoprotein binding to the emulsion surface. J Biol Chem 271:15515–15520
56. Listenberger LL, & Brown DA (2007) Fluorescent detection of lipid droplets and associated proteins. Curr Protoc Cell Biol 24(24.2)
57. Spandl J, White DJ, Peychl J, Thiele C (2009) Live cell multicolor imaging of lipid droplets with a new dye, LD540. Traffic 10(11):1579–1584
58. Sezgin E, Betul Can F, Schneider F, Clausen MP, Galiani S, Stanly TA et al (2016) A comparative study on fluorescent cholesterol analogs as versatile cellular reporters. J Lipid Res 57(2):299–309
59. Wustner D, Christensen T, Solanko LM, Sage D (2014) Photobleaching kinetics and time-integrated emission of fluorescent probes in cellular membranes. Molecules 19(8): 11096–11130
60. Saxton MJ (1997) Single-particle tracking: the distribution of diffusion coefficients. Biophys J 72(4):1744–1753
61. Ernst D, Kohler J (2013) Measuring a diffusion coefficient by single-particle tracking: statistical analysis of experimental mean squared displacement curves. Phys Chem Chem Phys 15(3):845–849
62. Davies M (2014) Long-lived reactive species formed on proteins induce changes in protein and lipid turnover. Free Radic Biol Med 75(Suppl 1):S6–S7
63. Qian H, Sheetz MP, Elson EL (1991) Single particle tracking. Analysis of diffusion and flow in two-dimensional systems. Biophys J 60(4): 910–921
64. Umansky M, Weihs D (2012) Novel algorithm and MATLAB-based program for automated power law analysis of single particle, time-dependent mean-square displacement. Comput Phys Commun 183:1783–1792

Chapter 11

Measurement of Cholesterol Transfer from Lysosome to Peroxisome Using an In Vitro Reconstitution Assay

Jie Luo, Ya-Cheng Liao, Jian Xiao, and Bao-Liang Song

Abstract

Low-density lipoproteins (LDLs) are taken up by the cell mainly through receptor-mediated endocytosis. LDL-derived cholesterol leaves lysosome and further transports to downstream organelles for specific cellular needs. We recently report that cholesterol transfers from lysosome to peroxisome through lysosome–peroxisome membrane contact (LPMC). Here, we use iodixanol density gradient centrifugation to isolate lysosomes and peroxisomes separately for the in vitro reconstitution of LPMC. We also apply ^{3}H-cholesterol-labeled lysosomes and peroxisomes in vitro to measure ^{3}H-cholesterol transfer through LPMC.

Key words Lysosome, Peroxisome, Lysosome–peroxisome membrane contact, Cholesterol transfer, In vitro reconstitution assay

1 Introduction

Cholesterol is an essential lipid that is dynamically transported within eukaryotic cells for utilization in membrane synthesis and regulation, steroid hormone generation, and bile acid synthesis [1–4]. Most mammalian cells acquire exogenous cholesterol from low-density lipoprotein (LDL) particles in the circulation through LDL receptor (LDLR)-mediated endocytosis [5]. Upon receptor binding, LDL is internalized in clathrin-coated pits and routed to early endosomes and late endosomes/lysosomes, where LDL-derived cholesteryl esters are hydrolyzed to unesterified cholesterol. Liberated cholesterol then exports from lysosomes and translocates to other organelles to execute specific functions [6].

The importance of proper intracellular cholesterol trafficking is underscored by Niemann-Pick Type C (NPC) disease, a fatal lysosomal disorder characterized by massive cholesterol accumulation in virtually all cell types, especially neurons and hepatocytes [7]. NPC patients exhibit cerebellar ataxia, dementia, hepatosplenomegaly, and usually die in the first or second decade of life. NPC disease is resulted from mutations in either the *NPC1* gene, which

Ingrid C. Gelissen and Andrew J. Brown (eds.), *Cholesterol Homeostasis: Methods and Protocols*, Methods in Molecular Biology, vol. 1583, DOI 10.1007/978-1-4939-6875-6_11,

encodes a large transmembrane protein, or the *NPC2* gene, which encodes a small soluble protein [8, 9]. Under normal physiological conditions, NPC2 binds to the 8-carbon isooctyl side chain of free cholesterol and escorts the molecule to the N-terminal domain of NPC1. NPC1, by attaching to the 3β-hydroxyl group of cholesterol, further intercalates the molecule into the lysosomal membrane [10]. Deficiency in NPC1 or NPC2 impedes the egress of cholesterol out of lysosomes, leading to NPC disease.

Our recent findings revealed a previously unappreciated component of intracellular cholesterol transport [11]. We demonstrated that the lysosomal protein synaptotagmin VII (Syt7) and the peroxisomal lipid PI (4, 5)P_2 mediated transient membrane contacts between lysosome and peroxisome, allowing cholesterol to move from one organelle to another. Intriguingly, we detected profound cholesterol accumulation well in advance of the manifestation of neurological deficits in mice with peroxisomal disorders (PDs), implying that a cholesterol trafficking blockage may account for the pathological mechanism of PDs.

In this chapter, we describe the detailed procedures of lysosome and peroxisome purification, in vitro reconstitution of lysosome–peroxisome membrane contact (LPMC), as well as in vitro ^{3}H-cholesterol transfer through LPMC.

2 Materials

2.1 Lysosome and Peroxisome Purification

1. Phosphate buffered saline (PBS; 10×): 1.37 M NaCl, 27 mM KCl, 40 mM Na_2HPO_4, 17.6 mM KH_2PO_4, pH 7.0–7.2. Weigh 80 g of NaCl, 2 g of KCl, 14.4 g of $Na_2HPO_4{\cdot}12\ H_2O$, and 2.4 g of KH_2PO_4 and transfer to a 1-L beaker containing about 850 mL of ultrapure water. Stir vigorously on a magnetic stirrer until everything dissolves completely. Make up to 1 L with ultrapure water and sterilize by autoclaving. Store at room temperature. To make 1 L of 1× PBS, add 100 mL of the stock solution to 900 mL of ultrapure water. Adjust pH to 7.4 with KOH.
2. Complete culture media: Dulbecco's Modified Eagle Medium (DMEM), 10 % (v/v) Fetal Bovine Serum (FBS), 100 units/mL penicillin and 100 mg/mL streptomycin. Prepare the media in a laminar flow hood. Add 50 mL of FBS and 5 mL of 100× penicillin/streptomycin to 445 mL of DMEM. Mix well and store at 4 °C. Preheat the media in a 37 °C water bath before use.
3. 0.25 % (w/v) trypsin–EDTA. Store at 4 °C (*see* **Note 1**).
4. Lysosome extraction buffer: Add 2 mL of a commercial Extraction Buffer 5× (e.g., from Sigma) to 8 mL of ultrapure water to make 10 mL of 1× lysosome extraction buffer. Store

at 4 °C. Ensure to add a protease inhibitor cocktail for mammalian cell and tissue extracts at a final concentration indicated by the supplier and keep on ice (*see* **Note 2**).

5. Peroxisome extraction buffer (5×): 25 mM 3-(N-Morpholino) propanesulfonic acid (MOPS) (pH 7.65), 1.25 M sucrose, 5 mM EDTA (pH 8.0), and 0.5 % (v/v) ethanol. Prepare the following stock solutions: To make 100 mL of 1 M MOPS (pH 7.65), weigh 20.926 g of MOPS and transfer to a 100-mL beaker containing about 70 mL of ultrapure water. Stir vigorously on a magnetic stirrer until everything dissolves completely. Adjust pH with NaOH. Make up to 100 mL with ultrapure water and sterilize by autoclaving. Store MOPS buffer at room temperature.

   To make 100 mL of 0.5 M EDTA (pH 8.0), weigh 14.612 g of EDTA and transfer to a 100-mL beaker containing about 80 mL of ultrapure water. Stir vigorously on a magnetic stirrer while adjusting pH with NaOH pellets. The suspension will become clear when the pH is approximately 8.0. Make up to 100 mL with ultrapure water and sterilize by autoclaving. Store your EDTA solution at room temperature.

   To make the peroxisome extraction stock buffer, weigh 42.79 g of sucrose and transfer to a 100-mL beaker containing about 50 mL of ultrapure water. Stir vigorously on a magnetic stirrer until everything dissolves completely. Then add 2.5 mL of 1 M MOPS (pH 7.65; see above), 1 mL of 0.5 M EDTA (pH 8.0; see above), and 0.5 mL of ethanol. Make up to 100 mL with ultrapure water. Store at 4 °C. To make 10 mL of 1× peroxisome extraction buffer, add 2 mL of the stock solution to 8 mL of ultrapure water. Ensure to add a protease inhibitor cocktail for mammalian cell and tissue extracts at a final concentration indicated by the supplier and keep on ice (*see* **Note 2**).

6. OptiPrep Density Gradient Medium (Sigma): a 60 % (w/v) solution of iodixanol in water. Store at room temperature.

7. OptiPrep dilution buffer for lysosome extraction: Add 0.5 mL of the OptiPrep dilution buffer 20× (Sigma) to 9.5 mL of ultrapure water to make 10 mL of 1× OptiPrep dilution buffer (L). Keep on ice until use.

8. OptiPrep dilution buffer for peroxisome extraction (20×): 100 mM MOPS (pH 8.0), 20 mM EDTA (pH 8.0) and 2 % (v/v) ethanol. Add 10 mL of 1 M MOPS (pH 8.0; see under 5 for recipe, adjust pH to 8.0), 4 mL of 0.5 M EDTA (pH 8.0; see under 5 for recipe) and 2 mL of ethanol. Make up to 100 mL with ultrapure water. Store at 4 °C. To make 10 mL of 1× OptiPrep dilution buffer (P), add 0.5 mL of the stock solution to 9.5 mL of ultrapure water. Keep on ice until use.

9. OptiPrep gradients for lysosome extraction: Prepare gradient solutions as indicated in Table 1. Keep all gradient solutions on ice until use (*see* **Note 3**). To make 100 mL of 2.3 M sucrose, weigh 78.729 g of sucrose and gradually pour into a 100-mL beaker containing 20 mL of ultrapure water and a fast stirring magnetic bar. Warm the suspension on a hot plate until everything dissolves completely. Make up to 100 mL with ultrapure water. Store sucrose solution at 4 °C.
10. OptiPrep gradients for peroxisome extraction: Prepare gradient solutions as indicated in Table 2. Keep on ice until use.
11. RIPA buffer: 50 mM Tris–HCl (pH 8.0), 150 mM NaCl, 0.1 % (w/v) sodium dodecyl sulfate (SDS), 1.5 % (v/v) Nonidet P-40 (NP-40), 0.5 % (w/v) sodium deoxycholate, 2 mM $MgCl_2$.

    Start with preparing the following stock solutions: To make 100 mL of 1 M Tris–HCl (pH 8.0), weigh 15.76 g of Tris–HCl and transfer to a 100-mL beaker containing about 80 mL of ultrapure water. Stir vigorously on a magnetic stirrer until every-

Table 1
Preparation of the OptiPrep gradients for lysosome extraction

Gradient	Final gradient percent (%)	OptiPrep density gradient medium volume (mL)	OptiPrep dilution buffer (L) volume (mL)	2.3 M sucrose volume (mL)	Final volume (mL)
1	27	0.864	0.941	0.115	1.92
2	22.5	0.9	1.351	0.149	2.4
3	19	OptiPrep fraction from **step 13** in Subheading 3.1			2.4
4	16	0.6408	1.6032	0.156	2.4
5	12	0.432	1.575	0.153	2.16
6	8	0.096	0.569	0.055	0.72
Total volume (mL)					12

Table 2
Preparation of the OptiPrep gradients for peroxisome extraction

Gradient	Final gradient percent (%)	OptiPrep density gradient medium volume (mL)	OptiPrep dilution buffer (P) volume (mL)	Final volume (mL)
1	27.5	1.374	1.626	3
2	22.5	OptiPrep fraction from **step 8** in Subheading 3.2		6
3	20	0.999	2.001	3
Total volume (mL)				12

thing dissolves completely. Adjust pH with NaOH. Make up to 100 mL with ultrapure water and sterilize by autoclaving. Store Tris–HCl solution at room temperature.

To make 100 mL of 10 % (w/v) SDS, weigh 10 g of SDS and transfer to a 100-mL beaker inside the hood containing about 80 mL of ultrapure water and a fast stirring magnetic bar. Warm the suspension to 68 °C on a hot plate until everything dissolves completely. Cool down and adjust pH with HCl to 7.2. Make up to 100 mL with ultrapure water. Store SDS solution at room temperature. Please avoid exposing fine crystals of SDS to oneself and coworkers. Wear a mask and weigh SDS in the fume hood. Clean up afterwards.

To make 100 mL of 10 % NP-40, slowly pour 10 mL of NP-40 into a 100-mL graduated cylinder containing 80 mL of ultrapure water and a fast stirring magnetic bar. Stir vigorously for about 30–40 min. Make up to 100 mL with ultrapure water. Store NP-40 solution at room temperature.

To prepare the RIPA buffer using the stock solutions listed above, weigh 4.383 g of NaCl, 2.5 g of sodium deoxycholate and 0.2033 g of $MgCl_2 \cdot 6\ H_2O$ and transfer to a 1-L beaker containing about 350 mL of ultrapure water. Stir vigorously on a magnetic stirrer until everything dissolves completely. Then add 25 mL of 1 M Tris–HCl (pH 8.0; see above), 5 mL of 10 % SDS (see above), and 75 mL of 10 % (v/v) NP-40 (see above). Make up to 500 mL with ultrapure water and sterilize by autoclaving. Aliquot and store at 4 °C.

12. HMGCR solubilization buffer: 62.5 mM Tris–HCl (pH 6.8), 15 % (w/v) SDS, 8 M urea, 10 % (v/v) glycerol, 100 mM DL-dithiothreitol (DTT). Slowly pour 50 mL of glycerol into a 100-mL graduated cylinder containing 50 mL of ultrapure water and a fast stirring magnetic bar. Stir vigorously for about 30–40 min and transfer (including the bar) to a 1-L beaker. Weigh 75 g of SDS (see above under 11 for safety considerations) and 240 g of urea and slowly pour into the beaker inside the hood. Add 31.25 mL of 1 M Tris–HCl (pH 6.8; see above under 11 for recipe, adjust pH to 6.8). Warm the suspension to 68 °C on a hot plate until everything dissolves completely (*see* **Note 4**). Cool down and add 7.71 g of DTT (*see* **Note 5**). Make up to 500 mL with ultrapure water. Aliquot and store at room temperature (*see* **Note 6**).

13. 4× Loading buffer: 150 mM Tris–HCl (pH 6.8), 12 % (w/v) SDS, 40 % (v/v) glycerol, 6 % (v/v) β-mercaptoethanol, 0.05 % (w/v) bromophenol blue. Weigh 60 g of SDS (see above under 11 for safety considerations) and transfer to a 1-L beaker inside the hood containing about 150 mL of ultrapure water and a fast stirring magnetic bar. Warm the suspension to 68 °C on a hot plate until everything dissolves completely. Slowly pour

(including the bar) into a 500-mL graduated cylinder and add 75 mL of 1 M Tris–HCl (pH 6.8; see above under 12) and 200 mL of glycerol. Stir vigorously for about 30–40 min. Then add 30 mL of β-mercaptoethanol (*see* **Notes 5** and **7**) and 0.25 g of bromophenol blue. Make up to 500 mL with ultrapure water. Save one aliquot at room temperature for current use and store the rest at −20 °C. To make 2× or 1× loading buffer, dilute the stock solution twofold or fourfold with ultrapure water respectively.

14. Reconstitution buffer: 20 mM HEPES (pH 7.2), 250 mM sucrose, 1 mM $MgCl_2$, 50 mM KCl, and 2 mM DTT. Start with preparing 100 mL of 1 M HEPES (pH 7.2). Weigh 23.83 g of HEPES and transfer to a 100-mL beaker containing about 70 mL of ultrapure water. Stir vigorously on a magnetic stirrer until everything dissolves completely. Adjust pH with NaOH. Make up to 100 mL with ultrapure water and sterilize by autoclaving. Store HEPES buffer at 4 °C.
For the reconstitution buffer, weigh 8.55 g of sucrose, 0.02 g of $MgCl_2 \cdot 6\ H_2O$, 0.37 g of KCl, and 0.031 g of DTT and transfer to a 100-mL beaker containing about 80 mL of ultrapure water. Stir vigorously on a magnetic stirrer until everything dissolves completely. Then add 2 mL of 1 M HEPES (pH 7.2; see above). Make up to 100 mL with ultrapure water. Store at 4 °C.

2.2 Cytosol Purification

1. Breaking buffer: 20 mM HEPES (pH 7.2), 250 mM sorbitol, 150 mM potassium acetate, 5 mM magnesium acetate, 0.3 mM DTT. Weigh 4.55 g of sorbitol, 1.47 g of potassium acetate, 0.107 g of $(CH_3COO)_2Mg \cdot 4H_2O$, and 0.0046 g of DTT and transfer to a 100-mL beaker containing about 80 mL of ultrapure water. Stir vigorously on a magnetic stirrer until everything dissolves completely. Then add 2 mL of 1 M HEPES (pH 7.2; see above under 14). Make up to 100 mL with ultrapure water. Store at 4 °C. Add a recommended amount of a protease inhibitor cocktail for mammalian cell and tissue extracts to 10 mL of the breaking buffer before use and keep on ice.
2. BCA Protein Assay Kit. Store at room temperature.

2.3 In Vitro Reconstitution of Lysosome–Peroxisome Membrane Contact (LPMC) and ^{3}H-Cholesterol Transfer

1. Ni Sepharose beads. Store at 4 °C.
2. Wash buffer: 20 mM HEPES (pH 7.2), 2 mM EGTA (pH 8.0), 250 mM sucrose, 1 mM $MgCl_2$, 50 mM KCl, 1 mM DTT (*see* **Note 8**). Start with preparing 100 mL of 0.5 M EGTA (pH 8.0). Weigh 19.018 g of EGTA and transfer to a 100-mL beaker containing about 70 mL of ultrapure water. Stir vigorously on a magnetic stirrer while adjusting pH with NaOH pellets. The suspension will become clear when the pH is approximately 8.0.

Make up to 100 mL with ultrapure water and sterilize by autoclaving. Store EGTA solution at room temperature.

For the wash buffer, weigh 8.55 g of sucrose, 0.02 g of $MgCl_2 \cdot 6H_2O$, 0.37 g of KCl, and 0.031 g of DTT and transfer to a 100-mL beaker containing about 80 mL of ultrapure water. Stir vigorously on a magnetic stirrer until everything dissolves completely. Then add 2 mL of 1 M HEPES (pH 7.2; see above under 14) and 0.4 mL of 0.5 M EGTA (pH 8.0; see above). Make up to 100 mL with ultrapure water. Store at 4 °C.

3. 0.1 M ATP. Weigh 0.0605 g of ATP and transfer to a 1.5-mL eppendorf tube containing 1 mL of ultrapure water. Mix on a rotator at 4 °C until everything dissolves completely. Aliquot and store at −80 °C.
4. 0.1 M GTP: Weigh 0.0589 g of GTP and transfer to a 1.5-mL eppendorf tube containing 1 mL of ultrapure water. Mix on a rotator at 4 °C until everything dissolves completely. Aliquot and store at −80 °C (*see* **Note 9**).
5. 3 M creatine phosphate: Weigh 0.908 g of creatine phosphate and transfer to a 1.5-mL eppendorf tube containing 1 mL of ultrapure water. Mix on a rotator at 4 °C until everything dissolves completely. Aliquot and store at −80 °C.
6. 50 mg/mL creatine kinase: Weigh 0.05 g of creatine kinase and transfer to a 1.5-mL eppendorf tube containing 1 mL of ultrapure water. Mix on a rotator at 4 °C until everything dissolves completely. Aliquot and store at 4 °C.
7. 1 mCi/mL ^{3}H-cholesterol. Store at −20 °C (*see* **Note 10**).
8. Scintillation cocktail. Store at room temperature in the dark.

3 Methods

Prepare cells in a laminar flow hood using proper aseptic technique. All procedures are carried out at 4 °C unless otherwise indicated. Ensure that you prechill reagents, supplies, and equipment in advance.

3.1 Lysosome Purification

1. Two days before harvesting, seed twelve 100 mm Petri dishes with 8×10^5 HeLa/NPC1-FLAG-mCherry cells each (*see* **Notes 11** and **12**).
2. Warm the culture media, sterile PBS and trypsin–EDTA in a 37 °C water bath for 20–30 min prior to harvesting (*see* **Note 13**).
3. Aspirate the culture media and rinse cells with 5 mL of PBS to remove any traces of serum that may inhibit the action of trypsin in the next step. Discard PBS.

4. Add 1 mL of trypsin–EDTA to the cell layer and rock the dish for complete coverage. Incubate cells in a 37 °C incubator for approximately 1–2 min. Examine cells under an inverted microscope to ensure most (≥90 %) have detached (*see* **Note 14**).
5. Add 2 mL of the culture media and pipette over the cell layer several times to dissociate any adherent cells from the bottom of the dish into the media.
6. Collect and transfer the cell suspension from all twelve dishes into a precooled 50-mL conical tube and centrifuge at 1000 × *g* for 5 min. Discard the supernatant.

   Steps 7–16 and **18–20** should be carried out at 4 °C. Ensure to use ice-cold reagents and pre-chilled supplies.
7. Resuspend the cell pellet in 10 mL of PBS and centrifuge at 1000 × *g* for 5 min. Discard the supernatant. Repeat this wash step one more time.
8. Resuspend the pellet in 2.7 packed cell volumes (PCV) of the lysosome extraction buffer (*see* **Note 15**). Vortex vigorously. Then equally split the suspension into two 5-mL eppendorf tubes (*see* **Note 16**).
9. Homogenize cells by passing through a 23G needle approximately 60–100 times so that 80–85 % cells have lysed (*see* **Note 17**).
10. Centrifuge at 1000 × *g* for 10 min (*see* **Note 18**).
11. Collect the supernatant in new eppendorf tubes. Keep 100–200 μL to assay for the degree of purification in **step 17**. Equally split the rest into four 1-mL ultracentrifuge tubes (*see* **Note 19**).
12. Centrifuge at 20,000 × *g* for 20 min using a HITACHI CS150GX ultracentrifuge or equivalent instrument. Discard the supernatant.
13. Resuspend the pellet of all four tubes in 1.28 mL of the lysosome extraction buffer. Transfer the suspension to a 5-mL eppendorf tube. Then add 0.808 mL of the OptiPrep Density Gradient Medium and 0.44 mL of the 1× OptiPrep dilution buffer (L) to make a final concentration of the 19 % (v/v) OptiPrep fraction (*see* **Note 20**).
14. Prepare a discontinuous density gradient in a 12-mL ultracentrifuge tube by adding the following solutions from the bottom to the top sequentially (Table 1): 1.92 mL of the 27 % OptiPrep media, 2.4 mL of the 22.5 % OptiPrep media, 2.4 mL of the above prepared 19 % OptiPrep fraction, 2.4 mL of the 16 % OptiPrep media, 2.16 mL of the 12 % OptiPrep media, and 0.72 mL of the 8 % OptiPrep media (*see* **Note 21**).
15. Centrifuge in a SW50.1 type rotor (Beckman Coulter) or equivalent instrument at 150,000 × *g* for 4 h with maximal acceleration and minimal deceleration (*see* **Note 22**).

16. After centrifugation, remove the tube and collect fractions of 0.6 mL in 1.5-mL eppendorf tubes. A total of 20 fractions will be taken. Number them individually (*see* **Note 23**).
17. Fractions collected from the above and that from **step 11** are now resolved by SDS-PAGE electrophoresis to assay for the degree of purification. Take 24 μL of each sample, add 40 μL of the 3:2 buffer (*see* **Note 6**) and incubate at 37 °C for 30 min (or add 24 μL of the 2× loading buffer and incubate at 95 °C for 10 min) (*see* **Note 24**). Then load 20 μL of the mixture onto 8 % (w/v) SDS-PAGE gels. Routine western blotting procedures are carried out afterwards. The blots are probed with anti-LAMP1 (lysosome marker), anti-NPC1 (lysosome marker), anti-prohibitin (PHB) (mitochondrial marker), anti-GM130 (Golgi marker), anti-ABCD1 (peroxisome marker), anti-Rab5 (early endosome marker), and anti-calnexin (ER marker). A typical example of fractions taken from the iodixanol density gradient is shown in Fig. 1.
18. Combine fractions with purest lysosomes together in a 12-mL ultracentrifuge tube. Make up the rest of volume with the reconstitution buffer. Vortex vigorously (*see* **Note 25**).
19. Centrifuge in a SW50.1 type rotor (Beckman Coulter) or equivalent instrument at 28,000 × *g* for 30 min with maximal acceleration and minimal deceleration. Discard the supernatant.
20. Resuspend the lysosome pellet in 200 μL of the reconstitution buffer and keep on ice until use (*see* **Note 26**).

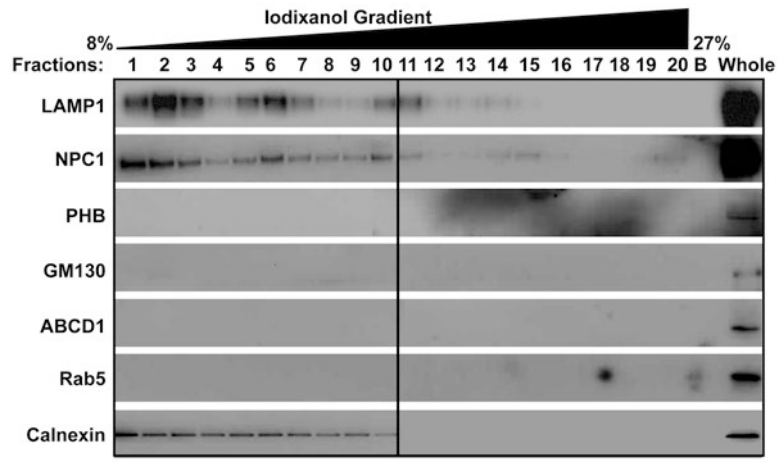

Fig. 1 The total 20 successive fractions along the iodixanol density gradient during lysosome purification. Lanes 11–15 represent purified lysosomes. B, blank; Whole, whole cell lysate

21. Proceed to Subheading 3.4.

3.2 Peroxisome Purification

Initial steps of preparing cells for peroxisome purification are quite similar to those for lysosome purification except that HeLa/EGFP-His_6-SKL cells are used (*see* **Note 27**). **Steps 1–7** are therefore omitted. Please refer to the relevant parts in Subheading 3.1 for the details.

1. Resuspend the pellet in 2.7 PCV of the peroxisome extraction buffer. Vortex vigorously. Then equally split the suspension into two 5-mL eppendorf tubes (*see* **Notes 15** and **16**).
2. Homogenize cells by passing through a 23G needle approximately 60–100 times so that 80–85 % cells have lysed (*see* **Note 28**. Also *see* **Note 17**).
3. Centrifuge at 1000 × *g* for 10 min (*see* **Note 18**).
4. Collect the supernatant in new eppendorf tubes. Keep 100–200 μL to assay for the degree of purification in **step 12**.
5. Centrifuge at 2000 × *g* for 10 min (*see* **Note 29**).
6. Collect the supernatant and further split into four 1-mL ultracentrifuge tubes (*see* **Note 19**).
7. Centrifuge at 25,000 × *g* for 20 min using a HITACHI CS150GX ultracentrifuge or equivalent instrument. Discard the supernatant.
8. Resuspend the pellet of all four tubes in 1.6 mL of the peroxisome extraction buffer. Transfer the suspension to a 10-mL conical tube. Then add 2.25 mL of the OptiPrep Density Gradient Medium and 2.15 mL of the 1× OptiPrep dilution buffer (P) to make a final concentration of the 22.5 % (v/v) OptiPrep fraction (*see* **Note 20**).
9. Prepare a discontinuous density gradient in a 12-mL ultracentrifuge tube by adding the following solutions from the bottom to the top sequentially (Table 2): 3 mL of the 27.5 % OptiPrep Media, 6 mL of the above prepared 22.5 % OptiPrep fraction, and 3 mL of the 20 % OptiPrep Media (*see* **Note 30**).
10. Centrifuge in a SW50.1 type rotor (Beckman Coulter) or equivalent instrument at 100,000 × *g* for 1.5 h with maximal acceleration and minimal deceleration (*see* **Note 22**).
11. After centrifugation, remove the tube and collect fractions of 0.6 mL in 1.5-mL eppendorf tubes. A total of 20 fractions will be taken. Number them individually (*see* **Note 31**. Also *see* **Note 23**).
12. Fractions collected from the above and that from **step 4** are now resolved by SDS-PAGE electrophoresis to assay for the degree of purification. Please refer to **step 17** in Subheading 3.1 for the details. The blots are probed with anti-ABCD1

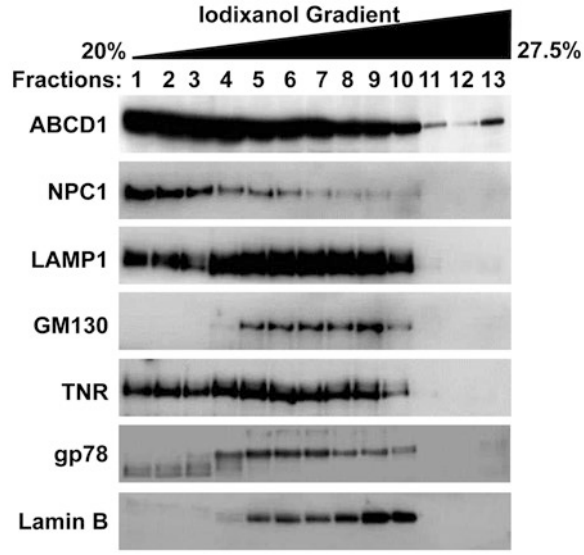

Fig. 2 The total 13 successive fractions along the iodixanol density gradient during peroxisome purification. Lanes 11–13 represent purified peroxisomes

(peroxisome marker), anti-NPC1 (lysosome marker), anti-LAMP1 (lysosome marker), anti-GM130 (Golgi marker), anti-transferrin receptor (TNR) (plasma membrane marker), anti-gp78 (ER marker), and anti-Lamin B (nucleus marker). A typical example of fractions taken from the iodixanol density gradient is shown in Fig. 2.

13. Combine fractions with purest peroxisomes together in a 5-mL eppendorf tube and keep on ice until use (*see* **Note 32**).
14. Proceed to Subheading 3.4.

3.3 Cytosol Purification

1. Two days before harvesting, seed thirty 100-mm Petri dishes with 2×10^6 HEK293T cells each (*see* **Note 33**).
   Perform **steps 2–7** as described in Subheading 3.1.
2. Resuspend the pellet in 1.5 PCV of the breaking buffer. Vortex vigorously. Then equally split the suspension into two 5-mL eppendorf tubes (*see* **Note 34**).
3. Homogenize cells by passing through a 23G needle approximately 100–150 times so that 80–85 % cells have lysed (*see* **Note 35**. Also *see* **Note 17**).
4. Transfer the supernatant to 1-mL ultracentrifuge tubes and centrifuge at 160,000 × *g* for 30 min.
5. Repeat **step 4** two more times (*see* **Note 36**).
6. Collect the supernatant in a 10-mL conical tube. Save about 10 μL to assay for protein concentration and keep the rest on ice until use (*see* **Note 37**). Prepare a series of diluted BSA standards ranging from 25 to 2000 μg/mL and the working

reagent following the instructions for BCA Protein Assay Kit. Dilute 2 μL of the supernatant in 98 μL of PBS. Combine 25 μL of each standard or sample replicate with 200 μL of the working reagent and incubate at 37 °C for 30 min. Measure the absorbance at 595 nm on a Bio-Rad iMark™ microplate reader or equivalent instrument (*see* **Note 38**).

7. Proceed to Subheading 3.4.

3.4 In Vitro Reconstitution of LPMC

1. Add 500 μL of Ni Sepharose bead slurry (250 μL packed beads) to 4 mL of PBS in a 5-mL eppendorf tube. Incubate with gentle rocking on a rotating shaker for 5 min (*see* **Note 39**).
2. Centrifuge at 800 × *g* for 1 min. Discard the supernatant (*see* **Note 40**).
3. Resuspend the beads in 4 mL of PBS. Incubate with gentle rocking for 5 min.
4. Repeat **steps 2–3** two more times.
5. Centrifuge at 800 × *g* for 1 min. Discard the supernatant.
6. Add purified peroxisomes prepared in Subheading 3.2 to the beads and incubate with gentle rocking for 2 h.
7. Centrifuge at 800 × *g* for 1 min. Discard the supernatant (*see* **Note 41**).
8. Wash the beads four times with the wash buffer (*see* **Notes 42** and **43**).
9. Resuspend the beads in 250 μL of the reconstitution buffer. Pipette to mix well.
10. Add the following components to a 1.5-mL eppendorf tube sitting on ice: 20 μL of purified lysosomes (prepared in Subheading 3.1), 40 μL of the above prepared slurry (20 μL packed beads), purified cytosol (prepared in Subheading 3.3) diluted to 1 mg/mL, 2.5 μL of 0.1 M ATP, 2.5 μL of 0.1 M GTP, 2.5 μL of 3 M creatine phosphate, and 0.25 μL of 50 mg/mL creatine kinase. Make up to 250 μL with the reconstitution buffer (*see* **Note 44**).
11. Incubate with gentle rocking at 37 °C for 30 min.
12. Centrifuge at 800 × *g* for 1 min. Discard the supernatant.
13. Wash the beads four times with the reconstitution buffer (*see* **Note 45**).
14. Resuspend the beads in 100 μL of the reconstitution buffer. Pipette to mix well. The overall workflow of the in vitro reconstitution of LPMC is summarized in Fig. 3. The suspension can be assayed for the following experiments:
    (a) Confocal microscopy. Place 12 μL of the mounting media onto a glass slide. Add 3–5 μL of the above suspension into the media, coverslip and examine under a confocal microscope. A typical example is shown in Fig. 4.

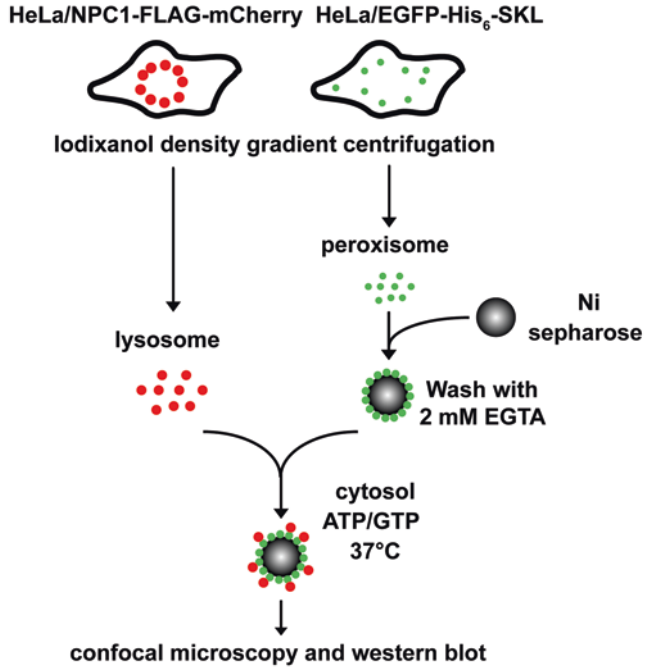

Fig. 3 A schematic summary of the in vitro reconstitution of LPMC (modified from [11] with permission from Elsevier)

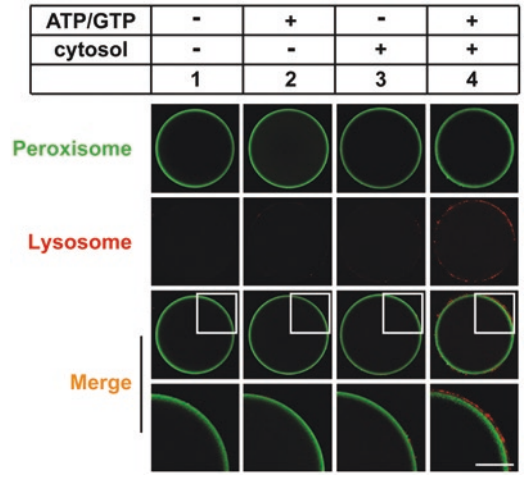

Fig. 4 The confocal images of Ni Sepharose beads from the in vitro reconstitution of LPMC in the absence (–) or presence (+) of the cytosol, ATP/GTP, and ATP-regenerating system as indicated. Boxed areas are shown at higher magnification in the bottom row. Scale bar, 20 μm (reproduced from [11] with permission from Elsevier)

(b) Western blot. Spin down the beads and resuspend in 40 μL of the 3:3:2 buffer (*see* **Note 6**) and incubate at 37 °C for 30 min (or 40 μL of the 1× loading buffer and incubate at 95 °C for 10 min). Then load 20 μL of the mixture onto

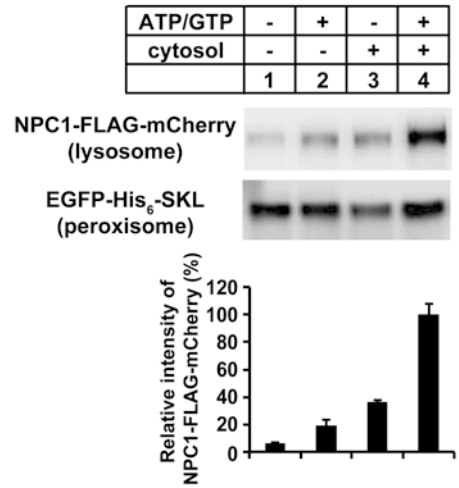

Fig. 5 The immunoblots from the in vitro reconstitution of LPMC in the absence (−) or presence (+) of the cytosol, ATP/GTP, and ATP-regenerating system as indicated. The intensity of $FLAG^+$ band was quantified to give an estimation of lysosomes associated with peroxisome-bound Sepharose beads. Data are mean ± SD (from 3 independent repeats of experiments) (reproduced from [11] with permission from Elsevier)

8 % SDS-PAGE gels. Routine western blotting procedures are carried out afterwards. The blots are probed with anti-FLAG and anti-EGFP. A typical example is shown in Fig. 5.

3.5 In Vitro ^{3}H-Cholesterol Transfer Through LPMC

Before starting your experiments, please observe **Note 10**.

3.5.1 ^{3}H-Cholesterol-Labeled Lysosome Purification

1. Two days before harvesting, seed twelve 100-mm petri dishes with 2×10^6 HEK293T cells each.
2. On the evening before harvesting, aspirate the culture media and rinse cells with 5 mL of PBS. Then add 10 mL of the culture media containing 1 μCi/mL ^{3}H-cholesterol. Return cells to the incubator (*see* **Note 46**).
3. 12 h later, aspirate the culture media and rinse cells with 5 mL of PBS containing 0.2 % (w/v) BSA (*see* **Note 47**). Discard radioactive media and PBS in accordance to institutional procedures.

Perform **steps 4–13** as described in Subheading 3.1 to get 200 μL of ^{3}H-cholesterol-labeled lysosomes.

3.5.2 Peroxisome Purification

Perform **steps 1–13** as described in Subheading 3.2 followed by **steps 1–9** as described in Subheading 3.4 to get 500 μL of peroxisome-bound bead slurry (250 μL packed beads).

Table 3
Reaction setup for the in vitro ^{3}H-cholesterol transfer assay

Tube #	A	B	C	D	E	F
^{3}H-cholesterol-labeled lysosomes (20 μL)	+	−	+	+	+	+
Peroxisome-bound bead slurry (40 μL)	−	+	+	+	+	+
Cytosol (1 mg/mL)	−	+	+	+	+	+
1 mM ATP, 1 mM GTP, 30 mM creatine phosphate, and 0.05 mg/mL creatine kinase	−	+	+	+	+	+
Reconstitution buffer	Make up volume to 250 μL					
Incubation time (min)	–	0	10	30	60	120

3.5.3 ^{3}H-Cholesterol Transfer Through LPMC

1. Set up the in vitro reconstitution of LPMC in 1.5-mL eppendorf tubes as follows (Table 3):
   (a) Start with tube F. Add 20 μL of ^{3}H-cholesterol-labeled lysosomes (prepared in Subheading 3.5.1), 40 μL of peroxisome-bound bead slurry (20 μL packed beads) (prepared in Subheading 3.5.2), purified cytosol (prepared in Subheading 3.3) diluted to 1 mg/mL, 1 mM ATP, 1 mM GTP, 30 mM creatine phosphate, and 0.05 mg/mL creatine kinase. Make up to 250 μL with the reconstitution buffer. Mix well and incubate with gentle rocking at 37 °C.
   (b) Prepare tube E in the same manner 1 h after **step a**. Incubate with gentle rocking at 37 °C.
   (c) Prepare tube D in the same manner 1.5 h after **step a**. Incubate with gentle rocking at 37 °C.
   (d) Prepare tube C in the same manner 1 h and 50 min after **step a**. Incubate with gentle rocking at 37 °C.
   (e) Prepare tube B 2 h after **step a**. Combine 40 μL of peroxisome-bound bead slurry (20 μL packed beads) (prepared in Subheading 3.5.2), purified cytosol (prepared in Subheading 3.3) diluted to 1 mg/mL, 1 mM ATP, 1 mM GTP, 30 mM creatine phosphate, and 0.05 mg/mL creatine kinase. Make up to 250 μL with the reconstitution buffer.
   (f) Prepare tube A immediately afterwards. Add 20 μL of ^{3}H-cholesterol-labeled lysosomes (prepared in Subheading 3.5.1) to 230 μL of the reconstitution buffer.
2. Centrifuge tubes B-F at 800 × *g* for 1 min. Discard the supernatant.
3. Wash the beads four times with the wash buffer (*see* **Notes 42** and **43**).

4. Add 1 mL of the scintillation cocktail into tubes A-F. Vortex vigorously.
5. Place tubes into plastic liquid scintillation vials and measure the radioactivity of each sample in units of disintegration per minute (dpm) using a Beckman LS 65004 liquid scintillation counter or equivalent instrument.
6. The radioactivity of tubes B-F is individually divided by that of tube A to get the percentage of ^{3}H-cholesterol transfer through LPMC at different time points. The overall workflow and the representative results are shown in Fig. 6.

4 Notes

1. For long-term storage, it is recommended to aliquot and store at −20 °C.
2. It is best to prepare the extraction buffer fresh every time.
3. The final osmolality of OptiPrep gradients should be balanced to around 290 mOsm using sucrose.
4. This process may take about 40–60 min. Cover the beaker with aluminum foil to prevent evaporation during the heating process.
5. The reducing reagent should be added after cooling down to avoid degradation.
6. The HMGCR solubilization buffer tends to solidify at low temperatures. Warm at 37 °C prior to use. In our laboratory, we prefer to prepare two ready-to-use versions by mixing HMGCR solubilization buffer with 4× loading buffer at a ratio of 3:2 (referred to as 3:2 buffer), or mixing RIPA buffer, HMGCR solubilization buffer, and 4× loading buffer at a ratio of 3:3:2 (referred to as 3:3:2 buffer) and store both at room temperature.
7. Due to the toxicity and strong odor, β-mercaptoethanol should be used in a fume hood.
8. The addition of 2 mM EGTA to the reconstitution buffer makes the wash buffer.
9. 0.1 M GTP aliquots may appear gel-like when thawing at room temperature. Warm at 37 °C before use.
10. Diligently follow the guidelines designated by your Institutions Radiation Safety Program when handling radioactive materials. Ensure that you wear personal protective equipment during operations. Dispose of radioactive waste properly according to guidelines designated by the Radiation Safety Program.

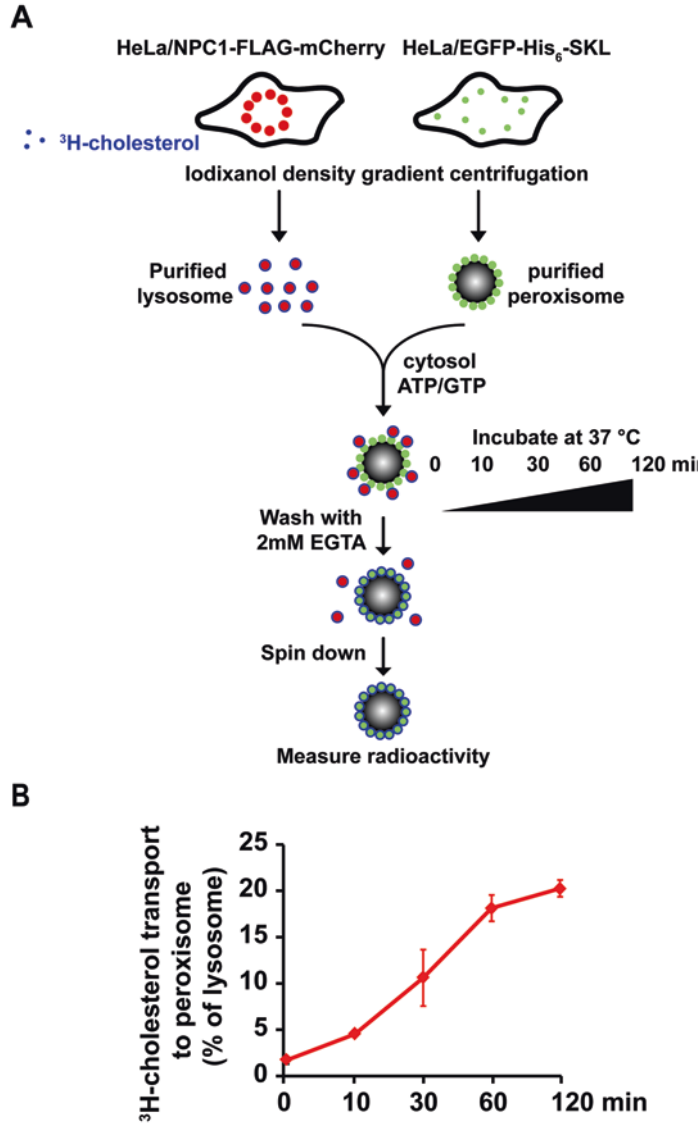

Fig. 6 In vitro ^{3}H-cholesterol transfer through LPMC. (**a**) A schematic summary of the in vitro ^{3}H-cholesterol transfer assay. (**b**) Percentages of ^{3}H-cholesterol retained on the peroxisome-bound Sepharose beads relative to the total ^{3}H-cholesterol in lysosomes were calculated to give an estimation of ^{3}H-cholesterol transfer from lysosome to peroxisome over time. Data are mean ± SD (from 3 independent repeats of experiments) (modified from [11] with permission from Elsevier)

11. The procedures of lysosome purification described here are applicable to HeLa cells stably expressing NPC1-FLAG-mCherry and HEK293T cells. Steps of establishing HeLa cells stably expressing NPC1-FLAG-mCherry: (a) Amplify *NPC1* from mouse liver cDNA by standard PCR; (b) Insert *NPC1*

and 3× FLAG tag into the pmCherry-N1 vector using quick-change method; (c) Transiently transfect HeLa cells with the NPC1-FLAG-mCherry plasmid using Fugene® HD transfect reagent (Promega) or an equivalent transfection reagent; (d) 48 h after transfection, change to the culture media containing 400 μg/mL G418; (e) Culture cells until single colonies are formed; (f) Select cells that stably express NPC1-FLAG-mCherry under a fluorescent microscope; (g) Maintain the stable cell line in the culture media containing 400 μg/mL G418.

12. Purifying lysosomes for the in vitro reconstitution assay requires a large amount of cells. Cells usually reach 80–90 % confluency on the day of harvesting.
13. It is best to use prewarmed solutions to minimize stress to cells.
14. The temperature and time duration for incubation vary depending on cell type. It is fine to increase the incubation time if necessary. However, one may need to check for cell dispersal more frequently. Gentle agitation of the dish may help detachment. If using HEK293T cells, we suggest incubating at room temperature since these cells are more easily detachable.
15. The PCV should be about 1–2 mL in volume.
16. Smaller volumes allow for more thorough homogenization during the next step.
17. The number of strokes varies depending on cell type and buffer composition and should be determined by end users. After every 20 strokes, place 5 μL of the lysate onto a glass slide, coverslip and examine under a microscope for lysis efficiency. The key of this step is to achieve enough cell breakage without jeopardizing lysosome integrity.
18. This step is to pellet unlysed cells, nuclei, and large debris.
19. It is necessary to split samples due to the limited tube capacity. Split samples will be pooled together later.
20. Ensure to perform sufficient resuspension in the extraction buffer using pipetting and vortexing. This step is a prerequisite of successful isolation of lysosomes/peroxisomes using the iodixanol density gradient in the next step. Avoid resuspending the pellet in the OptiPrep Density Gradient Medium since it is viscous. Vortex vigorously every time when adding a new component.
21. In this step, descending concentrations of solutions are overlaid progressively on one another. Start with the 27 % (v/v) OptiPrep Media first. Load and place an extra-long gel loading pipettor tip against the inside wall of the tube. Then pipette gently so that the solution flow down slowly and steadily. Allow

all volume to drain completely. Then proceed with the 22.5, 19, 16, 12, and 8 % OptiPrep Media successively.

22. For safety reasons, ensure to balance the rotor with tubes of the same mass (use weighing balance).
23. Avoid disturbing the layers when taking the tube out of the rotor. You will see several bands floating in the gradient. To collect fractions, snugly fit a white pipettor tip onto the end of a blue one and withdraw from the top of the gradient gently. It is fine to collect less fractions in a bigger volume, e.g., 15 × 0.8 mL fractions.
24. Reducing reagents such as DTT and β-mercaptoethanol are frequently used to break protein disulfide bonds. When examining membrane proteins with multiple transmembrane segments, we recommend warming samples in the HMGCR solubilization buffer because high concentration of urea may help to reduce protein aggregation and increase band resolution on the gels.
25. This step is to reduce the concentration of the OptiPrep Media in the lysosome fractions.
26. The pellet may be stored overnight at 2–8 °C if necessary. Never freeze since the freeze-thaw cycle may compromise lysosomal integrity.
27. Steps for establishing HeLa cells stably expressing EGFP-His_6-SKL: (a) Insert *SKL* and 6× His tag into the pEGFP-N1 vector using quick-change method; (b) Transiently transfect HeLa cells with the EGFP-His_6-SKL plasmid using Fugene® HD transfect reagent or an equivalent reagent; (c) 48 h after transfection, change to the culture media containing 400 μg/mL G418; (d) Culture cells until single colonies are formed; (e) Select cells that stably express EGFP-His_6-SKL under a fluorescent microscope; (f) Maintain the stable cell line in the culture media containing 400 μg/mL G418.
28. Please note that it requires more strokes when homogenizing samples for peroxisome purification, since the composition of the peroxisome extraction buffer differs from that of the lysosome extraction buffer.
29. This step is to pellet heavy mitochondria.
30. Similarly, descending concentrations of solutions are overlaid progressively on one another. Start with the 27.5 % (v/v) OptiPrep Media first. Then proceed with the 22.5 % OptiPrep fraction and the 20 % OptiPrep Media successively.
31. ER and lysosomes mainly float on the top of the gradient, and mitochondria restrict to the ring at the 27.5 %–22.5 % interface. Purest peroxisomes usually locate in the bottom layer.

32. The peroxisome fractions should be about 3 mL in volume. Purified peroxisomes may be stored overnight at 2–8 °C if necessary. Never freeze since the freeze–thaw cycle may compromise peroxisomal integrity.
33. HEK293T cells are smaller in size and a greater number of cells are required to start with. Cells usually reach 80–90 % confluency on the day of harvesting.
34. The PCV should be about 3–5 mL in volume.
35. This is the most labor-intensive homogenization of the whole procedure.
36. This step is to remove nuclei, vesicles and organelles from the cytosol. The pellet becomes smaller after each ultracentrifugation.
37. Purified cytosol may be stored at −80 °C for several weeks. It is best to aliquot to avoid freeze–thaw cycles.
38. The protein concentration should be about 5–10 mg/mL.
39. Ni Sepharose beads are often supplied as a 50 % slurry suspension in PBS containing 20 % ethanol. It is best to wash off ethanol before use. Mix the suspension well and withdraw gently using a yellow pipettor tip with the end cut off (which prevents damage to the beads and allows easy pipetting). After releasing the beads into PBS, pipette up and down several times to remove any traces that may stick to the tip.
40. Extra care should be taken when removing supernatant from the beads.
41. This step is to pellet EGFP-His_6-SKL-labeled peroxisomes bound to the beads.
42. The presence of EGTA in the wash buffer helps to dissociate organelles that may be in contact with peroxisomes.
43. During each wash, resuspend the beads in 4 mL of the wash buffer and incubate with gentle rocking for 5 min. Then centrifuge at 800 × *g* for 1 min and discard the supernatant.
44. Components listed here are for one standard reaction. You can also evaluate critical determinants of LPMC by adding Syt7-C2AB to or omitting ATP/GTP or cytosol from the system.
45. This wash step is to eliminate nonspecific binding to LPMC. Never use the wash buffer since the presence of EGTA may impair the formation of LPMC.
46. Prewarm PBS and the culture media to 37 °C before use. It is best to prepare a master mix for all the dishes by adding 150 μL of 1 mCi/mL ^{3}H-cholesterol to 150 mL of the culture media.

47. The presence of BSA helps to absorb excess ^{3}H-cholesterol that has not been taken up by cells during overnight incubation. We prepare PBS/0.2 % BSA fresh every time. Weigh 0.14 g of BSA and transfer to a 100-mL beaker containing about 65 mL of 1× PBS. Stir vigorously on a magnetic stirrer until everything dissolves completely. Make up to 70 mL with 1× PBS and filter through a 0.45-μm Millipore filter. Prewarm to 37 °C before use.

Acknowledgments

This work was supported by the National Natural Science Foundation of China (31430044, 31230020, and 81270155 to B.-L.S. and 31600651 to J.L.) and the Natural Science Foundation of Hubei Province (2015CFB215 to J.L.).

References

1. Goldstein JL, DeBose-Boyd RA, Brown MS (2006) Protein sensors for membrane sterols. Cell 124:35–46
2. Hanukoglu I (1992) Steroidogenic enzymes: structure, function, and role in regulation of steroid hormone biosynthesis. J Steroid Biochem Mol Biol 43:779–804
3. Wang TY, Liu M, Portincasa P (2013) New insights into the molecular mechanism of intestinal fatty acid absorption. Eur J Clin Invest 43:1203–1223
4. Jeong J, McMahon AP (2002) Cholesterol modification of Hedgehog family proteins. J Clin Invest 110:591–596
5. Brown MS, Goldstein JL (1986) A receptor-mediated pathway for cholesterol homeostasis. Science 232:34–47
6. Chang TY, Chang CC, Ohgami N, Yamauchi Y (2006) Cholesterol sensing, trafficking, and esterification. Annu Rev Cell Dev Biol 22:129–157
7. Vanier MT, Millat G (2003) Niemann-Pick disease type C. Clin Genet 64:269–281
8. Carstea ED, Morris JA, Coleman KG, Loftus SK, Zhang D, Cummings C, Gu J, Rosenfeld MA, Pavan WJ, Krizman DB et al (1997) Niemann-Pick C1 disease gene: homology to mediators of cholesterol homeostasis. Science 277:228–231
9. Sleat DE, Wiseman JA, El-Banna M, Price SM, Verot L, Shen MM, Tint GS, Vanier MT, Walkley SU, Lobel P (2004) Genetic evidence for nonredundant functional cooperativity between NPC1 and NPC2 in lipid transport. Proc Natl Acad Sci USA 101:5886–5891
10. Kwon HJ, Abi-Mosleh L, Wang ML, Deisenhofer J, Goldstein JL, Brown MS, Infante RE (2009) Structure of N-terminal domain of NPC1 reveals distinct subdomains for binding and transfer of cholesterol. Cell 137:1213–1224
11. Chu BB, Liao YC, Qi W, Xie C, Du XM, Wang J, Yang HY, Miao HH, Li BL, Song BL (2015) Cholesterol transport through lysosome-peroxisome membrane contacts. Cell 161: 291–306

Chapter 12

Measurement of Mitochondrial Cholesterol Import Using a Mitochondria-Targeted CYP11A1 Fusion Construct

Barry E. Kennedy, Mark Charman, and Barbara Karten

Abstract

All animal membranes require cholesterol as an essential regulator of biophysical properties and function, but the levels of cholesterol vary widely among different subcellular compartments. Mitochondria, and in particular the inner mitochondrial membrane, have the lowest levels of cholesterol in the cell. Nevertheless, mitochondria need cholesterol for membrane maintenance and biogenesis, as well as oxysterol, steroid, and hepatic bile acid production. Alterations in mitochondrial cholesterol have been associated with a range of pathological conditions, including cancer, hepatosteatosis, cardiac ischemia, Alzheimer's, and Niemann–Pick Type C Disease. The mechanisms of mitochondrial cholesterol import are not fully elucidated yet, and may vary in different cell types and environmental conditions. Measuring cholesterol trafficking to the mitochondrial membranes is technically challenging because of its low abundance; for example, traditional pulse-chase experiments with isotope-labeled cholesterol are not feasible. Here, we describe improvements to a method first developed by the Miller group at the University of California to measure cholesterol trafficking to the inner mitochondrial membrane (IMM) through the conversion of cholesterol to pregnenolone. This method uses a mitochondria-targeted, ectopically expressed fusion construct of CYP11A1, ferredoxin reductase and ferredoxin. Pregnenolone is formed exclusively from cholesterol at the IMM, and can be analyzed with high sensitivity and specificity through ELISA or radioimmunoassay of the medium/buffer to reflect mitochondrial cholesterol import. This assay can be used to investigate the effects of genetic or pharmacological interventions on mitochondrial cholesterol import in cultured cells or isolated mitochondria.

Key words Mitochondrial cholesterol import, Pregnenolone, F2-fusion protein, CYP11A1, Radioimmunoassay

1 Introduction

Cholesterol is an essential component of all animal membranes, regulating membrane fluidity, permeability, curvature, membrane fusion and fission, and membrane protein function. The distribution of cholesterol among subcellular membranes is highly heterogeneous, with highest levels in the plasma membrane and very low levels in the endoplasmic reticulum and in mitochondria, particularly in the inner mitochondrial membrane (IMM). Thus, cholesterol

Ingrid C. Gelissen and Andrew J. Brown (eds.), *Cholesterol Homeostasis: Methods and Protocols*, Methods in Molecular Biology, vol. 1583, DOI 10.1007/978-1-4939-6875-6_12,

levels in mitochondria have been estimated to be 40-fold lower than in the plasma membrane and even 4.5-fold lower than in the ER [1]. Nevertheless, mitochondria require cholesterol for structural maintenance, biogenesis and as the precursor for the synthesis of steroids, oxysterols, and hepatic bile acids. Increased mitochondrial cholesterol levels are associated with several pathological conditions, including cancer [2–4], myocardial ischemia [5, 6], hepatosteatosis [7–10], Alzheimer's disease [11–13], and NPC1 deficiency [13–15]. Elevated cholesterol levels decrease the fluidity and proton permeability of mitochondrial membranes [2, 16–18], and affect mitochondrial function (reviewed in [19–21]). Studies using cell or animal models with increased mitochondrial cholesterol have shown alterations in a wide variety of mitochondrial function parameters depending on the model system, cell type, genetic background, and other factors. However, certain commonalities of mitochondrial alterations associated with high cholesterol are beginning to emerge, for example increased oxidative stress and/or decreased mitochondrial antioxidant levels [7–13, 22–28], decreased mitochondrial respiration [2, 5, 15, 27–30], and impaired membrane permeabilization during the mitochondrial permeability transition [3, 16, 19, 31, 32], although the underlying mechanisms remain unclear and may vary among different model systems.

The mechanism of cholesterol import into mitochondria is best known for steroidogenic cells, where the steroidogenic acute regulatory protein (StAR, now Stard1) acts in conjunction with a multiprotein complex spanning both membranes to move cholesterol to the inner mitochondrial membrane (IMM), where the first step of steroidogenesis occurs (reviewed in [33–36]). At the IMM, cholesterol is converted to pregnenolone, which is the precursor for all other steroid hormones. In non-steroidogenic cells, trafficking to mitochondria has been described for cholesterol from the plasma membrane [37], the ER [18, 19], late endosomes [14, 38], and lipid droplets [39, 40], and may involve cytosolic carrier proteins, particularly for transport from the plasma membrane [37] and/or membrane contact sites, such as the mitochondria-associated membranes of the ER [41]. Stard1 and other members of the same protein family with a cholesterol-binding StAR-related lipid transfer (START) domain are key players in mitochondrial cholesterol import [14, 19, 33–36]. A multiprotein complex spanning both mitochondrial membranes is also required for cholesterol transport to the IMM [42, 43]. Even though many of the proteins involved in mitochondrial cholesterol import have been identified, the exact mechanisms and regulation of transport in different cell types and environmental conditions are still largely unclear. Recent work, disputing some long-standing models for mitochondrial cholesterol import, illustrates the need for further mechanistic studies [43, 44].

The association of diseases such as cancer with increased mitochondrial cholesterol levels has raised interest in the mechanisms of mitochondrial cholesterol import, and the consequences of altered mitochondrial cholesterol levels. However, the measurement of total mitochondrial cholesterol levels and of cholesterol transport to the mitochondrial membranes remains a key challenge. Investigations of other cholesterol trafficking pathways commonly rely on isotope-labeled tracers, either provided in the form of biosynthetic precursors, such as [^{3}H]- or [^{14}C]-labeled acetate or mevalonate, or in the form of exogenous isotope-labeled cholesterol or cholesterol esters, complexed to cyclodextrins or lipoproteins, to follow cholesterol. However, because of the relatively small amounts of cholesterol imported into mitochondria and the lengthy procedure to sufficiently purify mitochondria, the amounts of radiotracer and cells needed to quantify mitochondrial cholesterol with this approach would be prohibitively high. Fluorescent analogues of cholesterol have been used for real-time, single-cell monitoring of cholesterol transport [45], but the very low levels of cholesterol in mitochondria would make it nearly impossible to quantify fluorescent analogues in mitochondria in the presence of the cholesterol-rich plasma membrane and endosomal membranes. Moreover, the fluorescent analogues that best mimic the biophysical characteristics of cholesterol, namely dehydroergosterol and cholestatrienol, fluoresce in the low UV range, and are not easily detected with many microscopes [46]. More recently developed techniques, such as the tracing of cholesterol using the click chemistry probe alkyne-cholesterol [47, 48], may provide additional options for mitochondrial cholesterol measurements.

To circumvent the key challenge of quantifying very low levels of mitochondrial cholesterol in the presence of cholesterol-rich membranes, the assay described here uses the mitochondria-specific conversion of cholesterol to pregnenolone as an indicator for cholesterol arrival at the IMM. A similar approach of using an organelle-specific enzymatic process to monitor cholesterol trafficking is commonly used to follow cholesterol trafficking to the ER, where the formation of cholesterol esters from isotope-labeled cholesterol reflects cholesterol delivery to the ER. Pregnenolone synthesis is catalyzed by CYP11A1 (formerly cytochrome P450 side chain cleavage enzyme, P450scc) at the IMM, and the transport of cholesterol to CYP11A1 is the rate-determining step of steroidogenesis. Pregnenolone can be measured with high sensitivity and specificity using enzyme-linked immunosorbent assays (ELISA) or radioimmunoassays (RIA). Because pregnenolone is membrane-permeable, its concentration in the extracellular medium reflects pregnenolone synthesis—and thus cholesterol transport to the IMM—when downstream steroidogenesis from pregnenolone is inhibited. Pregnenolone formation has been used in steroidogenic cells to monitor cholesterol import to the IMM in studies that revealed the key role of Stard1 [49, 50].

To adapt this technique to non-steroidogenic cells, the group of Walter Miller at the University of California, San Francisco, CA, developed a mitochondrially targeted fusion construct of CYP11A1, ferredoxin reductase, and ferredoxin, which conferred the ability to synthesize pregnenolone to non-steroidogenic cells when expressed ectopically [51, 52]. Non-steroidogenic COS-1 cells transfected with the so-called F2-fusion protein synthesized measurable amounts of pregnenolone, which increased following co-transfection with Stard1, indicating increased mitochondrial cholesterol import in the presence of Stard1 [49, 50]. The approach relies on the key principle that through the activity of CYP11A1 in the F2-fusion protein, pregnenolone is exclusively formed from cholesterol at the IMM, so that the amount of pregnenolone in the medium reflects the sum of cholesterol that arrived at the IMM during the incubation period. It is crucial that CYP11A1 activity is high enough to ensure that cholesterol transport to the IMM (and not CYP11A1 activity) is the rate-determining step. The maximum CYP11A1 activity is determined using the membrane-permeable precursor 22-R-hydroxycholesterol (22-OH-Chol) for pregnenolone formation. 22-OH-Chol does not rely on active transport mechanisms to reach the F2-fusion protein, therefore its conversion to pregnenolone is only limited by CYP11A1 activity. One main caveat of this approach is that the ectopic expression of the F2-fusion protein could change mitochondrial cholesterol trafficking due to its CYP11A1 activity and removal of cholesterol from the IMM, especially if CYP11A1 activity is exceedingly high. Therefore, it should not be concluded that the amount of pregnenolone formed in cells transfected with the F2-fusion vector equals the amount of cholesterol that would reach the IMM in the parental cells not expressing the F2-fusion protein. However, when set up to ensure that CYP11A1 activity is not rate-limiting and that it is similar among cell models and conditions to be compared, this method can provide a powerful approach to investigate the effects of genetic or pharmacological manipulations—for example the depletion or overexpression of candidate transport proteins—on mitochondrial cholesterol import.

Our group has used this approach to elucidate the roles of Niemann–Pick Type C proteins and Stard3 in mitochondrial cholesterol import [14, 38]. Other studies have investigated the role of Stard1 and its binding partners, effects of different Stard1 mutations, other START proteins, and mitochondrial proteins potentially involved in cholesterol transport [41, 53–66]. Here, we describe the assay conditions for isolated mitochondria and cultured cells expressing the F2-fusion protein, as well as the analysis of pregnenolone by RIA. The measurement of pregnenolone formation in isolated mitochondria and other cell fractions also serves to verify the exclusively mitochondrial activity of

CYP11A1, which is a key feature of this transport assay. The transfection with the F2-fusion expression vector and the selection of cells stably expressing the F2-fusion protein must be adapted and optimized for each cell line of interest, and are not described in detail.

2 Materials

Prepare all solutions using ultrapure water and analytical grade reagents. Nondisposable glassware used for stock solutions and in the RIA should be cleaned thoroughly, soaked for at least 2 h in 1 M HCl, rinsed at least five times with deionized water, rinsed once with methanol, dried and capped until use.

2.1 Cell Culture and Expression Vector

1. F2 expression vector (*see* **Note 1**).
2. Cell lines of interest, stably expressing F2-fusion protein (*see* **Note 2**).
3. Growth medium suitable for the cell lines of interest.

2.2 CYP11A1 Activity Assay

1. Phosphate-buffered saline (PBS) 10× stock: Add 80 g NaCl, 2 g KCl, 14.4 g Na_2HPO_4, and 2.4 g KH_2PO_4 to 800 mL of water. Adjust the pH to 7.4 with 1 M NaOH, and fill up to 1 L with water. Dilute 100 mL of the 10× stock into 1 L of water for the final 1× PBS.
2. Mitochondria isolation buffer: 5 mM HEPES, 250 mM mannitol, 70 mM sucrose, 1 mM EGTA, pH 7.4. Add 0.65 g Na-HEPES, 22.77 g mannitol, 12 g sucrose, and 190 mg EGTA into 400 mL of water. Adjust the pH to 7.4 and fill up to a final volume of 500 mL with water. Add a protease inhibitor cocktail directly before use and keep on ice.
3. Dounce glass–glass homogenizer or nitrogen cavitation cell disruption vessel (*see* **Note 3**)
4. Mitochondria reaction buffer: 250 mM sucrose, 10 mM KH_2PO_4, 20 mM KCl, 15 mM triethylamine hydrochloride, 5 mM $MgCl_2$, pH 7.2. Dissolve 4.28 g sucrose, 68 mg KH_2PO_4, 74.5 mg KCl, 138.75 mg triethylamine hydrochloride, and 50.9 mg $MgCl_2$ in approximately 30 mL water, adjust pH to 7.2 with KOH, and fill up to a volume of 50 mL with water in a graduated cylinder.
5. Pyruvate/malate stock solution, 200 mM each: Dissolve 312.2 mg malic acid and 220 mg sodium pyruvate in 10 mL mitochondria reaction buffer. Prepare a 20 mM working stock by diluting the 200 mM pyruvate/malate solution 10 times in mitochondria reaction buffer.

6. NADPH: Prepare a 10 mM (7.44 mg/mL) working stock solution of NADPH in mitochondria reaction buffer.
7. 22-R-hydroxycholesterol (22-OH-Chol, 5-cholesten-3β,22(R)-diol, CAS 17954-98-2): 5 mM in ethanol. Dissolve 5 mg in 2.48 mL ethanol, and keep in screw-cap glass vial with Teflon-coated lid at −20 °C (*see* **Note 4**). On the day of the experiment, prepare a 50 μM working stock solution in mitochondria reaction buffer (1:100 dilution).
8. Trilostane (2(5α)-androsten-3-cyano-4α,5α-epoxy-3-ol-17--one, CAS 13647-35-3): 10 mM stock solution in ethanol. Dissolve 5 mg in 1.52 mL EtOH, and keep in screw-cap glass vial with Teflon-coated lid at −20 °C. On the day of the experiment, prepare a 100 μM working stock solution in mitochondria reaction buffer (1:100 dilution) (*see* **Note 5**).
9. Diethylether for lipid extraction of pregnenolone (*see* **Note 6**).
10. Evaporator to dry lipid extracts under a stream of nitrogen gas in a fume hood.

2.3 Mitochondrial Cholesterol Import Assay

1. Phenol red-free, serum-free medium suitable for the cell lines of interest (*see* **Note 7**).
2. 22-OH-Chol and trilostane stock solutions as above.
3. Protein assay, such as the bicinchinonic acid assay or assays based on the Lowry or Bradford methods.

2.4 Radioimmunoassay of Pregnenolone

1. Phosphate buffer: 0.1 M sodium phosphate buffer pH 7.0 (61 mM sodium phosphate dibasic and 39 mM sodium phosphate monobasic) with 15 mM sodium azide and 155 mM sodium chloride. Gelatin (0.2 %) is added as indicated. Add 8.175 g $Na_2HPO_4{\cdot}7H_2O$ (dibasic, m.w. 268 g/mol), 2.7 g $NaH_2PO_4{\cdot}H_2O$ (monobasic; m.w. 138 g/mol), 4.5 g NaCl (m.w. 58 g/mol), and 487.5 mg sodium azide (m.w. 65 g/mol) to approximately 350 mL water in a graduated cylinder and add water up to a volume of 500 mL. To prepare phosphate buffer with gelatin, add 0.2 g gelatin to 100 mL of complete phosphate buffer and heat the solution, until the gelatin is dissolved.
2. 12 × 75 mm disposable glass tubes.
3. Rabbit anti-pregnenolone antibody (MP Biomedicals #07172016).
4. [7-^{3}H(N)]-pregnenolone (1 mCi/mL, 11.5 Ci/mmol).
5. Pregnenolone: 1 μg/mL stock solution in ethanol.
6. Dextran-coated charcoal.
7. Scintillation vials and scintillation fluid.

3 Methods

3.1 Measurement of CYP11A1 Activity in Subcellular Fractions and Cholesterol Import Assay in Isolated Mitochondria

This section describes the isolation of mitochondria from cultured cells, and the conditions for the measurement of pregnenolone formation in isolated mitochondria and other subcellular fractions. This experimental design can be used to verify that the F2-fusion protein and CYP11A1 activity are restricted to mitochondria by measuring pregnenolone formation from the membrane-permeable precursor 22-OH-Chol in mitochondrial and non-mitochondrial cellular subfractions [14] (*see* **Note 8**). In the absence of 22-OH-Chol, the assay can serve to measure mitochondrial cholesterol import in isolated mitochondria, for example to study the effects of soluble recombinant proteins on the transport of cholesterol to the IMM [53, 67] (*see* **Note 9**).

1. Grow cells expressing the F2-fusion protein on six 10 cm dishes to 80 % confluency in full growth medium. The number of cells required depends on the cell type and yield of mitochondria.
2. Wash cells once with approximately 5 mL cold PBS per dish. Aspirate PBS, wash, and scrape cell layer into 1 mL ice-cold PBS per 10 cm dish.
3. Combine all cell suspensions into a 15 mL centrifuge tube and centrifuge at 800 × *g* for 4 min. Discard supernatant.
4. Resuspend cell pellet in 1 mL ice-cold mitochondria isolation buffer with protease inhibitors. Our preferred method of cell disruption is by nitrogen cavitation, which affords very high yields of functional mitochondria with minimal damage to the cell organelles as no heat is generated and the rupture is a single insult [14, 38, 68] (*see* **Note 3**). Cell suspensions are placed in a cell disruption vessel connected to a nitrogen tank and put under high nitrogen pressure. The rapid release of the pressure ruptures the plasma membrane due to the rapid escape of dissolved nitrogen gas from the cells. If a glass–glass Dounce homogenizer is used, precool the homogenizer, and lyse the cells on ice with 30 gentle strokes. Avoid pulling the pestle completely out of the solution to prevent foaming and bubble formation.
5. Transfer cell homogenate into a microcentrifuge tube and centrifuge at 800 × *g*, 4 °C for 5 min to remove nuclei and unbroken cells.
6. Discard the pellet, transfer the supernatant into a fresh microcentrifuge tube and centrifuge at 12,000 × *g*, 4 °C for 15 min to yield crude mitochondria. The supernatant can be collected as a non-mitochondrial fraction containing cytosol, ER and plasma membrane and be used to verify the absence of CYP11A1 activity outside of mitochondria.

7. Resuspend the pellet of crude mitochondria in 500 µL mitochondria reaction buffer.
8. Gently resuspend mitochondria in a small glass–Teflon homogenizer with two or three strokes.
9. Use samples immediately or freeze at −80 °C for no longer than 1 week (*see* **Note 10**).

3.2 Mitochondrial Cholesterol Import Assay in Isolated Mitochondria and Cellular Subfractions

1. Measure the protein content of the mitochondrial fraction, using a photometric protein assay, such as the bicinchinonic acid assay, or assays based on the Lowry or Bradford methods [69–74]. The amount of mitochondrial protein to use per reaction depends on the expression level of the F2-fusion protein and should be tested first by using increasing amounts of protein. For our F2-CHO cells, we used up to 60 µg protein of the crude mitochondrial fraction per reaction. To verify that CYP11A1 activity is exclusively in the mitochondrial fraction, also measure the protein content of the non-mitochondrial supernatant and an aliquot of the whole cell lysate, and include these fractions in the assay.
2. Pipette the appropriate volume of the mitochondrial fraction into a 1.5 ml microcentrifuge tube. Add mitochondria reaction buffer up to a volume of 60 µL. Then add 10 µL of each working stock of 20 mM pyruvate/malate, 10 mM NADPH, 100 µM trilostane, and 50 µM 22-OH-Chol for final concentrations of 2 mM pyruvate and malate, 1 mM NADPH, 10 µM trilostane, and 5 µM 22-OH-Chol (*see* **Note 11**). If several samples are measured, a mastermix of the four solutions can be prepared by mixing equal volumes of the four working stock solutions, and adding 40 µL per sample. It is recommended to prepare the mastermix for $n + 1$ samples.
3. Incubate samples for 60 min at 37 °C.
4. To stop the reaction, transfer the whole volume into a screw cap glass tube with Teflon-lined lid and add 400 µL PBS and 1 mL diethylether inside a fume hood (*see* **Note 6**). Vortex vigorously for 1 min.
5. Centrifuge the tubes at 2000 × *g* for 5–10 min.
6. Transfer the organic upper phase to a fresh screw cap glass tube.
7. Repeat the extraction of the aqueous phase once or twice to ensure complete extraction of the lipids (*see* **Note 12**).
8. Combine all organic (upper) phases in a screw cap glass vial. The extracts can be stored under nitrogen at −20 °C.
9. Dry the combined organic phases under a gentle stream of nitrogen gas in a fume hood.

10. Resuspend the lipids in warm (37 °C) phosphate buffer with gelatin (see below) and vortex vigorously. Samples can be frozen or used directly in the RIA for pregnenolone.

3.3 Mitochondrial Cholesterol Import Assay in Cultured Cells

1. Plate F2-cells into 48-well plates at 200 cells/mm^2 and grow for 48 h in the appropriate serum-containing growth medium.
2. Wash cells twice with serum-free, phenol red-free medium and incubate in 300 μL serum-free, phenol red-free transport medium (*see* **Note 13**). For CHO cells, we added 10 μM trilostane (final concentration) to the transport medium to minimize the conversion of pregnenolone to other steroids. To determine the maximum rate of pregnenolone formation, add 5 μM 22-OH-Chol (final concentration) to the transport medium (*see* **Note 14**). To determine the extent to which pregnenolone is degraded by the cells, add a known amount of pregnenolone at the beginning of the incubation period and determine its recovery at the end.
3. After 24 h (or shorter incubation periods, *see* **Note 15**), collect medium from each well into separate microcentrifuge tubes and centrifuge at 800 × *g* for 5 min to pellet and remove any cells. Transfer the resulting supernatant to a new tube.
4. Medium can be kept frozen at −80 °C until it is used in the RIA.
5. If pregnenolone formation is assessed for shorter time periods, or by cells that are producing lower levels of pregnenolone, it may be necessary to collect medium from more cells and to extract the pregnenolone. Lipid extraction is performed as described above for isolated mitochondria. The dried lipid extracts are resuspended in 500 μL warm phosphate buffer with gelatin and can be used directly in the RIA.
6. As a negative control, perform the same extraction with medium that has not been incubated with cells, but contains all treatments that have been added to the cells ("blank medium"). We also recommend preparing a positive control by adding a known amount of pregnenolone (we usually used 300 pg) to medium that was not incubated with cells, and performing the extraction (if applicable) and analysis in parallel to the extraction and analysis of the samples (*see* **Note 16**).

3.4 Pregnenolone RIA

In the RIA, the samples are mixed with a known amount of radiolabeled pregnenolone and antibodies specific for pregnenolone. The unlabeled pregnenolone in the sample and the radiolabeled trace pregnenolone compete for binding to the antibody. The pregnenolone antibody mixture is then mixed with a slurry of dextran-coated charcoal. Unbound pregnenolone, but not antibody-bound pregnenolone, is adsorbed by the dextran-coated

charcoal. The charcoal is pelleted by centrifugation, and radioactivity remaining in the supernatant is measured in a scintillation counter. The more unlabeled pregnenolone in the sample, the less radiolabeled pregnenolone will be bound to antibodies and remain in the supernatant. Therefore, radioactivity in the supernatant and pregnenolone levels in the sample are inversely related, and lower levels of radioactivity in the supernatant indicate higher amounts of pregnenolone in the sample. The assay relies on the specificity of the antibodies, and on the relative amounts of antibodies to radiolabeled trace pregnenolone and unlabeled sample pregnenolone. It is crucial that the amounts of antibody and radiolabeled trace pregnenolone are carefully controlled, and that a standard curve and the appropriate controls are included in every assay. Controls include a Total Count Control (TCC) without unlabeled pregnenolone, antibodies, or charcoal. The TCC reflects the maximum counts, as it only contains the radiolabeled pregnenolone trace. A second control is the nonspecific-binding NSBC control, which contains the pregnenolone trace and the dextran-coated charcoal to assess any nonspecific binding of pregnenolone that would prevent adsorption to the charcoal. This control should yield very low radioactivity in the supernatant, because the pregnenolone trace should be nearly completely bound to charcoal and removed from the supernatant. The third control is the maximum binding control (MBC), which contains the radiolabeled pregnenolone trace, antibodies, and dextran-coated charcoal. The radioactivity measured in the MBC should be close to the TCC, because virtually all radiolabeled pregnenolone trace should be bound by the antibodies and remain in the supernatant. If any of the controls do not yield the expected values, the results of the assay must be discarded. In addition to the controls, a standard curve with known amounts of unlabeled pregnenolone added should be measured in every assay, and it should be ensured that the samples are within the dynamic range given by the standard curve (*see* **Note 17**).

1. Prepare a serial dilution of nonradioactive pregnenolone: Warm 50 mL of phosphate buffer plus gelatin to 37 °C. Prepare four standard tubes (labeled "A–D") of 4, 2, 1, 0.5 ng/mL pregnenolone in warm phosphate buffer plus gelatin: Add 10 μL of the 1 μg/mL pregnenolone stock solution in ethanol to 2.5 mL warm phosphate buffer plus gelatin and vortex vigorously (tube A, 4 ng/mL). Add 500 μL from this solution to 500 μL of warm phosphate buffer plus gelatin (tube B, 2 ng/mL). Perform two more steps of a 1:1 serial dilution for tube C (1 ng/mL) and tube D (0.5 ng/mL). Tubes A to D are used to prepare the final standard curve in phosphate buffer plus gelatin as listed in Table 1.
2. Set up and label disposable 12 × 75 mm glass tubes for controls and standards in duplicate and for samples in triplicate as outlined in Table 1 (*see* **Note 18**).

Table 1
Pipetting scheme for the RIA

Tube #		Buffer (µL)	Standard	^{3}H trace (µL)	Antibody (µL)	Charcoal (µL)
1–2	TCC	800	–	100	–	–
3–4	NSBC	600	–	100	–	200
5–6	0 pg MBC	500	–	100	100	200
7–8	25 pg	450	50 µL of tube D	100	100	200
9–10	50 pg	400	100 µL of tube D	100	100	200
11–12	100 pg	400	100 µL of tube C	100	100	200
13–14	200 pg	400	100 µL of tube B	100	100	200
15–16	300 pg	425	75 µL of tube A	100	100	200
17–18	400 pg	400	100 µL of tube A	100	100	200
19–20	500 pg	375	125 µL of tube A	100	100	200
Samples						
1–3	Up to 75 µL	To 500	–	100	100	200

TCC total count control, *NSBC* nonspecific binding control, *MBC*—maximal binding control; tubes A to D contain unlabeled pregnenolone in phosphate buffer at 4, 2, 1, and 0.5 ng/mL pregnenolone, respectively

3. Pipette an appropriate volume of medium sample into each sample tube. We commonly use between 50 and 75 µL of medium (*see* **Note 19**). Use only up to 5 µL of medium from 22-OH-Chol treated cells, because of the much higher pregnenolone formation from 22-OH-Chol as precursor. Add blank medium (medium that was not incubated with cells but contains trilostane and any other treatments) to each sample as required to bring all samples up to the same volume of medium. Add cold phosphate buffer plus gelatin to a final volume of 500 µL. Include a negative control of pure blank medium.
4. Following appropriate radiation safety procedures, prepare a 1 µCi/mL (37 kBq/mL) ethanolic stock of [7-^{3}H(N)]-pregnenolone in a screw-cap glass tube with a Teflon-coated cap. We recommend measuing the radioactivity of this solution to ensure correct dilution and calibration of the scintillation counter. The stock solution can be stored at −20 °C in a radiation-approved site and used for subsequent experiments.
5. Dilute the [^{3}H]-pregnenolone stock solution to 1.67 kBq/mL (100 dpm/µL) in warm phosphate buffer plus gelatin. Vortex vigorously. Verify the concentration by measuring an aliquot (100 µL) of this solution in the scintillation counter. For each sample and standard, 100 µL of the diluted [^{3}H]-pregnenolone solution is required; we recommend preparing a sufficient

volume for $n + 4$ (where n = the number of standards plus the number of samples). Keep the solution on ice until use.

6. Prepare a 90-fold dilution of the anti-pregnenolone antibody in phosphate buffer plus gelatin. Prepare 100 µL for $n + 2$ and store on ice until use.
7. Add 100 µL of the 1.67 kBq/mL [^{3}H]-pregnenolone solution to each standard and sample. Add 100 µL of the diluted antibody into all samples and standards except the TCC and NSBC. Add 100 µL of cold phosphate buffer with gelatin to the TCC and NSBC tubes. Cover the tubes with Parafilm, gently swirl, and incubate overnight at 4 °C (*see* **Note 20**).
8. The following day, prepare a slurry of dextran-coated charcoal by mixing 100 mg of dextran-coated charcoal in 15 mL of cold phosphate buffer without gelatin. Because dextran-coated charcoal is not soluble, the solution must be continually stirred on ice for at least 30 min prior to use. Add 200 µL of diluted dextran-coated charcoal to all tubes except the TCC and NSBC tubes. Do not use a repeat pipettor as the charcoal can sediment during the pipetting, leading to uneven distribution across the samples. Stir the charcoal slurry while pipetting if possible. Swirl the tubes and incubate on ice for 30 min. After the incubation remove the dextran-coated charcoal by centrifugation at 2000 × *g* at 4 °C for 15 min.
9. Transfer the resulting supernatants into scintillation vials. Add 4 mL of scintillation fluid, cap, and vortex each tube.
10. Measure the radioactivity in a scintillation counter.
11. The amount of pregnenolone is calculated based on the standard curve (*see* **Note 21**).

4 Notes

1. The F2-fusion expression vector encodes a fusion construct (F2) of human CYP11A1, ferredoxin reductase, and ferredoxin with an N-terminal mitochondrial targeting sequence of the cytochrome c oxidase subunit VIII. The F2-fusion protein is targeted to the mitochondrial matrix and catalyzes the conversion of cholesterol to pregnenolone. The original expression vector was generated by Miller and coworkers in the pECE backbone [51, 52]. The F2 open reading frame was later cloned into the EcoRI and KpnI restriction sites of the pcDNA3.1(+) vector, which allows selection of transfected cells with G418.
2. Theoretically, any cell type/cell line can be used in these measurements. We have mostly used Chinese hamster ovary (CHO, ATCC CCL61) cells [14, 38]. Previous studies have described

the use of COS1 cells [53]. For better control of the expression levels of the F2-fusion protein, it is preferable to use cell lines that allow the selection and generation of monoclonal, stably transfected cell lines. We recommend generating several lines with different levels of expression of the F2-fusion protein. If mitochondrial cholesterol transport is to be compared in separate cell lines, for example to determine the influence of a different genetic background on mitochondrial cholesterol import, the expression and CYP11A1 activity of the F2 fusion protein must be comparable.

3. In our hands, nitrogen cavitation gave the highest yields of functional mitochondria. The disadvantage of this method is the necessity for a specialized high-pressure cell disruption vessel (available from Parr Instruments, 4639 Cell Disruption Vessel). Traditional mechanical homogenization is a good alternative. For cultured cells, glass–glass homogenizers are preferable to glass–Teflon homogenizers, which are more suitable for tissue samples where the more extensive extracellular matrix aids the disruption. To minimize damage to mitochondria and other cell organelles, it is important to keep the homogenizer on ice, and to avoid formation of bubbles.
4. 22-OH-Chol is a membrane-permeable precursor for pregnenolone synthesis catalyzed by CYP11A1. Pregnenolone formation from 22-OH-Chol is cholesterol transport-independent and is measured to determine maximum CYP11A1 activity. Therefore, it is important that the concentration of the stock solution remains constant. Avoid large volumes of air in the glass vial to minimize evaporation. Tightly close the stock vial and seal with Parafilm. If possible, aliquot the stock solution into smaller vials.
5. Trilostane inhibits 3-beta hydroxysteroid dehydrogenase, and thus the formation of most steroids downstream of pregnenolone. Trilostane is added to minimize the conversion of pregnenolone to downstream steroids, so that the amount of pregnenolone in the medium reflects its cumulative synthesis during the incubation period. Even non-steroidogenic cells may express some steroidogenic enzymes, and we therefore recommend measuring pregnenolone formation in the absence and presence of trilostane during the validation of the cell lines. If the addition of trilostane does not increase the amount of pregnenolone detected in the medium, trilostane can be omitted from the reaction mix (or cell culture medium). Given that genetic or pharmacological manipulations might affect steroidogenic enzyme expression, the effects of trilostane addition should be tested for all conditions investigated. Pregnenolone can also be converted to 17-hydroxypregnenolone and dehydroepiandrosterone through activity of CYP17A1

(17-alpha hydroxylase) and for some cell types it may be necessary to test whether pregnenolone is catabolized by CYP17A1 by including a CYP17A1 inhibitor, such as abiraterone. However, it must be verified that the inhibitor does not affect CYP11A1 activity and that the inhibitor does not interfere with the RIA. Because CHO cells do not express CYP17A1, we did not test any inhibitors of this enzyme. Alternatively, cells and medium can be analyzed for the presence of steroids to determine how far pregnenolone is converted to other steroids. For example, Huang et al. performed such an analysis for COS-1 cells, and concluded that these cells are not steroidogenic and do not require the presence of trilostane or other inhibitors [53].

6. When pregnenolone formation is measured in isolated mitochondria or other cellular fractions, lipid extraction is necessary to stop the reaction. We have used diethyl ether [38]; however, other solvents, for example dichloromethane or methyl tert-butyl ether, or solid phase extraction are also suitable [75–77]. The same procedure is used to extract and concentrate pregnenolone from larger volumes of medium when shorter incubation times or cells with very low levels of pregnenolone formation are used.
7. For CHO cells, we used phenol-red free DMEM:Ham's F12 (1:1, v:v).
8. The localization of the F2-fusion protein can also be confirmed by immunoblotting of subcellular fractions and/or immunofluorescence staining of cells cultured on glass coverslips, using antibodies against any one of the three enzymes of the fusion protein, human CYP11A1, ferredoxin reductase or ferredoxin. We have had good success with anti-ferredoxin reductase antibodies (Abcam; ab16874) in immunofluorescence staining [14]. For colocalization, we incubated the cells with Mitotracker Red, which is retained during fixation, prior to immunostaining. Alternatively, cells can be co-stained with antibodies against mitochondrial marker proteins such as Tom20, or cytochrome c oxidase subunits. A variety of immunoblotting and immunofluorescence protocols are easily available elsewhere, and will not be described in more detail here.
9. If this assay is used to study cell-type independent mitochondrial transport processes, mitochondria can be isolated from steroidogenic cells or—in larger quantities—from steroidogenic tissues, instead of cells with ectopic expression of the F2-fusion protein [78, 79].
10. The crude mitochondrial fraction still contains lysosomes and multivesicular endosomes. For a description of further purification of mitochondria by density gradient ultracentrifugation

or immunoisolation, the reader is referred to previously published protocols [14, 80–83].

11. The preparation of four separate working stock solutions may appear cumbersome, but allows for the measurement of control samples without 22-OH-Chol (to determine pregnenolone formation from endogenous cholesterol) and samples without trilostane (to determine the proportion of pregnenolone that may be metabolized to downstream steroids).
12. The assay relies on a quantitative extraction of pregnenolone formed in the reaction buffer during the 1 h incubation at 37 °C, because it is not possible to add an internal standard. We recommend extracting the aqueous phase two or three times and combining the organic phases. In addition, buffer and a mitochondrial sample taken at time 0 min (i.e., without incubation at 37 °C) should be spiked with different known amounts of pregnenolone and extracted in parallel to the samples. The recovery from buffer alone will show the efficiency of the lipid extraction. The mitochondrial sample should contain only the exogenously added pregnenolone and show whether any of its components prevent the efficient extraction of pregnenolone or interfere with the RIA. To determine whether some pregnenolone is degraded/metabolized during the incubation, a known amount of pregnenolone is added at the beginning of the incubation, and the difference in pregnenolone content of the spiked and non-spiked samples at 60 min is calculated. If pregnenolone is lost during the incubation, higher doses of trilostane or a CYP17A1 inhibitor should be considered.
13. Phenol red interferes with the pregnenolone RIA. Serum must be avoided, because it contains steroids, including pregnenolone. For cells that require serum, even during relatively short incubation times, serum-free alternatives may be available. It may also be possible to use serum that has been pre-adsorbed with charcoal ("charcoal-stripping") to remove steroid hormones; however, we have not tested this technique. Charcoal-treated medium can be prepared in the lab [84, 85] or obtained commercially. The amount of pregnenolone still detectable in the serum should be tested by RIA.
14. We recommend always including a measurement of maximum pregnenolone formation from 22-OH-Chol to verify that CYP11A1 activity remained constant between experiments and to ensure that the assay is working as expected. When unknown treatments are used, pregnenolone formation from 22-OH-Chol serves as a control that the treatment had no direct effects on CYP11A1 activity. Maximum CYP11A1 activity should be at least tenfold higher than pregnenolone formation

from endogenous cholesterol to ensure that CYP11A1 activity is not rate-limiting. Earlier studies used the ratio of pregnenolone formation from endogenous cholesterol to pregnenolone formation from 22-OH-Chol as a measure for mitochondrial cholesterol import [53]. However, this approach assumes that any effects of CYP11A1 activity on cholesterol trafficking change linearly with increasing maximum activity. We recommend avoiding comparisons between cell populations with widely different CYP11A1 expression and using the formation of pregnenolone from endogenous cholesterol directly as a measure for cholesterol arrival at the IMM without standardizing to maximum activity. As pointed out in the introduction, pregnenolone formation does not equal absolute rates of mitochondrial cholesterol import, as they would occur in cells without F2-fusion protein, but serve to compare the capacity for mitochondrial cholesterol import of cells under different conditions.

15. Pregnenolone levels in the medium reflect the cumulative cholesterol transport to the IMM within the incubation period. The most suitable incubation period over which to measure cholesterol import depends on the experimental conditions, the cell type, and the question to be addressed. We determined a time course of pregnenolone production when first establishing our F2-CHO lines, and then used single time point measurements (at 24 h) for the routine analysis of cholesterol import under different conditions; aiming to choose an incubation period during which sufficient pregnenolone had been formed for a reliable, direct measurement by RIA even under conditions of impaired mitochondrial cholesterol import, while not extending it too far beyond a time where pregnenolone levels have reached a plateau. We opted to use relatively long incubation times for our measurements, because it allowed us to select F2-cell lines with relatively low levels of maximum CYP11A1 activity and thus minimize the disturbance in overall cellular cholesterol homeostasis due to the ectopic expression of the F2-fusion protein.
16. It is crucial to include all pharmacological treatments in the negative control. For example, the drug U18666A, which is commonly used to interfere with lysosomal cholesterol trafficking, caused very high (false) readings in the pregnenolone RIA (unpublished observations). In particular sterol- and steroid-based compounds should be tested in the RIA.
17. Advantages of the RIA are the very low detection limit of about 50 pg per sample and the possibility to measure medium samples directly without extraction. Key challenges (in addition to working with radioactive material), are the sensitivity to interference (*see* **Note 16**) and the dependence on the rela-

tive amounts of three components, namely radiolabeled pregnenolone, antibodies, and charcoal, which all influence the sensitivity and dynamic range of the assay. Therefore, meticulous control of the assay conditions is crucial. The linear dynamic range is somewhat limited (between 50 and 500 pg pregnenolone under the conditions described here), and it may be necessary to repeat the measurements of some samples with a higher or lower volume of medium to ensure that the samples are within the dynamic range of the assay. Steroids, including pregnenolone, have also been measured using enzyme-linked immunosorbent assays (ELISA), and by gas or liquid chromatography coupled with mass spectrometric detection [65, 86–89]. Commercial kits are available for ELISA and RIA.

18. We always use disposable glass tubes for the preparation of the standard curve and samples for pregnenolone analysis to prevent nonspecific binding to the plastic and/or leaching of interfering substances out of the plastic. The use of special low-binding plastic tubes may be possible but we have not tested this.
19. We have not tested the use of larger volumes of medium directly in the RIA. Medium composition and pH could affect antibody binding to pregnenolone. If larger volumes of medium are used, the reliability of the RIA should be verified by measuring medium incubated with parental cells without the F2-fusion protein (to mimic the pH change during the incubation) and spiked with different known amounts of pregnenolone. Alternatively, medium samples can be extracted as described above for isolated mitochondria to concentrate pregnenolone from larger volumes of medium into one sample. Extraction can be useful if short incubation periods or cell lines with very low F2-fusion protein expression are used. As a negative control, the same volume of blank medium should be extracted in parallel, because medium components that interfere with the RIA are also concentrated during the extraction.
20. Samples must be incubated with trace and antibodies at least overnight at 4 °C to ensure equilibrium binding of unlabeled and labeled pregnenolone to the antibodies. Longer incubation times are possible, if the tubes are closed tightly.
21. The standard curve is fitted by linear or exponential regression analysis to calculate the amount of pregnenolone per sample in picograms. Samples must lie within the range given by the standard curve. Pregnenolone concentrations in the medium are calculated from the volume of medium per sample, and can be further standardized to cell protein based on the volume and total cellular protein per well.

Acknowledgments

We thank Dr. Walter Miller (UCSF San Francisco, CA) for generously sharing the original F2-fusion expression vector and the critical reading of the manuscript. Our work on mitochondrial cholesterol import was supported by the Canadian Institutes of Health Research, the Dalhousie Medical Research Foundation, and the Nova Scotia Health Research Foundation.

References

1. Horvath SE, Daum G (2013) Lipids of mitochondria. Prog Lipid Res 52:590–614
2. Baggetto LG, Clottes E, Vial C (1992) Low mitochondrial proton leak due to high membrane cholesterol content and cytosolic creatine kinase as two features of the deviant bioenergetics of Ehrlich and AS30-D tumor cells. Cancer Res 52:4935–4941
3. Montero J, Morales A, Llacuna L, Lluis JM, Terrones O, Basanez G, Antonsson B, Prieto J, Garcia-Ruiz C, Colell A, Fernandez-Checa JC (2008) Mitochondrial cholesterol contributes to chemotherapy resistance in hepatocellular carcinoma. Cancer Res 68:5246–5256
4. Parlo RA, Coleman PS (1984) Enhanced rate of citrate export from cholesterol-rich hepatoma mitochondria. The truncated Krebs cycle and other metabolic ramifications of mitochondrial membrane cholesterol. J Biol Chem 259:9997–10003
5. Rouslin W, MacGee J, Gupte S, Wesselman A, Epps DE (1982) Mitochondrial cholesterol content and membrane properties in porcine myocardial ischemia. Am J Physiol 242:H254–H259
6. Sangeetha T, Darlin Quine S (2009) Preventive effect of S-allyl cysteine sulphoxide (Alliin) on mitochondrial dysfunction in normal and isoproterenol induced cardiotoxicity in male Wistar rats: a histopathological study. Mol Cell Biochem 328:1–8
7. Colell A, Garcia-Ruiz C, Morales A, Ballesta A, Ookhtens M, Rodes J, Kaplowitz N, Fernandez-Checa JC (1997) Transport of reduced glutathione in hepatic mitochondria and mitoplasts from ethanol-treated rats: effect of membrane physical properties and S-adenosyl-L-methionine. Hepatology 26:699–708
8. Lluis JM, Colell A, Garcia-Ruiz C, Kaplowitz N, Fernandez-Checa JC (2003) Acetaldehyde impairs mitochondrial glutathione transport in HepG2 cells through endoplasmic reticulum stress. Gastroenterology 124:708–724
9. Coll O, Colell A, Garcia-Ruiz C, Kaplowitz N, Fernandez-Checa JC (2003) Sensitivity of the 2-oxoglutarate carrier to alcohol intake contributes to mitochondrial glutathione depletion. Hepatology 38:692–702
10. Mari M, Caballero F, Colell A, Morales A, Caballeria J, Fernandez A, Enrich C, Fernandez-Checa JC, Garcia-Ruiz C (2006) Mitochondrial free cholesterol loading sensitizes to TNF- and Fas-mediated steatohepatitis. Cell Metab 4:185–198
11. Barbero-Camps E, Fernandez A, Baulies A, Martinez L, Fernandez-Checa JC, Colell A (2014) Endoplasmic reticulum stress mediates amyloid beta neurotoxicity via mitochondrial cholesterol trafficking. Am J Pathol 184:2066–2081
12. Barbero-Camps E, Fernandez A, Martinez L, Fernandez-Checa JC, Colell A (2013) APP/PS1 mice overexpressing SREBP-2 exhibit combined Abeta accumulation and tau pathology underlying Alzheimer's disease. Hum Mol Genet 22:3460–3476
13. Fernandez A, Llacuna L, Fernandez-Checa JC, Colell A (2009) Mitochondrial cholesterol loading exacerbates amyloid beta peptide-induced inflammation and neurotoxicity. J Neurosci 29:6394–6405
14. Charman M, Kennedy BE, Osborne N, Karten B (2010) MLN64 mediates egress of cholesterol from endosomes to mitochondria in the absence of functional Niemann-Pick type C1 protein. J Lipid Res 51:1023–1034
15. Yu W, Gong JS, Ko M, Garver WS, Yanagisawa K, Michikawa M (2005) Altered cholesterol metabolism in Niemann-Pick type C1 mouse brains affects mitochondrial function. J Biol Chem 280:11731–11739
16. Colell A, Garcia-Ruiz C, Lluis JM, Coll O, Mari M, Fernandez-Checa JC (2003) Cholesterol impairs the adenine nucleotide translocator-mediated mitochondrial permeability transition through altered membrane fluidity. J Biol Chem 278:33928–33935

17. Paradis S, Leoni V, Caccia C, Berdeaux A, Morin D (2013) Cardioprotection by the TSPO ligand 4′-chlorodiazepam is associated with inhibition of mitochondrial accumulation of cholesterol at reperfusion. Cardiovasc Res 98:420–427
18. Bosch M, Mari M, Herms A, Fernandez A, Fajardo A, Kassan A, Giralt A, Colell A, Balgoma D, Barbero E, Gonzalez-Moreno E, Matias N, Tebar F, Balsinde J, Camps M, Enrich C, Gross SP, Garcia-Ruiz C, Perez-Navarro E, Fernandez-Checa JC, Pol A (2011) Caveolin-1 deficiency causes cholesterol-dependent mitochondrial dysfunction and apoptotic susceptibility. Curr Biol 21:681–686
19. Bosch M, Mari M, Gross SP, Fernandez-Checa JC, Pol A (2011) Mitochondrial cholesterol: a connection between caveolin, metabolism, and disease. Traffic 12:1483–1489
20. Martin LA, Kennedy BE, Karten B (2016) Mitochondrial cholesterol: mechanisms of import and effects on mitochondrial function. J Bioenerg Biomembr 2:137–151
21. Garcia-Ruiz C, Mari M, Colell A, Morales A, Caballero F, Montero J, Terrones O, Basanez G, Fernandez-Checa JC (2009) Mitochondrial cholesterol in health and disease. Histol Histopathol 24:117–132
22. Caballero F, Fernandez A, De Lacy AM, Fernandez-Checa JC, Caballeria J, Garcia-Ruiz C (2009) Enhanced free cholesterol, SREBP-2 and StAR expression in human NASH. J. Hepatol. 50:789–796
23. Llacuna L, Fernandez A, Montfort CV, Matias N, Martinez L, Caballero F, Rimola A, Elena M, Morales A, Fernandez-Checa JC, Garcia-Ruiz C (2011) Targeting cholesterol at different levels in the mevalonate pathway protects fatty liver against ischemia-reperfusion injury. J Hepatol 54:1002–1010
24. Fernandez A, Matias N, Fucho R, Ribas V, Von Montfort C, Nuno N, Baulies A, Martinez L, Tarrats N, Mari M, Colell A, Morales A, Dubuquoy L, Mathurin P, Bataller R, Caballeria J, Elena M, Balsinde J, Kaplowitz N, Garcia-Ruiz C, Fernandez-Checa JC (2013) ASMase is required for chronic alcohol induced hepatic endoplasmic reticulum stress and mitochondrial cholesterol loading. J Hepatol 59:805–813
25. Ha SD, Park S, Han CY, Nguyen ML, Kim SO (2012) Cellular adaptation to anthrax lethal toxin-induced mitochondrial cholesterol enrichment, hyperpolarization, and reactive oxygen species generation through downregulating MLN64 in macrophages. Mol Cell Biol 32:4846–4860
26. Mei S, Gu H, Yang X, Guo H, Liu Z, Cao W (2012) Prolonged exposure to insulin induces mitochondrion-derived oxidative stress through increasing mitochondrial cholesterol content in hepatocytes. Endocrinology 153: 2120–2129
27. Kennedy BE, Madreiter CT, Vishnu N, Malli R, Graier WF, Karten B (2014) Adaptations of energy metabolism associated with increased levels of mitochondrial cholesterol in Niemann-Pick type C1-deficient cells. J Biol Chem 289(23):16278–16289
28. Kennedy BE, Leblanc VG, Mailman TM, Fice D, Burton I, Karakach TK, Karten B (2013) Pre-symptomatic activation of antioxidant responses and alterations in glucose and pyruvate metabolism in niemann-pick type c1-deficient murine brain. PLoS One 8:e82685
29. Campbell AM, Chan SH (2007) The voltage dependent anion channel affects mitochondrial cholesterol distribution and function. Arch Biochem Biophys 466:203–210
30. Echegoyen S, Oliva EB, Sepulveda J, Diaz-Zagoya JC, Espinosa-Garcia MT, Pardo JP, Martinez F (1993) Cholesterol increase in mitochondria: its effect on inner-membrane functions, submitochondrial localization and ultrastructural morphology. Biochem J 289(Pt 3):703–708
31. Montero J, Mari M, Colell A, Morales A, Basanez G, Garcia-Ruiz C, Fernandez-Checa JC (2010) Cholesterol and peroxidized cardiolipin in mitochondrial membrane properties, permeabilization and cell death. Biochim Biophys Acta 1797:1217–1224
32. Lucken-Ardjomande S, Montessuit S, Martinou JC (2008) Bax activation and stress-induced apoptosis delayed by the accumulation of cholesterol in mitochondrial membranes. Cell Death Differ 15:484–493
33. Miller WL (2007) Steroidogenic acute regulatory protein (StAR), a novel mitochondrial cholesterol transporter. Biochim Biophys Acta 1771:663–676
34. Miller WL, Bose HS (2011) Early steps in steroidogenesis: intracellular cholesterol trafficking. J Lipid Res 52:2111–2135
35. Strauss JF 3rd, Kishida T, Christenson LK, Fujimoto T, Hiroi H (2003) START domain proteins and the intracellular trafficking of cholesterol in steroidogenic cells. Mol Cell Endocrinol 202:59–65
36. Stocco DM (2001) Tracking the role of a star in the sky of the new millennium. Mol Endocrinol 15:1245–1254
37. Lange Y, Steck TL, Ye J, Lanier MH, Molugu V, Ory D (2009) Regulation of fibroblast

mitochondrial 27-hydroxycholesterol production by active plasma membrane cholesterol. J Lipid Res 50:1881–1888

38. Kennedy BE, Charman M, Karten B (2012) Niemann-Pick type C2 protein contributes to the transport of endosomal cholesterol to mitochondria without interacting with NPC1. J Lipid Res 53:2632–2642
39. Lin Y, Hou X, Shen WJ, Hanssen R, Khor VK, Cortez Y, Roseman AN, Azhar S, Kraemer FB (2016) SNARE-mediated cholesterol movement to mitochondria supports steroidogenesis in rodent cells. Mol Endocrinol 30:234–247
40. Kraemer FB, Khor VK, Shen WJ, Azhar S (2013) Cholesterol ester droplets and steroidogenesis. Mol Cell Endocrinol 371:15–19
41. Prasad M, Kaur J, Pawlak KJ, Bose M, Whittal RM, Bose HS (2015) Mitochondria-associated endoplasmic reticulum membrane (MAM) regulates steroidogenic activity via steroidogenic acute regulatory protein (StAR)-voltage-dependent anion channel 2 (VDAC2) interaction. J Biol Chem 290:2604–2616
42. Issop L, Rone MB, Papadopoulos V (2013) Organelle plasticity and interactions in cholesterol transport and steroid biosynthesis. Mol Cell Endocrinol 371:34–46
43. Rone MB, Midzak AS, Issop L, Rammouz G, Jagannathan S, Fan J, Ye X, Blonder J, Veenstra T, Papadopoulos V (2012) Identification of a dynamic mitochondrial protein complex driving cholesterol import, trafficking, and metabolism to steroid hormones. Mol Endocrinol 26:1868–1882
44. Selvaraj V, Stocco DM, Tu LN (2015) Minireview: translocator protein (TSPO) and steroidogenesis: a reappraisal. Mol Endocrinol 29:490–501
45. Gimpl G, Gehrig-Burger K (2007) Cholesterol reporter molecules. Biosci Rep 27:335–358
46. Maxfield FR, Wustner D (2012) Analysis of cholesterol trafficking with fluorescent probes. Methods Cell Biol 108:367–393
47. Hofmann K, Thiele C, Schott HF, Gaebler A, Schoene M, Kiver Y, Friedrichs S, Lutjohann D, Kuerschner L (2014) A novel alkyne cholesterol to trace cellular cholesterol metabolism and localization. J Lipid Res 55:583–591
48. Jao CY, Nedelcu D, Lopez LV, Samarakoon TN, Welti R, Salic A (2015) Bioorthogonal probes for imaging sterols in cells. Chembiochem 16:611–617
49. Bose HS, Sugawara T, Strauss JF 3rd, Miller WL, International Congenital Lipoid Adrenal Hyperplasia Consortium (1996) The pathophysiology and genetics of congenital lipoid adrenal hyperplasia. N Engl J Med 335: 1870–1878
50. Lin D, Sugawara T, Strauss JF 3rd, Clark BJ, Stocco DM, Saenger P, Rogol A, Miller WL (1995) Role of steroidogenic acute regulatory protein in adrenal and gonadal steroidogenesis. Science 267:1828–1831
51. Harikrishna JA, Black SM, Szklarz GD, Miller WL (1993) Construction and function of fusion enzymes of the human cytochrome P450scc system. DNA Cell Biol 12:371–379
52. Black SM, Harikrishna JA, Szklarz GD, Miller WL (1994) The mitochondrial environment is required for activity of the cholesterol side-chain cleavage enzyme, cytochrome P450scc. Proc Natl Acad Sci U S A 91:7247–7251
53. Huang MC, Miller WL (2001) Creation and activity of COS-1 cells stably expressing the F2 fusion of the human cholesterol side-chain cleavage enzyme system. Endocrinology 142:2569–2576
54. Bose M, Whittal RM, Miller WL, Bose HS (2008) Steroidogenic activity of StAR requires contact with mitochondrial VDAC1 and phosphate carrier protein. J Biol Chem 283:8837–8845
55. LaVoie HA, Whitfield NE, Shi B, King SR, Bose HS, Hui YY (2014) STARD6 is expressed in steroidogenic cells of the ovary and can enhance de novo steroidogenesis. Exp Biol Med (Maywood) 239:430–435
56. Marriott KS, Prasad M, Thapliyal V, Bose HS (2012) Sigma-1 receptor at the mitochondrial-associated endoplasmic reticulum membrane is responsible for mitochondrial metabolic regulation. J Pharmacol Exp Ther 343:578–586
57. Katsumata N, Horikawa R, Tanaka T (2006) Replacement of alanine with asparagic acid at position 203 in human steroidogenic acute regulatory protein impairs the ability to enhance steroidogenesis in vitro. Endocr J 53:427–431
58. Sugawara T, Fujimoto S (2004) The potential function of steroid sulphatase activity in steroid production and steroidogenic acute regulatory protein expression. Biochem J 380:153–160
59. Baker BY, Lin L, Kim CJ, Raza J, Smith CP, Miller WL, Achermann JC (2006) Nonclassic congenital lipoid adrenal hyperplasia: a new disorder of the steroidogenic acute regulatory protein with very late presentation and normal male genitalia. J Clin Endocrinol Metab 91:4781–4785
60. Bose HS, Lingappa VR, Miller WL (2002) Rapid regulation of steroidogenesis by mitochondrial protein import. Nature 417:87–91
61. Kim JM, Choi JH, Lee JH, Kim GH, Lee BH, Kim HS, Shin JH, Shin CH, Kim CJ, Yu J, Lee DY, Cho WK, Suh BK, Lee JE, Chung HR, Yoo HW (2011) High allele frequency of the p.Q258X mutation and identification of a

novel mis-splicing mutation in the STAR gene in Korean patients with congenital lipoid adrenal hyperplasia. Eur J Endocrinol 165:771–778

62. Tee MK, Abramsohn M, Loewenthal N, Harris M, Siwach S, Kaplinsky A, Markus B, Birk O, Sheffield VC, Parvari R, Hershkovitz E, Miller WL (2013) Varied clinical presentations of seven patients with mutations in CYP11A1 encoding the cholesterol side-chain cleavage enzyme, P450scc. J Clin Endocrinol Metab 98:713–720
63. Rajapaksha M, Kaur J, Prasad M, Pawlak KJ, Marshall B, Perry EW, Whittal RM, Bose HS (2016) An outer mitochondrial translocase, Tom22, is crucial for inner mitochondrial steroidogenic regulation in adrenal and gonadal tissues. Mol Cell Biol 36:1032–1047
64. Nakae J, Tajima T, Sugawara T, Arakane F, Hanaki K, Hotsubo T, Igarashi N, Igarashi Y, Ishii T, Koda N, Kondo T, Kohno H, Nakagawa Y, Tachibana K, Takeshima Y, Tsubouchi K, Strauss JF 3rd, Fujieda K (1997) Analysis of the steroidogenic acute regulatory protein (StAR) gene in Japanese patients with congenital lipoid adrenal hyperplasia. Hum Mol Genet 6:571–576
65. Fluck CE, Pandey AV, Dick B, Camats N, Fernandez-Cancio M, Clemente M, Gussinye M, Carrascosa A, Mullis PE, Audi L (2011) Characterization of novel StAR (steroidogenic acute regulatory protein) mutations causing non-classic lipoid adrenal hyperplasia. PLoS One 6:e20178
66. Liu J, Rone MB, Papadopoulos V (2006) Protein-protein interactions mediate mitochondrial cholesterol transport and steroid biosynthesis. J Biol Chem 281:38879–38893
67. Bose HS, Lingappa VR, Miller WL (2002) The steroidogenic acute regulatory protein, StAR, works only at the outer mitochondrial membrane. Endocr Res 28:295–308
68. Kristian T, Hopkins IB, McKenna MC, Fiskum G (2006) Isolation of mitochondria with high respiratory control from primary cultures of neurons and astrocytes using nitrogen cavitation. J Neurosci Methods 152:136–143
69. Smith PK, Krohn RI, Hermanson GT, Mallia AK, Gartner FH, Provenzano MD, Fujimoto EK, Goeke NM, Olson BJ, Klenk DC (1985) Measurement of protein using bicinchoninic acid. Anal Biochem 150:76–85
70. Simpson RJ (2008) Quantifying protein by bicinchoninic acid. CSH Protoc. pdb.prot4722
71. Lowry OH, Rosebrough NJ, Farr AL, Randall RJ (1951) Protein measurement with the Folin phenol reagent. J.Biol.Chem. 193:265–275
72. Waterborg JH, Matthews HR (1994) The Lowry method for protein quantitation. Methods Mol Biol 32:1–4
73. Bradford MM (1976) A rapid and sensitive method for the quantitation of microgram quantities of protein utilizing the principle of protein-dye binding. Anal Biochem 72:248–254
74. Harlow E, Lane D (2006) Bradford assay. CSH Protoc 2006. doi:10.1101/pdb.prot4644
75. van der Pas R, Hofland LJ, Hofland J, Taylor AE, Arlt W, Steenbergen J, van Koetsveld PM, de Herder WW, de Jong FH, Feelders RA (2012) Fluconazole inhibits human adrenocortical steroidogenesis in vitro. J Endocrinol 215:403–412
76. Schloms L, Storbeck KH, Swart P, Gelderblom WC, Swart AC (2012) The influence of *Aspalathus linearis* (Rooibos) and dihydrochalcones on adrenal steroidogenesis: quantification of steroid intermediates and end products in H295R cells. J Steroid Biochem Mol Biol 128:128–138
77. Abdel-Khalik J, Bjorklund E, Hansen M (2013) Development of a solid phase extraction method for the simultaneous determination of steroid hormones in H295R cell line using liquid chromatography-tandem mass spectrometry. J Chromatogr B Analyt Technol Biomed Life Sci 935:61–69
78. Bose HS, Whittal RM, Huang MC, Baldwin MA, Miller WL (2000) N-218 MLN64, a protein with StAR-like steroidogenic activity, is folded and cleaved similarly to StAR. Biochemistry 39:11722–11731
79. Papadopoulos V, Guarneri P, Kreuger KE, Guidotti A, Costa E (1992) Pregnenolone biosynthesis in C6-2B glioma cell mitochondria: regulation by a mitochondrial diazepam binding inhibitor receptor. Proc Natl Acad Sci U S A 89:5113–5117
80. Sims NR, Anderson MF (2008) Isolation of mitochondria from rat brain using Percoll density gradient centrifugation. Nat Protoc 3:1228–1239
81. Clayton DA, Shadel GS (2014) Isolation of mitochondria from cells and tissues. Cold Spring Harb Protoc. pdb.top074542
82. Clayton DA, Shadel GS (2014) Purification of mitochondria by sucrose step density gradient centrifugation. Cold Spring Harb Protoc. pdb.prot080028
83. Clayton DA, Shadel GS (2014) Isolation of mitochondria from tissue culture cells. Cold Spring Harb Protoc. pdb.prot080002
84. Chen RF (1967) Removal of fatty acids from serum albumin by charcoal treatment. J Biol Chem 242:173–181

85. Cao Z, West C, Norton-Wenzel CS, Rej R, Davis FB, Davis PJ, Rej R (2009) Effects of resin or charcoal treatment on fetal bovine serum and bovine calf serum. Endocr Res 34:101–108
86. Kushnir MM, Rockwood AL, Roberts WL, Yue B, Bergquist J, Meikle AW (2011) Liquid chromatography tandem mass spectrometry for analysis of steroids in clinical laboratories. Clin Biochem 44:77–88
87. Couchman L, Vincent RP, Ghataore L, Moniz CF, Taylor NF (2011) Challenges and benefits of endogenous steroid analysis by LC-MS/MS. Bioanalysis 3:2549–2572
88. Taylor AE, Keevil B, Huhtaniemi IT (2015) Mass spectrometry and immunoassay: how to measure steroid hormones today and tomorrow. Eur J Endocrinol 173: D1–12
89. Krone N, Hughes BA, Lavery GG, Stewart PM, Arlt W, Shackleton CH (2010) Gas chromatography/mass spectrometry (GC/MS) remains a pre-eminent discovery tool in clinical steroid investigations even in the era of fast liquid chromatography tandem mass spectrometry (LC/MS/MS). J Steroid Biochem Mol Biol 121:496–504

Chapter 13

Identifying Sterol Response Elements Within Promoters of Genes

Laura J. Sharpe and Andrew J. Brown

Abstract

Cholesterol levels are under tight control within cells. This involves a complex interplay of balancing synthesis, uptake, and export. A major player in the transcriptional regulation of cholesterol levels is sterol regulatory element binding protein (SREBP). SREBP is upregulated in conditions of low cholesterol, and then binds to sterol regulatory elements (SREs) that exist within the promoters of genes involved in cholesterol synthesis and uptake.

Here, we describe a method to identify sterol response elements (SREs) using in silico and experimental approaches.

Key words Sterol response elements, SREBP, Transcription, Promoter, Regulation

1 Introduction

Cholesterol is a vital molecule in mammalian cells, but too much is toxic and can lead to disease. Cholesterol levels must therefore be maintained under tight control. This is achieved through a fine balance of synthesis, uptake, and export. The enzymes involved in each of these processes can be regulated by altering gene expression, protein levels, and activity. Gene expression levels are controlled transcriptionally, and one of the major transcription factors involved in cholesterol homeostasis is sterol regulatory element binding protein-2 (SREBP-2). SREBP-2 is activated in conditions of low cholesterol and then binds to sterol regulatory elements (SREs), largely found within the promoters of genes involved in cholesterol synthesis and uptake. This activates these genes, thus restoring cholesterol levels.

While most cholesterol synthesis genes have been shown to be SREBP-2 targets [1], only some of these have had their SREs mapped (for a review, *see* ref. [2]), meaning further work is required to pinpoint the precise regions required for regulation by SREBP-2. We have recently identified the SREs present in the two terminal enzymes of cholesterol synthesis, DHCR24 [3] and DHCR7 [4].

Ingrid C. Gelissen and Andrew J. Brown (eds.), *Cholesterol Homeostasis: Methods and Protocols*, Methods in Molecular Biology, vol. 1583, DOI 10.1007/978-1-4939-6875-6_13,

Interestingly, dual SREs were found in both these promoters, and we found evidence that they work cooperatively, a potential strategy for conserving energy. In completing this work, we found that prediction programs (e.g., MatInspector) for identifying putative SREs in promoters were ineffective, and we therefore devised our own methods. We also made use of Genome Browser [5] to examine experimental data regarding the binding of SREBP to the genome.

Here, we describe our approach to identifying SREs, including in silico predictions and in vitro promoter assays. Although we refer specifically to SREs, it is likely that these methods could be modified to find other regulatory elements under the control of different transcription factors where the consensus sequence is insufficiently prescriptive.

2 Materials

1. *Firefly* and *Renilla* luciferase plasmids (*see* **Note 1**).
2. Dual-luciferase reporter assay system, including passive cell lysis buffer and LAR II and STOP & GLO reagents (Promega).
3. HelaT cells and growth medium (RPMI supplemented with 10% (v/v) fetal calf serum (FCS; *see* **Note 2**), lipoprotein-deficient FCS (FCLPDS) and antibiotics.
4. Compactin (to decrease sterol status) and 25-hydroxycholesterol (to increase sterol status).
5. TransIT-2020 transfection reagent (Mirus Bio) and opti-MEM transfection medium.
6. Transcriptional Regulatory Element Database (TRED) https://cb.utdallas.edu/cgi-bin/TRED/tred.cgi?process=home.
7. Genome Browser https://genome.ucsc.edu/.

3 Methods

3.1 Identify the Sterol-Sensitive Region

1. From genomic DNA, clone approximately 1.5 kb of your promoter of interest into a *Firefly* luciferase construct (*see* **Note 3**).
2. Make progressive truncations of the promoter construct, e.g., 500 bp, 300 bp, 100 bp (*see* **Note 4**).
3. Set up HelaT cells in 24-well plates in RPMI supplemented with 10% (v/v) FCS. Use triplicate wells per condition.
4. Transfect cells with TransIT-2020 (per well):
   Mix 50 μl Opti-MEM with 250 ng *Firefly* luciferase plasmid (*see* **Note 5**) and 25 ng *Renilla* plasmid (*see* **Note 6**). Add 0.275 μl TransIT-2020.
5. Incubate at room temperature for 30 min.

6. Refresh media in the wells and do not include antibiotics (*see* **Note 7**).
7. Gently add 50 μl transfection mixture per well.
8. Incubate at 37°C with 5% CO_2 for 24 h.
9. Treat cells in RPMI supplemented with 10% (v/v) FCLPDS and either compactin (5 μM) to decrease sterol status and thus activate SREBP, or 25-hydroxycholesterol (10 μM) to increase sterol status and thus inhibit SREBP.
10. Incubate at 37°C with 5% CO_2 for 24 h.
11. Wash cells with PBS, and remove any residual liquid.
12. Add 100 μl passive lysis buffer per well.
13. Gently agitate the plate for 30 min, tapping after 15 min to ensure even distribution (*see* **Note 8**).
14. Pipette 20 μl lysate into wells of a white 96-well plate with clear, flat bottoms.
15. Measure luciferase output using a luminometer and LAR II and STOP & GLO reagents (*see* **Note 9**).
16. Normalize the *Firefly* luciferase values for transfection efficiency by dividing these values by the corresponding *Renilla* values for each well.
17. To determine the sterol-responsiveness of each construct, divide the normalized values of the compactin-treated wells (active SREBP) by the average values of the 25-hydroxycholesterol treated wells (inhibited SREBP) (*see* **Note 10**).
18. Graph these ratios and determine which constructs are sterol-responsive, and which are not, and thereby narrow down the region containing the SREs (*see* Fig. 1 for a mockup example).

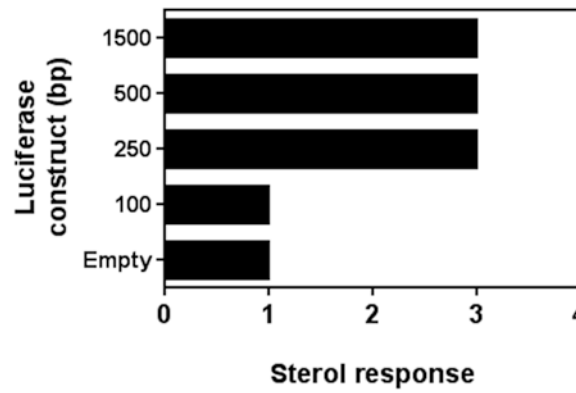

Fig. 1 Example luciferase data. In this example, the constructs containing at least 250 bp of the promoter are all sterol responsive (~3), whereas the empty vector and the 100 bp promoter are not (~1, indicating no difference between sterol and statin treatment). Therefore, the sterol responsive region is located between 100 and 250 bp in the promoter

3.2 Predict SREs

1. Survey the literature and record all available SRE sequences (*see* **Note 11**).
2. Create a matrix indicating the relative abundance of each nucleotide in each position. (For an example of our latest human SRE matrix and a sequence logo representation, *see* Fig. 2a and b).
3. Using the Matrix Search function in TRED (https://cb.utdallas.edu/cgi-bin/TRED/tred.cgi?process=home), input the known SRE sequences into the sequence box, and use the matrix in the positional weight matrix box and analyze the results.
4. Choose the lowest scoring SRE and use its score in the cutoff box to perform a search of your promoter of interest (*see* **Note 12**).
5. To check for existing information on SREBP binding sites, use Genome Browser (https://genome.ucsc.edu/). Use the Genome option to select Human GRCh37/hg19 (*see* **Note 13**).
6. Search for your gene of interest and select it.

A

		Nucleotide position									
		1	2	3	4	5	6	7	8	9	10
A	0.25	8	0	0	17	0	4	0	0	18	1
T	0.25	2	18	0	2	1	2	4	3	2	2
C	0.25	6	4	22	0	15	12	18	17	2	11
G	0.25	6	0	0	3	6	4	0	2	0	8

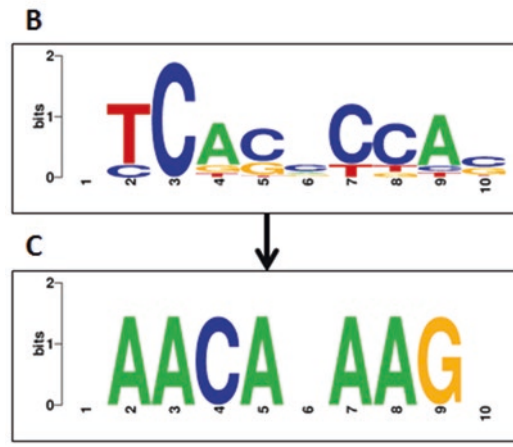

Fig. 2 SRE consensus sequences. (**a**) An example of an SRE matrix. The second column indicates the prior probability, i.e., the expected frequency of each nucleotide in any given sequence. Scores in the table are occurrence count for each position. (**b**) SRE sequences used to generate (a) were used to create a consensus sequence with WebLogo 3.3. (**c**) Suggested mutations to make in the predicted SRE sequence—each base represents to what the corresponding base should be mutated

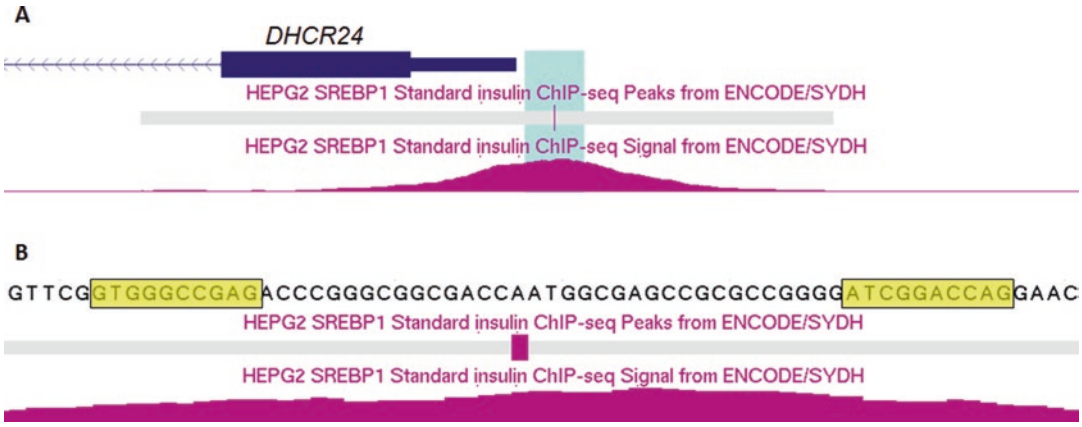

Fig. 3 Genome Browser for DHCR24. (a) A graphical view of Genome Browser showing SREBP data for DHCR24. (b) A zoomed in view of the *blue* highlighted section in A. The *yellow* highlighted sequences are the known SREs in DHCR24 [3]

7. Scroll in the browser to the 5′ untranslated region (*see* **Note 14**).
8. Click on track search and search for "SREBP".
9. Select all tracks (*see* **Note 15**) and click view in browser.
10. Peaks will be visible in the promoter region of the gene if it is an SREBP target (*see* Fig. 3a for an example with DHCR24).
11. Zoom in to view the bases surrounding the peaks to assist in narrowing down the region of SREBP binding (and thus the SRE sequences) (*see* Fig. 3b for an example with DHCR24) (*see* **Note 16**).

3.3 Confirm SREs

1. Using the predictions made in Subheading 3.2, create mutant SRE constructs in the smallest sterol-responsive construct made in Subheading 3.1 (*see* **Note 17**) (*see* Fig. 2b and c for suggested base mutations).
2. Perform luciferase assays as described in Subheading 3.1, **steps 3–18**.
3. Analyze the results to confirm the bona fide SREs based on the mutants that are no longer sterol-responsive (*see* **Note 18**).

4 Notes

1. We use pGL3-basic (*Firefly* luciferase) from Promega, and an in-house pRL-PBGD (*Renilla* luciferase) construct [3], but any *Renilla* luciferase driven by a housekeeping promoter should work.
2. We use HelaT cells as they are highly transfectable and can have their cholesterol status easily manipulated.

3. Any cloning method should work, but note that promoters may have a high GC content and therefore a specialized GC buffer may be of assistance.
4. In our experience, most SREs are located within 300 bp of the transcription start site.
5. Include an empty vector control in every experiment.
6. A master mix of OptiMEM and *Renilla* luciferase plasmid can be made, then *Firefly* plasmids and TransIT-2020 added separately.
7. We have found that refreshing the media at this step (rather than simply adding transfection mix directly) significantly increases transfection efficiency.
8. At this stage, the plate can be frozen at −20°C if desired.
9. This step will be highly dependent on your luminometer—please consult the manufacturer's instructions.
10. Dividing by the average values provides a method for obtaining error bars. We typically get a ratio of ~3 for a sterol-responsive construct, and a ratio of ~1 for a non-sterol-responsive construct or empty vector.
11. The reader should make value judgements on each paper to determine whether the published SRE has high confidence and should be included for the matrix.
12. Remember to also check the reverse complement, as the program does not automatically check this for you.
13. This build of the genome has the most SREBP information available.
14. The direction of the gene on the chromosome will be indicated by arrows.
15. Include SREBP1 as this will supply additional confirmation.
16. Many adjustments can be made to alter the appearance of the peaks and the browser window, and the reader is encouraged to experiment with these.
17. For example, we used 300 bp for DHCR24 [3] and 250 bp for DHCR7 [4].
18. This could then be followed up with creating double mutations if single mutations are still partially sterol-responsive.

References

1. Horton JD, Shah NA, Warrington JA, Anderson NN, Park SW, Brown MS, Goldstein JL (2003) Combined analysis of oligonucleotide microarray data from transgenic and knockout mice identifies direct SREBP target genes. Proc Natl Acad Sci 100:12027–12032
2. Sharpe LJ, Brown AJ (2013) Controlling cholesterol synthesis beyond 3-hydroxy-3-methylglutaryl-CoA reductase (HMGCR). J Biol Chem 288:18707–18715
3. Zerenturk EJ, Sharpe LJ, Brown AJ (2012) Sterols regulate 3beta-hydroxysterol Delta24-reductase (DHCR24) via dual sterol regulatory elements: Cooperative induction of key enzymes in lipid synthesis by Sterol Regulatory Element Binding Proteins. Biochim Biophys Acta 1821:1350–1360
4. Prabhu AV, Sharpe LJ, Brown AJ (2014) The sterol-based transcriptional control of human 7-dehydrocholesterol reductase (DHCR7): Evidence of a cooperative regulatory program in cholesterol synthesis. Biochim Biophys Acta 1842:1431–1439
5. Kent WJ, Sugnet CW, Furey TS, Roskin KM, Pringle TH, Zahler AM, Haussler D (2002) The human genome browser at UCSC. Genome Res 12:996–1006

Chapter 14

Membrane Extraction of HMG CoA Reductase as Determined by Susceptibility of Lumenal Epitope to In Vitro Protease Digestion

Lindsey L. Morris and Russell A. DeBose-Boyd

Abstract

Although many aspects of the endoplasmic reticulum (ER)-associated degradation (ERAD) pathway have been elucidated, methods to detect and examine intermediate steps in the process are lacking. Here, we describe the use of a protease protection assay to study the metabolically regulated ERAD substrate HMG CoA reductase. Studies utilizing this assay reveal that ubiquitinated reductase becomes extracted across the ER membrane prior to its cytosolic release and proteasomal degradation through reactions mediated by distinct AAA-ATPases. A similar approach could be applied to other substrates to determine whether membrane extraction is an intermediate step in their ERAD.

Key words Trypsin, Protease, Lumenal, Membrane extraction, ER-associated degradation

1 Introduction

Accelerated endoplasmic reticulum (ER)-associated degradation (ERAD) of the cholesterol biosynthetic enzyme 3-hydroxy-3-methylglutaryl coenzyme A (HMG CoA) reductase is triggered by its sterol-induced binding to ER membrane proteins called Insig-1 and Insig-2 [1, 2]. This binding is mediated by the membrane domain of reductase, which spans the ER membrane eight times. Subsequent ubiquitination of the reductase membrane domain by Insig-associated ubiquitin ligases marks the enzyme for cytosolic dislocation and proteasomal degradation through poorly understood mechanisms mediated by the AAA-ATPase Valosin-containing protein (VCP)/p97 and augmented by the nonsterol isoprenoid geranylgeraniol (GGOH) [2, 3].

Protease protection assays have been routinely used to define the topology of proteins that traverse membranes of the

Ingrid C. Gelissen and Andrew J. Brown (eds.), *Cholesterol Homeostasis: Methods and Protocols*, Methods in Molecular Biology, vol. 1583, DOI 10.1007/978-1-4939-6875-6_14,

endoplasmic reticulum (ER) one or more times [4–7]. In recent work [8], we developed an assay that measures sterol-induced extraction of reductase across ER membranes by determining susceptibility of a lumenal epitope in the enzyme to in vitro digestion with the protease trypsin. Intact membranes isolated from cells expressing a form of reductase containing T7 epitopes in the N-glycosylated lumenal loop between transmembrane domains 7 and 8 were subjected to in vitro digestion with the protease trypsin. Trypsinolysis produced protected fragments of reductase that were observed in anti-T7 immunoblots. A substantial fraction of the lumenal T7 epitopes became susceptible to trypsin digestion when cells were treated with the oxysterol 25-hydroxycholesterol (25-HC) and GGOH prior to harvest and subcellular fractionation, indicating exposure of the region to the cytosol. Importantly, sterol-induced membrane extraction of reductase as determined by susceptibility of the lumenal T7 epitopes to trypsin was inhibited by RNA interference (RNAi)-mediated knockdown of Insigs or VCP/p97 (an ATPase known to mediate membrane extraction and cytosolic dislocation of ERAD substrates [9]), confirming the physiologic relevance of the reaction. In combination with assays for cytosolic dislocation and degradation, the membrane extraction assay allows for the elucidation of sequential events in reductase ERAD and the identification of participating factors. Similar approaches can be utilized to examine mechanisms for ERAD of other types of substrates in cultured mammalian cells or model systems such as *Saccharomyces cerevisiae*.

2 Materials

This membrane protection assay is best used with a target protein that is engineered to contain an epitope tag in a lumenal loop or alternatively when an antibody is available that specifically recognizes a lumenal loop of the protein of interest. In addition, if studying membrane extraction of a protein, MG-132 treatment of cells may be necessary to acquire an accumulation of the protein on the cytosolic surface of the membrane, allowing a more substantial proportion of the protein to be susceptible to trypsin digestion.

All solutions should be prepared using Milli-Q water. Buffer C and 4× SDS loading buffer are stored at room temperature. All other solutions should be stored at 4 °C. Trypsin and trypsin inhibitor should be stored at −20 °C.

2.1 Cell Lysis Components

1. Cells expressing protein of interest: Triplicate 60-mm or 100-mm near-confluent dishes of cells for each condition that will be tested are usually sufficient. Studies reported in Morris et al. [8] utilized Chinese hamster ovary (CHO) cells to examine the sterol-regulated extraction of HMG CoA reductase from ER membranes.

2. Buffer A: 10 mM HEPES-KOH [pH 7.4], 10 mM KCl, 1.5 mM $MgCl_2$, 5 mM sodium EDTA, 5 mM sodium EGTA, 250 mM sucrose, 5 mM dithiothreitol (DTT), and 0.1 mM leupeptin (*see* **Note 1**).
   (a) Combine 5 mL of 1 M Hepes-KOH, 0.75 mL of 1 M $MgCl_2$, 2.5 mL of 2 M KCl, 5 mL of 500 mM EDTA, 5 mL of 500 mM EGTA, and 62.5 mL of 2 M sucrose. Add up to 400 mL of H_2O and adjust the pH to 7.6 using dropwise addition of 10 N KOH. Adjust the final volume to 500 mL with water. Solution should be filter sterilized and stored at 4 °C.
   (b) If adding 5 mM DTT and 0.1 mM leupeptin (please note, these are omitted in the recipe for buffer B, Subheading 2.2), add 2.4 mL of 10 mg/mL leupeptin and 2.5 mL of 1 M DTT after the pH has been adjusted.
3. 22.5-gauge needle.
4. 1 mL syringe.
5. 1× phosphate-buffered saline (PBS)
6. Microcentrifuge (Eppendorf 5415) or ultracentrifuge (Sorvall MX-120) depending on whether or not membrane and cytosolic fractions will be analyzed.

2.2 Trypsin Protection Assay Components

1. Buffer B: Buffer A (without DTT and leupeptin) supplemented with 100 mM NaCl. Prepared in same manner as Buffer A except 10 mL of 5 M NaCl is added prior to volume adjustment with water and pH adjustment with 10 N KOH. This solution should also be filter sterilized and stored at 4 °C.
2. Buffer C: 62.5 mM Tris–HCl [pH 6.8], 15% (w/v) SDS, 8 M urea, 10% (v/v) glycerol, and 100 mM DTT (*see* **Note 2**).
3. Coomasie Bradford Protein Assay.
4. Trypsin.
5. Trypsin inhibitor powder.
6. 10% (v/v) NP-40.
7. 4× SDS loading buffer: prepared using 12 g sodium dodecyl sulfate, 6 mL 2-mercaptoethanol, 30 g glycerol, 15 mL 1 M Tris–HCl pH 6.8 and adjusted to 100 mL with water. Bromophenol blue added to give solution color.
8. SDS-Page and Immunoblot equipment and reagents.

3 Methods

3.1 Isolation of Cell Membranes

1. Prechill all buffers on ice.
2. Scrape triplicate 60-mm or 100-mm dishes of cells into culture medium; combine and transfer cells to prechilled 15- or 50-mL Falcon tubes.

3. Pellet cells at 500 × *g* for 5 min at 4 °C.
4. Aspirate the medium and resuspend cell pellets in 1 mL cold PBS.
5. Transfer to prechilled 1.5 mL tube and pellet cells by spinning again for 5 min at 4 °C.
6. Resuspend cell pellets in 500 μL of Buffer A (*see* **Note 1**).
7. Homogenize cells by passing through a 22.5-gauge needle 30 times.
8. Pellet nuclei at 1000 × *g* for 7 min at 4 °C. Transfer 400 μL of the post-nuclear supernatant (PNS) to new 1.5 mL tubes.
9. Centrifuge the PNS at 16,000 x *g* for 12 min or 100,000 x *g* for 45 min at 4 °C. The supernatant from 100,000 x *g* spins may be saved if the cytosolic fraction is desired. The resulting pellets are designated as the membrane fraction.

3.2 Trypsin Proteolysis

1. Harvest cells and prepare membrane fractions according to Subheading 3.1 described above. Use of freshly isolated membrane fractions is recommended; these membranes can remain on ice for up to 2 h prior to trypsin digestion.
2. Resuspend membrane pellets in 100 μL Buffer B by pipetting up and down 30 times. Pool samples where appropriate.
3. Determine protein concentrations of membrane suspensions using Coomassie Bradford Protein Assay or equivalent assay.
4. Aliquot 56 μL of membrane suspensions to new 1.5 mL tubes (typical experiments utilizing 100-mm and 60-mm dishes will yield approximately 100 μg and 30 μg of membrane protein, respectively).
5. Prepare 5 mg/mL trypsin solution by dissolving trypsin in 200 μL Buffer B per mg trypsin (*see* **Note 3**).
6. Add 2 μL Buffer B (negative control) or 5 mg/mL trypsin to membrane suspensions. Gently mix and incubate at 30 °C for 30 min (*see* **Notes 4** and **5**).
7. Before trypsin reaction is complete, prepare a solution of trypsin inhibitor (50 μL Buffer B per mg trypsin inhibitor) (*see* **Note 3**).
8. Terminate trypsin proteolysis by transferring 1.5 mL tubes to ice and by the addition of 2 μL trypsin inhibitor solution. Vortex samples to ensure distribution of inhibitor.
9. To further terminate trypsinolysis and prepare samples for SDS-PAGE and immunoblot analysis, add Buffer C in equal volume to that of membrane suspensions and 4× SDS loading buffer (1× final concentration).
10. Heat samples at 37 °C for 20 min and subject to SDS-PAGE, followed by immunoblot analysis.
11. An example of SDS-Page of HMG CoA reductase, subjected to this assay, is presented in Fig. 1 (*see* **Notes 6–8**).

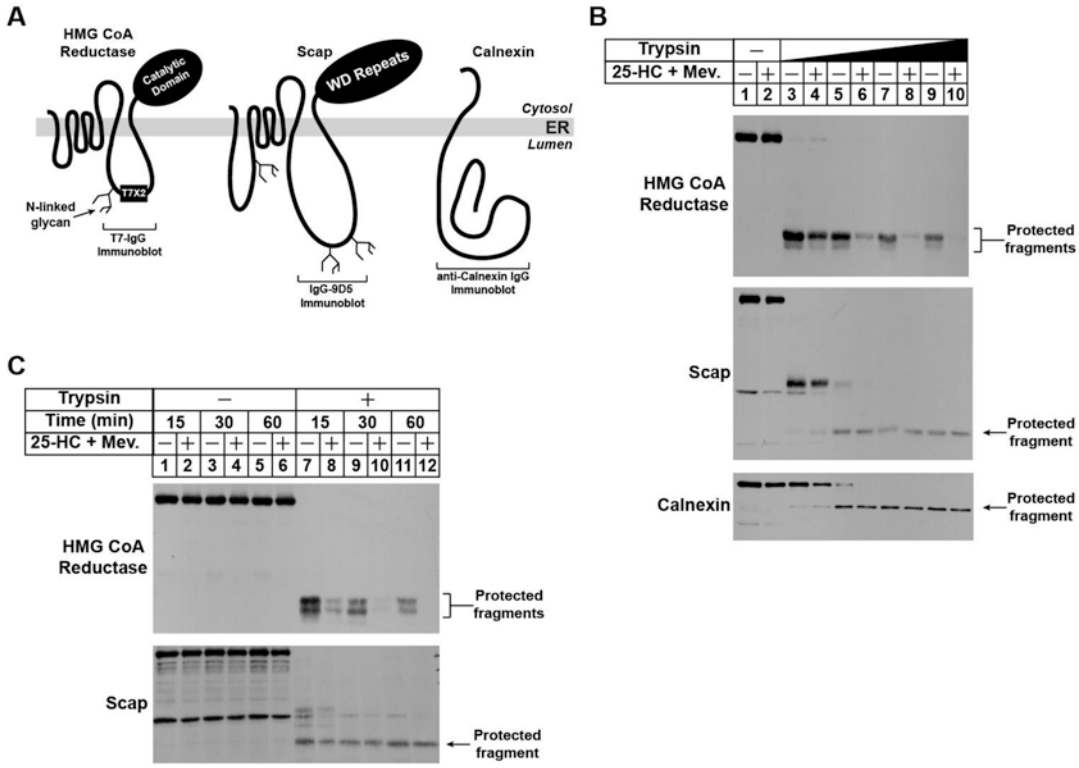

Fig. 1 Sterol and nonsterol isoprenoids enhance susceptibility of a lumenal T7 epitope in HMG-Red-T7 to trypsinolysis. (**a**) topology of HMG CoA reductase, Scap, and calnexin denoting the location of two T7 epitope tags in reductase encoded by pCMV-HMG-Red-T7, the epitope in Scap recognized by monoclonal IgG-9D5 [10], and the region in calnexin recognized by anti-calnexin IgG (Novus Biologicals, Littleton, CO). Sites for N-linked glycosylation in HMG CoA reductase and Scap are indicated (*see* **Note 6**). (**b** and **c**) UT-2/pHMG-Red-T7 cells, a line of reductase-deficient Chinese hamster ovary cells [11] expressing reductase containing lumenal T7 epitopes, were set up for experiments on day 0 at a density of 5×10^5 cells per 100-mm dish in a 1:1 mixture of Ham's F-12 medium and Dulbecco's modified Eagle's medium containing 100 units/mL penicillin and 100 μg/mL streptomycin sulfate (medium A) supplemented with 5% (v/v) fetal calf serum (FCS) and 0.2 mM mevalonate. On day 2, the cells were depleted of sterols by refeeding them medium A supplemented with 5% (v/v) lipoprotein-deficient serum (LPDS), 10 μM of the reductase inhibitor compactin, 50 μM mevalonate, and 1 μM MG-132 (to block reductase ERAD) in the absence or presence of 1 μg/ml 25-HC plus 10 mM mevalonate as indicated. Following incubation at 37 °C for 16 h, the cells were harvested for subcellular fractionation. The resulting membrane fractions were resuspended in Buffer B and digested with 2–20 μg trypsin for 30 min at 30 °C (**b**) or with 10 μg trypsin for the indicated amount of time at 30 °C (**c**). Following treatments, reactions were terminated and the samples were subjected to SDS-PAGE, followed by immunoblot analysis with anti-T7 IgG (against reductase, EMD Biosciences, Darmstadt, Germany), IgG-9D5 (against Scap), and anti-calnexin IgG (*see* **Note 7**)

4 Notes

1. While many cell lysis procedures include the use of protease inhibitors, this procedure does not include any to ensure trypsin will not be inhibited.
2. Buffer C, which is added at the end of trypsinization, is a buffer specifically used to solubilize reductase and may not be necessary or optimal for other proteins of interest.

3. Trypsin and trypsin inhibitor solutions were prepared fresh for each new experiment.
4. Prior to trypsin treatment, an aliquot of membrane suspension may be treated with a detergent, such as NP-40, to serve as a positive control for trypsin digestion.
5. While a trypsin concentration of 5 mg/mL was suitable for studying membrane extraction of reductase, it may be necessary to optimize trypsin concentrations with a concentration curve when studying other ERAD substrates.
6. The glycosylation state of protected fragments can be determined by: (1) treating membranes with 10 μL of 7× denaturation buffer (3.5% (w/v) SDS and 7% (v/v) 2-mercaptoethanol) and incubated at 100 °C for 10 min immediately following trypsin inhibitor treatment, (2) after samples cool add 9 μL 10× G5 buffer (500 mM sodium citrate, pH 5.5) plus either 5 μL H_20 (Endo H treatments) or 5 μL 10% (v/v) NP-40 (PNGase F treatments) containing 17× leupeptin, pepstatin, and aprotinin, (3) add 1 μL (500 units) Endo H or PNGase F to samples, spin briefly and incubate at 37 °C overnight, and (4) add 33 μL 4× sample buffer and incubate for 5 min at 100 °C.
7. Integral membrane proteins, such as calnexin, serve as valuable controls for membrane integrity when immunoblotting samples from trypsin protection assays. Commercially available antibodies can be found that recognize lumenal portions of calnexin.
8. RNA interference (RNAi) experiments can be conducted to verify that susceptibility of lumenal epitope(s) in proteins of interest to in vitro protease digestions results from extraction across the ER membrane and exposure to cytosol. For example, RNAi-mediated knockdown of VCP/p97, the ATPase that plays a key role in membrane extraction and cytosolic dislocation of ERAD substrates [9], blocks the in vitro trypsin digestion of the lumenal T7 epitopes in reductase [8].

Acknowledgments

This work was supported by NIH grants HL20948 and GM090216 to R.D.B.

References

1. Sever N, Yang T, Brown MS, Goldstein JL, DeBose-Boyd RA (2003) Accelerated degradation of HMG CoA reductase mediated by binding of insig-1 to its sterol-sensing domain. Mol Cell 11:25–33
2. Sever N, Song BL, Yabe D, Goldstein JL, Brown MS, DeBose-Boyd RA (2003) Insig-dependent ubiquitination and degradation of mammalian 3-hydroxy-3-methylglutaryl-CoA reductase stimulated by sterols and geranylgeraniol. J Biol Chem 278:52479–52490
3. Elsabrouty R, Jo Y, Dinh TT, DeBose-Boyd RA (2013) Sterol-induced dislocation of 3-hydroxy-3-methylglutaryl coenzyme A reductase from

membranes of permeabilized cells. Mol Biol Cell 24:3300–3308

4. Hua X, Sakai J, Ho YK, Goldstein JL, Brown MS (1995) Hairpin orientation of sterol regulatory element-binding protein-2 in cell membranes as determined by protease protection. J Biol Chem 270:29422–29427
5. Zelenski NG, Rawson RB, Brown MS, Goldstein JL (1999) Membrane topology of S2P, a protein required for intramembranous cleavage of sterol regulatory element-binding proteins. J Biol Chem 274: 21973–21980
6. Feramisco JD, Goldstein JL, Brown MS (2004) Membrane topology of human insig-1, a protein regulator of lipid synthesis. J Biol Chem 279:8487–8496
7. Nohturfft A, Brown MS, Goldstein JL (1998) Topology of SREBP cleavage-activating protein, a polytopic membrane protein with a sterol-sensing domain. J Biol Chem 273: 17243–17250
8. Morris LL, Hartman IZ, Jun DJ, Seemann J, DeBose-Boyd RA (2014) Sequential actions of the AAA-ATPase Valosin-containing Protein (VCP)/p97 and the proteasome 19 S regulatory particle in sterol-accelerated, Endoplasmic Reticulum (ER)-associated degradation of 3-hydroxy-3-methylglutaryl-coenzyme A reductase. J Biol Chem 289:19053–19066
9. Vij N (2008) AAA ATPase p97/VCP: cellular functions, disease and therapeutic potential. J Cell Mol Med 12:2511–2518
10. Sakai J, Nohturfft A, Cheng D, Ho YK, Brown MS, Goldstein JL (1997) Identification of complexes between the COOH-terminal domains of sterol regulatory element-binding proteins (SREBPs) and SREBP cleavage-activating protein. J Biol Chem **272**:20213–20221
11. Mosley ST, Brown MS, Anderson RG, Goldstein JL (1983) Mutant clone of Chinese hamster ovary cells lacking 3-hydroxy-3-methylglutaryl coenzyme A reductase. J Biol Chem 258:13875–13881

Chapter 15

Determining the Topology of Membrane-Bound Proteins Using PEGylation

Vicky Howe and Andrew J. Brown

Abstract

Biochemical methods can help elucidate the membrane topology of hydrophobic membrane proteins where X-ray crystallography is difficult or impractical, providing important structural data. Here, we describe the method of PEGylation, which uses a cysteine-reactive molecule, maleimide polyethylene glycol (mPEG), to determine the cytosolic accessibility of introduced cysteine residues. This accessibility is visualized using Western blotting to detect a band shift that indicates cysteine labeling by mPEG. Using scanning cysteine mutagenesis, followed by PEGylation, one can map the accessibility of the introduced cysteines, hence inferring the membrane topology of the protein.

We used PEGylation to determine the membrane topology of the sterol regulatory domain of a cholesterol synthesis enzyme, squalene monooxygenase, identifying that it is anchored to the membrane via a re-entrant loop.

Key words Membrane topology, Microsome, PEGylation, Western blot, Squalene monooxygenase

1 Introduction

The hydrophobic nature of membrane proteins often makes crystallization difficult or impossible, meaning structural data cannot be obtained using traditional X-ray crystallography techniques. For such proteins, alternative biochemical methods may be useful. One such technique, known as PEGylation, uses a membrane-impermeable cysteine-reactive reagent, maleimide polyethylene glycol (mPEG), to determine cysteine positions relative to the membrane [1, 2]. Single cysteine mutations are introduced systematically in regions of interest within the protein and PEGylation is performed on the single cysteine mutants. mPEG chemically labels cysteines that are cytosolically exposed, while membrane-buried or luminal residues remain unlabeled. This can be detected using SDS-PAGE and Western blotting, as PEGylation results in a band shift corresponding to the mass of mPEG. Triton X-100, a non-denaturing detergent, is used as a positive control. Triton X-100 solubilizes

Ingrid C. Gelissen and Andrew J. Brown (eds.), *Cholesterol Homeostasis: Methods and Protocols*, Methods in Molecular Biology, vol. 1583, DOI 10.1007/978-1-4939-6875-6_15,

membranes but does not disrupt secondary protein structures. Therefore, the level of PEGylation in a Triton X-100-treated microsome acts as a reference for the relative exposure of the residue when not treated with Triton X-100. For example, no PEGylation indicates that a residue is likely membrane-buried or luminal, while full accessibility (equal to the Triton X-100 condition) indicates a cytosolic orientation (Fig. 1). An mPEG-accessible residue that is less PEGylated than its Triton X-100-treated condition is likely to be on a membrane-cytosol interface. If however, the Triton X-100-treated control sample is unPEGylated, this may indicate that the residue is sterically hindered by protein structures. This can be confirmed by pretreating microsomes with a denaturing detergent, sodium dodecyl sulfate (SDS), prior to PEGylation, which should render the cysteine residue accessible, allowing it to be PEGylated (Fig. 1). By mapping the accessibility of the introduced cysteines relative to the Triton X-100 condition, the general membrane topology of a membrane protein can be inferred and regions such as re-entrant loops or transmembrane domains can be identified.

PEGylation can also be used to identify conformational changes that result in altered cysteine accessibility, e.g., the cholesterol-induced conformational change observed in squalene monooxygenase [3] or Ca^{2+}-induced conformational changes in inositol triphosphate receptors [4]. However, depending on the magnitude of the conformational change and whether this occurs in a membrane-spanning or sterically- hindered region, this may or may not be detectable by PEGylation.

PEGylation can be performed on purified protein or in cell lysates. As mPEG reacts with all cysteines in a sample, the quantity of mPEG must be in excess of that of cysteines in the reaction. -In

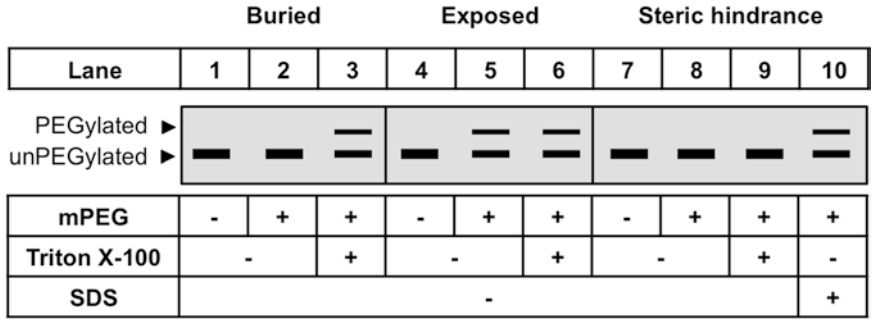

Fig. 1 Mock-up Western blots demonstrating that relative PEGylation indicates membrane orientation of cysteine residues. Residues that are membrane-buried or luminally-oriented are inaccessible to the membrane-impermeable mPEG, so no PEGylation is observed (lane 2). Triton X-100 solubilizes the membrane, allowing these residues to be PEGylated, acting as a positive control (lane 3). Cytosolically-exposed residues are able to be PEGylated in the absence of Triton X-100 (lane 5). Residues not PEGylated even with Triton X-100 are likely to be sterically hindered (lanes 8 and 9). Such residues can be PEGylated in the presence of SDS (lane 10). However, this gives no indication of the position of such residues relative to the membrane. Lanes 1, 4, and 7 are controls without the addition of mPEG

mixed protein samples, enrichment of the protein of interest can be helpful to reduce the number of cysteine-containing proteins. For example, for proteins residing in the endoplasmic reticulum (ER) membrane, intact microsomes can be isolated first, then PEGylation performed and detected using Western blot with an antibody specific to the protein of interest. Here, we describe a method for PEGylating an ER membrane protein (squalene monooxygenase) tagged with a V5 epitope tag.

2 Materials

2.1 Microsomal Harvest

1. Dulbecco's phosphate-buffered saline (PBS): 137 mM NaCl, 2.7 mM KCl, 8.1 mM disodium hydrogen phosphate, 1.47 mM potassium dihydrogen phosphate.
2. Buffer A: 10 mM HEPES-KOH pH 7.4, 10 mM KCl, 1.5 mM $MgCl_2$, 5 mM Na EDTA, 5 mM Na EGTA, 250 mM sucrose.
3. Protease inhibitors (PI): cocktails are suitable and available from various suppliers.
4. Protein quantification assay, e.g., bicinchoninic acid (BCA) assay.

2.2 PEGylation

1. mPEG: MAL-dPEG®$_4$-(m-dPEG®$_{12}$)$_3$, available from Quanta Biodesign, prepared as a 200 mM stock in dimethylsulfoxide (DMSO) (*see* **Note 1**).
2. Triton X-100: 10% (v/v) solution diluted in deionized water.
3. Dithiothreitol (DTT): 1 M stock.
4. 5× Laemmli buffer: 10% (w/v) SDS, 0.2% bromophenol blue, 0.25 M Tris–HCl (pH 6.8), 25% (v/v) glycerol.

2.3 Western Blotting

1. 12% (w/v) polyacrylamide gels for SDS-polyacrylamide gel electrophoresis (PAGE).
2. Phosphate-buffered saline with Tween-20 (PBST): 1× PBS, 0.1% (v/v) Tween-20.
3. Blocking solution: 5% (w/v) skim milk in PBST.
4. Antibody diluting solution: 5% (w/v) skim milk in PBST.
5. Primary antibody: Mouse anti-V5 1:5000 (Thermo Fisher).
6. Secondary antibody: Anti-mouse conjugated to horseradish peroxidase (HRP).
7. Immobilon™ Western Chemiluminescent HRP Substrate detection system (ECL, Millipore) or equivalent reagent.
8. LAS 500 Western imaging system (GE Healthcare) or equivalent imaging equipment.

2.4 Densitometry and Data Interpretation

1. ImageJ software package (imagej.nih.gov/ij).

3 Methods

3.1 Create a Plasmid Library

1. Using a plasmid containing the protein of interest (*see* **Note 2**), clone out any native cysteine residues and generate a cysteine-free mutant (*see* **Note 3**).
2. Use this cysteine-free mutant as a backbone to introduce systematic single cysteine substitution mutations at desired positions along the protein (*see* **Note 4** and Fig. 2).

3.2 Cell Culture and Microsomal Harvest

1. Culture mammalian cells in a 14.5 cm dish (*see* **Note 5**).
2. After 24 h, transfect cells with plasmids encoding the single-cysteine-containing protein of interest.
3. After a further 24 h, remove media from cells and wash cells twice with cold PBS (*see* **Note 6**).
4. Harvest cells by scraping into 20 mL of cold PBS (*see* **Note 7**). Transfer to a 50 mL centrifuge tube (*see* Fig. 3 for steps 4–11).
5. Pellet cells by centrifugation at 1300 × *g* for 5 min.
6. Remove supernatant. Resuspend pellet in 750 μL of cold Buffer A supplemented with PI.
7. Vigorously pass the cell lysate through a blunt 18G needle 50 times using a 1 mL syringe (*see* **Note 8**).

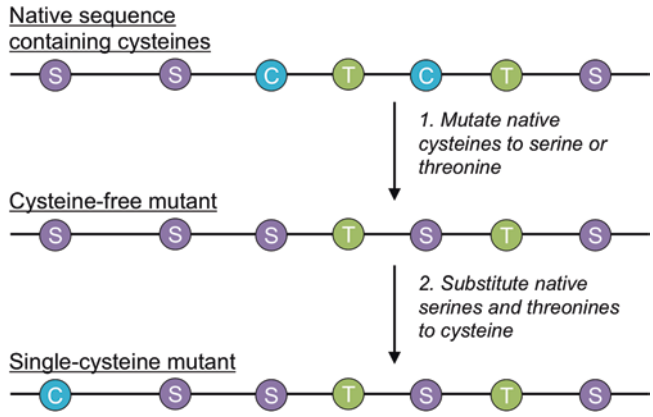

Fig. 2 Workflow of substituted cysteine mutagenesis. 1. Native cysteines (*blue*) are mutated to the chemically similar serine (*purple*), giving a cysteine-free mutant backbone. 2. This backbone is used to systematically mutate individual serines and threonines (*green*) to cysteine, producing a series of single cysteine mutants whose cytosolic accessibility can then be screened using PEGylation

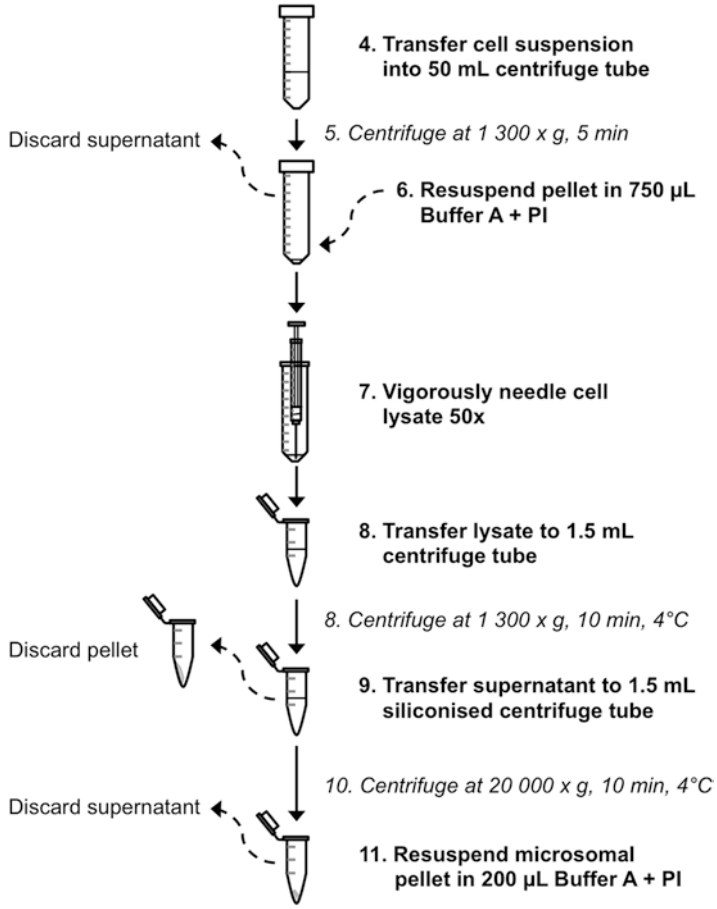

Fig. 3 Workflow for microsomal fractionation (Subheading 3.1, steps 4–10). Step numbers corresponding to Subheading 3.1 are indicated, with centrifugation steps indicated in italics

8. Transfer lysate to a 1.5 mL centrifuge tube. Centrifuge at 1300 × *g* for 10 min at 4 °C.
9. Transfer the resulting post-nuclear supernatant to a siliconized 1.5 mL centrifuge tube (*see* **Notes 9** and **10**).
10. Pellet microsomes by centrifugation at 20,000 × *g* for 30 min at 4 °C.
11. Remove all the supernatant and resuspend the microsomal pellet in 200 µL of Buffer A supplemented with PI using a siliconized tip (*see* **Note 11**).
12. Quantify protein using a protein quantification assay, e.g., bicinchoninic acid (BCA) assay (*see* **Note 12**).

3.3 PEGylation

1. In 1.5 mL centrifuge tubes, resuspend 40 µg of microsomal protein in a final volume of 54 µL of Buffer A (supplemented with PI) with or without 1% (v/v) Triton X-100 (5.4 µL of

10% v/v stock) detergent and with or without 5 mM mPEG (1.35 μL of 200 mM stock) (*see* **Notes 13** and **14**).

2. Mix by vortexing and spin tubes down.
3. Incubate for 30 min at the required temperature (*see* **Note 15**).
4. Quench the reaction with 10 mM DTT (*see* **Note 16**).
5. Vortex and spin tubes down.
6. Incubate for 10 min at room temperature.
7. Add 5× Laemmli buffer to a final concentration of 1× Laemmli buffer (*see* **Note 17**).

3.4 Western Blotting

1. Boil samples for 5 min at 95 °C before loading (*see* **Note 18**).
2. Load 30 μL of sample to 12% (w/v) polyacrylamide gels for SDS-PAGE (*see* **Note 19**).
3. Transfer proteins to a nitrocellulose membrane using a standard Western blotting transfer technique.
4. Block the membrane in blocking solution with gentle rocking for 1 h (*see* **Note 20**).
5. Incubate with the primary antibody (in our case, anti-V5) with gentle rocking for 1 h (*see* **Note 21**).
6. Wash three times for 10 min in PBST with rocking.
7. Incubate with the secondary antibody (anti-mouse) with gentle rocking for 1 h.
8. Wash three times for 10 min in PBST with rocking.
9. Visualize using ECL and LAS 500 imaging system (*see* **Note 22**). An example of the results from this method can be found in Fig. 4.

3.5 Densitometry and Data Interpretation

1. Quantify PEGylated bands using ImageJ, or any other suitable densitometric software.
2. In ImageJ, open the Western blot image file.
3. Convert the image to 8-bit by clicking on Image -> Type -> 8-bit.
4. Select Analyze -> Calibrate -> Uncalibrated OD.
5. Draw a rectangle around the PEGylated band to be analyzed, ensuring the same sized rectangle fits all bands while fitting as tightly as possible.
6. Use the same rectangle to take a blank measurement in a clean area of the blot above or below the PEGylated band to be measured.
7. Measure the PEGylated band.
8. Repeat for all remaining PEGylated bands, taking a blank measurement for each lane.

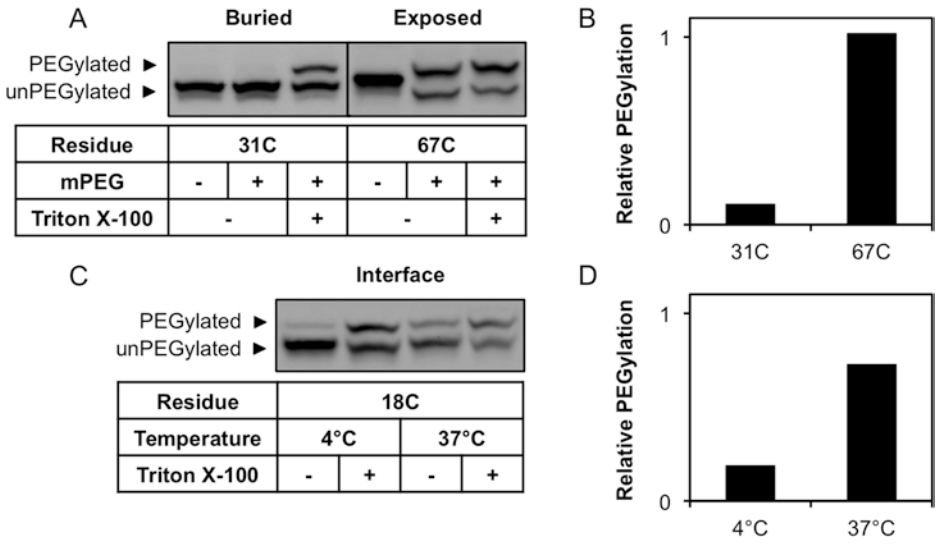

Fig. 4 Example Western blots and densitometry for a PEGylation assay using squalene monooxygenase. (**a**) Residues with no accessibility or complete accessibility to mPEG are easily identified, as is the case for residue 31C (buried) and 67C (cysosolically-exposed). (**b**) Densitometry of the PEGylated bands in (a). PEGylation is given relative to the Triton X-100 condition, which is set to 1. (**c**) Residues on a cytosol-membrane interface, such as 18C, are intermediately PEGylated relative to Triton X-100 and are differentially PEGylated at varying temperatures. (**d**) Densitometry of the PEGylated bands in (c). The extent of PEGylation is given relative to the Triton X-100 condition, which is set to 1

9. Subtract the blank measurement from all corresponding bands.
10. Normalize measurements to the detergent-treated condition for each mutant, which is set to 1.
11. Values approximately equal to 1 indicate that a residue is cytosolically-exposed. Values approaching zero indicate that a residue is membrane-buried or luminally-exposed. Intermediate values may indicate that a residue is on the cytosol-membrane interface (*see* Fig. 4).

4 Notes

1. mPEG should be prepared by dissolving in anhydrous solvent (we use dimethylsulfoxide, DMSO) and stored in single-use aliquots under an inert gas such as nitrogen or argon, as mPEG is reactive to water and sensitive to freeze-thaw cycles. Our 200 mM stock was prepared by dissolving 100 mg (density 1.02 g/mL, therefore 90.8 μL) in 121 μL anhydrous DMSO at 37 °C, vortexed periodically to dissolve, then frozen at −20 °C in 20 μL aliquots.
2. We used a pcDNA3.1-V5-His TOPO vector (Invitrogen) containing the first 100 amino acids of squalene monooxygenase fused to GFP [5].

3. We use site-directed mutagenesis to substitute native cysteine residues with the chemically similar serine residue. Any cloning method should work. We used a megaprimer method [6] with mutagenic forward primers and a generic reverse primer.
4. We used site-directed mutagenesis to systematically replace all serine and threonine residues with cysteine, due to their chemical similarity to cysteine, minimizing the likelihood of structural disruptions. We also substituted other amino acids for cysteines at strategic positions predicted to border membrane-spanning regions.
5. We use Chinese hamster ovary-7 (CHO-7) cells cultured in DF-12 medium supplemented with 5% (v/v) lipoprotein deficient serum.
6. If microsomes are to be treated with sterols, further pretreat cells with compactin (5 μM) and mevalonate (50 μM) overnight (~16 h) in media supplemented with lipoprotein deficient serum prior to harvest to lower their sterol status.
7. Keep cells and cell lysates on ice as much as possible to ensure microsomes remain intact.
8. Be as vigorous as possible without losing lysate through splashing. This is best achieved by pulling the plunger upward in a rapid motion and then pushing the plunger down gently. Vigorous needling is required to adequately break up cells to ensure a maximal microsomal yield.
9. A sticky, membranous film may be present on the top of the solution. Be sure not to take this with the supernatant as this fraction is insoluble and can interfere with protein quantification. The film can be pushed aside using a 1 mL pipette tip, then a clean tip can be used to remove the supernatant. If necessary, the 1300 × *g* centrifugation can be repeated to remove this fraction.
10. Siliconized tubes and tips should be used to obtain the microsomal fraction and resuspend the microsomal pellet as siliconized surfaces have lower affinity for the hydrophobic microsomes.
11. A larger volume may be required if the microsomal yield is high.
12. Keep microsomes on ice for immediate use or store at −20 °C for future use. It is not recommended that microsomes are stored for long periods of time (less than one month is best).
13. We found 5 mM to be an optimal concentration of mPEG; however, you may wish to test a range of concentrations as the amount of cysteines in a sample will depend on the quantity of total cysteine-containing proteins present.

14. mPEG should be added last and should be added to all tubes as quickly as possible. The reaction is both temperature- and time-dependent.
15. You may wish to pilot the experiment using a range of temperatures, such as 4 °C, room temperature and 37 °C. Residues bordering membrane/extramembrane interfaces or in dynamic regions of the protein may be differentially PEGylated at lower versus higher temperatures. Residues on this interface may be PEGylated at 37 °C but not at 4 °C due to lowered protein dynamics at 4 °C, indicating residues close to a sterically shielded interface. Important information may therefore be missed if PEGylation is only performed at higher temperatures.
16. DTT must be in excess of mPEG. If > 5 mM mPEG is used, a proportionally higher concentration of DTT will be required to quench the reaction.
17. Samples can be stored at −20 °C or used immediately for Western blotting.
18. Some proteins are prone to aggregation upon boiling. If your protein of interest is prone to such aggregation, heat samples at 37 °C for 30 min prior to loading to increase protein solubility, which makes it easier to load onto the gel and improves the band resolution.
19. 12% (w/v) SDS-PAGE gels should be run for sufficient time to separate the PEGylated and unPEGylated bands, noting that the band shift is only 2.3 kD. Our protein is 42 kD. Separation of the two bands required 12% polyacrylamide gels to be run in the separating gel for 1 h 45 min at 150 V. Running gels at a lower voltage, or at a lower temperature (e.g., in a 4 °C cold room) can aid in obtaining high-resolution gels. Excess detergent can also give poor-resolution gels. If this is a problem, consider loading less sample or diluting samples in Buffer A.
20. Blocking can be done overnight at 4 °C.
21. Weaker antibodies may require overnight incubations or higher concentrations of antibody.
22. Alternative imaging technologies can also be used, however if quantification is required then a digital imaging technique is preferred to using film exposure due to the greater sensitivity and linearity of response achieved through digital imaging. Film images should be scanned at 1200 dpi. Care should be taken to avoid over-exposure of the bands when quantification is required as over-exposed bands will give nonlinear results.

References

1. Guo Z-Y, Lin S, Heinen JA et al (2005) The active site His-460 of human acyl-coenzyme A:cholesterol acyltransferase 1 resides in a hitherto undisclosed transmembrane domain. J Biol Chem 280:37814–37826
2. Sun LP, Seemann J, Goldstein JL, Brown MS (2007) Sterol-regulated transport of SREBPs from endoplasmic reticulum to Golgi: Insig renders sorting signal in Scap inaccessible to COPII proteins. Proc Natl Acad Sci U S A 104:6519–6526
3. Howe V, Chua NK, Stevenson J, Brown AJ (2015) The regulatory domain of squalene monooxygenase contains a re-entrant loop and senses cholesterol via a conformational change. J Biol Chem
4. Anyatonwu G, Joseph SK (2009) Surface accessibility and conformational changes in the N-terminal domain of type I inositol trisphosphate receptors: studies using cysteine substitution mutagenesis. J Biol Chem 284:8093–8102
5. Gill S, Stevenson J, Kristiana I, Brown AJ (2011) Cholesterol-dependent degradation of squalene monooxygenase, a control point in cholesterol synthesis beyond HMG-CoA reductase. Cell Metab 13:260–273
6. Sanchis J, Fernández L, Carballeira JD et al (2008) Improved PCR method for the creation of saturation mutagenesis libraries in directed evolution: Application to difficult-to-amplify templates. Appl Microbiol Biotechnol 81:387–397

Chapter 16

Measuring Activity of Cholesterol Synthesis Enzymes Using Gas Chromatography/Mass Spectrometry

Anika V. Prabhu, Winnie Luu, and Andrew J. Brown

Abstract

The development of gas chromatography/mass spectrometry (GC/MS) technology has improved the ease and efficiency with which sterols in biological samples can be analyzed. Its advantages include that it needs only a small amount of sample, a short analysis time, and has enhanced specificity over traditional methods. Furthermore, a major benefit is its nonselective properties, which means that a complete scan of the sample will display the relative abundance of every sterol in the sample. This property has made it possible to define the abnormal, but distinctive, sterol profiles in a number of inborn errors of cholesterol synthesis. Here, we describe a semiquantitative method to determine relative activity of cholesterol synthesis enzymes. As an example, we measure the relative abundance of the substrate and product sterols of a cholesterol synthetic enzyme, 24-dehydrocholesterol reductase (DHCR24), which is defective in the hereditary developmental disease desmosterolosis.

Key words Lipids, Deuterated sterols, GC/MS, Enzyme activity

1 Introduction

Cholesterol synthesis is a complex and highly regulated process that involves more than 20 enzymatic steps in the mevalonate pathway. In addition to cholesterol synthesis, the pathway also produces vitamin D, isoprenoids, and ubiquinones. Changes in the activity of cholesterol synthesis enzymes can have significant consequences for levels of cholesterol, sterol intermediates, and products in the interacting pathways. Changes in the levels of these intermediates can affect cellular homeostasis, and thus their measurement can be crucial to studies exploring cholesterol and related pathways. Notably, a number of diseases causing human malformations have been identified as the result of inborn errors of cholesterol metabolism [1]. Specifically, mutations in many cholesterol synthetic enzymes are linked to fetal disorders, such as 7-dehydrocholesterol reductase (DHCR7) and 24-dehydrocholesterol reductase (DHCR24), causing Smith–Lemli–Opitz syndrome or desmosterolosis, respectively [2, 3].

Ingrid C. Gelissen and Andrew J. Brown (eds.), *Cholesterol Homeostasis: Methods and Protocols*, Methods in Molecular Biology, vol. 1583, DOI 10.1007/978-1-4939-6875-6_16,

As well as identifying such disease states, measurement of enzyme activity provides further insight into the biochemistry of cholesterol metabolism. We have recently uncovered novel aspects of the cholesterol synthetic pathway, and interacting pathways, by measuring the activity of the terminal enzymes DHCR7 and DHCR24 [4–6] via gas chromatography/mass spectrometry (GC/MS). This approach has superseded traditional biochemical methods such as radio-thin layer chromatography, which can often be limiting in its specificity and sensitivity, and requires the use of radioactive substrates. GC/MS offers a more precise and easily quantifiable methodology, where hazardous radioactive materials have been replaced with substrates specifically labeled with deuterium.

The general principles of GC/MS have been outlined previously [7]. Here, we describe our semiquantitative approach to specifically measure activity of cholesterol synthetic enzymes, using labeled sterol intermediates and measuring substrate conversion levels to determine relative enzymatic activity (*see* **Note 1**).

2 Materials

1. Deuterated sterol (e.g., [$^2H_6$]-desmosterol from Avanti Polar Lipids) complexed to cyclodextrin (*see* **Note 2**).
2. 0.1 M sodium hydroxide (NaOH). Add 0.2 g NaOH per 50 mL ultrapure water.
3. 1 mg/mL 5α-cholestane in chloroform (*see* **Note 3**).
4. Absolute ethanol.
5. 75% (w/v) potassium hydroxide (KOH). Add 37.5 g KOH per 50 mL ultrapure water.
6. 20 mM butylated hydroxytoluene (BHT). Make a 0.2 M stock (0.22 g BHT per 5 mL ultrapure water) and dilute to reach 20 mM.
7. 20 mM ethylenediaminetetraacetic acid (EDTA). Make a 0.2 M stock (0.58 g EDTA per 10 mL ultrapure water) and dilute to reach 20 mM.
8. 95% (or analytical grade) *n*-hexane.
9. *N*,*O*-bis(trimethylsilyl)trifluoroacetamide (BSTFA).
10. Nitrogen gas tank or vacuum centrifuge.
11. Heat block.
12. Pyrex glass tubes with polytetrafluoroethylene (PTFE)-lined caps (*see* **Note 4**).
13. Glass vials with fixed insert.
14. PTFE lids for glass vials.

15. Acetonitrile.
16. Protein assay that is compatible with cell lysates in NaOH, e.g., bicinchoninic acid (BCA) assay.
17. GC/MS equipment—the system at our institution includes the TRACE TR-50MS GC column (Thermo Fisher Scientific), which uses helium as a carrier gas and is 60 m × 0.25 mm with 0.25 μm film thickness. In addition, the TriPlus RSH™ Autosampler, Thermo Trace™ gas chromatograph and Thermo DSQ™ II mass spectrometer are used. Thermo Xcalibur software (version 2.2) is used for analysis of data. The conditions described in this method are optimized for this system.

3 Methods

3.1 Cell Culture

1. Seed cells in a 6-well plate at 60–80% confluence.
2. Label cells with 1 μg/mL deuterated sterol–cyclodextrin complex per mL of media (*see* **Note 2**), adding additional treatments to the media if needed.
3. Swirl the plate to mix and incubate at 37 °C for 4 h (*see* **Note 5**).

3.2 Harvest

1. Wash cells with PBS using 1 mL per well.
2. Add 500 μL of 0.1 M NaOH per well.
3. Rock plate for 5–10 min and tap plate to allow cell lysate to collect.
4. Add cell lysate solution to the Pyrex glass tubes.
5. Rinse well with 500 μL ultrapure water to collect remaining lysate, and add to the Pyrex glass tube. A final concentration of 0.05 M NaOH in the samples is obtained.
6. Vortex the tubes vigorously.
7. Store samples at −20 °C, or proceed with normalization.

3.3 Normalization

1. Measure the protein concentration using 20 μL of each sample, performed in duplicate (*see* **Note 6**).
2. Normalize samples to the least concentrated sample by using the equation below, where total volume refers to the 960 μL sample solution (*see* **Note 7**):

$$\text{Volume to Discard} = \text{Total Volume} - \left[\frac{\text{Total Volume} \times \text{Lowest Average Absorbance}}{\text{Average Absorbance of the Sample}}\right]$$

3. Adjust the volume of all samples (apart from the sample with the lowest protein concentration) with 0.05 M NaOH to a final volume of 960 μL.

4. Make a master mix of 40 μL 0.05 M NaOH and 0.2 μL 1 mg/mL 5α-cholestane (internal standard) for each sample and add 40.2 μL to each tube (*see* **Note 8**).
5. Store samples at −20 °C, or proceed with lipid extraction.

3.4 Lipid Extraction and Derivatization

1. Add 1 mL absolute ethanol (*see* **Note 9**), 500 μL 75% (w/v) KOH (for saponification), 1 μL 20 mM butylated hydroxytoluene (BHT), and 20 μL 20 mM EDTA to each sample (*see* **Note 10**).
2. Vortex well.
3. Saponify mixture by heating samples to 70 °C on a heat block for 1 h.
4. After cooling, add 1 mL absolute ethanol to each sample and vortex briefly.
5. Add 2.5 mL 95% *n*-hexane in a fume cupboard and vortex on high speed for 30 s (*see* **Notes 9** and **11**).
6. Centrifuge at high speed (4000 × *g*) for 5 min (*see* **Note 12**).
7. Transfer 2 mL of the *n*-hexane layer (top layer) into a new Pyrex glass tube (*see* **Note 13**).
8. Using nitrogen (or another inert) gas, or a vacuum centrifuge, to evaporate the hexane to dryness (*see* **Note 14**).
9. Store dried samples at −20 °C, or proceed to derivatization step.
10. Allow BSTFA derivatizing agent to reach room temperature, and add 50 μL BSFTA to each sample in fume cupboard (*see* **Note 15**).
11. Vortex samples and derivatize at 60 °C on a heat block for 1 h.
12. After cooling, transfer samples to glass vials with fixed insert and attach PTFE lids, for GC/MS analysis.

3.5 Sample Run and Data Analysis

1. Run two acetonitrile blanks prior to running samples to flush the column (*see* **Note 16** for suggestions of controls).
2. Run standards in scan (total ion chromatogram, TIC) mode using the Thermo Trace™ gas chromatograph coupled with the Thermo DSQ™ II mass spectrometer and Thermo TriPlus RSH™ Autosampler (*see* **Note 17**). To generate a standard, add ~0.1 μg of a known sterol of interest to a tube (in a small amount of ethanol for convenience). Dry sample, and derivatize as described in Step 11 (Subheading 3.4). An example chromatogram for a sterol standard (in this case, cholesterol) is provided in Fig. 1a, with the spectrum of the highest peak shown in Fig. 1b.
3. Identify retention times and ions (confirmation and molecular) to set up a single-ion monitoring (SIM) method (*see* **Note 18**). The ions selected align with the retention time of the chromatographic peak for the sterol of interest (Fig. 1c). As shown

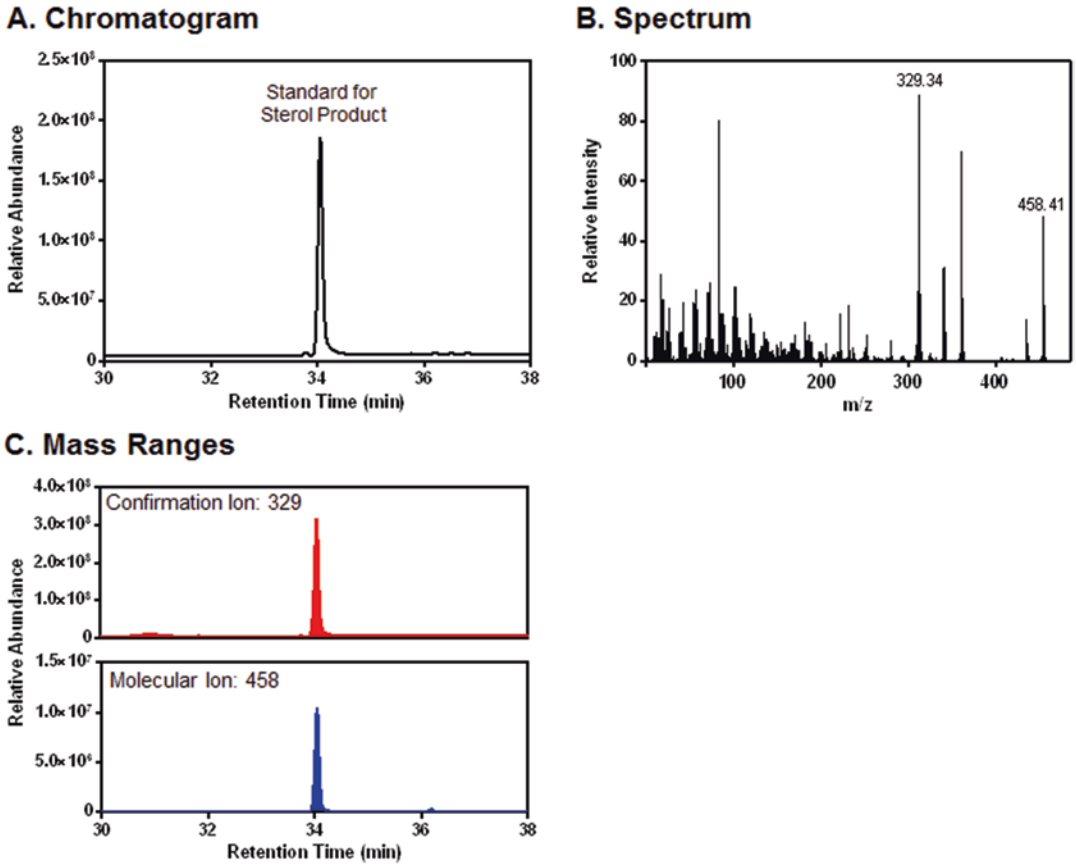

Fig. 1 Identifying confirmation and molecular ions in scan mode. A standard sample containing ~0.1 μg of the sterol of interest (in this case, cholesterol) was run in scan mode. (**a**) The total ion chromatogram (TIC) produced of the sample, with the highest peak corresponding to the sterol of interest, cholesterol. (**b**) The mass spectrum for the highest peak, with the confirmation ion (329.34) and molecular ion (458.41) marked. (**c**) Chromatograms monitoring only the confirmation or molecular ions, which appear at the correct retention time as cholesterol

in Fig. 2, the SIM method should monitor specific ions (*see* **Note 19**) over a specific time range when the sterol is known to be eluted.

4. Run samples in the newly established SIM mode. Example chromatograms of samples labeled with [$^2H_6$]-desmosterol and treated with and without a DHCR24 inhibitor are shown in Fig. 3. DHCR24 inhibition prevents the conversion of [$^2H_6$]-desmosterol to [$^2H_6$]-cholesterol.
5. Using Thermo Xcalibur software (version 2.2), identify the area under the curve for chromatographic peak of each sterol based on the confirmation ion (see Fig. 3a and b).
6. Calculate the product to substrate ratio to identify enzymatic activity relative to other samples. An example of the relative decrease in enzymatic activity with inhibition is provided in Fig. 3c.

A.

	Retention Time *(min)*	Time Range *(min)*	Ions *(m/z)*
Sterol Product	34.05	*to be excluded*	329, 458
Internal Standard	28.25	27.00 – 30.00	217, 372
[$^2H_6$]-Sterol Product	33.80	30.00 – 35.00	335, 464
[$^2H_6$]-Sterol Substrate	36.32	35.00 – 38.00	333, 462

B.

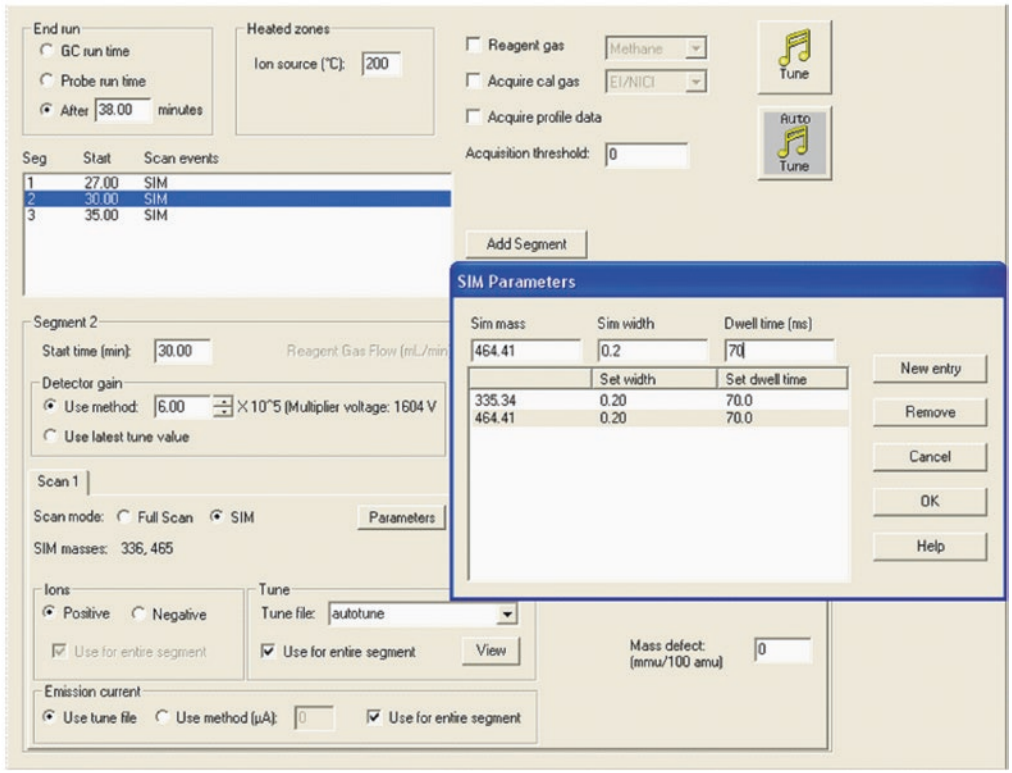

Fig. 2 Setting up a selected-ion monitoring (SIM) method for sterols of interest. (**a**) Retention times and ions for sterols of interest identified by running standards in scan mode. Note that certain information can be predicted for sterols that are not available (*see* **Note 19**). A specific range of retention times at which a particular sterol of interest appears is selected, and corresponding ions are measured during that time. Unlabeled, endogenous cholesterol is excluded from this SIM method. (**b**) Screenshot of the setup of SIM parameters, using Thermo Xcalibur software (version 2.2). Note the time ranges and corresponding ions that are inputted from (**a**)

4 Notes

1. The method presented here is semiquantitative, to allow comparison between samples and measure relative differences in the abundance of sterols. To achieve absolute quantification, standard curves for each sterol of interest must be created to measure exact amounts.

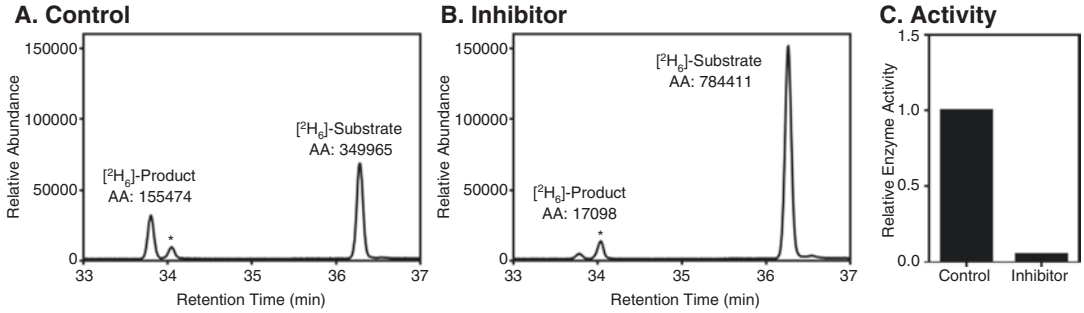

Fig. 3 Quantification of relative enzyme activity. (**a**, **b**) Cells were labeled with a deuterated substrate ([$^2H_6$]-desmosterol, in this case) for 4 h with or without an inhibitor of DHCR24, and lipids were extracted, derivatized, and subjected to GC/MS using the established selected-ion monitoring (SIM) method to monitor the confirmation and molecular ions of the deuterated substrate and product. (**c**) Relative enzymatic activity of (**a**, **b**) was calculated using the chromatographic peak analyte areas (AA) of the confirmation ion measured for [$^2H_6$]-product ([$^2H_6$]-cholesterol) and [$^2H_6$]-substrate ([$^2H_6$]-desmosterol), expressed as the ratio of product to substrate, and normalized to the control condition (set to 1). * indicates unlabeled, endogenous cholesterol which was not measured in this SIM method

2. The process of complexing sterols to cyclodextrin has been described previously [8]. Briefly, 15 mg/mL of the indicated sterol dissolved in 100% ethanol is added in five 10 μL aliquots to a stirring solution of 5% (w/v) methyl-β-cyclodextrin at 80 °C until a clear solution is achieved. The solution is lyophilized and the dried complex reconstituted in 375 μL ultrapure water to achieve a sterol–cyclodextrin complex at a concentration of 2 mg/mL.
3. 5α-cholestane can be used as an internal standard. As it is solubilized in chloroform, it is volatile and evaporation must be minimized to avoid dramatic changes in concentrations by using aliquots and sealing with parafilm during storage at −20 °C. Working concentrations of 5α-cholestane in heptane or ethanol can also be used.
4. Glass tubes are preferred for GC/MS as plastic can leach into samples and lipids can remain attached to the plastic. For this method, Pyrex glass tubes that can hold ~8 mL volume are used.
5. Concentration and time of labeling with deuterated sterol may require optimization. For instance, if enzymatic activity is very high, increasing the concentration or reducing labeling time can decrease substrate conversion, allowing differences in activity to be observed. When measuring the activity of a non-terminal enzyme, other sterol intermediates further downstream can also accumulate and may need to be measured. Efficient inhibition of enzymes downstream can be used to allow accumulation of the sterol product of the enzyme of interest.
6. A standard curve is not required for protein quantification since samples are being normalized relative to the sample with

the lowest concentration. However, inclusion of a standard curve can help during troubleshooting if a comparison of protein levels between experiments is needed.

7. As 40 μL was used for the protein assay, 960 μL of the sample remains. Discarding the sample and later replacing with 0.05 M NaOH minimizes sample loss and number of tubes required per experiment.
8. Make a master mix to avoid inaccuracy with addition of small volumes of volatile 5α-cholestane. Additionally, the amount of 5α-cholestane can be optimized, so that it remains the tallest peak in the trace for each sample.
9. To avoid evaporation of all volatile substances, such as ethanol-based solutions or *n*-hexane, minimize the opening of tubes, and improve accuracy of pipetting by pre-wetting the tip with the solution prior to dispensing.
10. The saponification step can be omitted in some circumstances by replacing the 75% (w/v) KOH with ultrapure water and skipping Step 3 (Subheading 3.4). Certain metabolites (such as vitamin D_3) may be negatively affected by saponification, which may warrant removal of this step. However, we have found that saponification has no effect on vitamin D_3 extraction.
11. 95% *n*-hexane is highly volatile and toxic, and hence it should always be used in a fume cupboard behind a shield.
12. Take precautions to ensure that if the glass tube breaks during centrifugation, hexane vapor will not be inhaled. Distinct layers should be visible, but avoid disrupting the interphase.
13. Although 2.5 mL hexane was added, remove a conservative 2 mL of hexane to avoid including contaminants from the interphase.
14. Specific vacuum centrifuges with solvent traps can also be used to safely dry down the hexane solution. Additionally, certain sterols such as 7-dehydrocholesterol are highly labile and readily oxidized to other products. A fast-drying method is preferable compared to drying by exposure to the air overnight or over several days.
15. After derivatization, any cloudiness or precipitate is indicative of contamination. Common causes include that the hexane or the glass tubes are not clean, or that the interphase was disrupted. Glass tubes and lids can be reused but need to be cleaned well with detergent and rinsed with acetone prior to reuse.
16. To test for any interference, run samples where the same harvest method is applied to an empty well (to account for any interference from the plastics used) and to unlabeled cells (to account for endogenous sterol levels).

17. Sample introduction involves a 1 μL injection via a splitless inlet heated to 290 °C into a Thermo Scientific™ TRACE TR-50MS GC column. Further details of GC/MS conditions have been outlined previously [4].
18. The confirmation ion typically appears with the highest relative intensity. The molecular ion corresponds to the molecular weight of the sterol of interest. Note that the addition of the BSTFA derivatizing agent forms trimethylsilyl (TMS) derivatives that give molecular ions that are 72 mass units above the molecular weight of the original compounds. Measuring the relative abundance of the confirmation and molecular ions only can help to determine whether they are appropriate ions to monitor.
19. Although not recommended, peak retention time or the mass to charge ratio (m/z) of the ions can be predicted, if the standard is not available. Moreover, deuterated versions of sterols typically have retention times very similar to the unlabeled counterparts, typically eluting marginally faster (e.g., the difference in retention time between cholesterol and [$^2H_6$]-cholesterol shown in Fig. 2a). Note that cells typically have high levels of endogenous cholesterol, which should be excluded from SIM methods to easily observe other sterols of interest. Furthermore, if the sterol of interest is labeled with six deuterium molecules [$^2H_6$], the mass units of the ions increase by six mass units (compare selected ions for Sterol Product and [$^2H_6$]-Sterol Product in Fig. 2a). In addition, molecular ions can be predicted based on the molecular weight (*see* **Note 18**).

References

1. Kelley RI, Herman GE (2001) Inborn errors of sterol biosynthesis. Annu Rev Genomics Hum Genet 2:299–341
2. Zerenturk EJ, Sharpe LJ, Ikonen E et al (2013) Desmosterol and DHCR24: unexpected new directions for a terminal step in cholesterol synthesis. Prog Lipid Res 52:666–680
3. Irons M, Roy Elias E, Salen G et al (1993) Defective cholesterol biosynthesis in Smith–Lemli–Opitz syndrome. Lancet 341:1414
4. Luu W, Zerenturk EJ, Kristiana I et al (2014) Signaling regulates activity of DHCR24, the final enzyme in cholesterol synthesis. J Lipid Res 55:410–420
5. Luu W, Hart-Smith G, Sharpe LJ et al (2015) The terminal enzymes of cholesterol synthesis, DHCR24 and DHCR7, interact physically and functionally. J Lipid Res 56 (4): 888–897
6. Prabhu AV, Luu W, Sharpe LJ et al (2016) Cholesterol-mediated degradation of 7-dehydrocholesterol reductase switches the balance from cholesterol to vitamin D synthesis. J Biol Chem 291:8363–8373
7. Honour JW (2006) Gas chromatography-mass spectrometry. Methods Mol Biol (Clifton, NJ) 324:53–74
8. Brown AJ, Sun L, Feramisco JD et al (2002) Cholesterol addition to ER membranes alters conformation of SCAP, the SREBP escort protein that regulates cholesterol metabolism. Mol Cell 10:237–245

Chapter 17

Sterol Analysis by Quantitative Mass Spectrometry

Andrew M. Jenner and Simon H.J. Brown

Abstract

Analysis of sterols by mass spectrometry is a fundamental technique allowing for both qualitative and quantitative characterization of sterol molecular lipid species. Lipids are isolated from matrix or matrices by homogenization and solvent extraction, and converted into species amenable for ionization either by derivatization or adduct formation. Chromatogaphy (either gas or liquid phase) can assist with the resolution of sterols. Tandem mass spectrometry allows the precise identification of sterol lipid species, while comparison to internal standards added during extraction enables accurate quantification.

Key words Sterol, GC-MS, LC-MS, Tandem mass-spectrometry, Electrospray

1 Introduction

Cholesterol synthesis and metabolism is significantly altered in several degenerative diseases including atherosclerosis, Alzheimer's, Huntington's, and Parkinson's disease and is believed to play an important role in development of pathophysiology [1–4]. Cholesterol is by far the most abundant sterol in animals (approximately 10^3 fold greater than other sterols). Plants generate phytosterols that are absorbed quite poorly by animals from their diet, but can be incorporated to a limited extent into tissues, together with other endogenous cholesterol synthetic intermediates and metabolites. Cholesterol also represents a major target for oxidative damage, and oxysterols generated by reactive oxygen species attack can be used as biomarkers of oxidative stress and lipid peroxidation [4].

In order to fully examine the importance of the multiple sterol mechanisms and pathways, there is an urgent need to develop efficient and reliable methods to measure sterols in different tissues by high-throughput lipidomic approaches. Sterols often share a very similar chemical structure and vary widely in tissue concentrations. Therefore, reliable measurement requires careful analytical method development and many methods have been established in different

Ingrid C. Gelissen and Andrew J. Brown (eds.), *Cholesterol Homeostasis: Methods and Protocols*, Methods in Molecular Biology, vol. 1583, DOI 10.1007/978-1-4939-6875-6_17,

laboratories, reviewed by [5]. Recent advances in mass spectrometry (MS) have greatly improved analytical throughput, while ever-improving sensitivity of instrumentation has rapidly increased the number of analytes routinely monitored. However, quantitative analysis of sterol molecular lipid species still presents unique challenges for analysis by MS, including relatively poor ionization and background cholesterol in great excess. In addition, oxysterols are thermally labile, poorly soluble in aqueous solvents and are weak chromophores.

Two approaches for quantitative characterization of sterols will be described here, a gas chromatography (GC) coupled to tandem mass spectrometry (GC-MS/MS) approach for sterols and oxysterols and direct-infusion (DI) tandem mass spectrometry (DI-MS/MS) technique for free cholesterol and cholesteryl esters.

Both approaches are based on identification of ionized lipids in the mass spectrometer by mass and collision-induced fragmentation, using a triple quadrupole instrument (Fig. 1). Lipid extraction is a crucial step in sterol analysis, and in both protocols described herein, the extractions have been optimized to balance efficiency and the purity of final extracts. In both cases internal

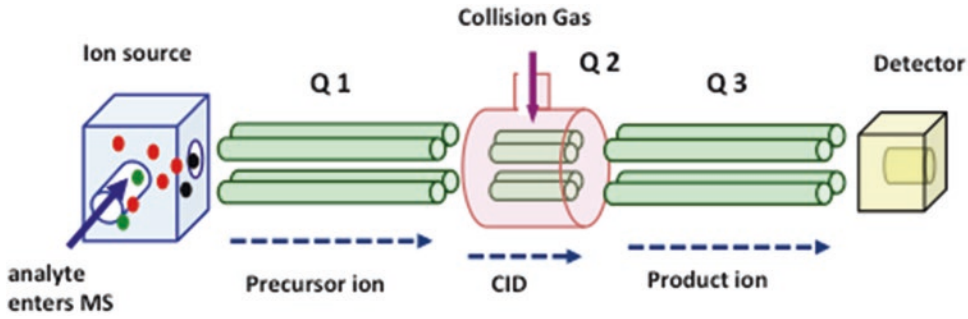

Fig. 1 Simple schematic of triple quadrupole analyte detection. Analytes entering the mass spectrometer are ionized in the ion source and then focused by a series of three quadrupoles before they reach the detector. During selective reaction monitoring (SRM), a precursor ion with an m/z specific to the analyte is initially selected by the first quadrupole, *Q1*. The ion then enters the collision cell *Q2*, where a product ion with a smaller m/z is produced after energetic impact with a collision gas molecule in a process of collision induced dissociation (CID). The final quadrupole *Q3* selects the product ion for detection. Therefore, only ions that have the selected precursor mass and fragment into the selected fragment mass reach the detector. In contrast, single quadrupole MS have only *Q1* and select the precursor ion for direct detection Selective reaction monitoring (SRM) has much higher discrimination against background signals and noise compared to SIM, which enhances analyte detection specificity and promotes sensitivity, provided that an abundant precursor ion and an efficient collision induced fragmentation can be determined.
In DI lipidomics, the tandem mass spectrometer is used to perform precursor-ion scans (PIS). In this mode, *Q1* operates in scan mode and is not selective. *Q3* acts as a filter to select a specific product ion produced after CID in *Q2* (in this case a dehydrated cholesterol ion) fragment. From the *Q1* full scan data, the *Q1* precursor molecular ion species that generated the *Q3* product ion is identified.
Quadrupole ion filtering can be controlled with very short time delays. Many SRM or PIS can be monitored with high frequency and sensitivity.

standards are added at the first step of the lipid extraction to normalize both the extraction steps and the MS analysis. Comparison of analyte peak areas to internal standard peak areas allows for accurate and reliable quantification.

GC fundamentally separates lipids by vapour pressure in a gas mobile phase over a liquid stationary phase prior to their ionization and characterization by MS. GC-MS in the electron ionization (EI) mode using a single quadrupole and selected ion monitoring (SIM) of a specific ion provides a robust and sensitive method for sterol analysis that was utilized early in sterol research. This technique still remains invaluable for sterol analysis today and has lead to the development of the GC-MS/MS (EI mode) protocol described in this chapter. The GC retention time, precursor ion mass and CID fragmentation allow for lipid identification. Through the use of single reaction monitoring (SRM), highly sensitive measurement of lipid molecular species is achieved (Fig. 1).

DI lipidomic approaches do not utilize a chromatographic step, and instead lipid extracts are directly infused into the MS. Lipids are ionized by electrospray ionization (ESI) and characterized by MS/MS. In this DI method, a MS/MS technique termed precursor-ion scanning is used to identify cholesterol-containing lipids (Fig. 1).

2 Materials

Use the highest quality solvents (LC-MS/MS grade when available), chemicals, and ultrapure water (prepared by purifying deionized water to attain a sensitivity of 18 MΩ cm at 25 °C). Prepare and store all reagents at room temperature (unless indicated otherwise). Carefully follow all health and safety and waste disposal regulations and procedures.

2.1 GC-MS/MS

2.1.1 Sterol Analytical Standards

1. Desmosterol-d_6, 14-demethyl-lanosterol-d_6, zymosterol-d_5, 14-demethyl-lanosterol (t-MAS or testis meiosis activating sterol), zymosterol, and lanosterol-d_6 (Avanti Polar Lipids).
2. Campesterol-d_3, 7α-hydroxycholesterol-d_7, 7β-hydroxycholesterol-d_7, β-sitosterol-d_7, lathosterol-d_4, 7-ketocholesterol-d_7, and 4-cholesten-3-one-d_5 (CDN Isotopes, Quebec, Canada).
3. 27-hydroxycholesterol-d_5, 24-hydroxycholesterol, and 24-hydroxycholesterol-d_7 (Medical Isotopes, Inc., Pelham, USA).
4. Squalene-d_6, 7-dehydrocholesterol-d_7, 4β-hydroxycholesterol-d_6, 25-hydroxycholesterol-d_6, and 24,25-dihydrolanosterol-d_6 (TRC, ON, Canada).
5. Cholesterol, α-cholestane, squalene, 7α-hydroxycholesterol, 7β-hydroxycholesterol, 7-dehydrocholesterol, 25-hydroxycholesterol, and 7-ketocholesterol (Sigma, St. Louis, USA).

6. Lathosterol, lanosterol, desmosterol, 27-hydroxycholesterol, 4β-hydroxycholesterol, coprostanol, epi-coprostanol, α-cholestanol, β-sitosterol, campesterol, stigmasterol, cycloartenol, fucostanol, 24,25-dihydrolanosterol, 4-cholesten-3-one, and β-sitostanol (Steraloids, Newport, USA).

2.1.2 Solid Phase Extraction (SPE) and Derivatization

1. Acetonitrile (100% anhydrous)
2. Toluene (100%)
3. n-hexane (99%)
4. Methanol (0.005% BHT): In a fume cupboard, add 15 mg of BHT (butylated hydroxytoluene) to a volume of 300 mL methanol and store at 4 °C.
5. Sodium hydroxide (10 M): In a fume cupboard, add 40 g of NaOH to 100 mL of water.
6. Sodium hydroxide (1 M): In a fume cupboard, slowly add water to 100 ml of 10 M NaOH to a final volume of 1000 mL.
7. Formic acid (1 M): In a fume cupboard, add 9.3 g of 99% formic acid (approximately 38.1 mL) to water to make a final volume of 200 mL.
8. Formic acid (0.13 M): Add water to 65 mL 1 M formic acid to make a final volume of 500 mL.
9. Formic acid (40 mM, pH 4.5): Add 2 mL formic acid (1 M) with water to make a final volume of 50 mL and adjust the pH with a few μL of NaOH (10 M).
10. Formic acid (40 mM, pH 4.5, 40% v/v methanol): Add 300 mL of 40 mM formic acid (pH 4.5) to 200 mL of methanol.
11. Hexane–MTBE (1:1 v/v): Add 250 mL of n-hexane to 250 mL MTBE (methyl *tert*-butyl ether, HPLC grade 99.9%).
12. Mixed mode SPE columns: C8/anion exchange quaternary amine, Clean-up 3 mL (UTC).
13. BSTFA (N,O-*bis*(trimethylsilyl)trifluoroacetamide) containing 1% (v/v) TMCS (trimethylchlorosilane).
14. 0.5 mL bead-beater homogenization tubes (tough-tubes).
15. 1.4 mm ceramic beads.
16. 5.0 mL screw top glass vials with PTFE/silicone lid inserts.
17. 2.0 mL glass auto sample vials auto sampler vials with PTFE/silicone lid inserts.
18. Narrow glass vial inserts.

2.2 DI-MS/MS

All standards obtained are of the highest purity (>95%).

2.2.1 Standards

1. Heavy isotope cholesterol (D_7) (Cambridge Isotope Laboratories,Tewksbury, USA).
2. Cholesteryl esters (Nu-Chek-Prep, Waterville, USA).

2.2.2 Extraction and Sample Preparation

1. MTBE (HPLC grade 99.9%).
2. Methanol (0.01% BHT): In a fume cupboard, add 30 mg of BHT to a volume of 300 mL methanol (LC-MS grade 99.9%).
3. 0.15 M ammonium acetate: Add 5.8 g ammonium acetate (LC-MS grade; 99.0%) to a volume of 500 mL ultrapure water in a glass bottle and dissolve. Store at 4 °C.
4. 1 M ammonium acetate: Add 7.7 g ammonium acetate (UHPLC-MS grade; 99.0%) to a volume of 100 mL ultrapure water in a glass bottle and dissolve. Store at 4 °C.
5. 2:1 (v/v) methanol–chloroform including 5 mM ammonium acetate: Add 200 mL methanol and 100 mL chloroform to a 500 mL glass bottle. Add 1.5 mL of 1 M ammonium acetate.
6. 2.0 mL bead-beater homogenization tubes (tough-tubes).
7. 1.4 mm ceramic beads.
8. 2.0 mL glass vials with PTFE/silicone lid inserts.
9. 2.0 mL centrifuge tubes.
10. 96-well plate (Eppendorf Twin-Tec).

3 Methods

3.1 GC-MS/MS

The GC-MS/MS method described in this paper (outline in Fig. 2) follows from GC methods developed in previous work that use GC-EI single quadrupole MS to analyze trimethysilyl (TMS) sterol derivatives. We have utilized faster, high-resolution GC capillary columns coupled with higher sensitivity triple quadrupole MS to improve routine, high-throughput sensitive measurement of sterols (listed in Table 1) that is often required for large lipidomic studies.

Carry out all procedures at room temperature unless otherwise specified. The GC-MS/MS instrument should be prepared so that it is in the EI mode ready for sterol analysis. The EI source should be installed and any GC or MS maintenance performed several days prior to sample analysis so that the instrument can be fully checked and validated with quality control samples.

3.1.1 Tissue Homogenization and Lipid Base Hydrolysis

1. Accurately and quickly weigh frozen tissue (5–20 mg depending on tissue) into a plastic homogenization tube containing 5 ceramic beads and add 150 µL methanol (0.005% BHT) (4 °C).

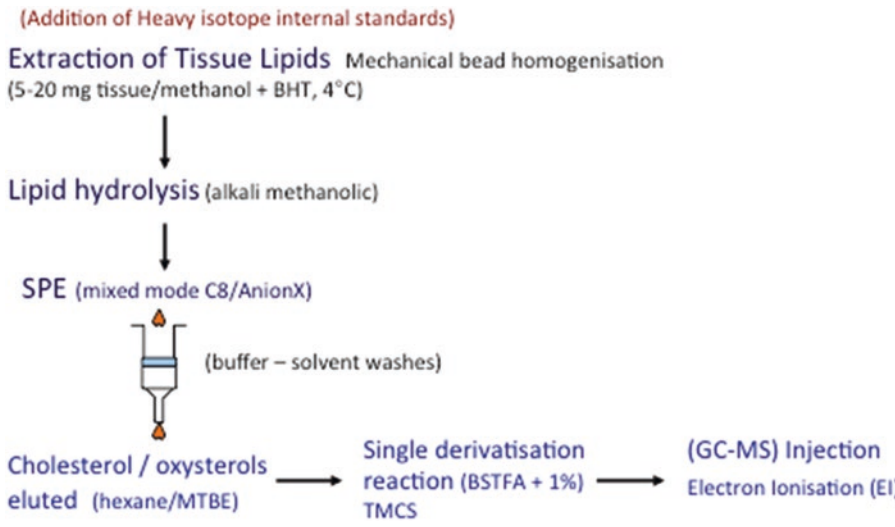

Fig. 2 Schematic overview of GC-MS sterol analysis in biological tissues

Table 1
Sterol analytes and their sources measured by GC-MS/MS

Cholesterol synthetic precursors	Cholesterol metabolites	Cholesterol oxidative damage biomarkers	Phytosterols (from diet)
lathosterol	24-hydroxycholesterol	7β-hydroxy cholesterol	campesterol
7-dehydrocholesterol	27-hydroxycholesterol	7-keto cholesterol	β-sitosterol
desmosterol	4-cholesten-3-one		stigmasterol
14-dimethyl-lanosterol (t-MAS)	25-hydroxycholesterol		brassicasterol
zymosterol	7α-hydroxycholesterol		cycloartenol
24,25 dihydrolanosterol	4β-hydroxycholesterol		β-sitostanol
lanosterol	coprostanol		fucosterol
squalene[a]	α-cholestanol		
	epicoprostanol		

[a]Squalene is not a sterol, but it is a major isoprenoid cholesterol precursor formed at the end of the mevalonate pathway

Add 20 μL of the internal standard mix, containing heavy isotopes (Table 2) in isopropanol (*see* **Note 1**). Cap the tube and homogenize for 2 × 20 seconds at 5000 rpm (4 °C) using a bead beater (*see* **Note 2**).

2. Transfer the homogenate to a clean 5 mL screw top glass vial and wash the tube with 100 μL methanol (0.005% BHT), then add the wash to the glass vial. Add 250 μL sodium hydroxide (1 M) to the homogenate and hydrolyze overnight for 16 h, rocking gently at room temperature in the absence of light

Table 2
Internal standards for GC-MS/MS analysis

Internal standard	Content per 5–12 mg brain sample (ng)	Individual stock concentration (mg/ml)	Volume of individual stock in final 4 ml mix (μl)
7α-hydroxycholesterol-d_7	10	0.1	20
7β-hydroxycholesterol-d_7	10	0.1	20
4β-hydroxycholesterol-d_6	10	0.1	20
27-hydroxycholesterol-d_5	10	0.1	20
7-ketocholesterol-d_7	20	0.1	40
7-dehydrocholesterol-d_6	40	0.1	40
lanosterol-d_6	10	0.1	20
24,25 dihydrolanosterold_6	10	0.1	20
squalene-d_6	40	0.1	80
25-hydroxycholesterol-d_6	10	0.1	20
24-hydroxycholesterol-d_7	200	1.0	40
desmosterol-d_6	100	1.0	20
lathosterol-d_4	100	1.0	20
zymosterol-d_5	10	0.1	20
4-cholesten-3-one-d_5	40	0.1	80
campesterol-d_3	100	1.0	20
β-sitosterol-d_7	100	1.0	20
14-demethyl-lanosterol-d_6	10	0.1	20
α-cholestane	200	1.0	40

Individual sterol stock solutions (0.1 or 1.0 mg/mL in isopropanol) were combined in relatively different volumes to achieve the desired amount in 20 μL internal standard mix

(*see* **Notes 3** and **4**). For plasma samples, 250 μL of methanol (0.005% BHT) and 25 μL 10 M sodium hydroxide is added to 225 μL plasma containing heavy (deuterated) internal standards before overnight hydrolysis.

3. The following morning, add 2.5 mL of 0.13 M formic acid to make a final volume of 3 mL (final pH 4.5, approx. 8% methanol) (*see* **Note 5**).

3.1.2 Solid Phase Extraction (SPE) of Sterols

1. Precondition the SPE column with 2 mL methanol followed by 2 mL 40 mM formic acid (pH 4.5). Load the sample and allow it to flow down the column under gravity (*see* **Note 6**).

2. Wash the column with 2 mL 40 mM formic acid (pH 4.5) containing 40% methanol. Preconditioning, loading, and washing eluates are discarded and the SPE column is then dried for 1–2 min by the flow of dry N_2 gas.
3. Elute the sterols into a clean glass tube with 2 mL hexane, followed by 2 mL hexane/MTBE 1:1 and dry this solvent fraction to approximately 1.5 mL using dry N_2 gas. Transfer the sterol solution to a 2 mL glass auto sample vial and dry using dry N_2 gas until all solvent has been removed (*see* **Note 7**).
4. In glass auto sample vials, pipette 5 or 6 different calibrations of sterols (triplicate) from a standard sterol mix in isopropanol (Table 3), using a range appropriate for the tissue samples. Also separately prepare cholesterol calibrations (triplicate) within the range 7.5–150 μg depending on the tissue to be analyzed. To all calibration samples, add 20 μL of the internal standard mix (Table 2) in isopropanol and dry using dry N_2 gas.

3.1.3 Sterol Derivatization

Once dry, 20 μL BSTFA + 1% (v/v) TMCS and 20 μL acetonitrile are added to the glass vial (samples and calibrations), capped and left to react for 1 h at 50 °C to generate trimethylsilyl ether derivatives (Fig. 3) (*see* **Notes 8** and **9**). The derivative mixture is dried briefly with dry N_2 gas and then reconstituted with 40 μL toluene and transferred into a narrow glass vial insert for GC-MS analysis.

3.1.4 GC-MS Quantitation of Oxysterols and Sterols

1. Derivatized samples are analyzed by an Agilent 7000B triple quadrupole mass selective detector interfaced with an Agilent 7890A GC system gas chromatograph, equipped with an automatic sampler and a computer workstation. The injection port and GC-MS interface are kept at 280 and 300 °C respectively. Separations are carried out on a fused silica capillary column (20 m × 0.18 mm i.d. × 0.18 μm film thickness; Rxi-5Sil MS Restek, Bellefonte, USA) (*see* **Note 10**). Helium is the carrier gas with a flow rate of 0.8 mL/min (average velocity = 59 cm/sec). Selected-reaction monitoring (SRM) is performed

Table 3
Concentration of different sterols (ng content) in calibration standards for brain samples

Calibration Level (ng)	L 1	L 2	L 3	L 4	L 5	L 6
"Low" abundance sterols	0.0375	0.15	0.6	2.25	7.5	22.5
"High" abundance sterols	0.375	1.5	6	22.5	75	225
Very high (24-hydroxycholesterol for brain samples)	1.5	6	24	90	300	900
Volume of final calibration std. mix to add (μl)	1	4	16	60	200	600

L1 to L6 are 6 levels of a calibration range. The two subjective categories "Lower" and "Higher" abundant sterols reflect the relatively different amounts of specific sterols in a variety of brain regions. "Higher" abundant sterols include squalene, 7-dehydrocholesterol, desmosterol, campesterol, β-sitosterol, lathosterol. 24-hydroxy cholesterol, a major brain cholesterol metabolite is at the highest calibration level

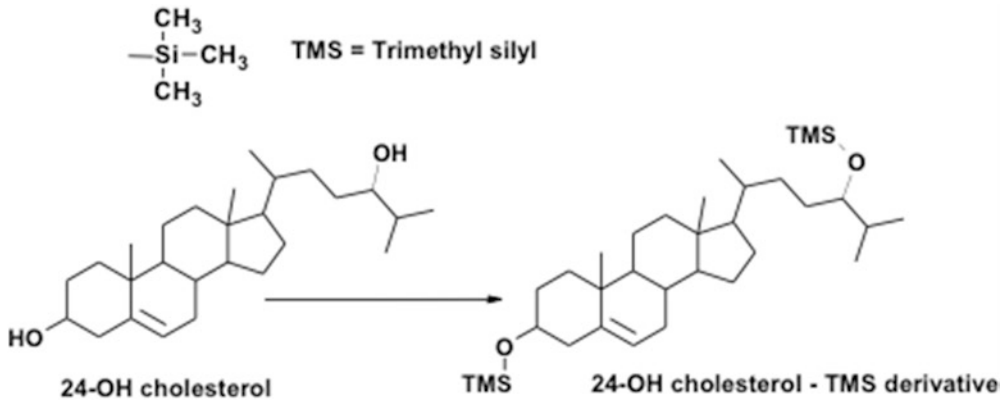

Fig. 3 Derivatization of 24-hydoxycholesterol forming a TMS ether. Trimethylsilylating reagents react with polar groups to form volatile, less polar derivatives suitable for GC

using the EI mode (60 eV) and nitrogen as the Q2 collision gas (1.5 mL/min) with 2.25 mL/min atomic He in the collision cell to reduce chemical noise from metastable He. The ion source is maintained at 280 °C and the quadrupoles at 150 °C. Target sterols, GC retention time and SRM transitions are listed in Table 4.

2. For sterol and oxysterol analysis, derivatized samples (1 μL) are injected split-less into the GC injection port. The column temperature is increased from 200 °C to 275 °C at 50 °C/min after 0.75 min at 200 °C, then temperature is raised to 300 °C at 2.5 °C/min with a final hold at 300 °C for 4 min. For cholesterol analysis, derivatized samples (0.4 μL) are injected with a 30:1 split into the GC injection port (270 °C). Column temperature is increased from 240 °C to 300 °C at 40 °C/min after 1 min at 240 °C, and then held at 300 °C for 7 min.
3. Quantification of oxysterols is calculated by comparison of specific SRM transitions with their heavy isotopes (Fig. 4). Where heavy isotopic standards are unavailable, analytes were compared to other heavy labeled standards. Cholesterol is quantified using α-cholestane. Relative molar response factors (RMRF) of all analytes are calculated from calibration curves constructed from different concentrations in triplicate that show good linearity ($r^2 > 0.99$) (*see* **Note 11**).

3.2 DI MS/MS for Cholesterol and Cholesteryl Esters

The DI-MS/MS extraction and MS analysis methods described herein was developed as part of a larger lipidomics platform. Cholesteryl ester (CE) MS approaches are based on published tandem MS methods [6], with optimized MS settings for instrumentation used in our group [7].

3.2.1 Lipid Extraction

1. Accurately and quickly weigh frozen tissue (between 5 and 50 mg) into plastic homogenizing tubes containing ceramic

Table 4
GC–MS triple quadrupole (MS/MS) analysis of squalene and sterols—analyte retention time, target and qualifier transitions

Name	Retention time (min)	Target SRM transition	Target collision energy	Qualifier SRM transition	Qualifier collision energy
squalene-d_6	5.00	416→ 373	5	416→ 401	8
squalene	5.06	410→ 367	5	410→ 395	8
5α-cholestane	5.53	217→ 121	4	217→ 135	4
coprostanol	6.93	370.→ 215.	8	370→ 355	8
α-cholestanol	7.04	355→ 186	12	460→ 355	12
epicoprostanol	7.07	370→ 215	8	257→ 175	8
7α-hydroxycholesterol-d_7	7.24	463→ 233	20	463→ 209	20
7α-hydroxycholesterol	7.31	456→ 233	20	456→ 209	20
cholesterol-d_7	7.82	463→ 449	8	463→ 373	8
cholesterol	7.90	458→ 443	8	458→ 368	8
7-dehydrocholesterol-d_7	8.05	463→ 211	20	463→ 448	10
desmosterol-d_6	8.09	447→ 357	2	447→ 315	2
7-dehydrocholesterol	8.10	456→ 209	20	456→ 441	10
desmosterol	8.15	441→ 351	2	441→ 309	2
brassicasterol	8.19	380→ 255	4	470→ 365	10
lathosterol-d_4	8.33	462→ 216	12	462→ 233	2
zymosterol-d_5	8.36	446→ 356	3	461→ 371	4
lathosterol	8.39	458→ 213	12	458→ 229	2
zymosterol	8.43	441→ 351	3	456→ 366	4
7β-hydroxycholesterol-d_7	8.58	463→ 233	20	463→73	40
7β-hydroxycholesterol	8.65	456→ 233	20	456→ 73	40
campesterol-d_3	8.76	385→ 255	2	475→ 385	2
campesterol	8.80	382→ 255	2	472→382	2
4-cholesten-3-one-d_5	8.84	345→ 232	7	345→ 260	7
4β-hydroxycholesterol-d_6	8.86	373→ 158	10	424→ 334	4
4-cholesten-3-one	8.89	342→ 229	7	342→ 257	7
4β-hydroxycholesterol	8.90	366→ 158	10	417→ 327	4
14-demethyl-lanosterol-d_6	9.06	385→ 181	8	400→ 247	12

(continued)

Table 4
(continued)

Name	Retention time (min)	Target SRM transition	Target collision energy	Qualifier SRM transition	Qualifier collision energy
stigmasterol	9.07	394→ 255	8	394→159	15
14-demethyllanosterol	9.13	379→ 175	8	394→ 241	12
24,25 dihydrolanosterol-d_6	9.26	492→ 402	4	402→ 187	15
24,25 dihydrolanosterol	9.30	485→ 395	4	395→ 187	15
β-sitosterol-d_7	9.71	403→ 255	2	493→ 403	2
lanosterol-d_6	9.73	489→ 399	4	504→ 399	10
fucosterol	9.75	386→ 281	15	386→ 296	5
lanosterol	9.80	483→ 393	4	498→ 393	10
β-sitosterol	9.81	396→ 255	2	486→ 396	2
sitostanol	9.92	473→ 383	2	488→ 215	10
24-hydroxycholesterol-d_7	10.37	334→ 95	25	448→ 75	30
24-hydroxycholesterol	10.46	327→ 95	25	441→ 75	30
cycloartenol	10.6	408→ 393	6	408→ 365	6
25-hydroxycholesterol-d_6	10.71	462→ 137	10	447→ 295	4
25-hydroxycholesterol	10.78	456→ 131	10	441→ 295	4
7-ketocholesterol-d_7	10.86	479→ 462	7	374→ 159	20
7-ketocholesterol	10.96	472→ 455	7	367→ 159	20
27-hydroxycholesterol-d_5	11.49	461→ 255	3	422→ 95	20
27-hydroxycholesterol	11.54	456→ 255	3	417→ 95	20

Note 1: Since collision cells between GC-MS/MS vendors are designed to different specification, optimal SRM and collision energies may vary between different manufacturers' instruments
Note 2: cholesterol SRM transitions are not measured during analysis of other sterols, but their details are included to illustrate cholesterols relative RT in this temperature program
Cholesterol is quantitated in the same sample, but using a different split injection and faster GC temperature gradient method (RT cholesterol = 4.10 min, 5α-cholestane = 3.21 min) as described in methods. GC-MS single quadrupole protocols may select different precursor ions to those described here for optimal sensitivity and specificity and these are reported in the scientific literature

beads. Add 300 μL methanol (0.01% BHT; 4 °C) and internal standards (*see* **Note 12**). Also include 3 extraction blanks with no tissue in homogenizing tubes. Cap the tubes and homogenize at 2 × 40 s at 6 m/s (*see* **Note 13**).

2. Transfer the homogenate to a clean 2 mL centrifuge tube and wash the homogenizing tube with 200 μL methanol (0.01% BHT) that is also added to the centrifuge tube (*see* **Note 14**).

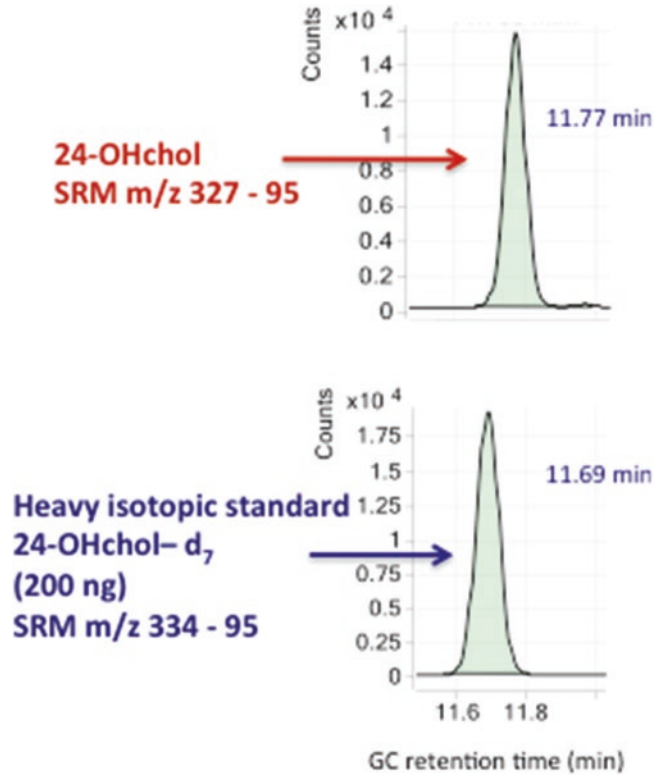

Fig. 4 Measurement of 24-hydroxycholesterol in mouse brain using GC-triple quadrupole (MS/MS) analysis and heavy isotope dilution. Quantification of sterols is calculated by comparison of specific SRM transitions with their corresponding heavy isotope internal standards

Add 1000 μL MTBE to the homogenate and vortex for 1 h at 4 °C (*see* **Note 15**). Add 300 μL 150 mM ammonium acetate and vortex for a further 15 min at 4 °C.

3. Transfer the tubes to a microcentrifuge and spin for 5 min at 20,000 × *g*. Remove the tubes and use a pipettor to remove the organic upper phase to a new glass vial without disturbing the aqueous phase (*see* **Note 16**). Cap the glass vials and store at −80 °C until MS analysis.

3.2.2 DI-MS/MS Analysis

1. Dilute extracts 200-fold into 2:1 methanol–chloroform including 5 mM ammonium acetate, for a total lipid content of approximately 10 μM (*see* **Note 17**).
2. Place a 96-well plate into a chiller block and rapidly load 40 μL of each sample into wells. Once samples and controls are loaded, seal the plate with heat-seal foil by heating for 2 s. Keep the 96-well plate in the chiller block until the plate returns to room temperature after sealing.
3. Bring the plate to the mass spectrometer and load into the appropriate location. Mass spectra are acquired using a chip

based nano-electrospray ionization source (TriVersa Nanomate®, Advion, Ithaca, USA) coupled to a hybrid linear ion trap-triple quadrupole mass spectrometer (QTRAP® 5500, Sciex, Foster City, USA). 10 μL of extract is aspirated from the sealed 96-well plate and delivered into the mass spectrometer via a nano-electrospray ionization (ESI) chip with an orifice diameter of 4.1 μm. The delivery gas is N_2 at a pressure of 0.4 psi and a spray voltage of 1.15 kV is used for positive ion acquisition.

A summary of MS settings is shown in Table 5. MS scan parameters and target lipids are shown in Tables 6 and 7, respectively. Mass spectra are averaged over 30–150 scans, dependent on the time available per sample and the abundance of cholesteryl

Table 5
DI-MS/MS general MS parameters

Setting	Value	Definition	Notes	Alternate names
Scan speed	200 m/z s^{-1}	Mass ramping speed of the spectrometer.	Trade-off between speed and sensitivity	May be defined as scan time
Curtain gas	20	Stream of inert gas that aids in solvent evaporation.	Aids to keep front end of instrument clean	Counter-current gas
De-clustering potential	100	Potential difference between the orifice and the skimmer in volts.	Prevents ions from clustering together.	n.a.
Entrance potential	10	Energy imparted on ion as they enter Q0	Instrument specific	n.a.
CAD pressure	med	Inert gas pressure in Q2	Some instruments have pressure setting	CID gas

Instrument parameter settings utilized for DI-MS/MS on a Sciex 5500 Qtrap instrument. A brief definition of each parameter and notes about the effects resulting from changes are supplied. These settings may have alternate names on different instruments and some alternates are noted

Table 6
DI-MS/MS tandem MS parameters

Lipid	Scan	Fragment mass (Q3)	Range	Collision energy
Cholesteryl ester	Precursor ion	369.3516	590–730	20
Free cholesterol	Precursor ion	369.3516	400–420	12
d_7 Free cholesterol	Precursor ion	376.3961	400–420	12

Parameters for three precursor-ion scans used for DI-MS/MS characterization of CE. Fragments masses are listed to high accuracy, although quadrupole instruments will not be capable of this high precision. The collision energy used in the Sciex 5500 Qtrap is listed; this will need to be optimized for other instruments

Table 7
Common cholesterol esters detected by DI-MS/MS

Cholesteryl ester	Mass (NH_4^+ adduct)	Isotope correction (of lipid)	Abundance (human plasma) nmol/mL [10]
14:0	614.5870	1.5928	80
14:1	612.5714	1.5925	30
15:0	628.6027	1.6108	30
15:1	626.5870	1.6105	30
16:0	642.6183	1.6291	190
16:1	640.6027	1.6287	111
16:2	638.5870	1.6284	31
17:0	656.6340	1.6475	32
17:1	654.6183	1.6472	31
18:0	670.6496	1.6662	59
18:1	668.6340	1.6658	533
18:2	666.6183	1.6655	1820
18:3	664.6027	1.6652	147
20:0	698.6809	1.7041	32
20:1	696.6653	1.7038	30
20:2	694.6496	1.7034	34
20:3	692.6340	1.7031	32
20:4	690.6183	1.7028	237
20:5	688.6027	1.7024	n.d.
22:0	726.7122	1.7429	23
22:1	724.6966	1.7426	10
22:2	722.6809	1.7422	10
22:3	720.6653	1.7419	n.d.
22:4	718.6496	1.7415	n.d.
22:5	716.6340	1.7412	n.d.
22:6	714.6183	1.7408	32

Common CE lipids that are detected in mammalian tissues. Isotope correction that is needed for accurate quantification is listed. The abundance in human plasma as determined by [10] is included

esters in the sample. Data are analyzed with LipidView® (Sciex) software, including smoothing, identification, removal of isotope contribution from lower mass species, and correction for isotope distribution. Ionized lipids detected with a signal-to-noise

ratio (s/n) over 10 are included in the analysis. Quantification was achieved in LipidView® software by comparison of the peak area of individual lipids to their internal standards after isotope correction (*see* **Notes 11** and **18**).

4 Notes

1. Internal standards are added at the very first extraction step. Whenever possible heavy labeled internal standards should be utilized to enable accurate quantitation using heavy isotope dilution. Table 2 illustrates the concentration of internal standards utilized for 5–12 mg brain tissue. To optimize analytical precision and accuracy, the level of internal standards should match as close as possible to the expected levels contained in the extracted tissue. Since different tissues contain relatively different proportions of sterols the amounts of internal standard added should be adjusted whenever possible for tissues with significantly dissimilar levels. This method also can be used to analyze plasma and serum (225 μL) as well as cultured cell pellets (containing $\approx 5 \times 10^5$ cells) with minor adjustments in internal deuterated standard concentrations and GC-MS injection conditions.
2. In our experience, multiple sample bead beaters offer great advantages of convenience, speed, efficiency, temperature control, and reliability of complete homogenization. They also improve sample handling and analytical reliability. Typically in our laboratory we extract batches of 20–40 samples at a time.
3. The majority of laboratories commonly measure total sample sterols (free sterols + esterified sterols) after lipid hydrolysis (saponification). The proportion of fatty acid esterified sterols varies widely between tissues. In non-hydrolyzed samples, GC-MS can detect fatty acid:sterol esters. However their larger molecular weight means higher, prolonged temperature gradients are necessary and longer columns that are resilient to higher temperatures are recommended. Longer columns and therefore more time is needed to resolve different steryl esters and EI mass spectra of steryl esters are typically predominated by the sterol ion so that sensitive identification of the fatty acid moiety is more challenging. For specific analysis of cholesterol esters, DI-MS/MS (described in this chapter) or LC-MS analysis using ESI is recommended. Alternatively, the sample can be split accurately into two parts with one hydrolyzed and one not and the proportion of steryl esterification estimated by the difference in sterol levels. In the latter method, specific identification of the fatty acid moiety in the sterol ester is not possible.
4. In the majority of lipid laboratories, hydrolysis is carried out at higher temperatures and shorter time periods, typically

50–70 °C for 30–60 min. Overnight processing allows tissue weighing and homogenization to be performed in the late afternoon of day 1 allowing the subsequent steps to proceed on day 2. This enables complete hydrolysis, while reducing degradation of certain sterols that are reported to be unstable at higher hydrolysis temperatures [8]. It also allows the GC-MS operator plenty of time to check that GC-MS sterol analysis is within analytical expectations and ready to immediately analyze samples on day 2.

5. Upon acidification, a cloudy mix may form with some tissues due to protein precipitation. Heavy precipitation can clog SPE frits and should be removed using either filtration or centrifugation. SPE equipment and buffers should be prepared as much as possible the day before.
6. Many laboratories extract sterols and oxysterols using simple liquid/liquid extraction by direct addition of organic solvents to the homogenate. SPE has the advantage of convenience, speed, extraction efficiency, and reduced use of organic solvents. It does require extra SPE columns and apparatus. SPE also allows us to fractionate more polar lipid classes from the same sample for separate targeted analysis [9].
7. Lipid classes of greater polarity (such as fatty acids and isoprostanes [9]) remain on the SPE column and can be eluted using increasing polarity solvent mixtures for extra analysis.
8. GC-MS requires a derivatization procedure in order to convert polar groups in the chemical structure of sterols and internal standards to volatile, thermally stable derivatives that possess characteristic mass spectra. Trimethylsilylation is the most widely used derivatization procedure for GC analysis, forming trimethylsilyl (TMS) derivatives (*see* Fig. 3). Different GC-MS laboratories have individually optimized TMS derivatization using a variety of trimethylsylating reagents and temperatures.
9. Tissue samples should be extracted, derivatized, and analyzed in a continuous process. If the GC-MS is unexpectedly not ready for sample analysis then sterol SPE extracts should not be derivatized, since sterol TMS derivatives will degrade over time, catalyzed by exposure to moisture and derivatized samples also slowly evaporate. If unavoidable then derivatized sample analytical viability can be prolonged by capping with new sealed septa and cooling in the absence of moisture. Sterol SPE eluted fractions can be dried in autosampler vials, capped and stored frozen for several weeks until derivatization and GC-MS analysis. They should be accompanied by appropriate calibrations.
10. In order to maintain high sensitivity, while increasing sample throughput we select shorter, narrower and thinner phase capillary column than the most common GC column used for

routine sterol quantitation (30 m × 0.25 mm × 0.25 μm). The smaller diameter and thinner stationary phase provide the equivalent number of chromatographic plates and resolving power of the 30 m column dimensions, with the advantage of shorter retention times. Optimization of the temperature gradient and GC-MS conditions provide similar high chromatographic resolution compared to previous analysis in our lab using 30 m columns. Sterols with close or overlapping peaks can be specifically measured by monitoring their unique SRMs. Longer columns exceeding 30 m can be utilized for improved sterol resolution, but suffer the disadvantage of extended run times. Since the 0.18 mm diameter column used has approximately 30% capacity of the common 0.25 mm column, sample overload was prevented by reducing the mass of tissue for lipid extraction and not exceeding the GC-MS injection volume. Good symmetrical peak shape and highly consistent retention times enabled easy and reliable integration of all sterols, except cholesterol, which exhibited large, skewed peak shape due to its high concentration. Consequently the MS ionization source and detector were routinely switched off during this chromatographic time period to safeguard MS long-term sensitivity. Accurate quantitation of cholesterol was performed using a separate shorter chromatographic run separate using a split injection.

11. It is outside the scope of this chapter to discuss all the analytical quality control protocols for collecting reliable sample data, since each analytical laboratory will have slightly different instruments, maintenance schedules, and quantitative strategies. It is the responsibility of each analyst to verify the performance of their MS and the reliability, reproducibility, and sensitivity of the sample analysis. The analyst should also become familiar with the integration parameters of the spectral and/or chromatographic peaks and MS signal data that confirm sterol peak authenticity and influence accuracy and precision. There are many available options for analysis of MS data, often supplied by the MS vendor. Our GC-MS/MS data is integrated using Agilent Masshunter to obtain sample sterol levels. DI-MS/MS data is processed using Lipidview to obtain cholesteryl ester and free cholesteryl levels (*see* **Note 18**). Data are then exported to Microsoft Excel for calculation of tissue contents and statistical analysis.

12. In our analytical protocol, internal standards are added at the very first extraction step to enable accurate quantification. Heavy isotope (D_7) cholesterol and non-endogenous (C13 and C22:1) cholesteryl esters are used here. However, if these esters are already present in samples, then other chain lengths will need to be selected for standards. Alternately deuterated

cholesteryl esters can be used for internal standards. The C13 ester is used to quantify short chain, saturated CE, while the C22:1 ester is used to quantify longer chain unsaturated CE. Internal standards are purchased individually from Nu Chek Prep (Waterville, MN) as pure solids and/or liquids. Each is dissolved individually into chloroform (including 0.01% BHT) at concentrations of approximately 1–10 mM to create bulk stocks and stored at −20 or −80 °C. For each set of samples, a mix of the appropriate internal standard is made at ~100 μmol concentration, and diluted into methanol before extraction. This dilution step is performed in bulk to improve accuracy of per sample addition.

13. As mentioned in **Note 2**, bead beaters offer many advantages for homogenization. The settings herein are described to process tissue (brain, liver muscle, heart) on an MPBio Fastprep homogenizer. We add approximately 20 beads to a 2 mL tough tube using a small scoop.
14. To rinse the homogenizing vials, briefly pulse on a vortex after adding the second aliquot of methanol. When removing liquid from the vials, the beads will retain some methanol. As internal standards have been added to the sample prior to this step, this retention does not affect quantification.
15. A 24-place vortex device in the cold room is used for this step. It is also possible to rotate the tubes gently overnight. MTBE is utilized in this step as it is less dense than the aqueous phase, and therefore the subsequent removal of the organic phase can be performed with less contamination [6].
16. As mentioned in **Note 15**, the MTBE organic phase is less dense and is therefore the upper phase, a benefit of the MTBE extraction. As internal standards have been added, the removal of the upper phase does not need to be complete, and often a few hundred microliters are left with the aqueous phase for speed and prevention of contamination.
17. Allow the extracts to come to room temperature before dilution, and vortex each vial to be sure the sample is dissolved and homogenized. Samples can also be diluted a few days prior and stored at −20 or −80 °C until MS analysis. The 200× dilution is based on 20 mg of liver tissue. Dependant on tissue quantity extracted and the relative sterol levels, it is helpful to test a few samples at different dilutions on the MS, and optimizing the dilution by optimal MS ion counts, before diluting a large batch for analysis. Additionally, it is very important to maintain total lipid content below 10 μM in the diluted samples for DI-MS/MS.
18. Lipidview is a commercial software that performs smoothing, identification, removal of isotope contribution from lower

mass species, and correction for isotope distribution. The second two steps are critical for accurate quantification. At the unit mass resolution of the mass spectrometers described here, for a lipid with Z double bonds, the (Z + 1) double bond variant of the same lipid will have an M + 2 isotope, which overlaps with the original lipid. The contribution of the M + 2 isotope must be calculated and subtracted (removal of isotope contribution from lower mass species). In addition, the total quantification of any given lipid must be the sum of all isotopes. This is calculated based on isotope abundance and peak areas adjusted (correction for isotope distribution). Isotope correction for common CE is shown in Table 7. As free cholesterol and D_7 have nearly identical isotope distributions, this step is not necessary.

References

1. Sharpe LJ, Burns V, Brown AJ (2014) A lipidomic perspective on intermediates in cholesterol synthesis as indicators of disease status. J Genet Genomics 41(5):275–282
2. Martín MG, Pfrieger F, Dotti CG (2014) Cholesterol in brain disease: sometimes determinant and frequently implicated. EMBO Rep 15(10):1036–1052
3. Poli G, Biasi F, Leonarduzzi G (2013) Oxysterols in the pathogenesis of major chronic diseases. Redox Biol 1(1):125–130
4. Iuliano L, Micheletta F, Natoli S, Ginanni Corradini S, Iappelli M, Elisei W et al (2003) Measurement of oxysterols and α-tocopherol in plasma and tissue samples as indices of oxidant stress status. Anal Biochem 312(2): 217–223
5. Griffiths WJ, Crick PJ, Wang Y (2013) Methods for oxysterol analysis: past, present and future. Biochem Pharmacol 86(1):3–14
6. Liebisch G, Binder M, Schifferer R, Langmann T, Schulz B, Schmitz G (2006) High throughput quantification of cholesterol and cholesteryl ester by electrospray ionization tandem mass spectrometry (ESI-MS/MS). BBA-Mol Cell Biol L 1761(1):121–128
7. Brown SH, Kunnen CM, Duchoslav E, Dolla NK, Kelso MJ, Papas EB et al (2013) A comparison of patient matched meibum and tear lipidomes. Invest Ophthalmol Vis Sci 54(12): 7417–7424
8. van de Bovenkamp P, Kosmeijer-Schuil TG, Katan MB (1988) Quantification of oxysterols in Dutch foods: egg products and mixed diets. Lipids 23(11):1079–1085
9. Lee CYJ, Huang SH, Jenner AM, Halliwell B (2008) Measurement of F2-isoprostanes, hydroxyeicosatetraenoic products, and oxysterols from a single plasma sample. Free Radic Biol Med 44(7):1314–1322
10. Quehenberger O, Armando AM, Brown AH, Milne SB, Myers DS, Merrill AH et al (2010) Lipidomics reveals a remarkable diversity of lipids in human plasma. J Lipid Res 51(11): 3299–3305

Chapter 18

Measurement of Rates of Cholesterol and Fatty Acid Synthesis In Vivo Using Tritiated Water

Adam M. Lopez, Jen-Chieh Chuang, and Stephen D. Turley

Abstract

Every organ in the body is capable of synthesizing cholesterol de novo but at rates that vary with a constellation of factors. A significant proportion of the hydrogen atoms present in cholesterol that is synthesized in the body are derived from water. Thus, although water ordinarily makes up the bulk of body mass, the acute enrichment of the body water pool with a sufficiently large amount of tritiated water over a short interval of time (usually 1 h) yields measurable rates of incorporation of the labeled water into newly generated cholesterol and also fatty acids. Such data can provide a quantitative measure of how specific genetic, dietary, and pharmacological manipulations impact not just the rate of cholesterol synthesis in particular organs but also rates of whole-body cholesterol production and turnover.

Key words Liver, Intestine, Brain, Extrahepatic, Digitonin-precipitable sterols, Lipogenesis

1 Introduction

In lean, healthy, young adult humans, the whole-body cholesterol content is about 140 g which equates to an average concentration throughout the body of ~2 mg /g wet weight of tissue [1]. Ultimately, this cholesterol, as is the case in the bodies of all mammals, derives from both endogenous (de novo synthesis within tissues), and exogenous (the diet) sources. In adult humans consuming a typical Western diet, the average amount of cholesterol ingested is ~5 mg/day/kg body weight [2], but on average only about half of this cholesterol is absorbed [3]. Hence, unless an individual hyper-absorbs cholesterol, the amount of exogenous cholesterol entering the body pool is generally less than the total quantity of cholesterol synthesized by the body each day. The latter figure, which in past years was arrived at using mainly the sterol balance technique, averages about 8–10 mg/day/kg body weight for adults, although this rate varies with a number of factors [4–6]. Methodology is now well established for measuring cholesterol synthesis rates in humans using deuterated water [7, 8].

Ingrid C. Gelissen and Andrew J. Brown (eds.), *Cholesterol Homeostasis: Methods and Protocols*, Methods in Molecular Biology, vol. 1583, DOI 10.1007/978-1-4939-6875-6_18,

There has long been an interest in determining what the principal sites of cholesterol synthesis in the body are, and also the association between cholesterol synthesis rates and the pathogenesis of various diseases. This question has been explored largely through the use of a range of animal models and a number of different techniques. Out of the multitude of publications on this topic has emerged a consensus that the rate of incorporation of tritiated water into cholesterol, in vivo, provides a reliable gauge for assessing the impact of specific dietary, pharmacological, and genetic manipulations on the rate of sterol synthesis in individual organs, and the body as a whole. This method has been used most extensively in mouse models whose cholesterol and/or fatty acid metabolism has been genetically altered. Thus, there are numerous examples in the literature of how application of the [^{3}H]-water technique in such models has greatly expanded our knowledge of the regulation of cholesterol metabolism in health and disease in multiple organ systems, especially the brain [9–12], small intestine [13–15], and liver [16–19].

Previous publications have discussed at length why the rates of cholesterol synthesis measured using [^{3}H]-water vs [^{14}C]-labeled substrates, either in vivo or in vitro, provide data that more closely reflect the true rate of synthesis in the intact animal [20–22]. Such in vivo data obtained using [^{3}H]-water can be converted into mg of sterol synthesized. This allows for the calculation of rates of whole-body cholesterol synthesis. These data are of particular value when the rates of cholesterol absorption, catabolism, and excretion are also measured in vivo in matching sets of animals because this gives an insight into how perturbations in any of these major pathways impacts whole-body sterol turnover [23, 24].

The major impediment to using the [^{3}H]-water method lies in the prohibitively high doses of radioactivity required. In adult mice with a normal body composition, water represents almost 60% of the body mass [25]. Thus, to achieve detectable incorporation rates into newly generated cholesterol, milliCurie amounts of [^{3}H]-water must be delivered into, and quickly equilibrated with, the body's pool of water. Another limitation of the method is that there is rapid transport of some newly generated [^{3}H]-cholesterol from the liver into the circulation, and therefore into the peripheral organs. There is also some movement of newly synthesized cholesterol from the liver through the bile into the lumen of the small intestine. While the amount of [^{3}H]-sterol leaving the liver through these routes is small compared to the rate at which it is being generated in the liver as a whole, this process nevertheless has to be taken into account when interpreting small differences between treatment groups in the rate of cholesterol synthesis determined for various extrahepatic organs. This subject has been dealt with in detailed studies in rats [21, 22, 26]. Clearly, the magnitude to which rates of cholesterol synthesis in specific

extrahepatic organs is impacted by "contamination" with liver-derived cholesterol will vary with factors such as the vasculature of each organ, but most of all by the rate of synthesis in the liver of each type of model (*see* **Note 1**).

2 Materials

2.1 Animal Labeling

1. Tritiated water (*see* **Note 2**): Stock [^{3}H]-water should be stored at about 4 °C, not frozen. After dilution in a graduated sterile polyallomer tube using sterile normal saline (sodium chloride 0.9% w/v), store the [^{3}H]-water at about 4 °C and bring slowly to room temperature before loading syringes for injection into the animal. Every effort should be made to keep the solution sterile.

2.2 Tissue Digestion and Saponification

1. Ethanolic KOH: Prepare aqueous KOH at ~9 N. Mix this solution with ethanol in the ratio of 3:47. Prepare fresh for each experiment and pipette 5 mL into tubes, noted below.
2. Glassware: 50 mL Kimax glass culture tubes (25 × 150 mm). These are supplied with black caps made of a phenolic resin, which should be replaced with polypropylene caps fitted with a polyvinyl liner (e.g., Wheaton Cat No 239201 or equivalent).
3. An electronic balance with tissue weight recording capability that measures to the third decimal place and is covered by a plexiglass shield to counter the effects of air flow under the fume hood.
4. Water bath.

2.3 Extraction of [^{3}H]-Sterols or/and [^{3}H]-Fatty Acids

1. Glass distilled water
2. Petroleum ether (ACS grade; boiling point range: 35–60 °C)
3. Hexane (hexanes; ACS grade)
4. HCl 37% (ACS grade)

2.4 Preparation, Washing, and Splitting of Sterol–Digitonin Precipitates (Digitonides)

1. Acetone–ethanol (1:1 v/v). Prepare using ACS grades of both solvents.
2. Digitonin (*see* **Note 3**): Dissolve 5 g of digitonin in 1000 mL of ethanol–water (1:1) with vigorous mixing and warming at ~45 °C if necessary to achieve solubilization. If pure digitonin is used, heating should not be required and the solution will remain clear for many weeks at room temperature. At a concentration of 0.5% w/v, 3 mL of the digitonin solution (the amount used per sample) contains 15 mg (12.2 μmol) of digitonin.
3. Carrier cholesterol (*see* **Note 4**): Prepare a solution of highly pure cholesterol in ethanol (~10 mg/mL) and store at ~4 °C.

4. Aluminum chloride (hexahydrate) (10% w/v): Dissolve 100 g in a final volume of 1000 mL water.
5. 1 N hydrochloric acid.
6. Acetone (ACS grade).
7. Diethyl ether (anhydrous, ACS grade).
8. Pyridine (ACS grade).
9. Glassware: 12 mL thick wall glass centrifuge tubes (Pyrex or equivalent).
10. Glass stirring rods that are ~200 mm length × 3.2 mm thick (these can be prepared from longer lengths of commercially available product).
11. Centrifuge (floor model with swinging bucket rotor), e.g., a Damon IEC model CRU-5000 centrifuge fitted with an IEC model 253 swinging bucket rotor (12 place) at 2000 rpm, which equates to 800 × *g*.
12. Vacuum oven.

2.5 Drying and Counting of [^{3}H]-Sterols or/and [^{3}H]-Fatty Acids

1. Methanol (ACS grade).
2. Scintillation cocktail suitable for efficient detection of ^{3}H.
3. Liquid scintillation counter.

3 Methods

Carry out all procedures under well-ventilated fume hoods.

3.1 Administration of Tritiated Water

Depending largely on the species and body mass of the animal, the [^{3}H]-water is administered either intravenously (iv) or intraperitoneally (ip). For iv delivery, this is best done through an indwelling catheter, but in species like the Golden Syrian hamster, direct injection into an exposed femoral vein (using a 30 G, 0.5 in. needle) is an alternative. This requires anesthesia followed by analgesics. In the case of adult rats, iv administration can be facilitated via a catheter in a tail vein, or by direct injection into a tail-vein or through an exposed femoral vein. Intraperitoneal injection works well for rats, especially at young ages when administration via a tail vein is more challenging. Certainly, in the case of virtually every mouse model, ip delivery is the most widely used route. As noted elsewhere, the formula for calculating the plasma water specific activity (a critically important term in the equation used to determine the rate of sterol or fatty acid synthesis) differs depending on how the [^{3}H]-water was administered. Irrespective of the route of delivery, the exact amount of [^{3}H]-water given to the animal is not needed except for record keeping on the total amount used in any

experiment. All procedures, including injection of the [^{3}H]-water into the animals and subsequent exsanguination and organ resection and processing must be carried out under well-ventilated hoods. After injection, the animals should be placed in a comfortable, secure holding cage, covered by a thick fabric to reduce the effects of the hood air flow on body temperature. During the 1 h period between injection and exsanguination, no food or drinking water are provided.

3.2 Exsanguination, Organ Resection, and Handling of Tissues

The procedures followed here will again vary with the study objectives, animal model and organs of interest but nevertheless are broadly oriented towards experiments involving adult mice. Irrespective of the model used, successful exsanguination of the animal is of key importance, not only for ensuring there is sufficient plasma for measurement of its water specific activity, but also to reduce the amount of residual blood in extrahepatic organs that contains [^{3}H]-cholesterol generated in and exported from the liver. In animal models where a dramatic increase in hepatic sterol synthesis is anticipated, the [^{3}H]-sterol content of the whole blood should be determined for potential use in assessing the extent to which the [^{3}H]-sterol content in some extrahepatic organs may significantly reflect the presence of labeled sterol of hepatic origin. This is done by taking an aliquot of whole blood (usually 0.1 mL) before centrifugation to obtain plasma for the water specific activity measurement. This aliquot of blood is treated in the same way as small organs and pieces of liver for digestion, extraction and sterol isolation.

1. Collect the target organs and rinse thoroughly in normal saline followed by blotting on filter paper.
2. Add small organs, with a total weight of less than 350 mg, after being weighed, (or plasma samples) directly to tubes containing 5 mL of ethanolic KOH solution.
3. Weigh larger organs such as the liver, and after weighing, cut into smaller sections on filter paper. An aliquot of combined sections weighing up to 350 mg should be treated as above.
4. If the rate of sterol synthesis is needed only for the liver and a few small extrahepatic organs, then the remaining animal carcass can be discarded (*see* **Note 5**). Should cholesterol synthesis rates in one or more regions of the gastrointestinal tract be needed, then remove the entire organ and rinse out the luminal contents of the stomach, small intestine and large intestine, blot gently on filter paper and record weight. Except for the small intestine, which typically weighs about 1 g or more in an adult mouse, the other regions of the gastrointestinal tract (stomach, cecum, colon) can each be added to 5 mL of ethanolic KOH. The entire small intestine should, after weighing,

be added to ~25 mL of ethanolic KOH in a sturdy 100 mL glass beaker, which is then firmly sealed with aluminum foil.

5. In those studies requiring measurement of whole-animal cholesterol synthesis, place the residual carcass, after weighing, on about 10 g of KOH crystals in the bottom of a sturdy 200 mL glass beaker followed by the addition of ~180 mL ethanol. Cover firmly with aluminum foil.
6. Keep those tissue aliquots contained in 5 mL alcoholic KOH in a water bath at about 70 °C with intermittent vigorous mixing until complete digestion is achieved. Depending on the tissue type and mass, the digestion step can take up to ~3 h.
7. Small intestine and carcass samples are best left for several days at room temperature before being placed on a steam bath or warming plate to achieve complete digestion. When that has occurred, the tissue extracts should be filtered through several layers of gauze cloth with rinsing into a volumetric flask (50 mL for the small intestine, 100 mL for the carcass).

3.3 Measurement of Plasma Water Specific Activity

1. Add 100 μL of plasma (or smaller known volume if necessary) in a 100 mL volumetric flask containing water and bring volume to 100 mL. Invert flask at least 30 times.
2. Pipette exactly 1.0 mL of this solution into another volumetric flask containing 99 mL of methanol and invert 30 times.
3. Pipette duplicate 1.0 mL aliquots of the methanolic solution into counting vials and quickly add 15 mL of a liquid scintillation cocktail suitable for ^{3}H detection. Mix well and count.
4. The plasma water specific activity is then calculated using the following equation (*see* **Note 6**):

$$\frac{\left(cpm\ {}^{3}\mathrm{H}\ /\ ml\ \text{plasma}\right)(0.87)}{\left(\text{nmol water}\ /\ ml\ \text{water}\right)\left(0.92\ ml\ \text{water}\ /\ ml\ \text{plasma}\right)}$$

3.4 Preparation and Processing of Sterol–Digitonin Precipitates

For the particular organs that labeled sterol isolation will be performed on, review published data for the species your project is using to estimate the likely amount of cholesterol mass present in the tube or flask containing the digested tissue. This is essential for determining what proportion of the petroleum ether extract is appropriate for preparing a workable sterol–digitonin precipitate, and whether or not the addition of some carrier cholesterol is necessary to achieve this objective.

1. In the majority of cases involving mouse organs, or portions thereof, the digested tissue is contained in 5 mL of ethanolic KOH in a 50 mL glass Kimax culture tube. For the whole small intestine or residual carcass, duplicate 5 mL aliquots are taken. Add add 5 mL of glass distilled water to all tubes, vortex

for 10 s, then add exactly 15 mL of petroleum ether. Cap tubes tightly and manually shake vigorously for at least 1 min. Let tubes stand for at least 15 min until a clear separation of the organic and aqueous phases is evident.

2. In the next step, portions of the organic phase are pipetted directly into 12 mL thick-walled glass centrifuge tubes. In the case of very small organs like adrenal glands or spleen, or in bulkier tissues that have an inherently low cholesterol content (such as skeletal muscle), a single aliquot of 10/15 mL of the organic phase should be taken. In most cases like this, additional carrier cholesterol will need to be added directly to this 10 mL of extract to ensure there is enough cholesterol to facilitate the development of a workable sterol–digitonin precipitate (see earlier text for carrier cholesterol). When it is determined there is likely to be <0.5 mg of tissue derived cholesterol in 10/15 mL of organic phase, add ~1 mg of carrier cholesterol (10 mg/mL in ethanol as described earlier). For other tissues like the adult brain, or liver from cholesterol-fed animals, duplicate or triplicate aliquots of the organic phase (i.e., 3/15 or 4/15 mL) can be taken for the digitonide formation step because of their comparatively high inherent cholesterol content. Ideally, the total amount of cholesterol in the centrifuge tube should be in the range of 1.0–1.5 mg (2.6–3.6 μmol). Amounts above 2 mg will result in copious digitonides that are slower to carry through the post-precipitation steps.
3. Dry aliquots of organic extracts under a gentle stream of air in a water bath at 38–40 °C. Then add 6 mL of acetone–ethanol (1:1 v/v) and place in a water bath at 45–50 °C for 5 min.
4. Add one drop of HCl (1 N) and mix tube contents briefly with a glass stirring rod. Then add 2 mL of $AlCl_3$ and 3 mL of digitonin to each tube (*see* **Note 7**). Mix with stirring rods.
5. Place tubes in water bath at 45–50 °C for 30 min (or 40 min if a large digitonin precipitate is likely to form as is usually the case in adult brain extracts). Leave the rods in tubes during incubation so tube contents can be stirred intermittently.
6. Set labeled stirring rods upright in a suitable holder and transfer tubes into a swinging bucket rotor that fits a refrigerated floor-model centrifuge. Ideally, this should be positioned immediately adjacent to a well-ventilated fume hood. Centrifuge the tubes at 800 × *g* for 30 min.
7. Draw off the clear phase down to ~0.5 cm above the surface of the digitonide and discard.
8. Wash the precipitates with 5 mL acetone. After adding the acetone, mix the precipitate with the stirring rod so that it breaks up into a powder.

9. Centrifuge tubes at 800 × *g* for 10 min, followed by aspiration and disposal of the acetone wash. Then repeat this wash step once.
10. After removal of the second acetone wash, add 5 mL of diethyl ether to the digitonide pellet and mix with stirring rod to yield an even suspension.
11. Centrifuge at 800 × *g* for 5 min, aspirate and discard most of the diethyl ether wash. Leave at least 0.5 cm of the diethyl ether on top of the pellet. Vortex so as to create a slurry and then roll the tube on a towel so as to spread the digitonide around the wall of the lower half of the tube.
12. Allow tubes to dry under hood for at least 20 min until no trace of ether is detectable.
13. The next step is to split the digitonides using pyridine. Place tubes in a metal rack in a vacuum oven at ~80 °C and under a vacuum of 15 mmHg for ~20 min.
14. Remove and quickly add ~1.0 mL of pyridine while the tubes are still warm.
15. Vortex vigorously until the digitonides have completely dissolved. Allow the tubes to stand ~20 min to ensure that splitting of the digitonide is complete (pyridine will be clear).
16. Add 5 mL diethyl ether, mix thoroughly with stirring rod and centrifuge at 800 × *g* for 10 min.
17. Carefully pour over supernatant into glass counting vial, gently turning the lip of the tube on that of the vial during the transfer.
18. Repeat extraction step with another 5 mL of diethyl ether and combine this extract with the first one.
19. Place vials in rack under hood with sash in a low position to strengthen air flow over the vial contents. Complete drying of the vial contents will take 6–18 h depending partly on the strength of the air flow.
20. When vials contain only crystals with no residual pyridine odor, place them in a metal tray inside a vacuum oven at ~80 °C at 15 mmHg pressure for 45 min. This step is critical as it eliminates any unreacted [^{3}H]-water adherent to the sterol crystals.
21. Remove vials from oven, allow to cool, then add 1.0 mL methanol followed immediately by 15 mL of the same counting cocktail used for the plasma water specific activity measurement. Mix well.
22. Add two vials with only methanol and scintillant cocktail to serve as blanks.

3.5 Calculation of Sterol Synthesis Rates

1. Calculate the "rate" of sterol synthesis using the following equation, with the units of nmol of water incorporated into sterol per hour per gram wet weight of tissue (nmol/h per gram).

$$\frac{\left(cpm\left[{}^{3}\mathrm{H}\right]\text{sterol} / 15ml \text{ of extract}\right)}{\left(\text{weight of organ or tissue aliquot}\,(\mathrm{g}) \times \text{plasma water specific activity}\,(cpm / \text{nmol})\right)}.$$

Note that for the small intestine, a further multiplication by 10 is needed to account for the use of only 5/50 mL of the digested organ for the sterol–digitonin precipitate preparation. Likewise, for the carcass, where 5/100 mL was taken for assay, use a multiplication factor of 20. In most cases, investigators require just the rate per gram of tissue for the liver and a few extrahepatic organs.

2. Other calculations that can be done, depending on the study objectives, include whole-organ and whole-body rates of synthesis. A focus on "whole-organ" rates becomes more important for animal models with various types of organomegaly [17, 19]. These various types of data are illustrated for a mouse model (Cyp27A1 knockout) in Fig. 1 (derived from Ref. 27). In Fig. 1A, the rates of sterol synthesis for multiple organs, including the small intestine and residual carcass, are shown as nmol/h per g wet weight of tissue. In Fig. 1B, these rates have been expressed in terms of the whole organ, normalized to 100 g body weight (μmol/h/organ per 100 g body weight). Summation of all the organ contents yields a "whole animal" [^{3}H]-sterol content, which is taken as a measure of the cholesterol synthesis rate in the body as a whole (inset in Fig. 1B).

3. An additional set of calculations is needed to convert the rates of water incorporation into sterol to milligrams of cholesterol generated per organ, or per whole animal. Of the various terms in the equation for making this calculation, one in particular has a complex derivation and remains somewhat hypothetical. This term is the ^{3}H/C incorporation ratio, the experimental determination of which has been discussed in detail elsewhere (see Table 1 in Ref. 22). The equation for calculating the whole-body sterol synthesis rate per day per kg body weight (bw) is as follows:

$$\frac{\mu\text{mol of water incorp'd into sterol} / \mathrm{h} / kg\ bw \times 0.387 \times 24}{18 \times 0.69}$$

0.387 converts μmol to mg; 24 converts the hourly rate to a daily rate; In the denominator, two values are used; 18 represents the number of acetyl CoA units utilized to synthesize one molecule of cholesterol, while 0.69 represents the "experimentally

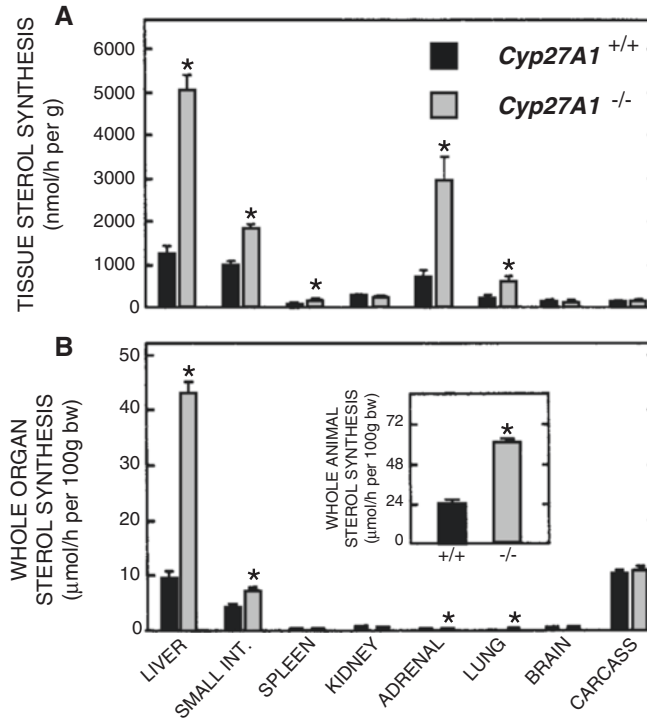

Fig. 1 Rates of sterol synthesis in the liver and extrahepatic organs of *Cyp27A1*$^{+/+}$ and *Cyp27A1*$^{-/-}$ mice. The rates of synthesis expressed per gram of tissue (**A**) were multiplied by respective whole organ weights to obtain whole-organ synthesis rates normalized per 100 g body weight (**B**). These whole-organ rates were added to give values for animal sterol synthesis per 100 g body weight (*inset* of **B**). Values represent the mean ± 1 S.E. of data from 4 to 7 mice of each genotype for all organs except the liver in which case measurements were made in 9 *Cyp27A1*$^{+/+}$ and 9 *Cyp27A1*$^{-/-}$ mice. Whole-animal sterol synthesis rates were determined in five mice of each genotype., $p < 0.05$ compared with value for *Cyp27A1*$^{+/+}$ animals. This research was originally published in Journal of Biological Chemistry. Repa JJ, Lund EG, Horton JD, Leitersdorf E, Russell DW, Dietschy JM, Turley SD (2000) Disruption of the sterol 27-hydroxylase gene in mice results in hepatomegaly and hypertriglyceridemia: reversal by cholic acid feeding. J Biol Chem 275:39685–39692. © [27]

determined" number of ^{3}H atoms found in cholesterol per atom of carbon that enters the biosynthetic pathway as acetyl CoA.

An example of the application of the tritiated water method in a much larger model was the determination of absolute rates of cholesterol synthesis in the major organs of a primate model that, like humans, exhibited marked individual variability in its cholesterolemic response to a lipid-rich diet [16]. As shown in Fig. 10 of this publication [16], irrespective of the animal's phenotype, the rates of synthesis for all organ compartments combined were in the range of 10–12 mg/day per kg body weight, which is comparable

to that found for adult human subjects using the sterol balance technique [4–6].

The numerous steps described for this method have not specifically included instructions on how to correct for procedural losses. Even with great care at every step, there will, on average, be a cumulative loss of labeled sterol of about 8%. Rather than introducing a radiolabeled internal standard like [^{14}C]-cholesterol into all samples at the tissue digestion step, it is better for each set of assays to run in parallel with the tissue samples quadruplicate [^{3}H]-cholesterol standards that contain sufficient carrier cholesterol. The percent recovery from these can be used to correct all the tissue [^{3}H]-sterol content data for an "average" procedural loss.

3.6 Determination of Tissue [^{3}H]-Fatty Acid Content

At least in mouse models, the two organs in which rates of fatty acid and sterol synthesis are most frequently determined are the liver and small intestine. The [^{3}H]-fatty acids are isolated and quantitated as follows:

1. Using the same tissue samples that were extracted for measurement of [^{3}H]-sterol content, aspirate the remaining organic phase and discard, unless needed for other purposes such as the determination of the cholesterol concentration in the organs for which rates of sterol synthesis were determined.
2. Acidify the lower phase containing the [^{3}H]-fatty acids with ~1.0 mL of conc. HCl and vortex for ~30 s.
3. Add 15 mL of hexane and shake vigorously for 1 min. To achieve rapid phase separation, centrifuge tubes at ~200 × *g* for ~20 min.
4. Pipette duplicate 2.0 mL aliquots of the hexane phase into counting vials, dry under hood, and place in vacuum oven for 30 min.
5. After cooling, add 1.0 mL methanol, 15 mL counting cocktail, cap and shake well.
6. Calculation of rate of fatty acid synthesis. Use the same expression as for determining the rate of sterol synthesis except, for tissues like liver and small intestine, which have very high rates of fatty acid synthesis. For these, divide rate by 1000 to convert from nmol to μmol. Examples of such data can be found in refs. 14 (Fig. 3) and 27 (Fig. 9).

4 Notes

1. Apart from the restrictions that arise with this method because of the very large amounts of [^{3}H]-water that are required, there is also the problem of rapid movement of [^{3}H]-sterol

from the liver to extrahepatic organs, particularly those with a pronounced vasculature like the spleen, kidneys, and lungs. This however is not a significant problem in animal models where cholesterol synthesis in the liver has been largely suppressed through dietary or genetic manipulation. For those models where this is not the case, there are sufficient published data for the residual blood volumes in a range of organs in various models including the mouse [28, 29] and rat [30]. When the [^{3}H]-sterol content in whole blood is determined, this value, together with the residual blood volume (μL/g wet weight tissue), can be used to calculate the amount of [^{3}H]-sterol that needs to be subtracted from the total [^{3}H]-sterol content found per gram of spleen, lung, or adrenal (or other organs of interest) to obtain a measure of the true rate of sterol synthesis in that organ. This correction procedure for numerous extrahepatic organs in the rat has been described in detail [30]. An alternate or adjunctive approach to determining how an experimental treatment impacts cholesterol synthesis specifically in organs like the lungs, kidneys, adrenals, and spleen is to measure the synthesis rate in vitro using [^{3}H]-water. This approach is beyond the scope of this chapter but has been described in earlier publications [30, 31]. When this is done, very high amounts of [^{3}H]-water have to be added to the incubation flasks to get clearly detectable rates of incorporation of the labeled water into new sterol because the rate of synthesis in any tissue under in vitro conditions is appreciably less than it is in vivo [31].

2. The amount and specific activity of the [^{3}H]-water to be acquired for any project will depend on multiple considerations including not only the species and study design, but also on governmental and institutional regulations. Even if the intention is to use the [^{3}H]-water only for cholesterol synthesis measurements in those organs of a small animal model that characteristically manifest high rates of sterol synthesis, it is still best to acquire the stock [^{3}H]-water at a concentration of 5 Ci in 1.0 mL of water. This allows for portions of the stock material to be diluted in sterile saline to fit the objectives of each experiment. For example, dilution of 1 Ci in a final volume of 5 mL (saline) yields an activity of ~200 mCi/mL. This is appropriate for most animal studies. Typically, for experiments with mouse models, the total amount of [^{3}H]-water administered per animal is around 40–50 mCi (ie 1.6–2 mCi/g body weight). The injection volume need not be identical for every mouse of the same body weight because it is the plasma water specific activity, and not the amount of [^{3}H]-water administered that is needed for calculating the cholesterol or fatty acid synthesis rates. There may be instances where the total amount

of [^{3}H]-water given per mouse needs to be significantly outside the range of 40–50 mCi. For example, if the only parameter of interest is the rate of hepatic fatty acid synthesis, then a total dose of about 5 mCi will suffice. On the other hand, if one needs to determine rates of cholesterol synthesis in different regions of the brain of mature mice, it will require that at least 150 mCi per mouse be used in order to get detectable levels of tritiated sterol in all regions. Clearly, in these special instances, the stock [^{3}H]-water should be diluted appropriately, given that the volume injected into each mouse should not exceed 0.1 mL per 10 g body weight.

Although [^{3}H]-water is available from several companies, a number of factors apart from cost need to be considered. Depending on the vendor, orders involving Curie amounts will likely require a custom synthesis as these are rarely available as stock items. Another key consideration is the type of container the [^{3}H]-water is supplied in. Although still commonly used, sealed glass ampoules do not provide the same level of safety and ease of handling as does the specially designed NENSure vial used by PerkinElmer Life Sciences. Our laboratory has routinely purchased custom made [^{3}H]-water (5.0 Ci/mL) from this supplier and found it to be of the highest quality.

3. The isolation and quantitation of cholesterol and several related sterols using digitonin has a long history [32]. A key discovery was that cholesterol, but not cholesteryl ester, forms a stable 1:1 molecular complex with digitonin [33]. Besides cholesterol, most naturally occurring sterols having a 3β-hydroxyl group are precipitable with digitonin. This includes several precursors of cholesterol in its biosynthetic pathway [34]. Thus, an argument can be made for presenting data as rates of sterol synthesis or, more precisely, incorporation rates of [^{3}H]-water into digitonin-precipitable sterols (DPS). Digitonin is available from multiple vendors but the purity and solubility varies from one source to another. Digitonin that is of 100% purity dissolves quickly and completely. To ensure that complete precipitation of all the cholesterol and its precursors extracted from tissues is achieved, only digitonin of high purity should be used.
4. Depending largely on the species studied, the amount of tissue cholesterol contained within an entire organ will often not be sufficient to facilitate the formation of a large enough sterol–digitonin complex needed for quantitative recovery of all the [^{3}H]-sterols present in that organ. In studies using mice, this is mainly a problem for organs like the adrenal glands, ovaries, and spleen, whose entire cholesterol content is less than the minimum amount needed (ideally 1.2–1.5 mg, 3.1–3.9 μmol). This mass of sterol is necessary to permit the

washing and splitting steps to be carried out without incurring significant and unknown loss of the labeled sterols in that organ. A solution of highly pure cholesterol in ethanol (~10 mg/mL) should be kept at ~4 °C for addition to those tissue extracts that are projected to contain sub-optimal levels of cholesterol as detailed later.

5. The majority of studies using this method will probably not need "whole animal" cholesterol synthesis rates. Therefore, the "residual" carcass will be discarded after the organs of interest have been harvested. However, when this is not the case, what defines "carcass" will be determined by which organs are taken for separate analysis. Thus, in studies with a focus on the liver and small intestine but which also require a "whole-animal" sterol synthesis rate, the carcass will contain not only the bulk organs of skin and muscle but numerous extrahepatic organs as well. An example of where the opposite situation applied can be seen in the data for the Cyp27A1 knockout mouse in Fig. 1.
6. The term 0.87 corrects the specific activity of plasma water determined at 1 h after injection of [^{3}H]-water to the mean specific activity of body water present throughout the 1 h period of time. Note that the factor of 0.87 applies when the [^{3}H]-water is given ip. If given iv, then this term should be 1.09 as described earlier [21]. The term 0.92 corrects the calculation for the concentration of water present in 1.0 mL of plasma from normolipidemic animals. Some investigators use a slightly higher value [26]. If the animal model has hyperlipidemia, then its plasma water content will likely be less than 92%. The water content can be determined by taking a precisely measured aliquot of plasma to dryness under a fume hood, followed by a ~30 min drying period in a vacuum oven. Typically, a plasma water specific activity in the range of 25–30 cpm/nmol will be sufficient to give detectable incorporation rates of [^{3}H]-water into newly synthesized sterols in all tissues. If rates of hepatic fatty acid synthesis are all that is required, then a plasma water specific activity of around 5 cpm/nmol will be sufficient.
7. At a concentration of 0.5% w/v, 3 mL of digitonin contains 12.2 μmol, which corresponds to about three times the amount of cholesterol it is to precipitate.

Acknowledgment

Much of the research described here was supported by US Public Health Service Grant R01HL009610. Each of the authors received salary support from this grant and also the Department of Internal

Medicine, University of Texas Southwestern Medical Center. The corresponding author also wishes to thank John M. Dietschy M.D. for the superb training he provided in the theoretical and technical aspects of using [^{3}H]-water for sterol synthesis measurements in many different types of experimental settings.

References

1. Cook RP (1958) Distribution of sterols in organisms and in tissues. In: Cook RP (ed) Cholesterol: chemistry, biochemistry, and pathology. Academic, New York, pp 145–180
2. Grundy SM (1983) Absorption and metabolism of dietary cholesterol. Annu Rev Nutr 3:71–96
3. Bosner MS, Lange LG, Stenson WF, Ostlund RE Jr (1999) Percent cholesterol absorption in normal women and men quantified with dual stable isotopic tracers and negative ion mass spectrometry. J Lipid Res 40:302–308
4. Bilheimer DW, Stone NJ, Grundy SM (1979) Metabolic studies in familial hypercholesterolemia. Evidence for a gene-dosage effect in vivo. J Clin Invest 64:524–533
5. McMurry MP, Connor WE, Lin DS, Cerqueira MT, Connor SL (1985) The absorption of cholesterol and the sterol balance in the Tarahumara Indians of Mexico fed cholesterol-free and high cholesterol diets. Am J Clin Nutr 41:1289–1298
6. Sudhop T, Reber M, Tribble D, Sapre A, Taggart W, Gibbons P, Musliner T, von Bergmann K, Lütjohann D (2009) Changes in cholesterol absorption and cholesterol synthesis caused by ezetimibe and/or simvastatin in men. J Lipid Res 50:2117–2123
7. Jones PJ, Leitch CA, Li ZC, Connor WE (1993) Human cholesterol synthesis measurement using deuterated water. Theoretical and procedural considerations. Arterioscler Thromb Vasc Biol 13:247–253
8. Cuchel M, Schaefer EJ, Millar JS, Jones PJH, Dolnikowski GG, Vergani C, Lichtenstein AH (1997) Lovastatin decreases de novo cholesterol synthesis and LDL Apo B-100 production rates in combined-hyperlipidemic males. Arterioscler Thromb Vasc Biol 17:1910–1917
9. Quan G, Xie C, Dietschy JM, Turley SD (2003) Ontogenesis and regulation of cholesterol metabolism in the central nervous system of the mouse. Brain Res 146:87–98
10. Xie C, Lund EG, Turley SD, Russell DW, Dietschy JM (2003) Quantitation of two pathways for cholesterol excretion from the brain in normal mice and mice with neurodegeneration. J Lipid Res 44:1780–1789
11. Bryleva EY, Rogers MA, Chang CC, Buen F, Harris BT, Rousselet E, Seidah NG, Oddo S, LaFerla FM, Spencer TA, Hickey WF, Chang TY (2010) ACAT1 gene ablation increases 24(S)-hydroxycholesterol content in the brain and ameliorates amyloid pathology in mice with AD. Proc Natl Acad Sci U S A 107: 3081–3086
12. Suzuki R, Ferris HA, Chee MJ, Maratos-Flier E, Kahn CR (2013) Reduction of the cholesterol sensor SCAP in the brains of mice causes impaired synaptic transmission and altered cognitive function. PLoS Biol 11:e1001532
13. Chuang JC, Valasek MA, Lopez AM, Posey KS, Repa JJ, Turley SD (2014) Sustained and selective suppression of intestinal cholesterol synthesis by Ro 48-8071, an inhibitor of 2,3-oxidosqualene:lanosterol cyclase, in the BALB/c mouse. Biochem Pharmacol 88:351–363
14. McFarlane MR, Liang G, Engelking LJ (2014) Insig proteins mediate feedback inhibition of cholesterol synthesis in the intestine. J Biol Chem 289:2148–2156
15. McFarlane MR, Cantoria MJ, Linden AG, January BA, Liang G, Engelking LJ (2015) Scap is required for sterol synthesis and crypt growth in intestinal mucosa. J Lipid Res 56:1560–1571
16. Turley SD, Spady DK, Dietschy JM (1997) Identification of a metabolic difference accounting for the hyper- and hyporesponder phenotypes of cynomolgus monkey. J Lipid Res 38:1598–1611
17. Horton JD, Shimomura I (1999) Sterol regulatory element-binding proteins: activators of cholesterol and fatty acid biosynthesis. Curr Opin Lipidol 10:143–150
18. Repa JJ, Turley SD, Quan G, Dietschy JM (2005) Delineation of molecular changes in intrahepatic cholesterol metabolism resulting from diminished cholesterol absorption. J Lipid Res 46:779–789
19. Aqul A, Lopez AM, Posey KS, Taylor AM, Repa JJ, Burns DK, Turley SD (2014) Hepatic entrapment of esterified cholesterol drives continual expansion of whole body sterol pool in lysosomal acid lipase-deficient mice. Am

J Physiol Gastrointest Liver Physiol 307: G836–G847

20. Andersen JM, Dietschy JM (1979) Absolute rates of cholesterol synthesis in extrahepatic tissues measured with 3H-labeled water and 14C-labeled substrates. J Lipid Res 20:740–752
21. Jeske DJ, Dietschy JM (1980) Regulation of rates of cholesterol synthesis in vivo in the liver and carcass of the rat measured using [^{3}H] water. J Lipid Res 21:364–376
22. Dietschy JM, Spady DK (1984) Measurement of rates of cholesterol synthesis using tritiated water. J Lipid Res 25:1469–1476
23. Schwarz M, Russell DW, Dietschy JM, Turley SD (1998) Marked reduction in bile acid synthesis in cholesterol 7α-hydroxylase-deficient mice does not lead to diminished tissue cholesterol turnover or to hypercholesterolemia. J Lipid Res 39:1833–1843
24. Xie CL, Turley SD, Dietschy JM (2000) Centripetal cholesterol flow from the extrahepatic organs through the liver is normal in mice with mutated Niemann-Pick type C protein (NPC1). J Lipid Res 41:1278–1289
25. Chapman ME, Hu L, Plato CF, Kohan DE (2010) Bioimpedance spectroscopy for the estimation of body fluid volumes in mice. Am J Physiol Renal Physiol 299:F280–F283
26. Jurevics H, Hostettler J, Barrett C, Morell P, Toews AD (2000) Diurnal and dietary-induced changes in cholesterol synthesis correlate with levels of mRNA for HMG-CoA reductase. J Lipid Res 41:1048–1054
27. Repa JJ, Lund EG, Horton JD, Leitersdorf E, Russell DW, Dietschy JM, Turley SD (2000) Disruption of the sterol 27-hydroxylase gene in mice results in hepatomegaly and hypertriglyceridemia. Reversal by cholic acid feeding. J Biol Chem 275:39685–39692
28. Satoh H (1979) Residual blood volumes in organs of pregnant mice and fetuses. Tohoku J Exp Med 129:41–44
29. Schumann K, Szegner B, Kohler B, Pfaffl MW, Ettle T (2007) A method to assess ^{59}Fe in residual tissue blood content in mice and its use to correct ^{59}Fe-distribution kinetics accordingly. Toxicology 241:19–32
30. Turley SD, Andersen JM, Dietschy JM (1981) Rates of sterol synthesis and uptake in the major organs of the rat in vivo. J Lipid Res 22:551–569
31. Spady DK, Turley SD, Dietschy JM (1983) Dissociation of hepatic cholesterol synthesis from hepatic low-density lipoprotein uptake and biliary cholesterol saturation in female and male hamsters of different ages. Biochim Biophys Acta 753:381–392
32. Sperry WM (1963) Quantitative isolation of sterols. J Lipid Res 4:221–225
33. Rosenfeld L (1999) Cholesterol. In: Rosenfeld L (ed) Four centuries of clinical chemistry. Taylor & Francis, New York, pp 377–394
34. Dietschy JM, Siperstein MD (1967) Effect of cholesterol feeding and fasting on sterol synthesis in seventeen tissues of the rat. J Lipid Res 8:97–104

Chapter 19

Methods for Monitoring ABCA1-Dependent Sterol Release

Yoshio Yamauchi, Shinji Yokoyama, and Ta-Yuan Chang

Abstract

Releasing sterols to the extracellular milieu is an important part of sterol homeostasis in cells and in the body. ATP-binding cassette transporter A1 (ABCA1) plays an essential role in cellular phospholipid and sterol release to lipid-free or lipid-poor apolipoprotein A-I (apoA-I), the major apolipoprotein in high-density lipoprotein (HDL), and constitutes the first step in the formation of nascent HDL. Loss-of-function mutations in the *ABCA1* gene lead to a rare disease known as Tangier disease that causes severe deficiency in plasma HDL level. Mammalian cells receive exogenous cholesterol mainly from low-density lipoprotein. In addition, they synthesize cholesterol endogenously, as well as multiple precursor sterols that are sterol intermediates en route to be converted to cholesterol. HDL contains phospholipids, cholesterol, and precursor sterols, and ABCA1 has an ability to release phospholipids and various sterol molecules. Recent studies using model cell lines showed that ABCA1 prefers to use sterols newly synthesized endogenously as its preferred substrate, rather than cholesterol derived from LDL or cholesterol being recycled within the cells. Here, we describe several methods at the cell culture level to monitor ABCA1-dependent release of sterol molecules to apoA-I present at the cell exterior. Sterol release can be assessed by using a simple colorimetric enzymatic assay, and/or by monitoring the radioactivities of radiolabeled cholesterol incorporated into the cells, and/or of sterols biosynthesized from radioactive acetate, and/or by using gas chromatography–mass spectrometry analysis of various sterols present in medium and in cells. We also discuss the pros and cons of these methods. Together, these methods allow researchers to detect the release not only of cholesterol but also of other sterols present in minor quantities.

Key words ABCA1, ApoA-I, Cholesterol, GC-MS, Lanosterol, HDL, Thin-layer chromatography

1 Introduction

Sterol is an essential lipid for the growth and maintenance of all eukaryotic cells. In mammalian cells, various elaborate regulatory mechanisms operate cooperatively to assure the ample supply of cholesterol, and to prevent the toxic accumulation of cholesterol in membranes [1, 2]. Within a single cell type, the release of cellular cholesterol to the extracellular milieu constitutes a critical step in optimizing cellular cholesterol level. Several ATP-binding cassette transporters including ABCA1, ABCG1, and ABCG4 all have the ability to release cholesterol from cells [3, 4]. ABCA1 plays a unique role in this step, being required for apolipoprotein-mediated

Ingrid C. Gelissen and Andrew J. Brown (eds.), *Cholesterol Homeostasis: Methods and Protocols*, Methods in Molecular Biology, vol. 1583, DOI 10.1007/978-1-4939-6875-6_19,

cholesterol and phospholipid release, which generates nascent HDL particles [5, 6]. Loss-of-function mutations in the *ABCA1* gene causes severe HDL deficiency, known as Tangier disease [7–9]. Patients with this disease display a higher risk for premature cardiovascular heart disease.

Mammalian cells acquire cholesterol from uptake of extracellular lipoproteins including low-density lipoprotein (LDL) [2]. In addition, almost all cells in the body synthesize cholesterol endogenously. The late stage of cholesterol biosynthesis occurs at the endoplasmic reticulum (ER), and involves the biosynthesis of a series of intermediate sterols (hereafter referred to as precursor sterols) as the cholesterol precursors (Fig. 1). These precursor sterols, with lanosterol being the first biosynthesized sterol, have structures similar but distinct from that of cholesterol; some of them display distinct roles from those of cholesterol. When their contents exceed certain threshold value, the precursor sterols are also toxic to cells [10]. For example, in humans, genetic defects in the conversion of precursor sterols to cholesterol are known to cause several malformation syndromes [11]. At the cell culture level, early results showed that certain precursor sterols including lanosterol, are transported to the plasma membrane (PM) shortly after their synthesis at the ER [12–15]. After arriving at the PM, cholesterol and various precursor sterol molecules immediately become available for ABCA1-dependent sterol release [16]. Alternatively, they are rapidly transported back to the ER for the conversion to cholesterol [15]. Our recent study [16] showed that ABCA1 prefers to use sterols newly synthesized endogenously, not cholesterol derived from LDL, or cholesterol being recycled within the cells, as its preferred substrates. HDLs are known to contain small but significant amounts of precursor sterols in addition to cholesterol [17]. Together, these studies suggest that ABCA1 mediates the release of phospholipids and not only cholesterol but also other structurally different sterols to apoA-I to generate nascent HDL. In addition to its well-known function of mediating the release of phospholipids and sterols to apoA-I present in the extracellular milieu, we have recently shown that ABCA1 also participates in retrograde sterol movement; lack of ABCA1 impairs sterol internalization from the PM and leads to a defect in sterol sensing at the ER [18].

In this chapter, we describe several methods used to monitor ABCA1-dependent sterol release. The first method is to measure cholesterol released into apoA-I by using a colorimetric enzyme assay. This method is based on the generation of H_2O_2 and cholestenone from cholesterol by the enzyme cholesterol oxidase. The second method is to feed cells with radiolabeled cholesterol and monitor the release of labeled cholesterol from cells. Third, we describe a method that uses radiolabeled acetate (a biosynthetic precursor of sterols) to produce radiolabel sterols

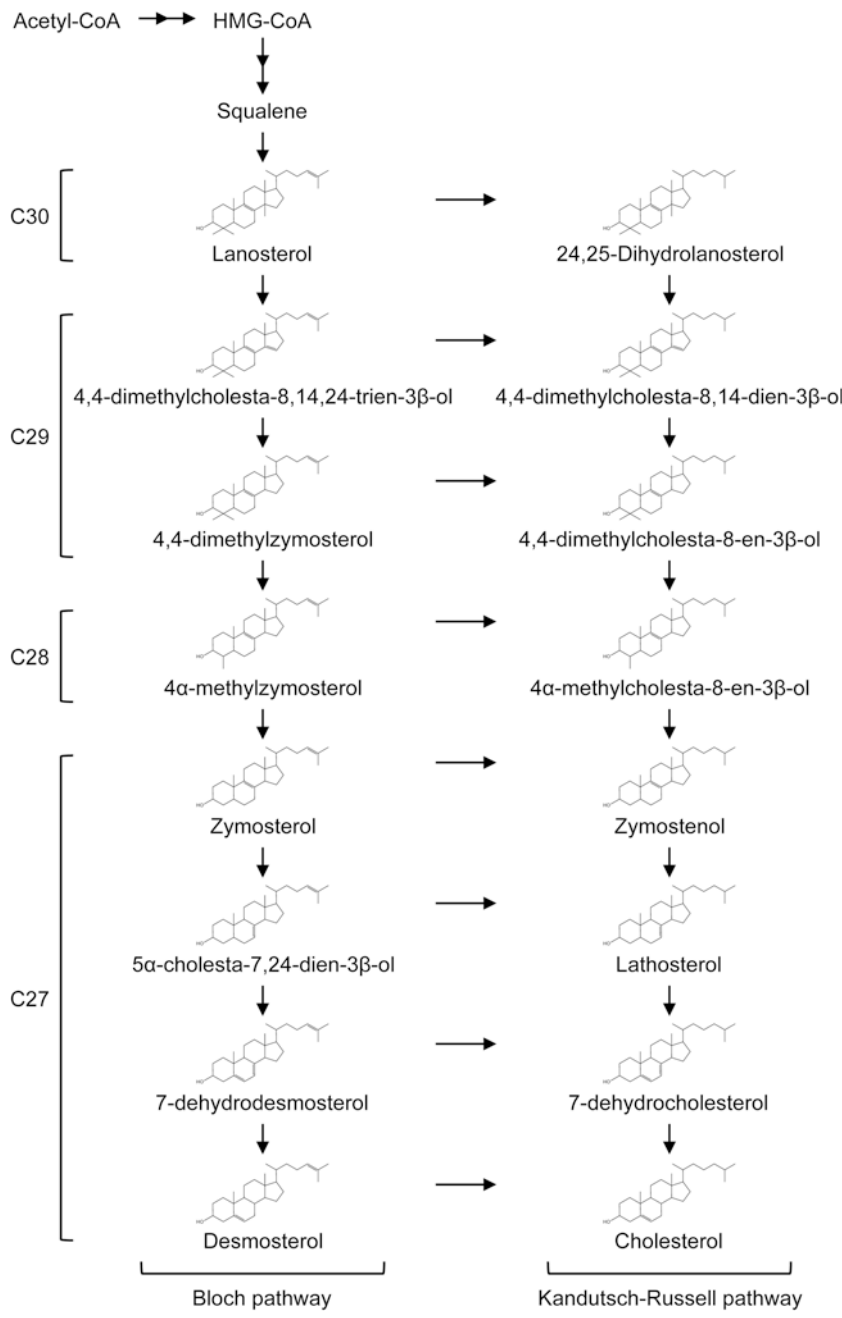

Fig. 1 Cholesterol biosynthetic pathway. Cholesterol biosynthesis proceeds through either the Bloch pathway or the Kandutsch-Russell pathway. The side-chain double bond at C24 position is reduced by the 24-dehydrocholesterol reductase DHCR24. The substrate for this enzyme may vary in a tissue/cell type-specific manner. The total number of carbons in each sterol is shown on the *left*

endogenously, and uses thin layer chromatography (TLC) to separate the radiolabeled sterols. This TLC method allows one to detect not only cholesterol but also precursor sterols with one or two methyl group(s) located at the steroid ring A. Finally, we

describe a method to identify sterol molecules by using gas chromatography-mass spectrometry (GC-MS). We also discuss the pros and cons of these methods.

2 Materials

2.1 Radioisotopes, Sterols, and Other Reagents

1. [^{3}H]-cholesterol and [^{3}H]-acetate are obtained commercially. [^{14}C]-cholesterol or [^{14}C]-acetate can be used instead.
2. Sterol standards for TLC and GC-MS: Epicoprostanol, cholesterol, lathosterol, desmosterol, zymosterol, and lanosterol, which are commercially available, are dissolved in chloroform at a concentration of 10 mg/mL. The stock solutions can be stored at −20 °C.
3. Sigma-Sil-A can be obtained from Sigma-Aldrich.
4. The BCA protein assay is commercially available.

2.2 Solutions

1. Phosphate-buffered saline (PBS): Dissolve 8 g of sodium chloride (NaCl), 0.2 g of potassium chloride (KCl), 1.15 g of disodium hydrogen phosphate (sodium phosphate, dibasic, anhydrous; Na_2HPO_4), and 0.2 g of potassium dihydrogen phosphate (potassium phosphate, monobasic, anhydrous; KH_2PO_4) in 1 L of deionized/distilled water (ddH_2O). After autoclaving, this solution is stable at room temperature.
2. 10% (w/v) bovine serum albumin (BSA): Dissolve 1 g of fatty acid-free BSA in 10 mL of sterile PBS. After filtration by using a 0.2 μm (or 0.45 μm) filter, the 10% stock can be stored at 4 °C for at least several months.
3. 0.1 M sodium hydroxide (NaOH): Dissolve 0.4 g of NaOH in 100 mL of ddH_2O. This solution is stable at room temperature.
4. 10 M potassium hydroxide (KOH): Dissolve 56.1 g of KOH in 100 mL of ddH_2O. This solution is stable at room temperature
5. 3% (w/v) sodium hydrogen carbonate ($NaHCO_3$) saturated with chloroform: Dissolve 3 g of $NaHCO_3$ in 100 mL of ddH_2O, and add 10–20 mL of chloroform. After vigorously mixing, use the top aqueous phase. This solution is stable at room temperature for only a few days.
6. ddH_2O saturated with chloroform: Add 10–20 mL of chloroform in 100 mL of ddH_2O and mix vigorously. This solution is stable at room temperature.

2.3 Cell Culture Media

The following media are used for experiments. All media listed below contain 100 U/mL of penicillin and 100 μg/mL of streptomycin.

1. Medium A: appropriate medium containing 10% (or 7.5%) fetal bovine serum (FBS).
2. Medium B: appropriate medium containing 0.1% fatty acid-free BSA (unless specified otherwise; from the 10% stock).
3. Medium D: appropriate medium containing 5% delipidated FBS [19] or lipoprotein-deficient FBS (LPDS; commercially available) (*see* **Note 1**).
4. Medium F: appropriate medium without any supplements.

2.4 ApoA-I

Lipid-free apoA-I is isolated/purified from human plasma as described [20]. Bacterially expressed recombinant apoA-I can also be utilized in the ABCA1-dependent lipid release assay [21–23]. ApoA-I and recombinant apoA-I can be obtained from commercial sources. All apoA-I forms are essentially devoid of lipids. Lyophilized apoA-I should be solubilized to obtain a homogeneous solution by dissolving in PBS for 1 h at room temperature followed by warming at 37 °C for 1 h [20]. After filtration by using a 0.22 μm filter, determine the protein concentration by using a protein assay and adjust to the concentration of 1 mg/mL with sterile PBS. The solution should be kept at 4 °C and can be used for at least a few months.

2.5 Organic Solvents

All organic solvents used are of analytical grade.

1. Chloroform–methanol (2:1). Mix 200 mL of chloroform and 100 mL of methanol, and store in a dark glass bottle. The mixture is stable at room temperature.
2. Hexane–2-propanol (3:2): Mix 150 mL of hexane and 100 mL of 2-propanol, and store in a dark glass bottle. The mixture is stable at room temperature.
3. Ethanol–benzene–water (80:20:5): Mix 80 mL of ethanol, 20 mL of benzene, and 5 mL of ddH_2O, and store in a dark glass bottle. The solution can be stored at room temperature for months.
4. Hexane–ether–acetic acid (260:80:3): Mix 45 mL of hexane, 20 mL of ether, and 0.75 mL of ddH_2O. Prepare this mixture just before the TLC analysis.
5. Methylene chloride–ethyl acetate (97:3): Mix 97 mL of methylene chloride and 3 mL of ethyl acetate. Prepare this mixture just before the TLC analysis.

2.6 Colorimetric Enzymatic Cholesterol Assay Kits

1. Determinar L FC (available from Kyowa Medex). Mix R-1 and R-2 reagents at the ratio of 3:1. Prepare mixture just before the assay (*see* **Note 2**).
2. An alternate kit that can be used is the Free Cholesterol E (available from Wako). Reconstitute appropriate amounts of

the lyophilized powder in appropriate volume of buffer provided in the kit. Reconstitute just before the assay (*see* **Note 3**).

3. Cholesterol standard: The Cholesterol stock solution can be prepared in chloroform as described in Subheading 2.1. Free Cholesterol E (Wako) provides a 2 mg/mL cholesterol stock solution.
4. Cholesterol esterase (if total amount of cholesteryl esters is also required): Dissolve in PBS at the final concentration of 10 U/mL. This solution can be stored at −20 °C.

2.7 Equipment

1. Evaporator with heater connected to nitrogen gas system.
2. Microplate reader with appropriate filters.
3. Channeled 20 cm × 20 cm thin layer chromatography (TLC) plates (Silica Gel 60 Å, 250 μm layer thickness) can be obtained from Analtech.
4. TLC developing tank.
5. Iodine TLC tank to visualize lipids. Add iodine to the tank for developing.
6. 80 °C oven.
7. GC-MS equipment; for example in our lab we use a Shimadzu GC-17A gas chromatograph connected to a Shimadzu QP5000 mass spectrometer and equipped with an XTI-5 (30 m × 25 μm × 0.25 mm) capillary column

3 Methods

Typically, seed cells into a 6-well plate and grow in Medium A essentially to a confluent stage at 37 °C with 100% humidity and 5% CO_2. Lipid extraction and analysis are performed at room temperature unless specified otherwise (*see* **Notes 4** and **5**).

3.1 Monitoring Cholesterol Release by Using Colorimetric Enzymatic Assay (See Note 6)

1. Seed cells into 6-well plates and grown to confuency in Medium A in an incubator with 100% humidity and 5% CO_2. Typically, cells are seeded at a density of 2–3 × 10^5 cells/well, and grown for 2–3 days (depending on cell lines/types) in Medium A. For cells that express low levels of ABCA1 (such as human fibroblasts and mouse embryonic fibroblasts), ABCA1 expression can be induced transcriptionally by incubating cells overnight with a ligand for liver X receptor (LXR) and/or for retinoid X receptor (RXR) (*see* **Note 7**).
2. Wash cells with PBS or with Medium F twice to remove FBS.
3. Incubate cells without or with apoA-I (5–10 μg/mL, 1 mL/well) in Medium B for 16–24 h at 37 °C in an incubator with 100% humidity and 5% CO_2 (*see* **Notes 8–11**).

4. Collect medium (~1 mL) into a 1.5 mL tube. Wash cells with PBS twice and let them dry.
5. Spin medium at 10,0000 × *g* for 5 min to precipitate floating cells and cell debris.
6. Transfer 0.9 mL of supernatant to a glass tube.
7. Add 4 vol (3.6 mL) of chloroform–methanol (2:1) into the glass tube and vortex vigorously.
8. Wrap the glass tube with aluminum foil and leave at 4 °C overnight.
9. Vortex again and spin the glass tube at 1000 × *g* for 10 min at room temperature.
10. Suck off the aqueous phase.
11. Add 1 mL of ddH_2O and vortex (*see* **Note 12**).
12. Spin the glass tube again at 1000 × *g* for 10 min at room temperature.
13. Suck off the aqueous phase.
14. Blow-dry the organic phase under nitrogen gas at 40–50 °C using a heat block (or a water bath).
15. Transfer extracted lipids into a well of 96-well plate with 2 × 100 μL of chloroform–methanol (2:1) to solubilize the dried lipid samples. Load onto a single well per sample (*see* **Note 13**).
16. Lipids present in the cells dried in the tissue culture wells (*see* **step 4**) can be extracted as follows: Add 1 mL of hexane–2-propanol (3:2) to a well, place for 1 h at room temperature, and transfer to a glass tube.
17. Extract cell lipids again by adding 1 mL of hexane–2-propanol (3:2) to a well, place for 30 min at room temperature, and transfer to a glass tube to combine with the first extract.
18. Blow-dry as describe above (*see* **step 14**).
19. Add 400 μL of chloroform–methanol (2:1) to a tube, vortex, and transfer a quarter (100 μL) of the extract (cell lipids) to a well of a 96-well plate.
20. Blow-dry the organic solvent in a 96-well plate using a hair dryer or under nitrogen gas.
21. Add the cholesterol standard (0–20 μg, typically 20, 10, 5, 2.5, 1.25, 0.625, 0.3125, 0 μg of cholesterol) into separate wells (*see* **Notes 14** and **15**).
22. Add 20 μL of 2-propanol into each well (both samples and standards) to dissolve lipids.
23. Add 150 μL of reaction mixture into each well and place the plate at 37 °C for 60 min.

24. Measure absorbance at 550–600 nm (optimal absorbance is 555 nm for Kyowa-Medics Kit, or at 600 nm for Wako kit; reference filter of 700 nm), and calculate cholesterol contents based on the standard curve. To obtain the calculated cholesterol contents in a sample, divide the values by 0.9 for medium extracts, or multiply the values by 4 for cell extracts.
25. Add 1 mL of 0.1 M NaOH into a well and place at 4 °C overnight to extract cell protein. This can be done after the cellular lipids are extracted. After cellular lipid extraction, the lipid free cell proteins remain in the well and can be measured by BCA protein assay after solubilization by using 0.1 M NaOH.
26. Normalize cholesterol content in the medium by using cell protein or cell cholesterol as the denominator (*see* **Notes 16** and **17**).

3.2 Monitoring the Release of Radiolabeled Cholesterol Added Exogenously

1. Seed and grow cells as above (*see* **step 1** of Subheading 3.1).
2. Wash cells with PBS or Medium F twice.
3. Incubate cells with [^{3}H]-cholesterol (without adding nonradioactive cholesterol as carrier; 0.1 μCi/mL, 1 mL/well) in Medium A overnight (Fig. 2a, Condition IV).
4. After washing cells with PBS or Medium F twice (to remove unincorporated labeled cholesterol), incubate cells in Medium A to equilibrate [^{3}H]-cholesterol in cells.
5. After washing cells with PBS or Medium F twice, incubate cells without or with apoA-I in Medium B for up to 24 h (*see* also Subheading 3.1).
6. Collect the medium (~1 mL) into a 1.5 mL tube. Wash cells with PBS twice and let them dry.
7. Spin medium at 10,0000 × *g* for 5 min to precipitate floating cells and cell debris.
8. Transfer 0.9 mL of supernatant to a glass tube.
9. Add 4 volumes (3.6 mL) of chloroform–methanol (2:1) into the glass tube, and vortex vigorously.
10. Wrap the glass tube with aluminum foil and leave at 4 °C overnight.
11. Vortex again, and spin the glass tube at 1000 × *g* for 10 min at room temperature.
12. Suck off the aqueous phase.
13. Blow-dry the organic phase under nitrogen gas at 40–50 °C using a heat block (or a water bath).
14. For cellular [^{3}H]-cholesterol analysis, extract cellular lipids as described above (*see* **steps 16** and **17** of Subheading 3.1).

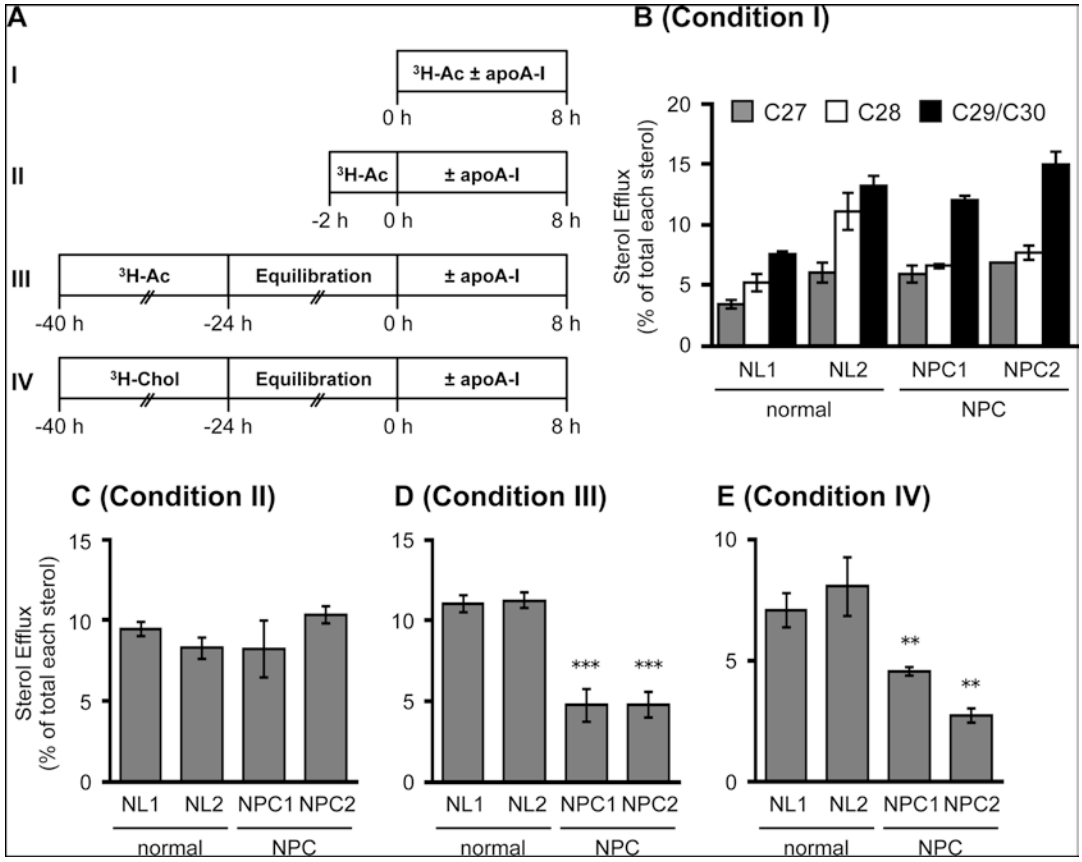

Fig. 2 Monitoring the ABCA1-dependent release of radiolabeled endogenously synthesized sterols in normal and mutant NPC cells. (**a**) Procedures used in pulse-chase experiments using radiolabeled-acetate or radiolabeled-cholesterol (Assay I–IV). Cells were labeled with either [^{3}H]-acetate (^{3}H–Ac) or [^{3}H]-cholesterol (^{3}H–Chol). (**b–e**) ABCA1-dependent release of labeled sterols in normal and NPC human skin fibroblasts (HSFs) evaluated under various conditions. HSFs from normal subjects (NL1 and NL2), and NPC patients (mutated in either *NPC1* or *NPC2* gene) were seeded in 6-well plates and grown in medium A to almost confluency. Cells were then subjected to the assay I, II, III, or IV by labeling cells with [^{3}H]-acetate or [^{3}H]-cholesterol as indicated below. For panel (**b**), cells pretreated with TO901317 (1 μg/mL) for 18 h were incubated with or without apoA-I (10 μg/mL) during the 8 h [^{3}H]-acetate (40 μCi/mL) labeling period in the presence of TO901317. For panel (**c**), cells were labeled with [^{3}H]-acetate (40 μCi/mL) for 2 h followed by washing off the label and incubation with or without apoA-I (10 μg/mL) in the presence of TO901317 for 8 h. For panels (**d**) and (**e**), cells were labeled with [^{3}H]-acetate (20 μCi/mL) for 16 h in Medium D (D) or with [^{3}H]-cholesterol (0.1 μCi/mL) in Medium A (**e**), followed by washing off the label and incubation with Medium D or Medium A for 24 h with TO901317 present. The cells were then incubated with or without apoA-I (10 μg/mL) for 8 h in the presence of TO901317. Sterols were analyzed by TLC. Data shown are means ± SD ($n = 3$). $^{**}P < 0.01$, $^{***}P < 0.001$ by Student's t-test. This research was originally published in J. Lipid Res. Yamauchi et al. (2016) ABCA1-dependent sterol release: sterol molecule specificity and potential membrane domain for HDL biogenesis, J Lipid Res 57:77–88. © The American Society for Biochemistry and Molecular Biology [16]

15. The extracted lipids (both from medium and cells) can directly be subjected to scintillation counting to determine radioactivity of [^{3}H]-cholesterol in medium and cells. For more detailed analysis, the extracted lipids are run on TLC with a solvent system of hexane–ether–acetic acid (260:80:3), which separates cholesterol and cholesteryl ester from other lipids. Cholesterol and cholesteryl ester fractions are scraped and their radioactivities are counted by a liquid scintillation counter.
16. Calculate % release of [^{3}H]-cholesterol by the following equation: counts in medium/(counts in medium + cell) × 100.

3.3 Monitoring the Release of Radiolabeled Sterols Synthesized Endogenously

1. Seed and grow cells in 6-well plates as above (*see* **step 1** of Subheading 3.1).
2. Wash cells twice with PBS or Medium F.
3. Incubate cells with [^{3}H]-acetate (20–40 μCi/mL, 1 mL/well) for 2–16 h in Medium B or in Medium D according to Fig. 2a (Condition I–III) (*see* **Note 18**).
4. After washing cells twice with PBS or Medium F, incubate cells without or with apoA-I for up to 24 h (typically 6–24 h) in Medium B.
5. Collect medium (~1 mL) into 1.5 mL tube. Wash cells twice with PBS and let them dry.
6. Spin medium at 10,0000 × *g* for 5 min to precipitate floating cells and cell debris.
7. Transfer 0.9 mL of supernatant to a glass tube.
8. Add 4 vol (3.6 mL) of chloroform–methanol (2:1) into the glass tube and vortex vigorously.
9. Wrap the glass tube in aluminum foil and leave at 4 °C overnight.
10. Vortex again, and spin the glass tube at 1000 × *g* for 10 min at room temperature.
11. Suck off the aqueous phase.
12. Cell lipids are extracted as above (*see* **steps 16** and **17** of Subheding 3.1).
13. Blow-dry sample under nitrogen gas at 40–50 °C using a heat block (or a water bath).
14. Saponify lipids (extracted from medium and from cells respectively) as follows (steps **14–16**): Add 3 mL of ethanol–benzene–water (80:20:5) and 0.33 mL of 10 M KOH (final concentration 1 M), and vortex.
15. Wrap the glass tube with aluminum foil.
16. Incubate the glass tube at 80 °C for 2 h in an oven.
17. Blow-dry under nitrogen gas at 40–50 °C using a heat block (or a water bath) to a final volume of ~0.1 mL.

18. Add 1 mL of ddH_2O and vortex.
19. Extract sterols by adding 3 mL of hexane and vortex.
20. Spin the glass tube at 1000 × *g* for 10 min at room temperature.
21. Collect organic (upper) phase (containing sterols) and transfer to a glass tube (*see* **Note 19**).
22. Repeat **steps 19–21** four times in total.
23. Blow-dry the organic phase to 3 mL.
24. Add 1 mL of 3% $NaHCO_3$ saturated with chloroform and vortex.
25. Spin the glass tube at 1000 × *g* for 10 min at room temperature.
26. Remove aqueous phase from the bottom using a glass Pasteur pipette.
27. Add 1 mL of water saturated with chloroform to the organic phase, and vortex.
28. Spin the glass tube at 1000 × *g* for 10 min at room temperature.
29. Remove aqueous phase from the bottom using a glass pasteur pipette.
30. Blow-dry the organic phase.
31. Add 40 μg of lanosterol and 60 μg of cholesterol as internal markers and 100 μL of chloroform to each tube, then vortex.
32. Spot onto a channeled 20 cm × 20 cm TLC plate and run in a TLC tank with 30–50 mL of methylene chloride/ethyl acetate (97:3).
33. Visualize cholesterol and lanosterol by iodine and mark the bands by a pencil.
34. Scrape off the corresponding bands (cholesterol band, C27 sterols; lanosterol band, C29 and C30 sterols; space between cholesterol and lanosterol bands, C28 sterols) and put into a scintillation vial.
35. After adding 3 mL of scintillation cocktail, count the radioactivity with a liquid scintillation counter.
36. Calculate % release of [^{3}H]-sterols as described earlier, using total (cell plus medium) [^{3}H]-sterols as the denominators (*see* Subheading 3.2).

3.4 Monitoring Sterol Release by GC-MS

1. Seed cells into two 100-mm dishes.
2. Incubate cells with apoA-I in Medium B for 24–48 h (6 mL/dish).
3. Collect and centrifuge medium at 10,0000 × g for 5 min to precipitate floating cells and cell debris.
4. Extract lipids as described earlier using chloroform–methanol (2:1) (*see* Subheading 3.1).

5. Saponify lipids as described earlier (*see* Subheading 3.3, **steps 14–18**).
6. Extract non-saponified fraction (containing sterols) using hexane four times (*see* Subheading 3.3, steps **19–30**).
7. Add 20 μg of epicoprostanol (as an internal standard) and 0.25 mL of Sigma-Sil-A to the tube and incubate at 60 °C for 30 min to achieve trimethylsilyl (TMS) derivatization of the sterols.
8. Blow-dry under nitrogen gas at 40–50 °C.
9. Resuspend in 50 μL of chloroform and transfer to a fresh glass vial with screw cap.
10. Inject appropriate amounts (typically 1–2 μL) of derivatized sterols into a GC-MS (*see* **Note 20**).
11. Analyze the GC profile (Fig. 3) with MS spectra of each peak (*see* **Note 21**).

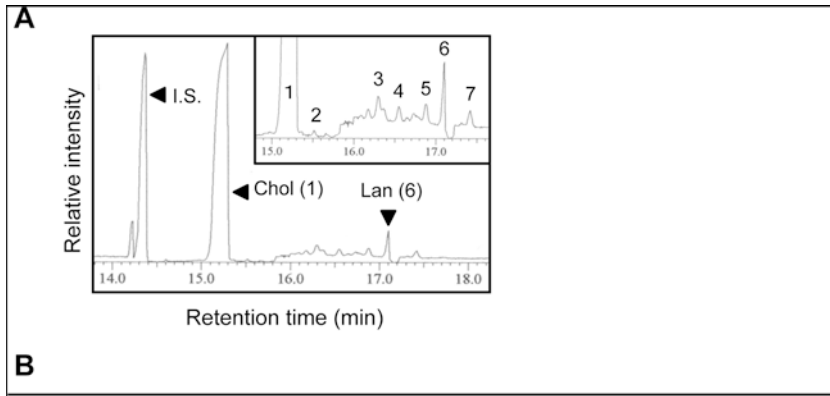

B

Peak	Sterol (number of carbons)	Sterol (ng/mg cell protein)
1	Cholesterol (C27)	4392.6
2	Desmosterol (C27)	10.7
3	Monounsaturated monomethylsterol (C28)	41.6
4	Monounsaturated monomethylsterol (C28)	40.3
5	Monounsaturated dimethylsterol (C29)	48.9
6	Lanosterol (C30)	119.7
7	Diunsaturated dimethylsterol (C29)	40.4

Fig. 3 GC-MS analysis of ABCA1-dependent sterol release. (**a**) HEK293 cells stably expressing human ABCA1-GFP (HEK/hABCA1) grown as a monolayer at subconfluency in two 100 mm dishes in Medium D were incubated with apoA-I (5 μg/mL) for 48 h in Medium B. Lipids were extracted from the medium, saponified, and analyzed by GC-MS. The peaks of epicoprostanol (internal standard, I.S.), cholesterol (Chol, peak 1), and lanosterol (Lan, peak 6) are indicated by *arrowhead*. Other minor peaks (2–5 and 7) are shown in the inset. This research was originally published in J. Lipid Res. Yamauchi et al. (2016) ABCA1-dependent sterol release: sterol molecule specificity and potential membrane domain for HDL biogenesis. J Lipid Res 57:77–88. © the American Society for Biochemistry and Molecular Biology [16]. (**b**) Identification and quantification of sterols released to apoA-I. Based on the GC-MS profile shown above, the identity of each peak and contents of each sterol were determined. The results are reproduced from Yamauchi et al. [16] with modification

4 Notes

1. The primary purpose to incubate cells in Medium D is to activate sterol regulatory element binding proteins and to upregulate sterol biosynthesis. Depending on cell types used, the concentration of delipidated FBS or LPDS may be reduced to 1 or 2%, but optimization is required.
2. Determinar L FC from Kyowa Medex is available only in certain Asian countries including Japan and China. Researchers who live in other countries can employ Free Cholesterol E (Wako).
3. Free Cholesterol E is supplied as lyophilized powder. If reconstituted all at once as described in the manufacture's instruction, the solution can be stored at 4 °C for up to 2 weeks only. To lengthen the usage time of the kit, we recommend that one measures a portion of the powder needed for a single experiment, and reconstitutes the powder in the buffer proportionally.
4. Not all cell lines express ABCA1. It is important to select correct cell lines/cell types to study ABCA1-dependent sterol release. With cells not expressing ABCA1 (such as HEK293 cells, HeLa cells, and COS-7 cells), sterol release to apoA-I cannot be detected. Cells that express ABCA1 include human fibroblast cell lines WI-38 and MRC-5, HepG2 cells, differentiated THP-1 cells, mouse embryonic fibroblasts, BALB/3 T3 cells, RAW264.7 cells treated with cAMP, and Chinese hamster ovary (CHO) cells [16, 24–26].
5. Niemann–Pick type C (NPC) disease is a lysosomal storage disease accompanied by severe neurodegeneration that often leads to death in affected patients before adulthood. NPC disease is caused by a mutation either in the *NPC1* or *NPC2* gene. Both NPC1 and NPC2 proteins bind cholesterol and function in transporting cholesterol out from the late endosome and lysosome [2]. In NPC1- or NPC2-deficient human fibroblasts and CHO cells, cholesterol and other lipids accumulate within the late endosome and lysosome compartments and fail to reach other membrane compartments. Mutant NPC cells serve as effective tools to study cholesterol transport pathways (*see* Fig. 2).
6. One needs to keep in mind that in addition to cholesterol, the colorimetric enzymatic assay described in this chapter may detect precursor sterols that can be the substrates of cholesterol oxidase.
7. ABCA1 expression is highly regulated at the transcriptional level. Treating cells with LXR and/or RXR ligands induces ABCA1 expression and significantly increases sterol release [27]. Several synthetic and natural LXR ligands including TO901317 and 22(*R*)-hydroxycholesterol, respectively, are

commercially available. The RXR ligand 9-*cis* retinoic acid is also commercially available. However, one needs to keep in mind that the colorimetric enzymatic assay described in this chapter can detect oxysterol used to induce ABCA1 expression.

8. When incubating with or without apoA-I, the BSA concentration in Medium B can be reduced to 0.02% instead of 0.1% (w/v).
9. ApoA-I is the most physiologically relevant lipid acceptor to assess ABCA1-dependent lipid release because apoA-I is the major apolipoprotein of HDL. However, other α-helix containing apolipoproteins such as apoA-II and apoE [28], and synthetic α-helical peptides [29, 30] can also induce lipid release in an ABCA1-dependent manner. In addition, sodium taurocholate can also mediate ABCA1-dependent lipid release [31].
10. Approximately 80% or 90–100% of lipid release ability can be observed by using 5 or 10 μg/mL of apoA-I, respectively.
11. A shorter incubation time can be used. In this case (for example; 6–8 h incubation with apoA-I), lipids extracted from two or more wells per assay may be required in order to exceed the detection limit of the assay employed.
12. This step is required to remove phenol red. When cholesterol contents are determined by using a colorimetric enzymatic assay, phenol red present in medium causes overestimation due to its color.
13. A 96-well plate used here should be resistant to organic solvent. Corning® Polypropylene Flat Bottom 96 Well Microplate is recommended.
14. 0.08–20 μg per well of cholesterol can be quantitatively measured by this method [26].
15. We use the cholesterol standard aqueous solution obtained from Wako. A cholesterol standard can also be prepared by dissolving cholesterol in chloroform–methanol. In this case, this step should be performed before **step 20**.
16. The same procedure can be applied to measure phospholipid content. In this case, Phospholipids B (Wako) or Determiner L PL (Kyowa Medex) kit is used as a colorimetric enzymatic assay. Because these assay kits are based on the use of choline oxidase, only choline-containing phospholipids (including phosphatidylcholine and sphingomyelin) are detected. The detection range is 0.15–20 μg per well.
17. When determining cell cholesterol levels, measuring both free cholesterol and total cholesterol (free cholesterol and cholesteryl esters) is recommended, which allows one to calculate the amounts of cholesteryl ester by subtracting free cholesterol from total cholesterol. Total cholesterol can be measured by

adding cholesterol esterase (at final concentration of 0.1 U/mL; available from Wako) to the free cholesterol assay reagent.

18. In order to monitor the fate of endogenously synthesized sterols, the labeling conditions are critical. The half-life of various precursor sterols is less than 1 h. Thus, ABCA1-dependent release of [^{3}H]-precursor sterols can only be detected under condition I (Fig. 2a). Even under condition II, it is difficult to detect the release of [^{3}H]-precursor sterols, due to their rapid conversion to cholesterol.

19. The bottom fraction contains saponified fatty acids. This fraction should not be discarded if fatty acid analysis is required. For fatty acid analysis, acidify the saponified fraction by adding 0.3 mL of 12 M hydrochloric acid (HCl). Extract fatty acids by 2 mL of hexane or petroleum ether 4 times as described in **steps 19–22**. Concentrate the hexane extract to ~3 mL under nitrogen gas, wash once with 1 mL of 5 mM HCl and once with 1 mL of ddH_2O. After blowing the sample to dryness under nitrogen gas, add oleic acid (40 μg/tube) as an internal standard, spot samples onto a TLC plate and run in a TLC tank with petroleum ether–ether–acetic acid (90:10:1). Afterwards, the fatty acid bands are identified by iodine staining, scraped and their radioactivities are counted in a liquid scintillation counter.

20. We use a Shimadzu GC-17A gas chromatograph connected to a Shimadzu QP5000 mass spectrometer and equipped with an XTI-5 (30 m × 25 μm × 0.25 mm) capillary column. For this system, the injector port is set at 290 °C. The temperature program for the column is as follows: the initial temperature of the oven is 110 °C and the temperature is increased at a rate of 15 °C/min to 290 °C and held for 10 min (total run time 22 min). Helium flow is maintained at a constant rate of 1.3 mL/min.

21. The sterol masses are quantified using epicoprostanol (as an internal standard) by comparing the relative areas of the individual peaks from the chromatogram. The mass spectrometer is operated in scan mode to observe both the molecular ions and the fragmentation patterns for the individual sterol derivatives. In our experiments, TMS-derivatives of five standard sterols, epicoprostanol, cholesterol, lathosterol, desmosterol, zymosterol, and lanosterol, were clearly separated under this condition. The GC-MS procedure also allowed us to identify TMS-derivatives of the following 10 cellular sterols; lanosterol (C30), monounsaturated 4,4-dimethyl sterol (C29), diunsaturated 4,4-dimethyl sterol (C29), two monounsaturated monomethyl sterols (C28), desmosterol (C27), 5α-cholesta-7,24-dien-3β-ol (C27), zymosterol (C27), lathosterol (C27), and cholesterol (C27) [15]. Also, refer to earlier works [32, 33].

Acknowledgments

We thank Dr. Catherine C.Y. Chang at Geisel School of Medicine at Dartmouth and Dr. Sumiko Abe-Dohmae at Nagoya City University Graduate School of Medical Sciences, who participated in developing and/or optimizing some of the methods described in this chapter. The authors' work was supported by JSPS KAKENHI grants (to Y.Y. and to S.Y.), by the CREST program from Japan Agency for Medical Research and Development, AMED (to Y.Y.), by MEXT-supported Program for the Strategic Research Foundation at Private Universities (S1201007) and by NIH grant HL060306 (to T.Y.C. and C.C.Y.C).

References

1. Goldstein J, DeBose-Boyd R, Brown M (2006) Protein sensors for membrane sterols. Cell 124:35–46
2. Chang T-Y, Chang CCY, Ohgami N, Yamauchi Y (2006) Cholesterol sensing, trafficking, and esterification. Annu Rev Cell Dev Biol 22:129–157
3. Tall A, Yvan-Charvet L, Terasaka N, Pagler T, Wang N (2008) HDL, ABC transporters, and cholesterol efflux: implications for the treatment of atherosclerosis. Cell Metab 7:365–375
4. Tarling EJ, de Aguiar Vallim TQ, Edwards PA (2013) Role of ABC transporters in lipid transport and human disease. Trends Endocrinol Metab 24:342–350
5. Hara H, Yokoyama S (1991) Interaction of free apolipoproteins with macrophages. Formation of high density lipoprotein-like lipoproteins and reduction of cellular cholesterol. J Biol Chem 266:3080–3086
6. Francis GA, Knopp RH, Oram JF (1995) Defective removal of cellular cholesterol and phospholipids by apolipoprotein A-I in Tangier disease. J Clin Invest 96:78–87
7. Brooks-Wilson A, Marcil M, Clee SM, Zhang LH, Roomp K, van Dam M et al (1999) Mutations in ABC1 in Tangier disease and familial high-density lipoprotein deficiency. Nat Genet 22:336–345
8. Bodzioch M, Orsó E, Klucken J, Langmann T, Böttcher A, Diederich W et al (1999) The gene encoding ATP-binding cassette transporter 1 is mutated in Tangier disease. Nat Genet 22:347–351
9. Rust S, Rosier M, Funke H, Real J, Amoura Z, Piette JC et al (1999) Tangier disease is caused by mutations in the gene encoding ATP-binding cassette transporter 1. Nat Genet 22:352–355
10. Bloch KE (1983) Sterol structure and membrane function. CRC Crit Rev Biochem 14:47–92
11. Porter FD (2002) Malformation syndromes due to inborn errors of cholesterol synthesis. J Clin Invest 110:715–724
12. Echevarria F, Norton R, Nes W, Lange Y (1990) Zymosterol is located in the plasma membrane of cultured human fibroblasts. J Biol Chem 265:8484–8489
13. Johnson WJ, Fischer RT, Phillips MC, Rothblat GH (1995) Efflux of newly synthesized cholesterol and biosynthetic sterol intermediates from cells. Dependence on acceptor type and on enrichment of cells with cholesterol. J Biol Chem 270:25037–25046
14. Lusa S, Heino S, Ikonen E (2003) Differential mobilization of newly synthesized cholesterol and biosynthetic sterol precursors from cells. J Biol Chem 278:19844–19851
15. Yamauchi Y, Reid PC, Sperry JB, Furukawa K, Takeya M, Chang CCY, Chang T-Y (2007) Plasma membrane rafts complete cholesterol synthesis by participating in retrograde movement of precursor sterols. J Biol Chem 282:34994–35004
16. Yamauchi Y, Yokoyama S, Chang T-Y (2016) ABCA1-dependent sterol release: sterol molecule specificity and potential membrane domain for HDL biogenesis. J Lipid Res 57:77–88
17. Koivisto PV, Miettinen TA (1988) Increased amounts of cholesterol precursors in lipoproteins after ileal exclusion. Lipids 23:993–996
18. Yamauchi Y, Iwamoto N, Rogers MA, Abe-Dohmae S, Fujimoto T, Chang CCY et al (2015) Deficiency in the lipid exporter ABCA1 impairs retrograde sterol movement and disrupts sterol sensing at the endoplasmic reticulum. J Biol Chem 290:23464–23477

19. Cham BE, Knowles BR (1976) A solvent system for delipidation of plasma or serum without protein precipitation. J Lipid Res 17:176–181
20. Yokoyama S, Tajima S, Yamamoto A (1982) The process of dissolving apolipoprotein A-I in an aqueous buffer. J Biochem 91:1267–1272
21. Saito H, Dhanasekaran P, Nguyen D, Holvoet P, Lund-Katz S, Phillips MC (2003) Domain structure and lipid interaction in human apolipoproteins A-I and E, a general model. J Biol Chem 278:23227–23232
22. Okuhira K, Tsujita M, Yamauchi Y, Abe-Dohmae S, Kato K, Handa T, Yokoyama S (2004) Potential involvement of dissociated apoA-I in the ABCA1-dependent cellular lipid release by HDL. J Lipid Res 45:645–652
23. Vedhachalam C, Duong PT, Nickel M, Nguyen D, Dhanasekaran P, Saito H et al (2007) Mechanism of ATP-binding cassette transporter A1-mediated cellular lipid efflux to apolipoprotein A-I and formation of high density lipoprotein particles. J Biol Chem 282:25123–25130
24. Yamauchi Y, Abe-Dohmae S, Yokoyama S (2002) Differential regulation of apolipoprotein A-I/ATP binding cassette transporter Al-mediated cholesterol and phospholipid release. BBA-Mol Cell Biol L 1585:1–10
25. Yamauchi Y, Chang CCY, Hayashi M, Abe-Dohmae S, Reid PC, Chang T-Y, Yokoyama S (2004) Intracellular cholesterol mobilization involved in the ABCA1/apolipoprotein-mediated assembly of high density lipoprotein in fibroblasts. J Lipid Res 45:1943–1951
26. Abe-Dohmae S, Suzuki S, Wada Y, Aburatani H, Vance D, Yokoyama S (2000) Characterization of apolipoprotein-mediated HDL generation induced by cAMP in a murine macrophage cell line. Biochemistry 39:11092–11099
27. Costet P, Luo Y, Wang N, Tall A (2000) Sterol-dependent transactivation of the ABC1 promoter by the liver X receptor/retinoid X receptor. J Biol Chem 275:28240–28245
28. Hara H, Hara H, Komaba A, Yokoyama S (1992) Alpha-helical requirements for free apolipoproteins to generate HDL and to induce cellular lipid efflux. Lipids 27:302–304
29. Mendez AJ, Anantharamaiah GM, Segrest JP, Oram JF (1994) Synthetic amphipathic helical peptides that mimic apolipoprotein A-I in clearing cellular cholesterol. J Clin Invest 94:1698–1705
30. Remaley AT, Thomas F, Stonik JA, Demosky SJ, Bark SE, Neufeld EB et al (2003) Synthetic amphipathic helical peptides promote lipid efflux from cells by an ABCA1-dependent and an ABCA1-independent pathway. J Lipid Res 44:828–836
31. Nagao K, Zhao Y, Takahashi K, Kimura Y, Ueda K (2009) Sodium taurocholate-dependent lipid efflux by ABCA1: effects of W590S mutation on lipid translocation and apolipoprotein A-I dissociation. J Lipid Res 50:1165–1172
32. Brooks CJ, Horning EC, Young JS (1968) Characterization of sterols by gas chromatography-mass spectrometry of the trimethylsilyl ethers. Lipids 3:391–402
33. Gerst N, Ruan B, Pang J, Wilson WK, Schroepfer GJ (1997) An updated look at the analysis of unsaturated C27 sterols by gas chromatography and mass spectrometry. J Lipid Res 38:1685–1701

Chapter 20

ABC-Transporter Mediated Sterol Export from Cells Using Radiolabeled Sterols

Alryel Yang and Ingrid C. Gelissen

Abstract

Cholesterol export from cells to extracellular acceptors represents the first step of the reverse cholesterol transport process and is an essential part of the multifaceted pathway for cells to control their cholesterol levels. Malfunction of this pathway leads to cholesterol accumulation in cells such as macrophages, which can form the basis of conditions like atherosclerosis. A number of ATP-binding cassette (ABC) transporters, namely ABCA1, ABCA7, ABCG1, and ABCG4, play an essential role in this process. In this chapter, we describe methods utilizing radiolabeled sterols for measuring ABC-transporter mediated sterol export, utilizing endogenously expressed transporters as well as overexpression systems.

Key words Cholesterol export, ABC-transporter, Reverse cholesterol transport, ABCA1, ABCG1, ABCA7, ABCG4

1 Introduction

Cells have multifaceted control mechanisms for regulating their cholesterol levels, of which ABC-transporter mediated cholesterol export is an important part. Humans express 48 ABC transporters, which transport a variety of substrates across cellular membranes, a process that depends upon ATP binding and consumption to facilitate transport. A number of family members have been implicated in the direct export of cholesterol and other sterols from cells, including ABCA1, ABCA7, ABCG1, and ABCG4 [1–4]. ABCA1 and ABCA7 are both part of the A-subfamily of ABC transporters and classified as full-transporters, containing two ATP-binding cassettes and two multipass transmembrane spanning domains. These two transporters are both localized on the plasma membrane [5, 6] and display significant amino acid sequence homology (~54% in humans; [7]); however, their cellular expression pattern and regulation are somewhat different. ABCA1 is ubiquitously expressed and associated with the regulation of lipid homeostasis in various cell types, including macrophages and other immune

Ingrid C. Gelissen and Andrew J. Brown (eds.), *Cholesterol Homeostasis: Methods and Protocols*, Methods in Molecular Biology, vol. 1583, DOI 10.1007/978-1-4939-6875-6_20,

cells, insulin-secreting β-cells and neurons [8–10]. Its function has been investigated extensively in the setting of atherosclerosis and other inflammatory conditions associated with lipid dysregulation (for recent reviews, see 11–13). ABCA1 is regulated by the liver X-receptor (LXR) family of transcription factors that upregulate a number of cholesterol-related genes, including ABCA1, ABCG1, and apolipoprotein E, in response to an increase in cellular cholesterol levels [14, 15]. On the other hand, ABCA7 is highly expressed in brain, lung, and hematopoietic tissues [5, 7, 16], and is thought to be important in the regulation of macrophage phagocytosis and regulation of lipid homeostasis in the brain [17]. ABCA7 expression has been shown to be regulated by cellular cholesterol levels via the sterol regulatory element-binding protein-2 (SREBP-2) pathway [18], whereby upregulation of ABCA7 was brought on by a depletion of cellular cholesterol, as opposed to ABCA1. In addition, inhibitors of 3-hydroxy-3-methylglutaryl-CoA (HMG-CoA) reductase, commonly known as statins, have been shown to upregulate expression of ABCA7 [19].

The other aforementioned pair of ABC family members associated with cholesterol transport, i.e., ABCG1 and ABCG4, share an even more significant amino acid sequence homology (~84% in humans; [20]). Unlike their ABCA-family members, ABCG1 and ABCG4 are part of the G-subfamily of half-transporters that require homodimerization or heterodimerization to form a functional transporter [8, 21]. Like ABCA1, ABCG1 has been predominantly investigated with regard to its role in macrophage lipid homeostasis while ABCG4 is thought to function predominantly in cells in the brain [4, 8]. As mentioned, ABCG1 is also regulated via the LXR pathway. However, it is less well established whether this is the case for ABCG4 in all cell types in brain, with reports of negligible or only modest upregulation of this transporter by LXR agonists [22–24]. The intracellular localization of these half-transporters may potentially differ from ABCA1 and ABCA7, with ABCG1 reported on the plasma membrane as well as exclusively intracellular [25].

Despite the differences in regulation, cellular expression, and localization described above, transport assays can be adapted to any cell type of interest, in particular when overexpression systems are used, as the end result of transporter activity is the same, i.e., cholesterol export to extracellular acceptors. A number of extracellular acceptors can stimulate ABC-transporter mediated cholesterol release, with apolipoprotein A-I (apoA-I) being the most physiologically relevant acceptor for ABCA1 and high density lipoprotein (HDL) subclasses for ABCG1 [8]. In this chapter, we describe a protocol for measuring cholesterol export from cells overexpressing ABCA1 or ABCG1, as well as cells that express the endogenous transporters, THP-1 macrophages. Cells can be preloaded with cholesterol if required by various means that are

included in the methodology. In addition, export of sterol substrates other than cholesterol, for example oxysterols, can also be measured utilizing these protocols.

2 Materials

Please follow your institute's radiation policy for storage, use and disposal of liquid and solid isotope contaminated materials. Note that this assay requires cell culture facilities that are approved for the use of [^{3}H]-containing reagents and cells.

2.1 Cells and Cellular Labeling

1. Cells of interest: CHO-K1 cells and THP-1 monocytes (*see* **Note 1**).
2. Culture media for CHO-K1: Ham's F12, containing 10% (v/v) fetal bovine serum (FBS), L-glutamine (2 mM), penicillin (100 U/mL), and streptomycin (100 μg/mL).
3. Zeocin (or other selection antibiotic) for selection of stable expressors in CHO-K1 cells.
4. Culture media for THP-1 monocytes: RPMI 1640 medium containing 10% (v/v) FBS, L-glutamine (2 mM), penicillin (100 U/mL), and streptomycin (100 μg/mL).
5. 24-well cell culture dishes.
6. Phorbol myristate acetate (PMA): Prepare a 500 μg/mL stock solution in DMSO and store aliquots at −20 °C. Prepare a 1:10 dilution in ethanol to achieve a 50 μg/mL stock and store at −20 °C.
7. Fatty acid-free bovine serum albumin (BSA): Prepare a 1% (w/v) BSA stock solution in the appropriate serum-free media, supplemented with antibiotics/L-glutamine. Filter-sterilize using a 0.22 μm syringe filter and store at 4 °C until use (*see* **Note 2**).
8. [1, 2-^{3}H(N)]-cholesterol: A stock of at least 1 μCi per μL in ethanol is required to achieve the necessary sensitivity (*see* **Note 3**).
9. Sterile phosphate-buffered saline (PBS).
10. TO-901317 (a synthetic LXR ligand): Prepare a 10 mM stock solution in DMSO and store at −20 °C.
11. ABC transporter overexpression constructs (*see* **Note 4**).

2.2 Cellular Cholesterol Enrichment and Acceptors for Efflux

All of the following reagents require filter sterilization through a 0.22 μm or 0.45 μm (in the case of lipoproteins) syringe filter before addition to cells.

1. Cholesterol/cyclodextrin (Chol/CD): Either prepare in-house [26] or purchase commercially (may be listed by suppliers as "water-soluble cholesterol").

2. Low-density lipoprotein (LDL): Prepare from human plasma as described by ultracentrifugation according to Chung et al. [27] or Sattler et al. [28] or purchase commercially (*see* **Note 5**).
3. Lipid-free apoA-I: Commercially available or isolate from HDL as described by Rye et al. [29].
4. HDL, either whole or subclasses such as HDL_2 or HDL_3: Prepare from human plasma via ultracentrifugation according to Rye et al. [29] or purchase commercially.

2.3 Cellular Harvesting and Scintillation Counting

1. 1.5 mL tubes.
2. Cell lysis buffer: 0.2 M NaOH in PBS or 0.1% (v/v) Triton X-100 in PBS.
3. Scintillation fluid (*see* **Note 6**).
4. Glass or plastic scintillation vials.
5. Scintillation counter for tritium-containing samples.
6. Non-refrigerated benchtop centrifuge for spinning 1.5 mL tubes that contain radiolabeled contents (10,000 × *g* for pelleting any non-adherent cells).

3 Methods

3.1 Cell Culture and Labeling: CHO-K1 Cells Overexpressing ABCA1 or ABCG1

1. Prepare media as follows: Media A (Ham's F12 supplemented with 10% FBS, penicillin/streptomycin, and glutamine) and Media B (serum-free Ham's F12 supplemented with penicillin/streptomycin and glutamine, as well as 0.1% (w/v) BSA by diluting the 1% BSA stock solution 1:10 with media).
2. On day 1, plate cells stably overexpressing ABCA1 or ABCG1 as well as CHO-K1 parental cells (for background subtraction) in 24-well plates in Media A (plus your selection antibiotic) at an appropriate density that assures that the cells are approximately 90% confluent at the end of the experiment. For CHO-K1 cells, 4×10^4 per well is a suitable density. Each condition should be set up at least in triplicate wells (or more), while a control condition (also in triplicate or more) to measure background efflux to Media B alone (without acceptor) should be included. Alternatively, if transporters are transiently expressed, plate CHO-K1 on day 1 and transfect on day 2 using standard transfection protocols and including a mock-transfected condition. This adds an extra day to the protocol described here, and hence plating densities should be adjusted.
3. On day 2, change media to 0.5 mL/well of fresh Media A with the addition of 1 μCi/mL of [1, 2-^{3}H(N)]-cholesterol, assuring

that the concentration of ethanol does not exceed 0.1% (v/v). If using stable overexpressors, include the selection antibiotic at suitable concentrations.

4. On day 3, remove media containing radiolabeled cholesterol, wash cells once with sterile PBS and incubate with 0.5 mL/well of Media B for 30 min to equilibrate (*see* **Note 7**).
5. After the 30 min equilibration period, remove media and wash cells twice with sterile PBS.
6. Add efflux media (0.5 mL/well), containing Media B with the required concentration of apoA-I, HDL or other acceptor and return cells to incubate for the remainder of the efflux period (*see* **Notes 8** and **9**).
7. At the end of the efflux period, collect media in pre-labeled 1.5 mL eppendorf tubes and spin immediately at 3000 × *g* to pellet any floating cells. Transfer 300–400 μL into a new pre-labeled 1.5 mL tube. Freeze at −20 °C until ready to process for scintillation counting.
8. Wash cells twice carefully with PBS, making sure that the last wash is removed completely.
9. Add 0.5 mL of cell lysis buffer to each well and freeze overnight (*see* **Note 10**).
10. Defrost cells and pipette lysis buffer up and down at least ten times, to create a homogenous sample. Transfer the cell lysate to pre-labeled 1.5 mL tubes, and add 50 μL to a pre-labeled scintillation vial. Store any unused cell lysate at −20 °C.
11. Defrost media and transfer 50 μL to a pre-labeled scintillation vial. Store any unused media at −20 °C.
12. Add the required amount of scintillation fluid to the scintillation vials and count (*see* **Note 11**). Make sure to include a blank sample (i.e., one sample containing background media B and one containing cell lysis buffer only) and subtract this from the counts in each of your respective samples.
13. Calculate % efflux for a particular condition as follows:

$$\frac{\text{Counts in media} \times (500/50) \times 100}{(\text{Counts in media} \times (500/50)) + (\text{Counts in cells} \times (500/50))}$$

14. If an intermediate time point was collected and counted, % efflux for this particular time point (indicated as t = a, with the final time as t = f) can be calculated as follows: Firstly, adjust the counts for time point t = a by multiplying your value from scintillation counting with the amount collected (e.g., 50 μL) over the amount counted (e.g., 30 or 40 μL). % Efflux for this time point is then calculated as follows:

$$\frac{\text{Counts in media}\left(t=\text{a}\right)\times\left(500/50\right)\times100}{\left(\text{Counts in media}\left(t=\text{a}\right)\right)+\left(\text{counts in media}\left(t=\text{f}\right)\times\left(450/50\right)\right)+\left(\text{Counts in cells}\times\left(500/50\right)\right)}$$

while calculation of efflux at the final time points is as follows:

$$\frac{\left(\text{Counts in media}\left(t=\text{a}\right)\right)+\left(\text{counts in media}\left(t=\text{f}\right)\times\left(450/50\right)\right)\times100}{\left(\text{Counts in media}\left(t=\text{a}\right)\right)+\left(\text{counts in media}\left(t=\text{f}\right)\times\left(450/50\right)\right)+\left(\text{Counts in cells}\times\left(500/50\right)\right)}$$

15. To calculate ABC transporter specific efflux to a particular acceptor, subtract the average % efflux of the parental non-expressing line from the cell line that overexpresses a particular transporter. Figure 1 shows an example of the % efflux calculated from CHO-K1 cells compared to cells overexpressing ABCG1.

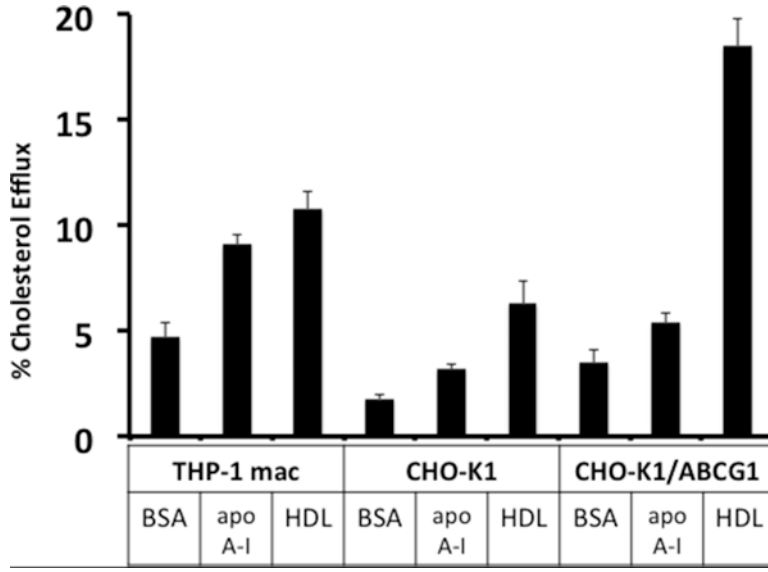

Fig. 1 Percentage cholesterol efflux from THP-1 macrophages, CHO-K1 cells and CHO-K1 cells overexpressing ABCG1. THP-1 monocytes were differentiated into macrophages (THP-1 mac) as described under Subheading 3.2 and loaded with Chol/CD at 5 μg/mL at the same time as [^{3}H]-cholesterol labeled. Efflux was performed for 8 h, to BSA alone or with apoA-I (20 μg/mL) or HDL_2 (20 μg/mL). CHO-K1 parental as well as cells overexpressing ABCG1 (CHO-K1/ABCG1) were cultured as described under Subheading 3.1. Efflux was performed for 6 h, to BSA alone or with apoA-I (20 μg/mL) or HDL_2 (10 μg/mL)

3.2 Cell Culture and Labeling: Macrophages that Express Endogenous ABCA1 and ABCG1

The protocol described here is an example and can be adjusted to other cell types and cholesterol loading conditions. We have used THP-1 monocyte-derived macrophages as our example as these are utilized extensively for ABC transporter mediated cholesterol export studies. The LXR agonist TO-901317 can be used to upregulate ABCA1 and ABCG1 expression when baseline levels are low, and can be replaced with other synthetic or endogenous LXR ligands, such as GW-3965 or oxysterols, respectively [30].

1. Prepare Media A and Media B (as described under Subheading 3.1, **step 1**, for CHO-K1 cells) for THP-1 monocytes.
2. Plate THP-1 monocytes in the presence of PMA (50 ng/mL) for 3 days to differentiate into macrophages (*see* **Note 12**). Plating densities for THP-1 cells in 24-well plates are 0.5×10^6 per well in 0.5 mL of media. Make sure to include a condition that has vehicle-only treatment in case an LXR ligand is used and Media B-only efflux (no acceptor).
3. In the case that cells require cholesterol-loading with native/modified LDL, this should preferably be done prior to labeling with [^{3}H]-cholesterol and in the case of LDL, requires a 24 h incubation for the cells to process the lipoproteins (hence this may add an additional day to the protocol; *see* **Note 13**).
4. On day 4, change media to 0.5 mL/well of fresh Media A with the addition of 1 μCi/mL of [1, 2-^{3}H(N)]-cholesterol, as well as TO-901317 (10 μM) if required, ensuring that the concentration of ethanol and/or DMSO does not exceed 0.2% (v/v).
5. On day 5, remove media containing radiolabeled cholesterol, wash cells once with sterile PBS and incubate with 0.5 mL/well of Media B (in the presence of PMA at 50 ng/mL) for 30–60 min to equilibrate (preferably longer if cells are preloaded with lipoprotein-derived cholesterol as the [^{3}H]-cholesterol is required to equilibrate into cholesteryl ester pools).
6. After equilibration, remove media and wash cells twice with sterile PBS.
7. Add efflux media (0.5 mL/well), containing Media B with the required concentration of apoA-I, HDL or other acceptor and return cells to incubate for the remainder of the efflux period (*see* **Note 14**).
8. Process media and cells as described from Subheading 3.1, **step 7**, onwards.

4 Notes

1. CHO-K1 and HEK293 cells are often used for cellular sterol export studies that utilize overexpressed ABC transporters. These cells can be transiently transfected with high efficiency

while the generation of stable expressors is also easily successful. THP-1 (a human monocytic cell line) and J774 murine macrophages are commonly used macrophage models, where upregulation of ABCA1 and ABCG1 can be easily achieved, either by cholesterol loading or incubation with a synthetic LXR agonist. Please note that J774 murine macrophages require treatment with cAMP to induce ABCA1 expression as the regulation of ABCA1 differs between human and murine cells [31].

2. Any BSA preparations need to be tested beforehand for background efflux as there can be considerable differences in background efflux between BSA from various suppliers. Although there will always be a small amount of cholesterol efflux expected to BSA alone, some preparations produce a larger than acceptable background due to leftover lipids in the BSA preparation. Concentrated BSA solutions can be stored for longer at −20 °C until needed.
3. Export of other sterols such as [1, 2-^{3}H(N)]-7-ketocholesterol can also be tested. If the sterol is in a different solvent that is toxic to cells, this may be removed by evaporation and replaced with ethanol.
4. ABCA1 and ABCG1: These can be transiently overexpressed in cells such as CHO-K1 or HEK293 cells; however, in our experience it is better to prepare stable overexpressors and in the case of ABCA1, inducible overexpression systems in the case when constructs are driven by strong promotors (e.g., CMV) as very high levels of ABCA1 overexpression can be toxic to cells.
5. The latter reference describes a protocol based on much smaller volumes of plasma and, subsequently, lipoproteins. Besides native LDL, acetylated or oxidatively modified LDL can be used to enrich macrophages with cholesterol that also leads to more extensive cholesterol but also cholesteryl ester accumulation as these will be internalized via scavenger receptor uptake. Methods for these modifications are described in Brown et al. [32] and Kritherides et al. [33].
6. The scintillation fluid needs to be compatible with the cell lysis buffer used as well as the media used for the efflux assay. This can be tested by performing a standard curve with a small consistent amount of [1, 2-^{3}H(N)]-cholesterol added to increasing amounts of cell lysis buffer or background media to test whether these quench the tritium signal.
7. All media and washes from now on need to be collected and processed as radioactive waste according to your institution's radiation control procedures.
8. To achieve maximal cholesterol efflux, 10 μg/mL of apoA-I is generally sufficient for CHO-K1 cells overexpressing ABCA1,

while 10 μg/mL of HDL_2 is sufficient for CHO-K1 cells overexpressing ABCG1. If other cell types or transporters are utilized, an acceptor concentration curve might first be performed to make sure that the acceptor concentration is not limiting.

9. Apart from measuring total efflux at the final time point, samples can be collected at intermittent time points. As the total efflux volume is 500 μL, we recommend that a maximum of two time points of 50 μL volume can be collected without reducing the media volume to levels that will affect cell viability. These intermediate samples can be collected, spun immediately to remove non-adherent cells and 30–40 μL counted for [^{3}H]–cholesterol release. Considering that [^{3}H]-counts may be low, it might be necessary to increase the amount of [^{3}H]-cholesterol that is used to label the cells.
10. We found that an overnight freeze makes it easier to harvest all the cellular materials without the need for scraping (which is not feasible in the small wells).
11. In our lab, we have scaled down this procedure and only use 5 mL of scintillation fluid in 7 mL plastic scintillation vials.
12. PMA should be included during the entire experiment at the same concentration but should be left out during the efflux phase (without the cells floating off) as any ethanol or other carriers can interfere with the acceptors.
13. Chol/CD loading at a low concentration (e.g., 5 μg cholesterol/mL) can be done simultaneously with the labeling (*see* Fig. 1 for example data).
14. Generally, concentrations of apoA-I and HDL needed to induce maximum cholesterol efflux may be higher for THP-1 cells compared to other cell lines, while efflux time required is generally longer compared to cells overexpressing the transporters (e.g., 6–24 h).

References

1. Oram JF, Vaughan AM (2000) ABCA1-mediated transport of cellular cholesterol and phospholipids to HDL apolipoproteins. Curr Opin Lipidol 11:253–260
2. Abe-Dohmae S, Ikeda Y, Matsuo M, Hayashi M, Okuhira K, Ueda K, Yokoyama S (2004) Human ABCA7 supports apolipoprotein-mediated release of cellular cholesterol and phospholipid to generate high density lipoprotein. J Biol Chem 279:604–611
3. Klucken J, Buchler C, Orso E, Kaminski WE, Porsch-Ozcurumez M, Liebisch G, Kapinsky M, Diederich W, Drobnik W, Dean M, Allikmets R, Schmitz G (2000) ABCG1 (ABC8), the human homolog of the Drosophila white gene, is a regulator of macrophage cholesterol and phospholipid transport. Proc Natl Acad Sci U S A 97:817–822
4. Wang N, Yvan-Charvet L, Lutjohann D, Mulder M, Vanmierlo T, Kim TW, Tall AR (2008) ATP-binding cassette transporters G1 and G4 mediate cholesterol and desmosterol efflux to HDL and regulate sterol accumulation in the brain. FASEB J 22:1073–1082
5. Wang N, Lan D, Gerbod-Giannone M, Linsel-Nitschke P, Jehle AW, Chen W, Martinez LO, Tall AR (2003) ATP-binding cassette transporter A7 (ABCA7) binds apolipoprotein A-I and mediates cellular phospholipid but not cholesterol efflux. J Biol Chem 278:42906–42912

6. Wang N, Silver DL, Costet P, Tall AR (2000) Specific binding of ApoA-I, enhanced cholesterol efflux, and altered plasma membrane morphology in cells expressing ABC1. J Biol Chem 275:33053–33058
7. Kaminski WE, Orso E, Diederich W, Klucken J, Drobnik W, Schmitz G (2000) Identification of a novel human sterol-sensitive ATP-binding cassette transporter (ABCA7). Biochem Biophys Res Commun 273:532–538
8. Gelissen IC, Harris M, Rye KA, Quinn C, Brown AJ, Kockx M, Cartland S, Packianathan M, Kritharides L, Jessup W (2006) ABCA1 and ABCG1 synergize to mediate cholesterol export to apoA-I. Arterioscler Thromb Vasc Biol 26:534–540
9. Brunham LR, Kruit JK, Pape TD, Timmins JM, Reuwer AQ, Vasanji Z, Marsh BJ, Rodrigues B, Johnson JD, Parks JS, Verchere CB, Hayden MR (2007) Beta-cell ABCA1 influences insulin secretion, glucose homeostasis and response to thiazolidinedione treatment. Nat Med 13:340–347
10. Kim WS, Rahmanto AS, Kamili A, Rye KA, Guillemin GJ, Gelissen IC, Jessup W, Hill AF, Garner B (2007) Role of ABCG1 and ABCA1 in regulation of neuronal cholesterol efflux to apolipoprotein E discs and suppression of amyloid-beta peptide generation. J Biol Chem 282:2851–2861
11. Rosenson RS, Brewer HB Jr, Ansell BJ, Barter P, Chapman MJ, Heinecke JW, Kontush A, Tall AR, Webb NR (2016) Dysfunctional HDL and atherosclerotic cardiovascular disease. Nat Rev Cardiol 13:48–60
12. Westerterp M, Bochem AE, Yvan-Charvet L, Murphy AJ, Wang N, Tall AR (2014) ATP-binding cassette transporters, atherosclerosis, and inflammation. Circ Res 114:157–170
13. Van Eck M (2014) ATP-binding cassette transporter A1: key player in cardiovascular and metabolic disease at local and systemic level. Curr Opin Lipidol 25:297–303
14. Venkateswaran A, Laffitte BA, Joseph SB, Mak PA, Wilpitz DC, Edwards PA, Tontonoz P (2000) Control of cellular cholesterol efflux by the nuclear oxysterol receptor LXR alpha. Proc Natl Acad Sci U S A 97:12097–12102
15. Costet P, Luo Y, Wang N, Tall AR (2000) Sterol-dependent transactivation of the ABC1 promoter by the liver X receptor/retinoid X receptor. J Biol Chem 275:28240–28245
16. Broccardo C, Osorio J, Luciani MF, Schriml LM, Prades C, Shulenin S, Arnould I, Naudin L, Lafargue C, Rosier M, Jordan B, Mattei MG, Dean M, Denefle P, Chimini G (2001) Comparative analysis of the promoter structure and genomic organization of the human and mouse ABCA7 gene encoding a novel ABCA transporter. Cytogenet Cell Genet 92: 264–270
17. Li H, Karl T, Garner B (2015) Understanding the function of ABCA7 in Alzheimer's disease. Biochem Soc Trans 43:920–923
18. Iwamoto N, Abe-Dohmae S, Sato R, Yokoyama S (2006) ABCA7 expression is regulated by cellular cholesterol through the SREBP2 pathway and associated with phagocytosis. J Lipid Res 47:1915–1927
19. Tanaka N, Abe-Dohmae S, Iwamoto N, Fitzgerald ML, Yokoyama S (2011) HMG-CoA reductase inhibitors enhance phagocytosis by upregulating ATP-binding cassette transporter A7. Atherosclerosis 217:407–414
20. Engel T, Lorkowski S, Lueken A, Rust S, Schluter B, Berger G, Cullen P, Assmann G (2001) The human ABCG4 gene is regulated by oxysterols and retinoids in monocyte-derived macrophages. Biochem Biophys Res Commun 288:483–488
21. Kerr ID, Haider AJ, Gelissen IC (2011) The ABCG family of membrane-associated transporters: you don't have to be big to be mighty. Br J Pharmacol 164:1767–1779
22. Tarr PT, Edwards PA (2008) ABCG1 and ABCG4 are coexpressed in neurons and astrocytes of the CNS and regulate cholesterol homeostasis through SREBP-2. J Lipid Res 49:169–182
23. Abildayeva K, Jansen PJ, Hirsch-Reinshagen V, Bloks VW, Bakker AH, Ramaekers FC, de Vente J, Groen AK, Wellington CL, Kuipers F, Mulder M (2006) 24(S)-hydroxycholesterol participates in a liver X receptor-controlled pathway in astrocytes that regulates apolipoprotein E-mediated cholesterol efflux. J Biol Chem 281:12799–12808
24. Nelissen K, Mulder M, Smets I, Timmermans S, Smeets K, Ameloot M, Hendriks JJ (2012) Liver X receptors regulate cholesterol homeostasis in oligodendrocytes. J Neurosci Res 90:60–71
25. Tarling EJ, Edwards PA (2011) ATP binding cassette transporter G1 (ABCG1) is an intracellular sterol transporter. Proc Natl Acad Sci U S A 108:19719–19724
26. Sharpe LJ, Rao G, Jones PM, Glancey E, Aleidi SM, George AM, Brown AJ, Gelissen IC (2015) Cholesterol sensing by the ABCG1 lipid transporter: Requirement of a CRAC motif in the final transmembrane domain. Biochim Biophys Acta 1851:956–964
27. Chung BH, Segrest JP, Ray MJ, Brunzell JD, Hokanson JE, Krauss RM, Beaudrie K, Cone

JT (1986) Single vertical spin density gradient ultracentrifugation. Methods Enzymol 128: 181–209

28. Sattler W, Mohr D, Stocker R (1994) Rapid isolation of lipoproteins and assessment of their peroxidation by high-performance liquid chromatography postcolumn chemiluminescence. Methods Enzymol 233:469–489
29. Rye KA (1990) Interaction of apolipoprotein A-II with recombinant HDL containing egg phosphatidylcholine, unesterified cholesterol and apolipoprotein A-I. Biochim Biophys Acta 1042:227–236
30. Janowski BA, Grogan MJ, Jones SA, Wisely GB, Kliewer SA, Corey EJ, Mangelsdorf DJ (1999) Structural requirements of ligands for the oxysterol liver X receptors LXRalpha and LXRbeta. Proc Natl Acad Sci U S A 96:266–271
31. Kiss RS, Maric J, Marcel YL (2005) Lipid efflux in human and mouse macrophagic cells: evidence for differential regulation of phospholipid and cholesterol efflux. J Lipid Res 46: 1877–1887
32. Brown AJ, Dean RT, Jessup W (1996) Free and esterified oxysterol: formation during copper-oxidation of low density lipoprotein and uptake by macrophages. J Lipid Res 37:320–335
33. Kritharides L, Jessup W, Mander EL, Dean RT (1995) Apolipoprotein A-I-mediated efflux of sterols from oxidized LDL-loaded macrophages. Arterioscler Thromb Vasc Biol 15: 276–289

Chapter 21

Measurement of Macrophage-Specific In Vivo Reverse Cholesterol Transport in Mice

Wendy Jessup, Maaike Kockx, and Leonard Kritharides

Abstract

Reverse cholesterol transport (RCT) is one of the main processes that is thought to protect against cardiovascular disease. RCT constitutes the removal of cholesterol from peripheral sites, its transport through the plasma compartment for delivery to the liver for excretion. Here, we describe an in vivo RCT method that incorporates these steps, measuring movement of cholesterol from macrophages to the plasma, the liver, and finally to the feces in mice.

Key words Reverse cholesterol transport, In vivo RCT, Macrophage-specific RCT

1 Introduction

Reverse cholesterol transport is the process whereby cholesterol is removed from peripheral tissues and transported through the blood to the liver, where it is excreted via the bile into the feces. RCT is thought to be one of the most important mechanisms for removal of excess cholesterol from foam cell macrophages in the arterial wall, leading to inhibition of atherosclerotic plaque formation and progression. Although in vitro protocols can be used to investigate aspects of RCT, such as which transporters are involved in cholesterol efflux from macrophages, the overall process of RCT requires a whole animal. In 2003, a model to study macrophage RCT in vivo in mice was developed in the laboratory of Daniel Rader [1]. This chapter describes the in vivo RCT model as used in our laboratory and is based on the previously reported method of Zhang et al. [1].

The method is summarized in Fig. 1. [^{3}H]-cholesterol-enriched macrophages are prepared in advance. This involves (1) preparation of L929-conditioned medium as a source of m-CSF for macrophage cell survival, (2) isolation and culture of primary bone marrow derived macrophages (BMDM) (*see* **Note 1**), and (3) preparation of acetylated LDL (AcLDL) to cholesterol-enrich

Ingrid C. Gelissen and Andrew J. Brown (eds.), *Cholesterol Homeostasis: Methods and Protocols*, Methods in Molecular Biology, vol. 1583, DOI 10.1007/978-1-4939-6875-6_21,

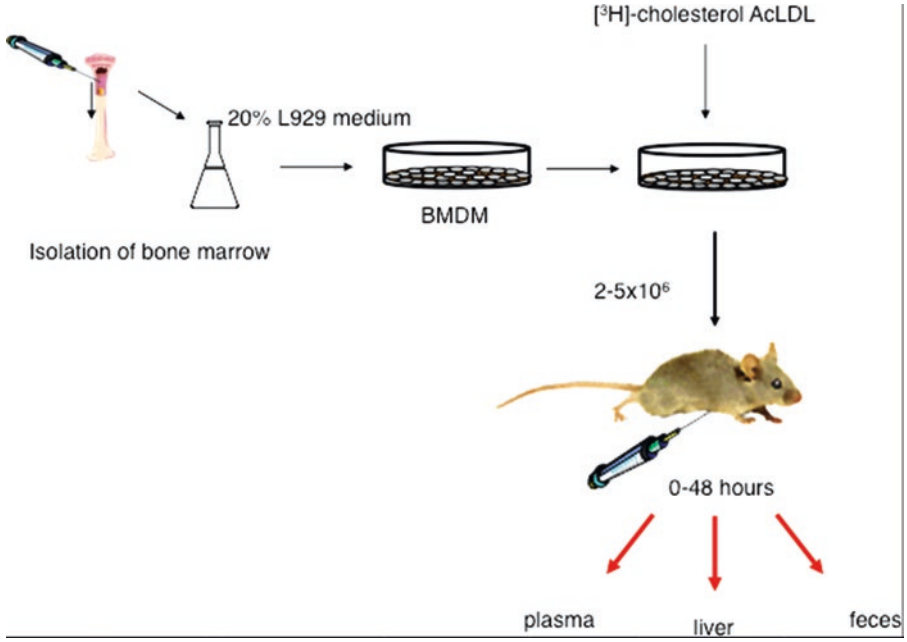

Fig. 1 Schematic of reverse cholesterol transport experiment. After isolation of bone marrow-derived monocytes (BMDM) are cultured in 20% L929-conditioned medium for differentiation into macrophages. Cells are then cholesterol-enriched by incubation with acetylated LDL containing [^{3}H]-cholesterol as a tracer. Cells are harvested and intraperitoneally injected into mice. Movement of [^{3}H]-dpm into plasma, liver, and feces is traced over time. Alternatively, J774 cells can be used instead of BMDM

the macrophages. The [^{3}H]-cholesterol-enriched macrophages are injected into the peritoneum of a mouse. Small blood samples are taken at intervals before euthanasia of the mice. Blood, liver, and fecal samples are collected after euthanasia and radioactivity is determined in all samples to trace movement of [^{3}H]-cholesterol.

2 Materials

2.1 Preparation of [^{3}H]-cholesterol-Enriched Macrophages

2.1.1 L929-conditioned Medium

1. Class II Biological Safety Cabinet (BSCII).
2. Water bath set at 37 °C.
3. 37 °C and 5% CO_2 cell incubator.
4. 150 cm^2 tissue culture flasks (T150).
5. L929 medium: Dulbecco's Modified Eagle's Medium (DMEM) containing 10% (v/v) heat-inactivated fetal calf serum (FCS), 2 mM L-glutamine, 50 U/mL penicillin, 50 μg/mL streptomycin.
6. Sterile phosphate buffered saline (PBS: 137 mM NaCl, 2.7 mM KCl, 4.3 mM Na_2HPO_4; 1.47 mM KH_2PO_4).
7. 0.25% (w/v) trypsin with 5 mM EDTA in PBS.
8. Hemocytometer.

9. L929 murine fibroblast cell line (American Type Culture Collection).
10. 50 mL sterile capped tubes.

2.1.2 Acetylation of Low Density Lipoprotein (LDL)

1. Isolated human LDL [2].
2. Magnetic stirrer.
3. Small stir bars.
4. 3–5 mL containers with flat bottom.
5. Ice bucket with ice.
6. Saturated sodium acetate solution in nanopure water.
7. Acetic anhydride.
8. Dialysis tubing with 10 kDa molecular weight cutoff.
9. Dialysis buffer: PBS containing 0.01% (w/v) chloramphenicol and 0.1% (w/v) Chelex-100 (sodium form, 50–100 mesh) (*see* **Note 2**).
10. 0.45 μm sterile syringe filter.
11. Bicinchoninic acid assay (BCA) reagents and equipment for protein assay.
12. SAS-MX lipoprotein Kit for gel electrophoresis (Helena Laboratories).

2.1.3 Materials for Bone Marrow Isolation

1. Surgical scissors and forceps (blunt and sharp).
2. 70% (w/v) ethanol.
3. Tray for mouse dissection.
4. CO_2 to euthanize animals or equivalent method.
5. Sterile 5 mL tube.
6. Ice.
7. RPMI 1640 medium without additions.
8. Complete medium: RPMI 1640 containing 10% (v/v) heat-inactivated fetal calf serum, 20% (v/v) L929-conditioned medium, 10 mM HEPES, 2 mM L-glutamine, 50 U/mL penicillin, and 50 μg/mL streptomycin.
9. Class II Biological Safety Cabinet (BSCII).
10. Water bath set at 37 °C.
11. 37 °C and 5% CO_2 cell incubator.
12. Sterile plastic petri dishes (10 mm).
13. Sterile PBS.
14. Timer.
15. 50 mL sterile capped tubes.
16. 70 μm nylon filter fitted for 50 mL tube.

17. 20 mL syringe fitted with 25 G needle.
18. Containers to hold surgical tubes.
19. Centrifuge to spin 50 mL tubes.
20. Tris buffered ammonium chloride (TBAC): Mix 90 mL 0.16 M NH_4HCL and 10 mL 0.17 M Tris–HCL (pH 7.2). Adjust pH to 7.2 and filter-sterilize (0.22 μm membrane).
21. 150 cm^2 sterile petri dishes.
22. Hemocytometer.
23. Trypan Blue.
24. 5, 10, and 25 mL pipettes.
25. [1,2-^{3}H(N)]-cholesterol in ethanol (e.g., from PerkinElmer).
26. Loading medium: RPMI 1640 containing FCS, L929, HEPES, 2 mM L-Glutamine, 50 U/mL penicillin and 50 μg/mL streptomycin, 2 μCi/mL [^{3}H]-cholesterol, and 25 μg/mL AcLDL (*see* Subheading 2.1.2).
27. Fatty acid free bovine serum albumin (BSA): 1% (w/v) stock in RPMI 1640 medium, filter-sterilized with 0.22 μm filter.
28. Synthetic LXR ligand T0901317 (T09): 1 mM Stock in DMSO
29. Equilibration medium: RPMI 1640 containing HEPES, 0.1% (w/v) BSA and 1 μM T09.
30. Lidocaine–EDTA solution: 4 mg/mL Lidocaine, 10 mM EDTA in PBS.

2.1.4 In vivo Reverse Cholesterol Transport (RCT)

1. Metabolic cages or cages that will ensure all feces can be accurately harvested (*see* **Note 3**).
2. 26 G needles and 1 mL syringes for intraperitoneal injection and cardiac puncture.
3. 23 G needles and 20 mL syringes for perfusion.
4. Blood taking capillaries.
5. PBS.
6. Tubes for liver storage.
7. Container with liquid nitrogen.
8. Microcentrifuge tubes.
9. Anticoagulant tubes (optional).
10. Microcentrifuge with temperature control.
11. Glass scintillation vials.
12. Solvable (PerkinElmer) or equivalent solubilizer.
13. Isopropanol.
14. Hydrogen peroxide (H_2O_2; 30% v/v).
15. Scintillation fluid and vials.

16. Scintillation counter.
17. 60 °C incubator with shaking option.

3 Methods

It is important that all procedures involving mice are approved by local animal ethics committees. In addition, all steps involving radiation (including waste disposal) should be carried out according to institutional radiation safety guidelines.

3.1 Preparation of L929-condition Medium

Macrophages need m-CSF to adhere and differentiate. L929 mouse fibroblast-conditioned medium is used as a source of m-CSF.

1. Plate L929 cells at 0.3×10^6 in 150 mL of L929 medium in each of 4 × T150 flasks.
2. Incubate in a 37 °C and 5% CO_2 cell incubator.
3. After 7 days, remove the medium from the flasks to 50 mL sterile capped tubes. Replace flasks with fresh medium.
4. Centrifuge the collected medium for 10 min at 1500 × *g* to remove any detached cells and collect the supernatant. Repeat after 7 days with the second batch of media.
5. Pool the two batches of medium.
6. Store the collected medium in aliquots at −80 °C (*see* **Note 4**).

3.2 Preparation of Acetylated LDL

Chemical modification of human LDL by acetylation promotes efficient uptake by macrophages and cholesterol ester accumulation. Isolation of LDL is described in detail elsewhere (Schumaker and Puppione [2]). The AcLDL concentration should preferably be >1 mg/mL, to prevent excessive dilution of the loading medium. Therefore the starting LDL concentration should be >2 mg/mL (*see* **Note 5**).

1. Calculate the amount of LDL protein required to treat cells with 25 μg protein/mL AcLDL (*see* **Note 6**).
2. Calculate the volume of acetic anhydride required (multiply micrograms of LDL protein by 6: e.g., for 1 μg protein, 6 μl of acetic anhydride is required).
3. Add required amount of LDL to a small flat bottom tube on ice over a magnetic stirrer (*see* **Note 7**).
4. Add a similar volume of saturated sodium acetate (*see* **Note 8**).
5. Add small magnetic stirrer bar to each tube and ensure that the bars are moving slowly (*see* **Note 9**).
6. Add the calculated volume of acetic anhydride to each tube in 2 μl aliquots every 10 min with constant gentle stirring, until the total amount has been added.

7. Transfer the acetylated LDL to a dialysis tube and dialyze against 100 volumes of dialysis buffer, protected from light at 4 °C. Refresh dialysis buffer four times over a 24 h period.
8. Filter-sterilize the AcLDL using a 0.45 μm filter (*see* **Note 10**).
9. Determine the protein concentration using a BCA protein assay as per manufacturer's instruction (*see* **Note 11**).
10. Confirm the successful acetylation by agarose gel electrophoresis using SAS-MX agarose gels. Load 2 μl LDL and 4 μl AcLDL per lane. Typically the mobility of AcLDL is threefold greater than unmodified LDL.
11. Store AcLDL at 4 °C wrapped in foil, stored under nitrogen and use within 1 month (*see* **Note 12**).

3.3 Isolation and Preparation of BMDM

Typically, 4–6 × 10^6 cells containing 4–6 × 10^6 dpm are injected per mouse. To achieve this, use 1 donor mouse for 8–10 recipient mice.

3.3.1 Dissection of Hind Legs

1. Add 5 mL of RPMI 1640 with no additions to a sterile tube and keep on ice.
2. Euthanize mouse using CO_2 or other local approved protocol.
3. Pin mouse out on a surgical board securing each leg.
4. Spray mouse with 70% ethanol.
5. Remove the skin from each leg, from backbone to foot, exposing the muscles.
6. Remove muscles and tissue around the hip joint until the top of the femur (upper leg bone that looks like a white ball) is visible and cut through the joint to remove the leg.
7. Cut the ligaments at the ankle (*see* **Note 13**).
8. Separate the fibula from the tibia and remove the fibula (*see* **Note 14**).
9. Leave top (femur) and bottom leg attached and remove all external muscle tissue from the bones, using a scalpel and sharp scissors (*see* **Note 15**).

3.3.2 Harvest of Bone Marrow

All steps from this point should be performed under sterile conditions (in BSCII cabinet).

1. Prepare Complete medium and warm to 37 °C.
2. Sterilize blunt forceps and scissors in 70% ethanol and rinse in sterile PBS.
3. Prepare three petri dishes: one containing 70% ethanol and two containing sterile PBS.

4. Prepare a 20 ml syringe containing cold RPMI 1640 with no additions and a 25 G needle.
5. Dispense the bones onto the upturned lid of a sterile petri dish.
6. Using the sterile forceps, transfer the bones into the prepared petri dishes, first with 70% ethanol and then two sequential dishes with PBS, leaving them for 1 min in each dish.
7. Using forceps to hold the bone, cut at the knee to separate the upper and lower leg.
8. Holding each leg section, cut off the bottom and top as close to the knuckle as possible.
9. Flush the interior of the bone with 5 mL RPMI (using the 20 mL syringe with a 25 G needle) onto a clean sterile petri dish (*see* **Note 16**).
10. Repeat with the remaining bones.
11. Filter the pooled cell suspension through a 70 μm filter fitted onto a 50 mL tube.
12. Using the plunger of a 3 mL syringe, separate cell clumps that are lodged on the filter.
13. Rinse the petri dish and filter with 10 mL RPMI 1640 and add to the 50 mL tube.
14. Spin the cell suspension at 335 × *g* for 10 min.
15. Discard the supernatant and resuspend the pellet in 5 mL TBAC; incubate for 6 min to lyse red blood cells
16. Dilute TBAC with 10 mL RPMI 1640
17. Spin at 335 × *g* for 5 min.
18. Wash cell pellet three times in RPMI 1640, centrifuging between each wash (*see* **Note 17**).
19. Dilute 10 μL of cell suspension 1:1 in trypan blue and count the number of live cells (i.e., those that are not blue) using a hemocytometer.
20. Plate cells at 15–17 × 10^6 cells per 150 mm^2 dish in 25 mL complete medium. Incubate at 37 °C in a CO_2 incubator for 3 days (*see* **Notes 18** and **19**).
21. After 3 days, add an extra 25 mL of fresh pre-warmed complete medium to each plate (*see* **Note 20**).
22. After another 2 days, remove old medium and replace with fresh complete medium (*see* **Note 21**).
23. By day six, the cells should be almost confluent and can be enriched with cholesterol. Remove medium and replace with 25 mL loading medium (*see* **Note 22**).
24. After 48 h, remove the loading medium and wash the cells twice with warm PBS.

25. Incubate cells in equilibration medium for 16 h (*see* **Note 23**).
26. Wash the cells twice with cold (4 °C) PBS
27. Add 10 mL of cold (4 °C) lidocaine–EDTA solution and incubate for 10 min to detach the cells.
28. Using a 10 mL pipette, vigorously pipette the lidocaine/EDTA solution up and down the plate to dislodge all of the cells from the plate surface.
29. Transfer the cell suspension to 50 mL tubes.
30. Rinse the plates with 15 mL RPMI and add this to the 50 mL tubes.
31. Centrifuge at 335 × *g* for 5 min.
32. Resuspend the pellet in the required amount of RPMI 1640 with no additions (500 μl per mouse).
33. Use a small aliquot to determine the cell number injected as described in **step 20**.
34. Count 5 μl cell of suspension on a scintillation counter to determine the total amount of [^{3}H]-dpm injected.
35. Separate the cell suspension into 500 μl aliquots (one aliquot per mouse) into the appropriate number of sterile microcentrifuge tubes.
36. Keep aliquots on ice until injection.

3.4 In vivo RCT

Acclimatize mice to RCT cages (one mouse per cage) 48 h before initiation of the RCT experiment. It is preferable to use see-through cages placed close together, as this reduces the stress of separation.

3.4.1 RCT

1. Weigh mice (record weight) and assign to the various treatment groups, ensuring mice are equally distributed.
2. Using a 25 G needle, slowly inject the 500 μl cell suspension into the peritoneal cavity. Record the time of injection (*see* **Note 24**).
3. At allocated time points, take a small amount of blood by orbital puncture. Alternatively, blood can be taken from a small tail cut.
4. Use a small aliquot (approx. 10 μl) to determine radioactivity released by scintillation counting (*see* **Notes 25** and **26**).
5. At the final time point, anaesthetize the mouse according to institutional guidelines, perform a cardiac puncture and store blood on ice.
6. Cut through the spine and the abdominal aorta at the base of the tail. Perfuse mouse via the left ventricle with at least 12 mL of PBS using a 20 mL syringe with 23 G needle and harvest the

liver. Rinse liver in PBS to remove external blood, record weight, and snap-freeze in liquid nitrogen. Livers can then be stored at −80 °C until analysis (*see* **Note 27**).

7. Collect all feces for each mouse in a separate tube. Store at room temperature.

3.4.2 Plasma Analysis

1. Prepare plasma (centrifuge 20 min, 2100 × *g* at 4 °C) or serum (leave at room temperature for 15 min) and transfer to a clean tube.
2. Transfer an aliquot to a scintillation vial.
3. Add 5 mL of scintillant.
4. Determine counts on scintillation counter.
5. Determine the amount of [^{3}H]-dpm in the total plasma compartment by using formula 1 [3].

   Formula 1: Plasma volume = 0.04706 × gram body weight

3.4.3 Liver Analysis

1. Pipet 1 mL of Solvable into a glass scintillation vial.
2. Accurately weigh a piece of liver of 20 mg or less and add to the vial.
3. Shake for 2 h at 60 °C.
4. Cool and add 10 mL of scintillant.
5. Determine counts on scintillation counter.
6. Based on weight of the piece used, the amount of [^{3}H]-dpm for the total liver from each mouse can be determined (*see* **Note 28**).

3.4.4 Analysis of Feces.

1. Weigh all uncapped tubes (each containing all fecal pellets from a single mouse) and place all tubes uncapped in a 60 °C oven to desiccate. Weigh every 24 h until a stable (dry) weight is reached. This generally takes 2–3 days.
2. Place the dried feces from a single mouse in a small zip-locked plastic bag and pulverize with a hammer to a fine powder.
3. Using a sheet of paper folded into a cone, transfer pulverized feces to a clean pre-weighed tube.
4. Record the weight of the feces.
5. Transfer an accurately weighed sample of 20 mg or less of feces powder to a clean glass scintillation vial.
6. Add 100 µl of ultrapure water and leave at room temperature for 30 min (*see* **Note 29**).
7. Add 1 mL of Solvable.
8. Shake for 90 min at 50–60 °C.
9. Add 1 mL of isopropanol.

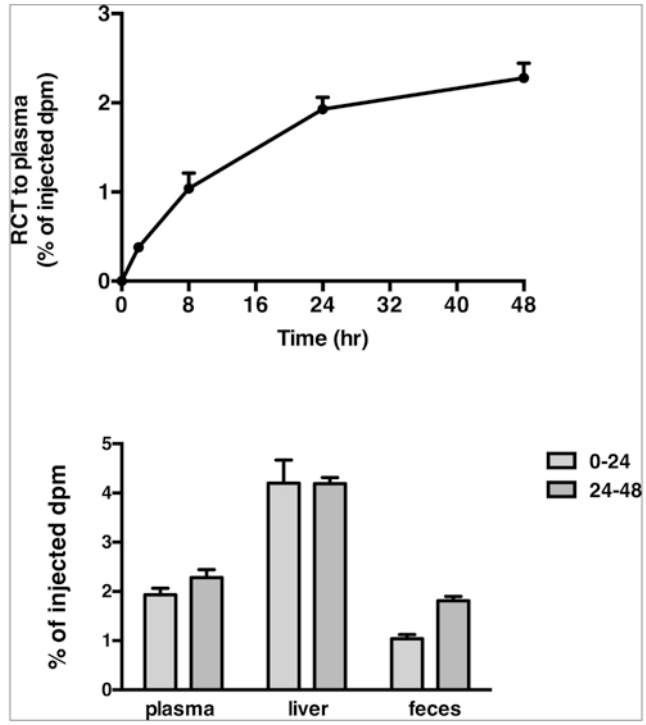

Fig. 2 C57Bl6/J mice were injected with [^{3}H]-cholesterol labeled macrophages. Appearance of [^{3}H] in plasma over time (**a**) and in plasma, liver, and feces during the first and second 24 h. time intervals (**b**) is shown. Data is mean ± SEM from 5 mice and is depicted as % of injected dpm

10. Shake for 2 h at 50–60 °C.
11. Add 200 μl of 30% H_2O_2.
12. Mix and leave at room temperature for 30 min.
13. Cap tightly and incubate overnight at 50–60 °C.
14. Add 10 mL of scintillant.
15. Determine counts on scintillation counter.
16. Based on weight of feces powder used, the amount of [^{3}H]-dpm for the total feces excreted from each mouse can be determined.

Express [^{3}H]-dpm in plasma, liver, and feces as % of injected [^{3}H]-dpm. In general 1–2%, 4–6% and 1–2% of total injectable dpm will be recovered in plasma, liver, and feces, respectively (Fig. 2).

4 Notes

1. Alternatively the macrophage cell line J774 can be used [1]. J774 cells are more readily available and easier to use; however, they lack expression of certain proteins (some of which affect

cholesterol efflux) such as apolipoprotein E. Importantly, BMDM can be isolated from knockout mouse models, providing the ability to investigate involvement of specific proteins in RCT from macrophages.

2. Chelex-100 chelates trace free metals, protecting the LDL from oxidation.
3. Standard cages fitted with a grate can be used.
4. The amount of medium prepared can be scaled up or down depending on needs. The frozen medium is stable at −80 °C for at least a year.
5. Alternatively, if AcLDL concentration <1 mg/mL, the AcLDL can be concentrated using centrifugation filter units (Amicon® Ultra-10).
6. For each mg of AcLDL protein required, it is necessary to acetylate at least 3 mg of LDL, to account for losses during the procedure.
7. Depending on the amount of LDL that is acetylated it may be faster to divide the LDL between multiple tubes, each containing 1 mL of LDL. Add an equal volume of saturated sodium acetate solution.
8. Add sodium acetate slowly in drops along the side of the tube; do not vortex.
9. Fast spinning as well as vortexing can cause aggregation of LDL.
10. Filtering through a 0.22 μm filter will reduce the yield substantially.
11. Incubate at 56 °C rather than 37 °C to allow for efficient dissociation of protein and lipids.
12. If final AcLDL concentration is below 1 mg protein/mL, concentrate using a 10 kDa Amicon® Ultra-15 filter device, to avoid excessive dilution of the cell loading medium.
13. It is easier to cut through the joint by moving the lower leg towards the foot.
14. The fibula is the very thin bone.
15. The cleaner the bones, the easier it is to isolate the bone marrow. Place the bones in a tube containing ice-cold RPMI 1640.
16. The flushed cell suspension is slightly brown. Occasionally, cells may come out as a long “string”.
17. Cells will be lost with every wash. When isolating cells from less than 3 mice wash only twice.
18. Do not disturb the cells during the first 3 days.
19. Cells will adhere less firmly to petri dishes than tissue culture plastic and are therefore easier to dislodge from the plate when harvesting.

20. Do not remove the old medium. At this stage some monocytes will have adhered but they are still easy to detach. They have a stretched fibroblast-like appearance. There will also be many non-adherent cells.
21. The cells should be dividing now.
22. If the plates are very confluent, the medium will be depleted of nutrients within 24 h and the cells will round up. Replace with fresh loading medium when this occurs. Also, please note that cells and media now contain [^{3}H]-cholesterol, and hence Institutional guidelines regarding disposal of radioactive waste need to be observed.
23. The addition of LXR agonist maximizes upregulation of expression of the cholesterol transporters ABCA1 and ABCG1.
24. The cells will sediment whilst sitting on ice. Before preparing the injection syringe, gently resuspend the cells by tapping the microfuge tube; do not use the syringe and needle to resuspend, as this may shear some cells.
25. The maximum blood volume taken at each time point will depend on the number of time points needed.
26. The blood will contain [^{3}H]-radioactivity. If mice are bleeding, take care to contain contamination of equipment and containers.
27. It is very important the liver is sufficiently perfused, as any remaining blood will affect the determination of liver-associated [^{3}H]-cholesterol.
28. Ensure that the liver piece is totally dissolved. If undissolved chunks persist after 2 h in Solvable, ensure they are submerged and incubate for longer period or overnight.
29. Add water directly on top of the fecal powder, not on the sides of the vial.

Acknowledgments

This work was supported by the National Heart Foundation (Grant in aid G10S5192) and the National Health and Medical Research Council of Australia (Program grant 1037903).

References

1. Zhang Y, Zanotti I, Reilly MP, Glick JM, Rothblat GH, Rader DJ (2003) Overexpression of apolipoprotein A-I promotes reverse transport of cholesterol from macrophages to feces *in vivo*. Circulation 108:661–663
2. Schumaker VN, Puppione DL (1986) Sequential flotation ultracentrifugation. Methods Enzymol 128:155–170
3. Berbée JFP, Boon MR, Khedoe PPSJ, Bartelt A, Schlein C, Worthmann A, Kooijman S, Hoeke G, Mol IM, John C, Jung C, Vazirpanah N, Brouwers LPJ, Gordts PLSM, Esko JD, Hiemstra PS, Havekes LM, Scheja L, Heeren J, Rensen PCN (2015) Brown fat activation reduces hypercholesterolaemia and protects from atherosclerosis development. Nat Commun 6:6356

INDEX

Ingrid C. Gelissen and Andrew J. Brown (eds.), *Cholesterol Homeostasis: Methods and Protocols*, Methods in Molecular Biology, vol. 1583, DOI 10.1007/978-1-4939-6875-6,

L

M

N

P

R

S

T

W